TRANSPORT OF ADSORBED GASES THROUGH

GRAPHITISED CARBON MEMBRANES

by

CHRISTOPHER LINLEY MURRAY

B.Sc., A.R.C.S.

A thesis submitted for the degree of

Doctor of Philosophy

in the University of London

Chemistry Department,                                    August 1976

Imperial College,

London, SW7 2AY.

## ABSTRACT

Isothermal diffusion of n-paraffins (up to $n-C_4H_{10}$) and non-isothermal flow of $C_3H_8$, $n-C_4H_{10}$ and $neo-C_5H_{12}$ through microporous carbon membranes compacted from Graphon, have been investigated. Adsorption isotherms have been determined for most of these hydrocarbons, to establish the relationship between gas and surface phase concentrations. Additionally, to complete a previous study, isotherms for $H_2$, Ne, Kr and Xe have been determined. Measurements have been made between 308.15 and 393.15K.

Time-lags, L and permeabilities, $K$, have been determined for isothermal diffusion, and diffusion coefficients for the transient and steady-state flows derived. Empirical relationships between $K$ and L, and the Henry law coefficient, polarizability and boiling point of the gas have been tested.

In the non-isothermal studies a flow apparatus involving a capacitance membrane manometer to monitor pressure was used, a temperature drop of 60K being imposed on the carbon plug. From the steady-state pressure ratios, heats of transport, $Q_m$, have been obtained. Non-ideal values, unexpectedly found for non-sorbed gases, are discussed. A method has been developed for independently determining the thermo-osmotic flux in an open system, and hence an isobaric permeability, $B(T_o)/p_o$.

Analysis of $K$, $B(T_o)/p_o$ and $Q_m$ has been made in terms of gas and surface (or 'extra') flow components, using helium as a calibrating gas. For strongly sorbed hydrocarbons it is found that 'extra' flow can greatly exceed gas phase flow.

Pressure dependence of flow parameters has been investigated. $K$ is found to be constant for $CH_4$ and $C_2H_6$, decreases slightly with ingoing pressure in the case of $C_3H_8$ but with $n-C_4H_{10}$ $K$ decreases

markedly with increasing pressure. Similar behaviour is observed with $-B(T_o)/p_o$ and $-Q_m$, evidence for a maximum, occurring at progressively lower pressures with increasing adsorption, being found. This behaviour is related to the surface concentration of the adsorbate.

ACKNOWLEDGEMENTS

I would like to thank Professor R M Barrer and Mr R Ash for their sustaining encouragement and guidance throughout this work.

Thanks are also due to the technical staff of the Chemistry Department for their help with the construction of the more specialised parts of the apparatus.

I also wish to express my deepest thanks to my father and mother for their continued help, support and advice throughout my education.

I am indebted to Mrs June Banks for many hours of patient and painstaking work in transforming an untidy manuscript into a very neat typescript.

Finally, I wish to acknowledge the award of a maintenance grant by the Science Research Council during the period 1970-1973.

TABLE OF CONTENTS

LIST OF TABLES

LIST OF FIGURES

CHAPTER 1

INTRODUCTION

*"The motion of gases through minute channels such*

*as capillary tubes, porous plugs and apertures in*

*thin plates, has been the subject of much*

*attention during the last fifty years."*

*Reynolds, 1879*

These words, expressed nearly one hundred years ago, are equally true today. Porous membranes are now used for a variety of separation processes ranging from the desalination of sea water to uranium isotope separation. In this work we are concerned with the diffusion of gases through high area microporous membranes in which a concentration gradient exists. The more significant developments leading to the work will now be outlined.

Graham (1846) made the observation that effusion rates of different gases through stucco plates and apertures were inversely proportional to the square root of the gas density. In 1909 Knudsen found that the proportionality held for gases flowing through long tubes, provided that the tube diameter was small in comparison with the mean free path of the gas molecules. He proceeded to derive an expression for this so-called molecular streaming or Knudsen flow, in which the flux was proportional to the pressure gradient across the tube. Subsequent workers verified his expression for capillaries (Gaede, 1913; Clausing, 1932; Adzumi, 1937 a, b). Smoluchowski (1910) modified Knudsen's expression to take into account the fractions of diffuse and specular reflections contributing to the flow, in an attempt to bring the measured and calculated fluxes into closer agreement. Deviations from the

theoretical Knudsen permeability have been found at low pressures (Adzumi, 1939; Brown et. al., 1946; Berman and Lund, 1958) and attributed to non-diffuse scattering.

Permeability has been determined over a range of pressures extending into the Poiseuille flow region, and a linear relationship between permeability and mean pressure was generally found. In some systems at low pressures minima have been observed which were less than the value for Knudsen flow (Klose, 1931; Huggill, 1952; Hanley and Steele, 1964, 1965). A two-term equation of flow (Adzumi, 1937b; Flood et al, 1952a) and a three-term equation (Weber, 1954; Barrer, 1963a) have been advanced to account for the permeability-pressure relationship.

When porous media are considered the situation becomes more complicated since a knowledge of the pore shape and diameter, and the pore size distribution are required for a complete analysis of the flow data. Frequently this is not available but several models have been proposed for the porous system. The cylindrical capillary model (Adzumi, 1937c; Barrer and Barrie, 1952) is probably the simplest, wherein it is considered that the medium can be represented by a bunch of parallel cylindrical capillaries. Another popular model is that of the Dusty Gas Theory (Mason, Evans and Watson, 1961). Here the porous medium is represented by a 'dust' consisting of giant molecules. The 'dust' and diffusing gas are then considered as a two-phase system. Lassettre (1956) used a similar model where the porous medium was considered as a bed of spheres and equations for permeability were derived which could account for diffuse and specular reflection.

Experimental work on the flow of gases through porous membranes is now quite extensive. Carman and co-workers studied diffusion and flow of gases through compacts of silica and carbon black (Carman, 1950;

Carman and Malherbe, 1950; Carman and Raal, 1951a,b). Ash and

Grove (1960) used a porous ceramic and tested several equations of

flow, whilst Hirsch (1961) fitted a three-term equation to flow

through a Pyrex disc. These investigations did not reveal minima in

the permeability-pressure curves but a flattening tended to occur at

low pressures. Pollard and Present (1948) postulated that in

capillaries an extra contribution to flow arises from long axial

flights at very low pressures. Since a porous bed is tortuous with

many kinks, then no long flights are possible and no minimum occurs.

In recent years the research group of Barrer has been concerned

primarily with the flow of single gases and binary gas mixtures under

conditions where there is no viscous flow component. Microporous

membranes compacted from high area carbons have been used in these

studies (Barrer and Strachan, 1955; Barrer and Gabor, 1959; Ash,

Barrer and Pope, 1963a; Ash, Baker and Barrer, 1967; Ash, Barrer, Clint,

Dolphin and Murray, 1973). Except for very weakly sorbed gases it was

found that the permeability was enhanced by a condensed phase flow

arising as a result of adsorption on the membrane surface (Barrer and

Gabor, 1960; Ash, Baker and Barrer, 1967). Diffusion through membranes

under such circumstances can be highly selective, being closely related

to the sorbability of the gas. Binary gas mixtures have been considered

(Ash, Barrer and Pope, 1963b; Ash, Barrer and Lowson, 1973; Ash, Barrer

and Sharma, 1976).and with a pair of gases where one is strongly sorbed

and the other weakly sorbed, very high steady-state separation factors

can be achieved.

From the experimental measurement of permeability, a time-lag

can be derived which characterises the transient flow of gas into a

membrane when initially exposed to the diffusing gas. The original

proposals relating time-lags to a diffusion coefficient were made by

Barrer (1939) and Frisch (1957, 1958 and 1959) and experimental

investigations have included those by Barrer and Grove (1951b), Barrer

and Gabor (1959), Goodknight and Fatt (1961), Ash, Barrer and Pope

(1963a) and Ash, Baker and Barrer (1968).

Under conditions where Knudsen flow occurs, the existence of

a temperature difference between the ends of a capillary or the faces

of a porous medium causes a flow of gas from the cold to the hot side.

This is termed thermal transpiration and in a closed system flow

continues until a pressure difference has built up which causes an

equal and opposite flow of gas. This equilibrium state is characterised

by a steady-state pressure ratio, $(p_o/p_\ell)_\infty$ where $p_o$ and $p_\ell$ are the

gas pressures at the hot $(T_o)$ and cold $(T_\ell)$ faces respectively.

The effect was first predicted in 1872 by Neumann and then

experimentally observed by Fedderson in 1873 on porous palladium and

platinum membranes. Reynolds independently rediscovered the effect in

1879, coining the term thermal transpiration, and making measurements on

porous stucco plates and meerschaum. Maxwell (1879) also discussed

thermal transpiration and Knudsen (1910a) considered the effect in

more detail, deriving from kinetic theory the value of $(T_o/T_\ell)^{\frac{1}{2}}$ (the

Knudsen limit) for $(p_o/p_\ell)_\infty$ ; Reynolds had also suggested this value.

Knudsen derived an expression for $(p_o/p_\ell)_\infty$ which allowed for the

departure from the Knudsen limit with increasing gas pressure.

Liang (1951, 1953) and Weber (1936) produced more elaborate

equations to describe the variation in $(p_o/p_\ell)_\infty$ with pressure. Their

equations were generally applied to single capillaries, but even so it

was frequently observed that the Knudsen limit was not achieved, even

using inert gases (Miller, 1963; Hobson, Edmonds and Verreault, 1963;

Edmonds and Hobson, 1965). Recently several workers have suggested that

this is due to a kinetic theory defficiency in not allowing for

interaction of gas molecules with the potential field of the capillary

wall (Wu, 1968; Sandler, 1972a; Siu, 1973) and for the degree of specular reflection varying with the gas velocity (Edmonds and Hobson, 1965; Miller and Buice, 1966).

Transport of gases in a temperature gradient through non-porous membranes, such as natural rubber, was investigated by Denbigh and Raumann (1952a,b), Crowe (1957) and Bearman (Bearman 1957; Bearman and Bearman, 1966). In these systems some transport occurred by sorption within the membrane matrix.

Thermal transpiration measurements in porous systems have been made on porous ceramic (Hanley, 1965; Hopfinger and Altman, 1969), on Vycor porous glass (Gilliland, Baddour and Engel, 1962), on unglazed porcelain (Rastogi, Singh and Singh, 1969) and on microporous carbon membranes (Clint, 1966; Dolphin, 1971; Ash et al, 1973). The Dusty Gas Theory has been extended to accommodate thermal transpiration (Mason, Evans and Watson, 1963) and an expression derived to predict the behaviour of $(p_0/p_\ell)_\infty$ with pressure outside the region of molecular streaming.

For non-adsorbed, or very slightly adsorbed gases, $(p_0/p_\ell)_\infty$ is less than the Knudsen limit (Ash et al 1973), in line with the findings on capillaries. However, for more strongly sorbed gases a surface analogue of thermal transpiration can occur which substantially augments the gas flow and leads to very high values for $(p_0/p_\ell)_\infty$ and large heats of transport (Ash et al 1973).

When thermal transpiration occurs in an open system without allowing any pressure difference to build up, then an isobaric permeability can be measured (Gilliland, Baddour and Engel, 1962; Ash et al 1973). This may be more effective than isothermal flow in gas separation (Ash et al 1973).

The scope of this work was to investigate the transport of low

molecular weight paraffin hydrocarbons through microporous carbon membranes compacted from Graphon, a high area carbon black. Flow under isothermal and isobaric conditions was measured as well as steady-state thermal transpiration ratios.

CHAPTER 2

THEORETICAL AND REVIEW

## 2.1 ISOTHERMAL TRANSPORT

### 2.1.1 *Flow through capillary tubes*

(i) Low pressure region, $\lambda >> d$.

When the mean free path ($\lambda$) of gas molecules flowing through a capillary tube is much greater than the tube diameter (d), then molecular streaming or Knudsen flow can occur (Knudsen, 1909). From the kinetic theory of gases we can derive the following expression for Knudsen flow in a cylindrical capillary of radius r and length $\ell$:

$$G = \left\{ \frac{4}{3} r \left( \frac{2RT}{\pi M} \right)^{\frac{1}{2}} \left( \frac{2-f}{f} \right) \right\} \pi r^2 \cdot \left( \frac{p_o - p_\ell}{\ell} \right) \qquad (2.1)$$

G is the steady-state energy flow per unit time; T and M are the temperature and molecular weight of the gas; $p_o$ and $p_\ell$ are the pressures at each end of the tube. The term in brace brackets is defined as a Knudsen permeability $K_k$. The factor (2-f)/f was not included by Knudsen, but was added by Smoluchowski (1910) to account for a fraction, f, of the molecules being diffusely reflected from the walls of the tube and a fraction (1-f) being specularly reflected. Specular reflections have a greater probability of being reflected in the direction of flow.

If the Fick relationships can be applied, then

$$\frac{J}{A_c} = - D \frac{\partial c}{\partial x} \quad ; \quad \frac{\partial c}{\partial t} = \frac{\partial}{\partial x} D \cdot \left( \frac{\partial c}{\partial x} \right) \qquad (2.2)$$

where $c = c(x,t)$; $J = J(x,t)$; $D = D(c,x,t)$.

Here c is the concentration of the diffusing gas at point x and time t, D is a diffusion coefficient, $A_c$ ($=\pi r^2$) is the cross-sectional area of the tube and $J$ is the gas flow rate or mass flux (moles per unit time).

In the steady-state of flow $J$ will be constant and frequently D is found to be independent of c, x and t. Steady-state values of G and $J$ can then be related as follows:

$$G = RT.J \qquad ; \qquad G\frac{dc}{dx} = J\frac{dp}{dx} \qquad (2.3)$$

By identifying dp/dx with $-(p_o-p_\ell)/\ell$, equation (2.1) can be written as :

$$\frac{J}{A_c} = -\left\{ \frac{4}{3} r \left(\frac{2RT}{\pi M}\right)^{\frac{1}{2}} \left(\frac{2-f}{f}\right) \right\} \frac{dc}{dx} \qquad (2.4)$$

Comparison of (2.2) and (2.4) allows the Knudsen permeability, $K_k$, to be identified with the diffusion coefficient, D thus;

$$D = K_k = \frac{G\ell}{\pi r^2.(p_o-p_\ell)} = \frac{4}{3} r \left(\frac{2RT}{\pi M}\right)^{\frac{1}{2}} \left(\frac{2-f}{f}\right) \qquad (2.5)$$

The characteristic of this type of flow is that it is determined solely by molecule-wall collisions, molecule-molecule collisions in the rarified gas being insignificant. It can be seen that for two gases flowing at the same temperature through the same capillary, $K_1/K_2 = (M_2/M_1)^{\frac{1}{2}}$, where subscripts 1 and 2 denote the different gases.

(ii) Intermediate flow, $\lambda \simeq d$.

At higher pressures when $\lambda$ is comparable to, or less than, the tube diameter, molecule-molecule collisions become more important in determining flow through the tube. Three components of flow can be recognised in this region (Weber, 1954; Barrer, 1963a):

(a) Self-diffusion in a pressure gradient. In the low pressure limit this is equivalent to molecular streaming, but decays asymptotically to zero as the pressure increases.

(b) Conduction flow arising from slipping of the gas layer adjacent to the tube wall. This rises from zero at low pressures to achieve a constant value at a high pressure.

(c)   Viscous flow obeying Poiseuille's law and being a linear

function of the mean pressure.

The total flow in this region is expressed by:

$$G = - \left\{ \frac{1}{1 + (2\ r/\lambda)} + \frac{\pi}{4} \frac{2r/\lambda}{[1 + (2r/\lambda)]} + \frac{3\pi}{64} \frac{r}{\lambda} \right\} K_k \cdot A_c \cdot \frac{dp}{dx} \qquad (2.6)$$

where the first, second and third terms represent, respectively, self-

diffusion, conduction and Poiseuille flow.

(iii)   High pressure region, $\lambda \ll d$.

At sufficiently high pressures self-diffusion and conduction flow

are insignificant, Poiseuille or streamline flow predominating.  This is

the continuum region and the gas can be treated as a fluid in which

molecule-wall collisions are negligible compared with molecule-

molecule collisions.

The contributions of the three components of flow to the

permeability are shown below.



(i)   Self-diffusion
(ii)   Conduction
(iii)  Poiseuille
(iv)   Overall

*Variation of flow*
*components with*
*pressure*
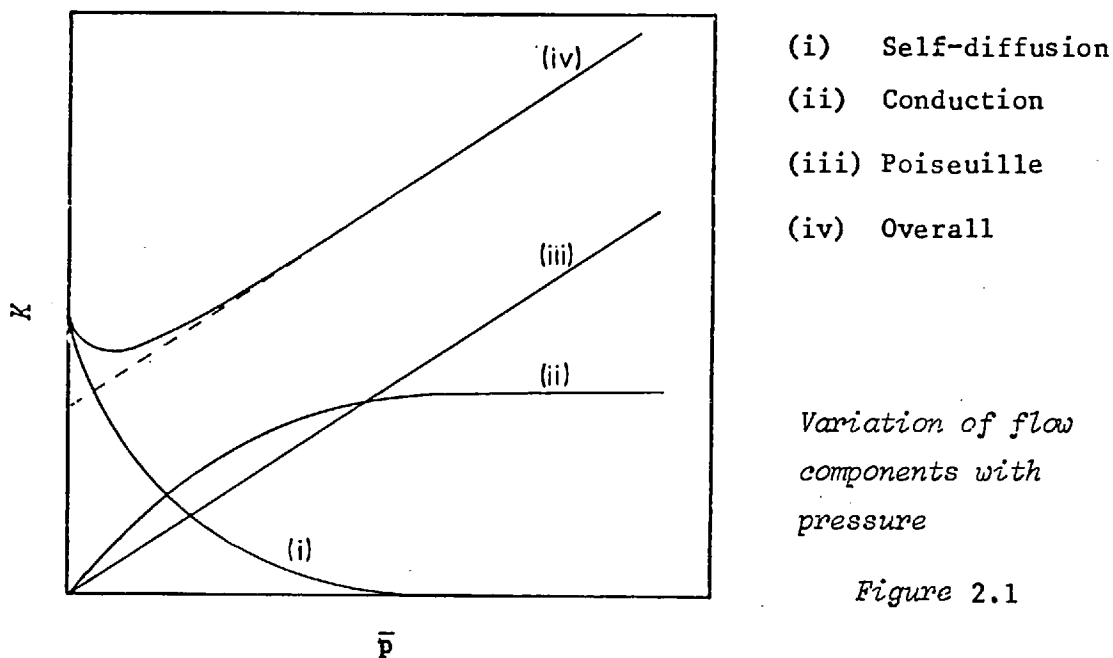
*Figure* 2.1

In the intermediate region the permeability often goes through

a minimum as the mean pressure ($\bar{p}$) is increased (figure 2.1), see

for example Knudsen, 1909; Adzumi, 1937b and Hanley and Steele, 1964,

1965. The depth and shape of the minima can be related to the length, shape, and material of the capillary and to the nature of the flowing gas (Brown et al, 1946; Huggill, 1952). Adzumi (1939) expressed the permeability as $K = a\bar{p} + \gamma b$ (a and b are constants, $\gamma = f/(2-f)$); he attributed the minimum to specular reflection.

Pollard and Present (1948) proposed that the minimum was due to an extra flow occurring as $\bar{p} \to 0$. This flow was due to axial flights of gas molecules down very long tubes, which suffered *no* collisions with the walls before leaving the capillary. As $\ell$ is reduced, the proportion of such flights diminishes and so does the depth of the minimum. Berman and Lund (1958) used very short capillaries and found no minima. In porous media no long axial flights are possible and again we find the absence of minima (Carman, 1950).

A model based on a multiply kinked ('vielfach geknickte') tube was developed by Hiby and Pahl (1956). Its permeability was compared with that of an infinitely long tube – the permeability ratio was found to be 0.8 when $\ell/d = 3$.

### 2.1.2 *Porous media*

The Knudsen permeability of a porous membrane is more difficult to interpret than that of a capillary, as a membrane is composed of a large number of non-uniform pores which vary in length and diameter. The 'long' capillary situation can not occur, and the diffusing gas molecule will undergo many collisions with the pore walls whilst within the membrane. Pore dimensions are usually several magnitudes smaller than in capillary tubes and so the Knudsen regime can be observed at much higher pressures.

Several models for porous media will now be considered.

(i) Capillary models.

The porous medium can be represented by a bunch of parallel, single capillaries which are, in the simplest form of the model, of

equal length and diameter. Adzumi (193?c) proposed the model but considered the pores to be of variable diameter and arranged as bunches of capillaries in parallel and in series. The model has been applied to streamline and intermediate flow through synthetic analcite crystals (Barrer and Grove, 1951a) and a porous ceramic (Ash and Grove, 1960), as well as to Knudsen flow through porous glass (Barrer and Barrie, 1952) and porous carbon membranes (Barrer and Strachan, 1955). More recently Nicholson and Petropoulos (1971) have developed a capillary network model in which the porous medium is represented by a number of voids linked by a three-dimensional cubic network of capillary tubes.

Barrer and Gabor (1959) related flow through a porous medium to flow through a reference capillary. To represent the pore radius of the medium, the concept of a hydraulic radius, $r_h$, was introduced (Blake, 1922; Kozeny, 1927).

$$r_h = \frac{\Sigma \ (\text{cross-sectional area of pores})}{\Sigma \ (\text{circumference of pores})}$$

For a medium composed of cylindrical capillaries, $r_h = r/2$ where r is the capillary radius. $r_h$ can be related to the porosity, $\varepsilon$, and internal surface area of the pores, A, by $r_h = \varepsilon/A$. When these relations are substituted into equation (2.5) (ignoring specular reflections) then we get (Barrer and Gabor, 1959):

$$K_k^{cyl} = D_g^{cyl} = \frac{8}{3} \frac{\varepsilon}{A} \left( \frac{2RT}{\pi M} \right)^{\frac{1}{2}} \tag{2.7}$$

$D_g^{cyl}$ is the gas phase diffusion coefficient for Knudsen flow in a reference capillary of radius $2\varepsilon/A$, where $\varepsilon$ and A take on the values of the medium being considered.

For a real porous medium,

$$D = \kappa \cdot D_g^{cyl} = \frac{8}{3} \frac{\varepsilon}{A} \kappa \left( \frac{2RT}{\pi M} \right)^{\frac{1}{2}} \tag{2.8}$$

where D is an experimentally determined diffusion coefficient and

κ is a structure factor which allows for tortuosity and non-ideality

of the porous medium. It has been considered to be equal to $\varepsilon/k^2$

(Carman, 1950), where k is the tortuosity of the membrane (= path length

of pores divided by the membrane length, $\ell$).

Nicholson and Petropoulos (1973) have replaced the reference

capillary of Barrer and Gabor by a reference pore considered to be a

parallel sided narrow slit. They were then able to calculate an

adsorption potential energy due to interaction of the gas molecule with

the plane surfaces of the slit.

(ii) Dusty gas model.

Originally proposed by Maxwell in 1860, it was rediscovered

independently by Deriagin and Bakanov (1957a,b) and by Mason (Mason et

al, 1961). The model considers the medium to be a uniform distribution

of 'dust' particles, constrained to be stationary. When the 'dust' is

visualized as giant molecules, then it is possible to treat the flow of

gas through this medium from the kinetic theory, with gas plus 'dust'

being considered as a two-component mixture.

From this model an expression analogous to equation (2.7) can be

obtained for the Knudsen limit, $D_k$ in which $\varepsilon/A$ is replaced by another

constant, $K_o$, containing terms for the number density, $n_d$, and radius,

$r$, of the dust particles, tortuosity and porosity of the medium and a

diffuse scattering factor, $a_1$. $K_o$ is determined empirically and was

expressed as:

$$(K_o)^{-1} = \frac{128}{9} \cdot n_d \cdot \frac{k}{\varepsilon} \cdot r^2 \cdot \left( 1 + \frac{\pi\, a_1}{8} \right)$$

Some evidence was found that $a_1$ was gas dependent, but for most gases

$a_1 \simeq 1$.

An equation for permeability in the intermediate region was also

derived and the model could be extended to accommodate binary gas mixtures

(Mason and Malinauskas, 1964) and thermal transpiration (Mason, Evans and Watson, 1963).

(iii) Other models.

Representation of a porous medium as a bed of randomly dispersed spheres of variable diameters was proposed by Weissberg (1963). Williams (1973) also advanced a random sphere model in which the spheres were small compared with the mean free path of molecule-sphere collisions, and where the spheres acted as scattering centres. Both Williams and Lassettre (1956) considered that reflections in the medium could be diffuse, specular or a mixture of both, and back scattering was also allowed.

Several models based on the Dusty Gas Theory (D.G.T.) have been developed. Johnson and Stewart (1965) used the D.G.T. for diffusion within each pore and obtained a total flow rate by integration over the pore size distribution. The model was extended by Feng and Stewart (1973) who introduced a term for surface diffusion as well as viscous flow and gas phase diffusion. They then considered a system of main pores with extensive cross-linking and dead-end pore branches.

### 2.1.3 *Flow through porous membranes*

The experimental technique employed for isothermal flow measurements in this work employed the following boundary conditions:

$$c(0,t) = c_o \qquad = \text{constant for } t > 0$$

$$c(\ell,t) = c_\ell(t) \qquad t > 0, c_\ell(t) \ll c_o$$

$$c(x,0) = 0 \qquad\qquad 0 < x < \ell$$

Here t denotes time and flow is in the direction of x-increasing between membrane faces bounded by $x = 0$ and $x = \ell$. c represents the total concentration of diffusant in the gas and surface phase per unit volume of membrane. The flow rate was determined by observing the build up in pressure $p (Nm^{-2})$ in a calibrated volume $V$ $(m^3)$ at $x = \ell$. A steady-state energy flux G $(J\ s^{-1})$, reduced to the temperature of the membrane, T (Kelvin),

was calculated from

$$G = \frac{d(pV)}{dt} \cdot \frac{T}{T_R} = V \cdot \frac{dp}{dt} \cdot \frac{T}{T_R} \qquad (2.9)$$

$T_R$ (Kelvin) is the temperature of the calibrated volume.

A permeability, $K$ ($m^2 s^{-1}$), was defined as the flux though unit membrane cross-sectional area, normal to the direction of flow per unit pressure gradient.

$$K = \frac{G \cdot \ell}{A_c \cdot \Delta p} = \frac{J \cdot \ell}{A_c \cdot \Delta c_g'} \qquad (2.10)$$

Here $J$ is the molar flux (mol $s^{-1}$) and $\Delta c_g'$ is the gas phase concentration drop (mol $m^{-3}$) between the membrane faces.

If adsorption occurs within the membrane, then the permeability will be composed of a gas phase component, $K_g$, and a surface or 'extra', condensed phase flow component, $K_s$, related by

$$K = K_s + K_g \qquad (2.11)$$

In several systems surface flow has been found to be much larger than the gas phase flow while in some cases very strong adsorption has led to pore blockage. Transport can then only take place by surface diffusion and in a binary mixture, flow of a non-sorbed gas could be severely reduced (for example $SO_2$ and $H_2$, Ash, Barrer and Pope, 1963b).

It can be seen (equation (2.5)) that in pure gas phase Knudsen flow $K(M/T)^{\frac{1}{2}}$ is constant for non-sorbed gases. Hence $K_g$ in equation (2.11) can be obtained from the relation

$$K_g = K^{He} \cdot (M_{He}/M)^{\frac{1}{2}} \qquad (2.12)$$

where $M_{He}$, $M$ are molecular weights and $K^{He}$ is the experimental helium permeability at the temperature of the $K$ determination (Barrer and Gabor, 1959). Here helium is assumed to be a non-sorbed calibrating gas but this practice has been questioned by Hwang and Kammermeyer (1966a,b; 1967)

who claimed that helium exhibited sorption and surface flow. However Ash, Barrer and Lowson (1970) carried out an extensive investigation of the temperature dependence of $K^{He}$ and only found a 3% variation in $KT^{-\frac{1}{2}}$ over the temperature range 77.6 to 573K. Sandler (1972a) advanced a treatment of Knudsen diffusion taking account of the potential field interaction between the gas molecules and the pore walls and Nicholson and Petropoulos (1973) adopted a similar treatment. Sandler's approach does not yield an exact $T^{\frac{1}{2}}$ dependence of $K$, but the discrepancy is small and within experimental error. Insufficient evidence is available to adopt anything other than a $T^{\frac{1}{2}}$ dependence of $K^{He}$.

Barrer and Gabor (1959) defined a steady-state gas phase diffusion coefficient as

$$D_{gs} = K_g/\varepsilon \tag{2.13}$$

where the factor $\varepsilon$ allows for the fraction of $A_c$ which exists as pores and is thus available for gas phase diffusion. Hence from (2.12) we can write

$$D_{gs} = D_{gs}^{He} (M_{He}/M)^{\frac{1}{2}} \tag{2.14}$$

Barrer and Gabor also defined a surface phase diffusion coefficient

$$D_{ss} = K_s/Ak_s \tag{2.15}$$

where $k_s$ is the Henry law constant (m ).

Besides the steady-state diffusion coefficients so far obtained, we can also determine $D_g$ and $D_s$, diffusion coefficients for gas phase and surface phase transport pertaining to the transient state, when gas is first admitted to the membrane. These will be characteristic of diffusion not only in through channels, but also into dead-end blind-pores and crevices which may exist within the membrane. Consequently they may be expected to differ from $D_{gs}$ or $D_{ss}$, which are concerned solely with flow through the membrane by as direct a path as possible.

The gas phase diffusion coefficient, $D_g$, can, in the absence of adsorption, be determined from the measured time-lag, L, by the relation

$$L = \ell^2/6D_g \qquad (2.16)$$

Here $D_g$ is considered to be independent of concentration, c, x and t. Frisch (1957; 1958; 1959) established an expression for L when $D_g$ was a function of c. Ash, Baker and Barrer (1968) derived an expression for L from the conservation of mass condition and independent of any assumed equation of flow. The treatment could be applied to diffusion according to Fick's equation where D was a function of c, x or t, or combinations of these.

If helium is again used as a non-sorbed calibrating gas, then $D_g$ can be calculated from

$$D_g^{He} = \frac{\ell^2}{6\,L_{He}} \qquad ; \qquad D_g = D_g^{He}\left(\frac{M_{He}}{M}\right)^{\frac{1}{2}} \qquad (2.17)$$

The fourth diffusion coefficient, $D_s$, can be obtained using an expression for L of a sorbed gas (Barrer and Grove, 1951b):-

$$L = \frac{\ell^2}{6} \cdot \frac{(1 + A\,k_s/\varepsilon)}{(D_g + D_s\,A\,k_s/\varepsilon)} \qquad (2.18)$$

By substituting $D_g$ from (2.17) in (2.18) and rearranging we obtain:-

$$D_s = \frac{\ell^2}{6\,Ak_s/\varepsilon}\left[\frac{(1 + Ak_s/\varepsilon)}{L} - \frac{(M_{He}/M)^{\frac{1}{2}}}{L_{He}}\right] \qquad (2.19)$$

Comparison with a cylindrical reference capillary can be made for the gas phase diffusion coefficients by evaluating the following structure factors:

$$\kappa_g = \frac{D_g}{D_g^{cyl}} \qquad ; \qquad \kappa_{gs} = \frac{D_{gs}}{D_g^{cyl}} \qquad (2.20)$$

The magnitude of the $\kappa$'s reflects the tortuosity and character of

the main flow channels. If $\kappa < 1$ then tortuosity and bottlenecks are

important. When $\kappa > 1$, then flow is greater than that predicted for a

cylindrical capillary and some channels of radii greater than $2\varepsilon/A$

govern the flow.

It has been observed that the surface diffusion coefficients

exhibit a temperature dependence (Carman and Raal, 1951a; Barrer and

Barrie, 1952; Barrer and Strachan, 1955; Barrer and Gabor, 1960) and

hence an Arrhenius-type relation can be obtained:

$$D_s = D_o \exp \ (-E_s/RT) \quad ; \quad D_{ss} = D_{os} \exp \ (-E_{ss}/RT) \qquad (2.21)$$

$E_s$ and $E_{ss}$ represent activation energies for surface diffusion in the

transient- and steady-states.

The treatment so far has assumed that adsorption is in the Henry

law region and hence that $D_s$ and $D_{ss}$ are independent of concentration

at constant temperature. Outside Henry's law two effects occur. With

large amounts of sorption the thickness of the adsorbed layer may be

such that partial blockage of pores occurs. This will have the effect

of decreasing the number of 'through' pores and hence $K_g$ calculated from

equation (2.12) will be too great and the derived $K_s$ (equation (2.11))

will be too small. This effect will be strongly pressure dependent and

the true situation will be between the extremes of $K_g = K^{He} \ (M_{He}/M)^{\frac{1}{2}}$

(no blockage) and $K_g = 0$ (complete blockage, only surface flow occurs).

Secondly, if the isotherm is curved, then equation (2.15) must

be replaced by (Ash, Baker and Barrer, 1967; Ash, Barrer, Clint, Dolphin

and Murray, 1973):

$$K_s = \frac{\varepsilon}{c_{og}} \int_0^{c_{og}} D_{ss} A \left( \frac{dc_s{}'}{dc_g} \right)_T . \ dc_g \qquad (2.22)$$

Here $c_{og}$ is the gas phase concentration (moles per unit volume of porous

membrane) at $x = 0$ and $c_g$ is the concentration within the membrane such that $c_g$ at $x = \ell$ is zero. Provided that $D_{ss} (dc_s'/dc_g)_T$ is independent of $c_s'$ (the Gibbs excess concentration per unit surface area of carbon) then $K_s$ will remain independent of $c_s'$, even if the isotherm is curved.

It may be noted that whereas $K_s$ (and $D_{ss}$) will not be expected to be concentration dependent until blockage occurs, the time lag, L, will become pressure dependent as soon as the isotherm departs from Henry law linearity. As the average pressure increases, the quantity of gas required to be adsorbed in the steady-state does not increase as rapidly. Hence a decrease in L is expected.

### 2.1.4 *Transient-state flow*

We have so far derived diffusion coefficients for the transient state, but the significance of the time-lag has not been discussed. Blind-pore character and time-lags were considered by Barrer and Gabor (1959) and Ash, Baker and Barrer (1968).

Blind (or dead-end) pores, cracks and crevices in porous media are irregularities which do not play any part in the steady-state flow. They are involved in the approach to the steady-state because flow occurs into them until sorption equilibrium and pressure equilibration with the adjacent through-stream has taken place. Subsequently they take no further part in flow.

Since blind pores need not have the same pore geometry and $\varepsilon/A$ as through pores and may not be distributed uniformly, it can be expected that $D_s$ and $D_g$ will be time-dependent as well as being averages over the length of the membrane. Ash et al (1968) defined a time-lag, $L_1$, as follows:

$$\ell \cdot J_\infty (c_o) \cdot L_1 = \int_0^\ell x \cdot c(x) \cdot dx \qquad (2.23)$$

where $c(x)$ is the adsorbate concentration (per unit volume of membrane) at $x$ ; $c(x) = c_o$ at $x = 0$ . $J_\infty (c_o)$ is the total molar flux through unit

cross-section under these conditions.

$L_1$ may be compared with the measured time-lag, L, by the quantity, $\Delta$ (= $L_1$ - L). $\Delta$ will reflect any progressive change in pore structure (x - dependence of D) and also time-dependence in D during the transient-state of flow. Ash et al (1968) derived the relation

$$2 \Delta \ J_\infty (c_o) = Q_B(0) \qquad (2.24)$$

where $Q_B(0)$ is the quantity of gas associated with flow solely into blind pores in the +x direction through unit area of the ingoing face between t = 0 and $\infty$. It can be used as a measure of the blind pore character. Ash et al also showed that the x - dependence of D can be minimised by constructing the membrane in a large number of equal increments.

If Henry's law adsorption occurs then :

$$Q_B(0) = (\varepsilon_b + A_b \ k_s). \ c_{og}'.\ell \qquad (2.25)$$

where $\varepsilon_b$ and $A_b$ are the porosity and internal surface area associated with blind pore character and $c_{og}'$ is the value of $c_g'$ (the gas phase concentration) at x = 0. Since we can write equation (2.10) as

$$K = \frac{J_\infty (c_o). \ \ell}{c_{og}'} \qquad (2.26)$$

then using (2.24) and (2.25) to eliminate $J_\infty (c_o)$ and $c_{og}'$ we get

$$K\Delta = \frac{\ell^2}{2} \ (\varepsilon_b + A_b. \ k_s) \qquad (2.27)$$

For a linear concentration gradient between c(x) = $c_o$ at x = 0 and c(x) = 0 at x = $\ell$, then c(x) = $c_o(1 - x/\ell)$. Hence on integration equation (2.23) becomes:

$$L_1 = \frac{\ell}{6} \ \frac{c_o}{J_\infty (c_o)} \qquad (2.28)$$

Using (2.26) for $J_\infty (c_o)$ and $c_o = c_{og}'(\varepsilon + Ak_s)$ (see Appendix A) then (2.28) becomes:

$$KL_1 = \frac{\ell^2}{6} (\epsilon + Ak_s) \qquad , \qquad (2.29)$$

Combining (2.27) and (2.29) we get:

$$KL = \frac{\ell^2}{6} [(\epsilon - 3\epsilon_b) + k_s (A - 3A_b)] \qquad (2.30)$$

Hence for a series of gases adsorbed according to Henry's law, a plot of $KL$ vs $k_s$ should give a straight line from which $\epsilon_b$ and $A_b$ can be determined.

### 2.1.5 *Experimental evidence for surface diffusion*

The presence of an additional component of flow in the Knudsen region, a surface flow of adsorbed molecules, is of interest in this work. First evidence for such a flow was provided by Volmer (1921) and Clausing (1930), while Wicke and Kallenbach (1941) observed an unusually high flow rate in counter-diffusion experiments on porous membranes. They attributed this to surface diffusion and identified three components of flow - viscous flow, Knudsen diffusion and surface diffusion.

Today there is extensive evidence for surface diffusion (or condensed flow) of a wide variety of sorbates on many types of porous media. Carman has investigated permeability and surface diffusion of $SO_2$, $CF_2Cl_2$ and n-butane on compacts of Linde silica and Carbolac I (Carman and Raal, 1951a, 1951b, 1954; Carman and Malherbe, 1950). Here adsorption was in the multilayer region. Large flow rates and maxima in diffusion coefficients have been observed by Flood et al (1952a-c) using activated carbon rods.

The magnitude of surface flow can often be considerably larger than the predicted gas flow (Gilliland, Baddour and Russell, 1958; Ash, Baker and Barrer, 1967). Extensive surface flow has been observed on micro-porous membranes when strong adsorption occurs. Ross and Good (1956) and Haul and Peerbooms (1958) have reported maxima in $D_{ss}$ for

n-butane on Graphon at around monolayer coverage. Ash, Barrer and Pope (1963a) and Ash, Baker and Barrer (1967) found points of inflection or maximum-minimum behaviour for $SO_2$, $SF_6$ and Ar at low temperatures where flow was almost completely in the surface phase. The strong adsorption led to extensive blockage of gas phase flow so that high separation factors were obtained for $H_2/SO_2$ mixtures (Ash, Barrer and Pope, 1963b).

Surface flow has also been observed in the sub-monolayer region. In the transient state Barrer and Barrie (1952) found a limited amount of surface flow for the Henry law adsorption of $NH_3$ and $SO_2$ on Vycor porous glass. However in the steady-state, surface flow made only a very small contribution to the flow. In contrast with this behaviour Barrer and Strachan (1955) and Ash et al (1973) have found appreciable surface diffusion on carbon membranes even within the Henry law range. Recently Patel and Butt (1972) observed a surface flux of propane on a molybdenum sulphide compact which contributed more than 30% to the total flux at $\theta \simeq 0.2$.

The influence of the nature of the membrane surface, and its energetic heterogeneity, has been investigated. Horiguchi et al (1971) have compared the permeabilities of several gases on membranes of Vycor and Graphon (the former being energetically heterogeneous and the latter energetically homogeneous). Both membranes gave similar adsorption isotherms and heats of adsorption. However the surface permeability on Graphon was more than twenty times that on Vycor, being up to five times the gas phase permeability, while on Vycor $K_s$ was never more than 30% of $K_g$. Horiguchi thought that these marked differences could be attributed to surface roughness causing a decrease in mobility of adsorbed molecules on Vycor.

Ash et al (1973) embarked on a similar comparison using membranes compacted from two carbon blacks, Carbolac, a somewhat energetically heterogeneous material of high surface area, and Graphon, a more energetically

homogeneous carbon of lower area. It was found that surface diffusion

coefficients for Graphon were comparable with or greater than gas phase

diffusion coefficients whereas for Carbolac the $D_{ss}$ were always

considerably smaller than $D_{gs}$. Ash et al related this behaviour to

the greater surface uniformity of Graphon, so that translational

freedom gave long surface mean free paths of adsorbed molecules. On

Carbolac, the rougher surface texture allowed less translational freedom

and shorter surface mean free paths. Carbolac was also found to have a

higher activation energy for surface diffusion which was consistent with

lower mobility. Although $K_s/K_g$ for a given gas was greater for Carbolac

than Graphon, the surface permeability per unit area of surface was very

much greater on Graphon.

Sandler (1972b) proposed a method for determining surface diffusion

coefficients without the use of helium as a calibrating gas. Flow

measurements in the presence of a pressure *and* a temperature gradient

were used, together with thermal transpiration measurements.

It is also possible to obtain surface diffusion coefficients

independent of gas phase permeability measurements. Haul (1950) used a

direct weighing technique for diffusion of organic vapours into porous

silica and carbon sorbents. Radioactively labelled $SO_2$ was employed by

Pope (1967) to determine a 'true' surface diffusion coefficient at high

sorbate concentrations. Finally, by the use of Spin Echo N.M.R.,

Boddenberg et al (1970) were able to determine surface self-diffusion

coefficients for Ar, $C_6H_{12}$, $C_6H_6$ on a silica compact.

2.1.6 *Mechanisms for surface diffusion*

(i) Hydrodynamic flow model

The driving force for surface flow is considered to be

proportional to the spreading pressure gradient, $d\phi/dx$, a two-dimensional

analogue of pressure gradient. Viscous flow occurs with the adsorbed

film moving as a whole over the surface with a velocity u. A characteristic of this flow mechanism is that no separation or 'unmixing' occurs when binary gas mixtures are used, and it is more correctly termed 'condensed' flow. Fick's law (equation (2.2)) takes the form where $D = D(c)$ and hydrodynamic flow is thought to become important at high sorbate concentrations $(\theta \geqslant 1)$.

For adsorption on a porous medium Babbitt (1950; 1951) expressed the flow by the equation:

$$C_R \cdot u = -d\phi/dx \qquad (2.31)$$

$C_R$ $(gs^{-1}cm^{-2})$ is a coefficient of resistance and an empirical constant. $\phi$, the spreading pressure, is the force per unit surface area which must be applied to prevent the adsorbed film from spreading; it can be obtained from isotherm data.

Gilliland et al (1958) used Babbitts equation and obtained an expression for the 'condensed' flux in the steady-state:

$$\frac{J_s}{A_c} = - \frac{\rho_{app} \cdot A_g \cdot RT}{\kappa \cdot C_R} \frac{(c_s')^2}{p} \frac{dp}{dx} \qquad (2.32)$$

$c_s'$ is the concentration of adsorbed molecules per unit surface area of membrane; $\rho_{app}$ is the apparent density of the membrane and $\kappa$ is a structure factor. If $C_R$ is independent of pressure then we can integrate from $x = 0$ to $x = \ell$, yielding:

$$\frac{J_s}{A_c} = \frac{\rho_{app} \cdot A_g \cdot RT}{\ell \cdot \kappa \cdot C_R} \int_0^{p_0} \frac{(c_s')^2}{p} \cdot dp \qquad (2.33)$$

The integral here can be evaluated from the isotherm data. Assuming Fick's equation to hold, Gilliland proceeded to derive an expression for a surface diffusion coefficient, $D_{ss}$:

$$\frac{J_s}{A_c} = D_{ss} \cdot \frac{\rho_{app} \cdot A_g}{\kappa} \cdot \frac{\Delta c_s'}{\ell} \qquad (2.34)$$

where $\Delta c_s'$ is the surface concentration difference between the plug

faces. A good correlation over the concentration range $\theta = 0.1$ to the

capillary condensation region was claimed.

Flood et al (1952c) had previously adopted a similar approach and

concluded that viscous flow of a compressed gas and flow of a liquid film

could not be distinguished, but pure diffusive flow was thought to be

small. When multilayer adsorption or capillary condensation occurred,

the controlling flow mechanism was laminar viscous flow of a liquid film.

Popielawski (1967) also favoured a two-dimensional viscous flow mechanism

in cases of strong sorption.

(ii) Activated diffusion mechanism

At sub-monolayer concentrations a random walk or activated diffusion

model appears to give the best interpretation of surface diffusion. The

adsorbed molecules are localised at particular sites and flow occurs by

a series of adsorption-desorption steps between sites. Since the hopping

molecules are more likely to be re-adsorbed at vacant sites than at

occupied ones, a net flux of adsorbed molecules occurs in the direction

of decreasing surface concentration. For small surface concentrations

the flow obeys Fick's equation having a constant D. The mechanism was

first advanced by Wicke and Kallenbach (1941) and supported by

Kammermeyer (1958) and the research groups of Carman (Carman and Raal,

1951a; Carman and Malherbe, 1950) and Barrer (Barrer and Strachan, 1955;

Aylmore and Barrer, 1966; Ash et al, 1973).

Kruyer (1953) suggested that for random walk the diffusion

coefficient could be expressed as :

$$D_{ss} = D_{os} \, \exp \, (-E/RT) \; ; \; D_{os} = \tfrac{1}{4} a^2 / \tau_m \qquad (2.35)$$

where $a$ represents the mean jump distance of a molecule on the surface

and $\tau_m$ is its mean residence time on a particular site (cf. equation (2.21)). Activation energies (E) for surface diffusion indicate that localised adsorption occurs. Diffusion coefficients for this type of mechanism are obtained from equation (2.15) in the Henry law range and equation (2.22) outside it.

Diffusive flow is distinguished since (a) on energetically homogeneous surfaces and at low surface concentrations $D_{ss}$ should be independent of concentration; (b) flow of binary gas mixtures leads to separation of the components; (c) independent migration is found; (d) $D_{ss}$ is strongly temperature dependent.

(iii) Other models

Metzner and co-workers (Smith and Metzner, 1964; Weaver and Metzner, 1966) have derived a general equation for surface transport by a hopping mechanism in which the actual trajectory and path of the molecule is considered in detail. Both the jump distance, $a$, and jump frequency, F, may vary with surface concentration. The formula obtained was:

$$\frac{J_s}{A_c} = \frac{A_g \, \rho_{app}}{2 \, \pi \, k^2} \left[ F \left( \frac{\partial a^2}{\partial p} \right)_T + \frac{\pi a^2}{2} \cdot \left( \frac{\partial F}{\partial p} \right)_T \right] \frac{dp}{dx} \qquad (2.36)$$

Roybal and Sandler (1972) used this equation to derive a mathematical model for surface diffusion.

A novel statistical mechanical treatment, recently developed by Lee and O'Connell (1972), used a single model to predict both adsorption isotherms and surface diffusion coefficients for partially mobile sorbents on homogeneous surfaces. The model was applied to the data of Ash, Baker and Barrer (1967) and Pope (1967) for the flow of $SO_2$ and $SF_6$ on Graphon. Reasonable agreement was found below $\theta = 1$.

Horiguchi et al (1971) evaluated several models for surface diffusion including hydrodynamic, diffusive and Metzner's model. A Fick's law

diffusive mechanism was found to give the best fit to sub-monolayer experimental data.

## 2.2   THE PHENOMENON OF THERMAL TRANSPIRATION

Following Reynolds discovery of thermal transpiration, Knudsen (1910a) showed that when $\lambda \gg d$, molecular streaming in a temperature gradient gave rise to a pressure gradient in a closed system. From kinetic theory he obtained the molecular collision frequency, per unit area, $Z$, as

$$Z = p/(2\pi mkT)^{\frac{1}{2}} \qquad (2.37)$$

where m is the molecular mass and k is the Boltzmann constant.

When a capillary or porous membrane connects two vessels of different temperatures $T_0$ and $T_\ell$ ($T_0 > T_\ell$), then a state of equilibrium will be set up such that no net flow occurs through the capillary. In this state the collision frequencies on each capillary entrance must be equal (assuming diffuse reflection to occur within the tube) and so:

$$\frac{p_0}{(2\pi mk T_0)^{\frac{1}{2}}} = \frac{p_\ell}{(2\pi mk T_\ell)^{\frac{1}{2}}} \qquad ; \qquad \left(\frac{p_0}{p_\ell}\right)_\infty = \left(\frac{T_0}{T_\ell}\right)^{\frac{1}{2}} \qquad (2.38)$$

Hence a pressure gradient is set up to oppose the flux due to the temperature gradient.

When $\lambda \ll d$, then we are in the viscous flow region and no transpiration will be expected, hence $p_0/p_\ell = 1$. In the intermediate region, $\lambda \sim d$, a smooth transition in $(p_0/p_\ell)_\infty$ will occur between the limits of unity and $(T_0/T_\ell)^{\frac{1}{2}}$. This is illustrated in figure 2.2; it is generally considered that the limits are achieved at $\lambda \geqslant 10d$ and $10\lambda \leqslant d$.
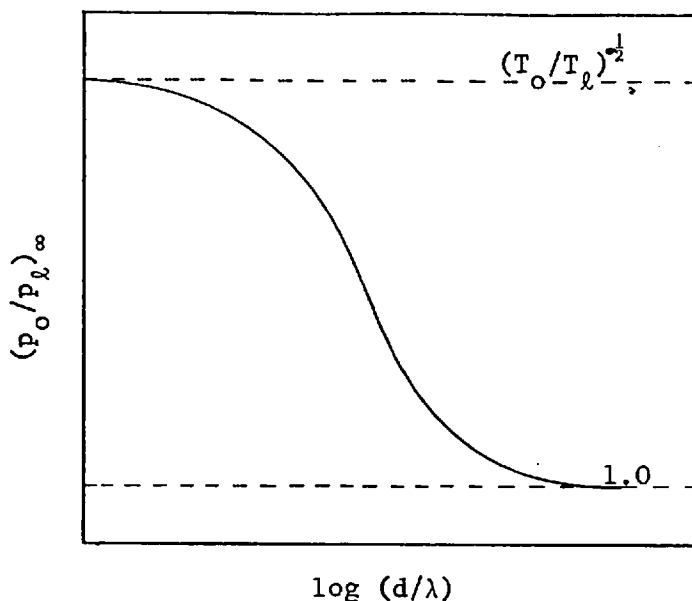
Variation of thermal
transpiration pressure
ratio with d/λ

Figure 2.2

In the transition region, a 'thermal creep' mechanism has been postulated for the thermal transpiration effect (Kennard, 1938, p 330; Williams, 1971). A steady creep of gas occurs along the surface from the cold region to the hot region and an equilibrium is set up with a viscous back flow. Kennard suggested that 'creep' was caused by a preferential back scattering of obliquely impinging molecules, and this was greater for a molecule travelling from a hot to cold region than for one travelling from cold to hot.

Although a $(p_o/p_\ell)_\infty$ value of $(T_o/T_\ell)^{\frac{1}{2}}$ (the Knudsen limit) can be obtained for apertures (Edmonds and Hobson, 1965), a satisfactory explanation of why the Knudsen limit is rarely achieved for capillaries, even though $\lambda \gg d$, has not yet been proposed.

2.2.1 *Thermal transpiration through capillaries*

Several theories and equations have been proposed to describe the behaviour of the pressure ratio in the transition region. The effect of overall gas pressure, temperature difference, capillary diameter, the internal surface of the capillary and the nature of the gas have all been considered. The more important treatments will now be considered.

(i) Weber's equation

A semi-empirical formula was proposed by Weber, Keesom and Schmidt (1936) and investigated by van Itterbeck and de Grande (1947), Los and Fergusson (1952), and Miller (1963). The formula proposed by Weber et al, which they applied to He, Ne and $O_2$, was:-

$$\frac{dp}{dT} = \frac{p}{2T} \cdot \frac{1}{k_1 y^2 + k_2 y + \mu} \qquad (2.39)$$

where $y = d/\lambda$ and $k_1$ ($\simeq \pi/128$), $k_2$ ($\simeq \pi/12$) and $\mu$ are semi-empirical constants which vary with the gas. The equation can be expressed in an integrated form as :

$$(2.40)$$

$$\ln\left(\frac{p_o}{p_\ell}\right)_\infty = \frac{1}{2} \ln\left(\frac{T_o}{T_\ell}\right) + \frac{(1+2n)}{2(1+n)} \left[ B \ln\left(\frac{y_\ell+m}{y_o+m}\right) + C \ln\left(\frac{y_\ell+m'}{y_o+m'}\right) + D \ln\left(\frac{y_\ell+m''}{y_o+m''}\right) \right]$$

Here B, C, D, m, m', m" are constants which could be calculated from the semi-empirical constants $k_1$, $k_2$ and $\mu$. n is obtained from the temperature dependence of gas viscosity $(\eta)$ in $(\eta_o/\eta_\ell) = (T_o/T_\ell)^{\frac{1}{2}+n}$.

Besides being cumbersome to operate since $k_1$, $k_2$ and $\mu$ must be obtained for each gas, both Los and Fergusson and Miller found it necessary to modify the equation to obtain a fit for the transition curve of such simple gas molecules as $H_2$, $N_2$ and Ar. Hence Weber's equation has found very limited application.

(ii) Liang's equation

An empirical formula with only one adjustable parameter was proposed by Liang (1951, 1952), covering the entire pressure regime, from the low pressure limit to continuum flow. This was much simpler to use than Weber's equation, and is generally employed in preference, when thermal transpiration effects have to be estimated eg. in pressure measurements at low temperatures and pressures (Rosenberg, 1956). In its original form Liang's equation used $N_2$ as a standard with which to compare

the transition curve. He subsequently proposed another form (Liang, 1953, 1955) in which helium was used as the standard, since with helium the effect can be more easily observed at higher pressures. The form of this equation was:

$$\left(\frac{P_o}{P_\ell}\right)_\infty = \frac{\alpha_{He}(\phi_g X)^2 + \beta_{He}(\phi_g X) + 1}{\alpha_{He}(\phi_g X)^2 + \beta_{He}(\phi_g X) + R_m} \qquad (2.41)$$

where $R_m = (T_\ell/T_o)^{\frac{1}{2}}$, $X = p_o \cdot d$ and $\phi_g$ is a pressure shifting factor for the gas; for helium $\phi_{He} = 1$. Once $\alpha_{He}$ and $\beta_{He}$, empirical constants, have been determined accurately from helium measurements, then we are left with an equation containing one adjustable parameter, $\phi_g$.

Equation (2.41) can also be written as:

$$\frac{\Delta p}{P_o} = \frac{1 - R_m}{\alpha_{He}(\phi_g X)^2 + \beta_{He}(\phi_g X) + 1} \qquad (2.42)$$

This equation predicts a maximum at $\alpha_{He}(\phi_g X)^2 = 1$ when $\Delta p$ is plotted against $p_o$ and this was investigated by Bennett and Tompkins (1957). They also tried to allow for a temperature dependence of $\phi_g$ (Liang assumed that $\alpha_{He}$, $\beta_{He}$ and $\phi_g$ were independent of temperature), and reported poor agreement with the experimental transition curve at large tube diameters.

(iii) Dusty Gas Theory

This theory, originally proposed as a model for transport phenomena in porous media (section 2.1.2), has recently been applied to thermal transpiration and extended to include capillaries (Mason, Evans and Watson, 1963). When diffuse flow and viscous back flow were considered a differential approximation for capillaries was obtained as:

$$\frac{\Delta p}{P_o} = \frac{\frac{1}{2}(1 - R_m^2)}{[1 + (\pi/12)y][1 + \frac{1}{8}(y)]} \qquad (2.43)$$

This has the same basic form as Weber's and Liang's equations (cf equations (2.42) and (2.43)) and gave a reasonable prediction of experimental transition curves, even at relatively large pressures where viscous back flow is significant. A maximum in $\Delta p/p_o$ is again predicted: the Knudsen limit of $(T_o/T_\ell)^{\frac{1}{2}}$ is assumed.

(iv) Departure from the Knudsen limit

Experimental verification of Liang's equation was carried out by several workers. It was soon reported that the expected Knudsen limit of $(T_o/T_\ell)^{\frac{1}{2}}$ for the thermal transpiration pressure ratio was frequently not achieved, even when $\lambda \gg d$ (Takaishi and Sensui, 1963). Miller (1963) using the Weber equation found similar behaviour. It was observed that $(p_o/p_\ell)_\infty$ was a function of the tube diameter, the closest approach to $(T_o/T_\ell)^{\frac{1}{2}}$ being achieved at low d (Podgurski and Davis, 1961; Hobson et al, 1963; Edmonds and Hobson, 1965). It is interesting to note that Liang (1955) indicated that thermal transpiration can be expected to be a function of the capillary tube since the accommodation coefficient of the surface plays a part in the flow mechanism.

Thus several factors appear to be important in determining the pressure ratio. The influence of the length of the tube and its entrance geometry were considered by Hobson and co-workers, and Siu (1973). Surface roughness and the microscopic nature of the capillary surface has also been investigated (Hobson et al, 1963; Hobson, 1969; Siu, 1973). It became evident that the kinetic theory treatment, which considered gas molecules to be hard spheres which do not interact with the surface, was inadequate.

Treatments by Siu (1973), McCormick and Kuščer (1972) and Cha and McCoy (1972) considered the nature of the molecule-surface collision. Their treatments invoked energy and momentum accommodation coefficients for the surface reflection, and they allowed for deviations from the Maxwell distribution of molecular velocities. It was realised that

molecules travelling from a hot region to a cold one could differ from
molecules travelling in the other direction in regard to their proportion
of specular and diffuse reflections. An equation was developed for the
pressure ratio which could account for the non-Knudsen limit:

$$\left(\frac{p_o}{p_\ell}\right)_\infty = \left(\frac{T_o}{T_\ell}\right)^\gamma \quad ; \quad \gamma = \frac{1}{2} - f(\sigma) \tag{2.44}$$

$\sigma$ is the degree of specular reflection ($0$ for complete diffuse reflection;
1 for complete specular reflection). The form of $f(\sigma)$ varied with the
treatments of Siu, McCormick and Cha. $\gamma$ (and hence $\sigma$) were determined
empirically and varied with the gas.

Another approach (Edmonds and Hobson, 1965; Miller and Buice, 1966)
adopted the transmission probability theory of Clausing (1932), and
produced the simple result:

$$\left(\frac{p_o}{p_\ell}\right)_\infty = \left(\frac{T_o}{T_\ell}\right)^{\frac{1}{2}} \frac{W_\ell}{W_o} \tag{2.45}$$

where $W_o$ is the transmission probability for a molecule travelling from
hot to cold and $W_\ell$ for one travelling from cold to hot. If specular
reflection occurs which is greater for a hot molecule striking a colder
surface than for a cold molecule striking a hotter surface, then $W_o > W_\ell$
and a lower pressure ratio is obtained.

Wu (1968) produced an equation for $(p_o/p_\ell)_\infty$ from general kinetic
theory, but allowed for a deviation of the velocity distribution function
from classical theory. He introduced a geometric factor, I, as a measure
of this deviation.

In Chapter 6 the implication of specular reflections and departure
from classical kinetic theory will be considered in more detail.

2.2.2 *Thermal transpiration through porous media*

When we turn our attention to porous media we find that a physical
definition of a membrane is rather more difficult than for a capillary.

Some of the uncertainties were considered in section 2.1.2. In addition when Knudsen flow in a temperature gradient occurs in porous media an adsorbed film is frequently present which could itself exhibit a temperature gradient flow. The interpretation of the diffuse - specular nature of molecule - wall collisions is also more complicated.

(i) D.G.T. model

Mason, Evans and Watson (1963) extended the Dusty Gas Theory (D.G.T.) for a porous medium to thermal transpiration. They derived an expression (2.46) for the total flux $(J_{tot})$ under thermal transpiration conditions which applied to the entire pressure range and allowed for viscous back-flow close to the high pressure limit.

$$J_{tot} = - \frac{pD_k}{RT} \left[ \left( 1 + \frac{B_o p}{\eta D_k} \right) \frac{d\ln p}{dx} - \left( \frac{\alpha_Q n_d RT}{p + 2\alpha_Q n_d RT} \right) \frac{d\ln T}{dx} \right] \quad (2.46)$$

Here $D_k$ is the Knudsen diffusion coefficient (section 2.1.2), $\eta$ is the gas viscosity, $\alpha_Q$ represents a thermal diffusion factor and $B_o$ is a geometric tortuosity factor (proportional to $\epsilon/k$, where k is the tortuosity). The term involving $B_o p/\eta D_k$ allows for viscous flow. An equation representing the transition curve in the steady-state $(J_{tot} = 0)$ was obtained as

$$\frac{\Delta p}{\bar{p}} = \frac{(1 - R_m^2) \, (\alpha_Q \, n_d \, R\bar{T}) \, (\eta D_k/B_o)}{(\bar{p} + 2\alpha_Q \, n_d R\bar{T}) \, [\bar{p} + (\eta D_k/B_o)]} \quad (2.47)$$

where $\bar{T} = \frac{1}{2} (T_o + T_\ell)$ and $\bar{p} = \frac{1}{2}(p_o + p_\ell)$. This equation predicts a maximum in $\Delta p$ at :

$$(\bar{p})_{max} = [ 2\alpha_Q \, n_d \, R\bar{T} \, (\eta D_k/B_o) ]^{\frac{1}{2}} \quad (2.48)$$

which can be related to the isothermal Knudsen permeability. Mason et al also suggested using equation (2.47) to predict the thermal transpiration curve from permeability measurements, and this approach has

been adopted by Hopfinger and Altman (1969).

In the Knudsen limit the viscous flow component does not occur and so (2.46) becomes:

$$J = - \frac{pD_k}{RT} \left[ \frac{d\ln p}{dx} - \left( \frac{\alpha_Q n_d RT}{p + 2\alpha_Q n_d RT} \right) \frac{d\ln T}{dx} \right] \qquad (2.49)$$

In the steady-state $J = 0$ and the Knudsen limit for $(p_o/p_\ell)_\infty$ of $(T_o/T_\ell)^{\frac{1}{2}}$ can readily be obtained from (2.49).

Another interpretation of a porous medium was given by Lassettre who derived theoretical expressions for the permeability of a porous bed of spherical particles (Lassettre, 1956). He considered that a fixed proportion of diffuse and specular reflections occurred and he extended the treatment to mass and heat transport in a temperature gradient (Lassettre, 1958).

(ii) Experimental evidence.

Until recently the only published data on thermal transpiration through porous media was that of Reynolds (1879) and Knudsen (1910b) who used stuccoplates, meerschaum, and plugs of powdered magnesia and asbestos.

Following Mason's publication in 1963 several workers attempted to verify his equation and commenced investigations of thermal transpiration *and* permeabilities on the same membrane. Hanley (1965) used a porous ceramic while Hopfinger and Altman (1969) used both porous ceramic and Millipore filters - materials of well characterised porosity and tortuosity.

From measurement of isothermal permeability as a function of p, for $H_2$, He, Ne, Kr, $CO_2$ and $SO_2$, Hanley obtained $B_o$ and $D_k$, from which $(\alpha_Q n_d RT)$ could also be deduced knowing the membrane porosity and tortuosity and the gas viscosity. Using equation (2.48) he then predicted the shape of a $\Delta p$ vs $p_o$ (or $\ln\Delta p$ vs $\ln p_o$) curve and compared this with the

experimental curve. He found good agreement between theory and experiment except (a) at low pressures, where he considered that second order temperature effects and pressure gradient contributions become important and (b) for appreciably adsorbed gases. He also found that the geometric factor, $B_o$, varied slightly with the gas.

Hopfinger carried out investigations in the intermediate range, $d/10 < \lambda < 10d$, using $H_2$, He, Ar and $CO_2$, and found that the D.G.T. gave a satisfactory explanation of the transition curve when $\lambda > d/10$. Like Hanley he found that $B_o$ was gas dependent and was a function of $\varepsilon/k^2$ (k = tortuosity) rather than $\varepsilon/k$. Consistent deviations were found in both the low and high pressure limits, the latter being due to significant viscosity effects. The experiments were not sufficiently accurate to distinguish between experimental error and deviations from the Knudsen limit.

Recently Ash et al (1973) have carried out a high precision study of thermo-osmotic transport through carbon membranes, in the Knudsen flow regime ($\lambda > > 10d$). For non-sorbed gases the limiting value of $p_o/p_\ell$ was less than the Knudsen limit, $(T_o/T_\ell)^{\frac{1}{2}}$ and varied with the gas, $(p_o/p_\ell)_\infty$ being in the order Ne < He < $H_2$.

2.2.3 *Surface analogue of thermal transpiration*

Hill (1956) realised that when adsorption occurs within a capillary, then a surface analogue of thermal transpiration can occur. This surface flow in a temperature gradient will augment the gas phase flow, thus causing $p_o/p_\ell$ to exceed the Knudsen limit of $(T_o/T_\ell)^{\frac{1}{2}}$, at low pressures. The flow is a diffusive one caused by a gradient in surface concentration within the membrane.

Using the approach of Sears (1954) Hill derived a steady-state transport equation for $\dot{n}$, the number of moles transported per second in the x direction per unit cross-section.

$$\dot{n} = -2\pi r \, D_{ss} \frac{dc_s'}{dx} - \frac{8}{3} \left( \frac{\pi r^3}{(2\pi \, mk)^{\frac{1}{2}}} \right) \cdot \frac{d \, (p/T^{\frac{1}{2}})}{dx} \qquad (2.50)$$

where $c_s'$ is the surface concentration, r is the tube radius, m is the molecular mass and $D_{ss}$ is a surface diffusion coefficient. The first term represents surface transport and the second gas phase transport. The expression reduces to the Knudsen limit when $\dot{n} = 0$ and there is no surface transport.

It can be seen that the surface flow component depends on $c_s'$ and this is obtained from the adsorption isotherm. Hill considered specific cases of mobile and localised adsorption. Clint (1966) modified Hill's expression and included $D_{ss}$ in the integration w.r.t. x. His equation will be considered further in Chapter 6.

Lassettre and Brooks (1961) used Hill's approach and applied it to surface flow and thermal transpiration in a porous medium. In the steady-state $\dot{n} = 0$, hence either (i) gas and surface fluxes become zero or (ii) they are equal but opposite (countercurrent flow). We have already seen (section 2.1.6) that at low surface concentrations a diffusive, random walk, mechanism exists for surface transport and this leads to separation of gas mixtures. At higher coverages when a hydrodynamic mechanism operates surface flow is non-separative. However if, in this latter case, flow is in a temperature gradient and at low pressures, then Lassettre and Brooks suggested that the flow could still be separative since the adsorbed surface phase would be in equilibrium with the gas phase where separative Knudsen flow would operate. The situation is analogous to distillation under reflux - in this case the countercurrent surface flow is the reflux and separation occurs in the gas phase flow. Repetitive fractionation is now possible. The countercurrent argument has been used more recently by Ash, Barrer, Clint, Dolphin and Murray (1973).

Sandler (1972b) attempted to relate the thermal transpiration

flux ($J_{TT}$) and pressure ratio with the isothermal fluxes for surface

diffusion ($J_s$) and Knudsen gas flow ($J_g$). He used the D.G.T. to obtain

$J_g$ and $J_{TT}$ and assumed that in the Knudsen flow regime the total flux

$J_{tot}$ was the sum of $J_s$, $J_g$ and $J_{TT}$. When the steady-state pressure ratio

was achieved then $J_{tot}$ = 0 and he deduced the relationship.

$$\left( \frac{p_o}{p_\ell} \right)_\infty = \left( \frac{T_o}{T_\ell} \right)^R \quad \text{where} \quad R = \frac{\alpha_L}{1 + (J_s/J_g)}$$

$\alpha_L$ is an empirical constant having the value of $\frac{1}{2}$ in the Knudsen limit.

If $\Delta T (= T_o - T_\ell)$ is not very large then $J_s$ and $J_g$ can be considered to

be constant.

The limitations of this approach are that (i) it assumes the ideal

Knudsen limit, $\alpha_L = \frac{1}{2}$; and (ii) although allowing for flow of a condensed

film in isothermal surface diffusion, it takes no account of surface flow

in a temperature gradient which will be significant if $J_s \neq 0$. The form

of R predicts that in the presence of adsorption a reduced thermal

transpiration ratio will be obtained because of the pressure gradient

causing a surface back flow. In fact recent work with strongly sorbed

gases on carbon membranes (Ash et al 1973) has shown that $(p_o/p_\ell)_\infty$ is

actually increased.

Gilliland et al (1962) used a hydrodynamic approach. He considered

that for dilute films the driving force for surface flow in a temperature

gradient was a function of the gradient in :

$$\phi / T^{\frac{1}{2}} \exp(E_{ss}/RT)$$

A surface flow rate, $J_s$, was obtained as:

$$\frac{J_s}{A_c} = - \frac{\rho_{app} \cdot A_g}{k^2 \cdot C_R} \frac{(c'_s)^2}{T} \left[ \Delta H + \frac{\phi}{2c'_s} \left( \frac{2 E_{ss}}{RT} - 1 \right) \right] \frac{dT}{dx} \quad (2.51)$$

where $\bar{T}$ is the mean temperature, $E_{ss}$ is an activation energy for surface flow and $\Delta H$ is the enthalpy of adsorption. Other parameters are defined in section 2.1.6.

Since $\Delta H < 0$ and $E_{ss} > 0$, then this equation predicts that surface flow can be from 0 to $\ell$ or vice - versa, depending on the relative magnitudes of $\Delta H$ and $\phi \quad \left( \dfrac{2 E_{ss}}{RT} - 1 \right)$.
$\overline{2c}_s'$

Wright (1971) treated surface thermal transpiration by considering the stochastic theory of Brownian motion in a temperature gradient. He deduced expressions for the surface flux in terms of gradients in (i) surface concentration, $c_s'$; (ii) temperature and (iii) spreading pressure , $\phi$. The interrelation between $c_s'$, $\phi$ and $p_{eq}$, the gas phase pressure in local equilibrium with the surface, was:

$$\frac{\partial \phi}{\partial x} = - c_s' \cdot \frac{Q}{T} \cdot \frac{\partial T}{\partial x} + RT \cdot \frac{c_s'}{p_{eq}} \cdot \frac{\partial p_{eq}}{\partial x}$$

where Q is an equilibrium heat of adsorption.

Experimental evidence for surface thermal transpiration has been provided by Hanley (1965), who obtained some curious results for strongly sorbed gases. Hopfinger and Altman (1969) also obtained anomalous thermal transpiration results which could have been due to surface flow. However they worked in the intermediate (slip flow) pressure region and viscous back flow could occur.

Ash et al (1973) on the other hand, working in the Knudsen regime have found pronounced enhancement of $(p_0/p_\ell)_\infty$ for strongly sorbed gases, the degree of enhancement increasing with the degree of adsorption.

2.3. THERMO-OSMOSIS

Thermo-osmosis is the mass transport of a fluid through a diaphragm under the influence of a temperature gradient. It is closely associated

with thermal transpiration (section 2.2) but can occur outside the Knudsen flow regime and is exhibited by liquids as well as by gases on both porous and non-porous membranes. In this section we are concerned with the thermodynamics of the process, heats of transport associated with thermo-osmotic flow and the relationship with isothermal and isobaric permeabilities.

### 2.3.1 *Theoretical treatment*

The approach used here is based on non-equilibrium thermodynamics (Denbigh, 1951) and makes use of the Onsager reciprocal relationship (Onsager, 1931); it has been presented more fully by Ash and Barrer (1963) and Ash, Barrer, Clint, Dolphin and Murray (1973). Similar treatments have been used by Denbigh and Raumann (1952a) and Bearman (1957) for solubility and flow through a rubber membrane, by Hanley and Steele (1965) for gas flow through a bundle of steel capillaries, and by Siu (1973) for flow through a single capillary.

If we denote mass flow by subscript 1 and heat flow by subscript 2, then for the total mass and heat fluxes ($J_1$ and $J_2$) through a membrane per unit cross-section we can write:

$$J_1 = J_1^s + J_1^g \qquad (2.52)$$

$$J_2 = J_2^s + J_2^g + J_2^i \qquad (2.53)$$

Here $J_1^s$ denotes the extra mass transport caused by the presence of an adsorbed phase and $J_1^g$ is the gas phase mass transport which would occur in the absence of adsorption. $J_2^s$, $J_2^g$ and $J_2^i$ are heat transport due to extra flow, gas phase flow and heat flow through the particles ($J_1^i$ does not occur as the membrane constituent particles are considered to be non-porous).

We can now invoke non-equilibrium thermodynamics and write:

$$J_1 = (L_{11}{}^S X_1 + L_{12}{}^S X_2) + (L_{11}{}^g X_1 + L_{12}{}^g X_2) \qquad (2.54)$$

$$J_2 = (L_{22}{}^S X_2 + L_{21}{}^S X_1) + (L_{22}{}^g X_2 + L_{21}{}^g X_1) + L_{22}{}^i X_2 \qquad (2.55)$$

The fluxes are assumed to be linear functions of the driving forces $X_1$ and $X_2$, and the L's are proportionality coefficients. $L_{12}$ is a cross-coefficient which allows for a coupling effect of the heat driving force on the mass flow ($L_{21}$ refers to mass driving force on heat flow). Expressions for the driving forces are:

$$X_1 = - T \text{ grad } (\mu/T) \quad ; \quad X_2 = - \frac{1}{T} \text{ grad } T \qquad (2.56)$$

which for flow in one dimension become :

$$X_1 = - T \frac{\partial(\mu/T)}{\partial x} \quad ; \quad X_2 = - \frac{1}{T} \frac{\partial T}{\partial x} \qquad (2.57)$$

The Onsager reciprocal relationship is expressed by :

$$L_{12}{}^S = L_{21}{}^S \quad \text{and} \quad L_{12}{}^g = L_{21}{}^g \qquad (2.58)$$

Several special cases will now be considered which simplify considerably equations (2.54) and (2.55).

(i)  isothermal transport,  $X_2 = 0$ and $J_2 = 0$

$$J_1{}^{iso} = L_{11}{}^S X_1 + L_{11}{}^g X_1$$

$$= - (L_{11}{}^S + L_{11}{}^g) \frac{\partial \mu}{\partial x} \qquad (2.59)$$

(ii) No net flow of heat,  $X_2 = 0$  but  $J_2 \neq 0$

$$\left( \frac{J_2}{J_1} \right)_{X_2 = 0} = \frac{L_{21}{}^S + L_{21}{}^g}{L_{11}{}^S + L_{11}{}^g}$$

$$= \frac{L_{12}{}^s + L_{12}{}^g}{L_{11}{}^s + L_{11}{}^g} \quad . \tag{2.60}$$

This ratio represents the energy transported per mole of gas when there is no net flow of heat.

(iii) Thermo-osmotic steady-state. In this condition there is no net flow of mass through any cross-section within the membrane i.e. $J_1 = 0$. From equation (2.54),using (2.57) we get

$$\frac{\partial(\mu/T)}{\partial x} = -\left(\frac{L_{12}{}^s + L_{12}{}^g}{L_{11}{}^s + L_{11}{}^g}\right) \frac{\partial T}{\partial x} . \frac{1}{T^2} \tag{2.61}$$

Integrating from $x = 0$ to $\ell$ :

$$\left(\frac{\mu}{T}\right)_\ell - \left(\frac{\mu}{T}\right)_o = - \int_{T_o}^{T_\ell} \left(\frac{L_{12}{}^s + L_{12}{}^g}{L_{11}{}^s + L_{11}{}^g}\right) . \frac{\partial T}{T^2} \tag{2.62}$$

From classical thermodynamics we have the relationships :

$$\mu = \mu^\ominus + RT \ln a = \mu^\ominus + RT \ln p \tag{2.63}$$

$$H^\ominus_g = - T^2 \frac{\partial}{\partial T} \left(\frac{\mu^\ominus}{T}\right) \tag{2.64}$$

where 'a' is the activity, $\mu^\ominus$ is the standard chemical potential and $H^\ominus_g$ is the standard gas enthalpy. By differentiation of (2.63) we obtain :

$$\frac{\partial(\mu/T)}{\partial T} = \frac{\partial(\mu^\ominus/T)}{\partial T} + R \frac{\partial \ln p}{\partial T} \tag{2.65}$$

Substituting from (2.64) and integrating from $x = 0$ to $\ell$ gives

$$\left(\frac{\mu}{T}\right)_\ell - \left(\frac{\mu}{T}\right)_o = - \int_{T_o}^{T_\ell} \frac{H^\ominus_g}{T^2} . dT + \int_{P_o}^{P_\ell} R d \ln p \tag{2.66}$$

Equation (2.62) can now be written as

$$-\int_{T_o}^{T_\ell} \frac{H_g^\ominus}{T^2} \cdot dT \quad - \quad R \ln \left( \frac{p_o}{p_\ell} \right)_\infty \quad = \quad -\int_{T_o}^{T_\ell} \left( \frac{L_{12}^s + L_{12}^g}{L_{11}^s + L_{11}^g} \right) \frac{dT}{T^2} \qquad (2.67)$$

which can be rearranged to give

$$R \ln \left( \frac{p_o}{p_\ell} \right)_\infty \quad = \quad \int_{T_o}^{T_\ell} \left( \frac{L_{12}^s + L_{12}^g}{L_{11}^s + L_{11}^g} - H_g^\ominus \right) \frac{dT}{T^2} \qquad (2.68)$$

We now define a heat of transport, $Q_o$ $(= Q_o(T_o))$, as

$$Q_o \quad = \quad \frac{L_{12}^s + L_{12}^g}{L_{11}^s + L_{11}^g} - H_g^\ominus \qquad (2.69)$$

It can be seen from relation (2.60) that $Q_o$ is the amount by which the total energy transported per mole when there is no net flow of heat exceeds the standard enthalpy of the gas.

By differentiating (2.68) w.r.t. $T_o$ at constant $T_\ell$ and substituting $Q_o$ under the integral we obtain:

$$\frac{\partial}{\partial T_o} \left[ R \ln \left( \frac{p_o}{p_\ell} \right)_\infty \right]_{T_\ell} \quad = \quad - \frac{Q_o}{T_o^2} \qquad (2.70)$$

which can be rearranged to give

$$Q_o \quad = \quad R \frac{\partial}{\partial (1/T_o)} \left[ \ln \left( \frac{p_o}{p_\ell} \right)_\infty \right]_{T_\ell} \qquad (2.71)$$

Thus $Q_o$ can be obtained as a function of $T_o$ from plots of $\ln(p_o/p_\ell)_\infty$ versus $1/T_o$. It has been found (Ash et al 1973) that through microporous carbon membranes $Q_o$ was always negative and its magnitude decreased with increasing $T_o$.

If the heat of transport is assumed to be independent of temperature, then we can obtain a mean integral heat, $Q_m$, from (2.68):

$$R \ln \left( \frac{P_o}{P_\ell} \right)_\infty = - Q_m \left[ \frac{1}{T_\ell} - \frac{1}{T_o} \right] = - Q_m \frac{\Delta T}{T_o T_\ell} \qquad (2.72)$$

where $\Delta T = T_o - T_\ell$

For an ideal Knudsen gas which is non-sorbed, only gas phase flow

occurs and so equation (2.69) reduces to

$$Q_o = \frac{L_{12}^g}{L_{11}^g} - H_g^\ominus \qquad (2.73)$$

Kinetic theory predicts that $Q_o = -\frac{1}{2} RT_o$ (Kennard, 1938), however

deviations from this ideal value have been found. Clint (1966) and Ash

et al (1973), on the basis of experimental observations, proposed that

$$Q_o = - \beta . \frac{RT}{2} \qquad (2.74)$$

The factor $\beta$ probably arises from limitations of the kinetic theory

treatment which neglects interaction of gas molecules with the attractive

potential of the pore walls (Sandler, 1972b).

Experimental measurements of thermo-osmosis have been confined

to a small number of membrane systems. Denbigh and Raumann (1952b) studied

the flow of $H_2$, $N_2$, $CO_2$ and $H_2O$ vapour through a natural rubber membrane

whilst Bearman and Bearman (1966) used butyl- and gum-rubber membranes with

inert gases. In these systems transport by solution in the membrane was

possible and $Q_o$, calculated from (2.72) and assumed to be independent of

T, was quite different from the ideal gas value, and could be positive

(He, Ne, $H_2$) or negative (more strongly sorbed gases).

Hanley and Steele (1965) measured the flow of He, Ne and Ar through

a bundle of stainless steel tubes over a wide range of pressures. After

correction for temperature and pressure dependence, limiting values of

$-Q_o$ were obtained which were less than $\frac{1}{2} RT_o$. Argon most closely

approached this ideal value but He and Ne gave significantly smaller

values of $Q_o$. As $d/\lambda$ increased and the-slip flow region was entered, then $Q_o$ decreased. Hanley (1966) found similar behaviour for the flow of He, Ne, Kr, $CO_2$ and $SO_2$ through a porous ceramic membrane.

Rastogi, Singh and co-workers studied thermo-osmosis through porous unglazed porcelain as a function of pressure and temperature, up to $\Delta T = 130K$. They worked with $N_2$, $O_2$, $CO_2$, $H_2S$ and $C_2H_4$ in the intermediate pressure regime. At high pressures $Q_m$ tended to zero, but even at the lowest pressures used the ideal value of $-\frac{1}{2}RT_o$ was not achieved (Rastogi, Singh and Singh, 1969; Singh, 1971). Thermo-osmosis of binary, ternary and quaternary gas mixtures have also been studied (Rastogi and Rai, 1974; Rastogi, Rai and Yadava, 1974) but again the measurements were outside the Knudsen regime. They did, however, show that:

$$Q_m = \sum c_i \cdot [Q_m]_i \qquad (2.75)$$

where $Q_m$ and $[Q_m]_i$ are mean heats of transport for the mixture and the pure component i. $c_i$ is the mass fraction of component i.

Thermo-osmosis in the Knudsen regime has been studied by Ash et al (1973) for $H_2$, He, Ne, Ar and Kr, through carbon membranes of Carbolac and Graphon, and also for $D_2$, Xe and $N_2$ through Graphon and $CO_2$, $CH_4$, and $C_3H_8$ through Carbolac. $T_\ell$ was held at a constant value and $T_o$ varied between 320.65 and 393.15K. For $H_2$, $D_2$, He and Ne, $-Q_o$ was always below the value for a Knudsen gas and increased with increasing $T_o$. When stronger adsorption occurred, especially on Carbolac, $-Q_o$ could be much greater than $\frac{1}{2}RT_o$ and decreased sharply with increasing $T_o$.

2.3.2 *Relationship with isothermal permeability*

(i) Theoretical

The Fick equation can be expressed in several ways thus:

$$J = -D \cdot \frac{dc}{dx} \quad ; \quad J = -L_{11} \frac{d\mu}{dx} \qquad (2.76)$$

It should therefore be possible to relate the phenomenological coefficients to diffusion coefficients. Using equation (2.63) we can write (2.76) as:

$$J = - L_{11} RT \frac{d\ln a}{dc} \cdot \frac{dc}{dx} \qquad (2.77)$$

and hence we can make the identification:

$$D = L_{11} \cdot RT \cdot \frac{d\ln a}{dc} \qquad (2.78)$$

If 'a' is proportional to c, then (2.78) becomes

$$D = L_{11} RT \frac{d\ln c}{dc} = L_{11} \cdot \frac{RT}{c} = \ell_{11} RT \qquad (2.79)$$

Here we have defined a mobility coefficient, $\ell_{11}$ as $L_{11}/c$. Similar relationships can be obtained when we consider gas and surface flow (Ash et al, 1973):

$$c_g \ell_{11}^g = L_{11}^g \; ; \; c_g \ell_{12}^g = L_{12}^g \; ; \; c_s \ell_{11}^s = L_{11}^s \; ; \; c_s \ell_{12}^s = L_{12}^s \qquad (2.80)$$

$Q_o$ can be expressed as (from (2.69)):

$$Q_o = \frac{1}{(L_{11}^s + L_{11}^g)} \left[ \left( \frac{L_{12}^s}{L_{11}^s} - H_g^\ominus \right) \cdot L_{11}^s + \left( \frac{L_{12}^g}{L_{11}^g} - H_g^\ominus \right) \cdot L_{11}^g \right] \qquad (2.81)$$

Making use of (2.80) allows (2.81) to be written as:

$$Q_o = \left( \frac{\ell_{12}^s}{\ell_{11}^s} - H_g^\ominus \right) \cdot \frac{c_s \ell_{11}^s}{c_s \ell_{11}^s + c_g \ell_{11}^g} + \left( \frac{\ell_{12}^g}{\ell_{11}^g} - H_g^\ominus \right) \cdot \frac{c_g \ell_{11}^g}{c_s \ell_{11}^s + c_g \ell_{11}^g} \qquad (2.82)$$

Heats of transport pertaining to surface and gas phase flow can be identified as:

$$Q_s = \left( \frac{\ell_{12}^s}{\ell_{11}^s} - H_g^\ominus \right) \quad ; \quad Q_g = \left( \frac{\ell_{12}^g}{\ell_{11}^g} - H_g^\ominus \right) \qquad (2.83)$$

If we define the quotients $\ell_{12}^g/\ell_{11}^g$ and $\ell_{12}^s/\ell_{11}^s$ as $Q*_g$ and $Q*_s$, isothermal heats of transport for gas phase, and 'extra' flow respectively (cf. equation (2.60)) then we can write:

$$Q_g = Q*_g - H_g^{\ominus} \quad ; \quad Q_s = Q*_s - H_g^{\ominus}$$

For an ideal monatomic gas $H_g^{\ominus} = 5/2 RT_o$ hence $Q*_g = 2RT_o$ and for an ideal diatomic gas $H_g^{\ominus} = 7/2 \; RT_o$ and so $Q*_g = 3RT_o$. Interpretation of these heats is given by Ash et al, 1973.

The remaining factors in (2.82) can be related to isothermal permeability measurements and this will now be shown.

From equations (2.10) and (2.11) we can write:

$$J = K_s \cdot \frac{\Delta c_g'}{\ell} + K_g \cdot \frac{\Delta c_g'}{\ell} \tag{2.84}$$

where $J$ is now the flux per unit cross-sectional area. Using (2.13) and (2.15) this can be written as

$$J = -D_{ss} \cdot \frac{dc_s}{dx} - D_{gs} \cdot \frac{dc_g}{dx} \tag{2.85}$$

where $c_s$ is the Gibbs excess concentration per unit volume of porous medium and $c_g$ is the gas phase concentration per unit volume of porous medium (see Appendix A for inter-relation of $c_s$, $c_s'$, $c_g$ and $c_g'$).

The equivalent Fickian expressions to (2.85) in terms of phenomenological and mobility coefficients are:

$$J = -L_{11}^s \cdot \frac{d\mu}{dx} - L_{11}^g \cdot \frac{d\mu}{dx} \tag{2.86}$$

$$= -c_s \ell_{11}^s \frac{d\mu}{dx} - c_g \ell_{11}^g \cdot \frac{d\mu}{dx} \tag{2.87}$$

If $K_s$ and $K_g$ are assumed independent of concentration, then gas phase components of (2.84) and (2.87) can be equated:

$$K_g \cdot \frac{\Delta c_g'}{\ell} = - c_g \, \ell_{11}^g \cdot \frac{d\mu}{dx} \tag{2.88}$$

and using (2.63) for $\mu$ with $p = c_g' \, RT$ and putting $c_g = \varepsilon \, c_g'$,

$\Delta c_g'/\ell = - dc_g'/dx$, gives:-

$$K_g = \varepsilon \ell_{11}^g \, RT \tag{2.89}$$

Similarly by equating 'extra' flow components we can obtain

$$K_s = \varepsilon RT \cdot \frac{c_s}{c_g} \cdot \ell_{11}^s \tag{2.90}$$

and so $K$ can be expressed as:

$$K = \varepsilon \, RT \left[ \ell_{11}^g + \frac{c_s \cdot \ell_{11}^s}{c_g} \right] \tag{2.91}$$

Thus using relations (2.83) and (2.91), equation (2.82) can be written as:-

$$Q_o = Q_s \cdot \frac{K_s}{K} + Q_g \frac{K_g}{K} \tag{2.92}$$

A similar comparison of equations (2.85) and (2.87) yields:

$$D_{gs} = RT \, \ell_{11}^g \tag{2.93}$$

$$D_{ss} = RT \, \ell_{11}^s \cdot \frac{d \ln c_g}{d \ln c_s} \tag{2.94}$$

We have shown therefore that isothermal permeabilities may be related to thermo-osmotic heats of transport. The above relationships were investigated experimentally by Ash et al (1973) where from $Q_o$ and permeability data $Q_g$ and $Q_s$ were derived, the latter assuming upper and lower limits to $Q_g$. $Q^*_g$ and $Q^*_s$ were also derived, as well as values for $\ell_{11}^g$, $\ell_{12}^g$, $\ell_{11}^s$ and $\ell_{12}^s$. It was shown that $Q_s$ is always negative and $Q^*_s$ positive.

### 2.3.3 *Relationship with isobaric permeability*

The effectiveness of thermo-osmotic flow can be measured by an isobaric permeability. When thermo-osmosis occurs in an open system, flow takes place through the membrane unchecked by the build-up of a pressure difference which occurs in a closed system. Under such circumstances the pressures at $x = 0$ and $x = \ell$ will be the same and there will be a constant flux throughout the length of the membrane. Since there is a temperature gradient within the membrane, then the surface or gas phase flux will vary slightly with x, and so to keep the flux constant then a pressure profile must exist within the membrane.

Experimentally isobaric flow is observed by having a closed system but with a horizontal mercury slug forming a barrier between the reservoirs at $T_o$ and $T_\ell$. The slug will move under a minute pressure gradient thus maintaining substantially equal pressures at $T_o$ and $T_\ell$ (Gilliland et al, 1962). Alternatively we can arrange to have large volumes at $T_o$ and $T_\ell$, and use a sensitive differential pressure transducer to measure $\Delta p (=p_o - p_\ell)$; since $\Delta p$ is small then $p_o \simeq p_\ell$. The only reported measurements of isobaric fluxes are due to Gilliland et al (1962) who measured the isobaric flow of ethylene and propylene through a Vycor membrane.

A quantity, $B(T_o)$, can be defined as the energy transported at $T_o$ by isobaric flow through unit membrane cross-section in unit time and under unit temperature gradient,

ie
$$B(T_o) = RT_o \cdot {}^J\!B(T_o) \cdot \frac{\ell}{\Delta T} \tag{2.95}$$

where ${}^J\!B(T_o)$ is the isobaric flux (mol s$^{-1}$) per unit cross-section and $\Delta T = T_o - T_\ell$. The isobaric permeability is then defined as $B(T_o)/p_o$ (and under isobaric conditions $p_o = p_\ell$):

$$\frac{B(T_o)}{p_o} = \frac{RT_o}{p_o} \cdot \frac{{}^J\!B(T_o) \cdot \ell}{\Delta T} \tag{2.96}$$

This expression can be compared with the isothermal permeability (equation (2.10)) which can be written as:

$$K(T_o) = J_I(T_o) \cdot \frac{\ell}{\Delta c_g'} = RT_o \cdot \frac{J_I(T_o) \cdot \ell}{\Delta p'} \qquad (2.97)$$

where $J_I(T_o)$ is the isothermal flux per unit area at a temperature of $T_o$ and $\Delta p'$ is the pressure difference across the membrane in the isothermal experiment.

A relationship between the thermo-osmotic steady-state pressure ratio, $(p_o/p_\ell)_\infty$, and the isobaric permeability can also be derived.

From equations (2.54), (2.57) and (2.80) we can write

$$J_1 = -(c_s \ell_{11}^s + c_g \ell_{11}^g) T \cdot \frac{\partial(\mu/T)}{\partial x} - (c_s \ell_{12}^s + c_g \ell_{12}^g) \cdot \frac{1}{T} \cdot \frac{\partial T}{\partial x} \qquad (2.98)$$

$$= -\frac{(c_s \ell_{11}^s + c_g \ell_{11}^g)}{T} \left[ T^2 \cdot \frac{\partial(\mu/T)}{\partial T} + \frac{(c_s \ell_{12}^s + c_g \ell_{12}^g)}{(c_s \ell_{11}^s + c_g \ell_{11}^g)} \right] \frac{\partial T}{\partial x} \qquad (2.99)$$

Making use of relations (2.91), (2.64) and (2.65) and (2.69) and (2.80) we can express (2.99) as:-

$$J_1 = -\frac{K c_g'}{RT^2} \left[ RT^2 \frac{\partial \ln p}{\partial T} + Q_o \right] \frac{\partial T}{\partial x} \qquad (2.100)$$

Putting $p = c_g' RT$ we get:

$$J_1 = -\frac{K}{RT} \left[ \frac{\partial p}{\partial T} + \frac{p Q_o}{RT^2} \right] \frac{\partial T}{\partial x} \qquad (2.101)$$

which, after manipulation, becomes (for fixed $T_\ell$):

$$J_1 = -\left[\frac{K}{RT} \cdot \exp\left(-\int_{T_\ell}^{T} \frac{Q_o}{RT^2} dT\right)\right] \frac{d}{dx}\left[p \cdot \exp\left(\int_{T_\ell}^{T} \frac{Q_o}{RT^2} \cdot dT\right)\right] \quad (2.102)$$

For constant $J$ (we now omit subscript 1), we can integrate from 0 to $\ell$ and from x to $\ell$ to give the equations:

$$J = \frac{p_o \exp\left(\int_{T_\ell}^{T_o} \frac{Q_o}{RT^2} \cdot dT\right) - p_\ell}{\int_{o}^{\ell}\left[\frac{RT}{K} \cdot \exp\left(\int_{T_\ell}^{T} \frac{Q_o}{RT^2} dT\right)\right] dx} \quad (2.103)$$

$$\text{and } J = \frac{p(x) \cdot \exp\left(\int_{T_\ell}^{T} \frac{Q_o}{RT^2} dT\right) - p_\ell}{\int_{x}^{\ell}\left[\frac{RT}{K} \exp\left(\int_{T_\ell}^{T} \frac{Q_o}{RT^2} \cdot dT\right)\right] dx} \quad (2.104)$$

Therefore substituting $J$ from (2.103) for $J_B(T_o)$ in equation 2.96 and putting $\ell/\Delta T = - dx/dT$ we get:-

$$\frac{B(T_o)}{p_o} = - \frac{T_o\left[\exp\left(\int_{T_\ell}^{T_o} \frac{Q_o}{RT^2} \cdot dT\right) - \left(\frac{p_\ell}{p_o}\right)\right]}{\int_{T_o}^{T_\ell}\left[\frac{T}{K} \exp\left(\int_{T_\ell}^{T} \frac{Q_o}{RT^2} \cdot dT\right)\right] dT} \quad (2.105)$$

Under isobaric conditions $p_o = p_\ell$ and the thermo-osmotic steady-state quantities can be found from equations (2.68) and (2.69):

$$\exp\int_{T_\ell}^{T_o} \frac{Q_o}{RT^2} \cdot dT = \left(\frac{p_\ell}{p_o}\right)_\infty \quad ; \quad \exp\int_{T_\ell}^{T} \frac{Q_o}{RT^2} \cdot dT = \left(\frac{p_\ell}{p(x)}\right)_\infty \quad (2.106)$$

Therefore,

$$-\frac{B(T_o)}{P_o} = \frac{T_o \left[ 1 - (p_\ell/P_o)_\infty \right]}{\displaystyle\int_{T_\ell}^{T_o} \left[ \frac{T}{K}\left(\frac{p_\ell}{p(x)}\right)_\infty \right] dT} \qquad (2.107)$$

This treatment was derived by Ash et al (1973). There it was also shown from experimental data that the isobaric permeability was often more effective than the isothermal permeability in producing differences in ratios of flow rates between each of two gases through the same membrane. However, with real binary mixtures cross-coefficients are likely to be important ie the presence of a second gas will affect the flow of the first gas. For sorbed gases $-B(T_o)/p_o$ was found to decrease with increasing temperature, but for non-sorbed gases (He, Ne and $H_2$) a slight increase was found.

A study of isobaric and isothermal permeabilities has also been made by Gilliland, Baddour and Engel (1962). They used the Knudsen permeability for $K$ $(T_o)$ at a temperature of $T_o$, and an expression due to Kennard (1938, p330) for $B(\bar{T})/p_o$ (valid for small $\Delta T$), where $\bar{T}$ is the mean temperature of the membrane:

$$\frac{B(\bar{T})}{P_o} = \frac{4}{3} \cdot \frac{\varepsilon}{A} \cdot \left(\frac{2R}{\pi M \bar{T}}\right)^{\frac{1}{2}} \qquad (2.108)$$

It then followed that:

$$\frac{B(\bar{T})}{P_o} = \frac{K(T_o)}{2(\bar{T}\,T_o)^{\frac{1}{2}}} \qquad (2.109)$$

However this expression neglects any surface contribution to both the isothermal and isobaric flows. Gilliland then considered surface flow, caused by a gradient in spreading pressure and derived expressions for the surface flow rate under a pressure gradient at constant temperature (isothermal) and under a temperature gradient at constant pressure (isobaric). A surface isobaric permeability, $B_s(T_o)/p_o$, was then derived

using equation (2.51) and (2.95), and this could be obtained entirely

from adsorption isotherms and isothermal permeabilities. The equation

predicted a maximum in $B_s(T_o)/p_o$ as a function of pressure, and

experimental measurements with $C_2H_4$ and $C_3H_6$ at several temperature

gradients and pressures suggested that this was the case.

The pressure distribution within the membrane may also be derived.

In the steady-state we can equate the fluxes in equations (2.103)

and (2.104), then making the substitutions from (2.106) with a linear

temperature gradient, $dT/dx$, and with $p_o = p_\ell$ for isobaric transport, we

obtain:-

$$\frac{\left(\dfrac{p_\ell}{p_o}\right)_\infty - 1}{\displaystyle\int_{T_\ell}^{T_o}\left[\frac{T}{K}\left(\frac{p_\ell}{p(x)}\right)_\infty\right]dT} = \frac{\left(\dfrac{p(x)}{p_\ell}\right)\cdot\left(\dfrac{p_\ell}{p(x)}\right)_\infty - 1}{\displaystyle\int_{T_\ell}^{T}\left[\frac{T}{K}\left(\frac{p_\ell}{p(x)}\right)_\infty\right]dT} \qquad (2.110)$$

Here $(p_\ell/p_o)_\infty$ can be determined from steady-state thermo-osmotic measurements

and the integrals can be evaluated graphically knowing $T$, $K$ and $(p_\ell/p(x))_\infty$

for several values of x at fixed $T_\ell$.

The profiles of $p(x)/p_\ell$ versus $x/\ell$ obtained by Ash et al (1973) are

almost parabolic with a maximum close to $x/\ell = 0.5$. The value of $p(x)$

at the maximum differred from $p_\ell$ by about 5% for a $\Delta T$ of 85K for strongly

sorbed gases ($CO_2$, Xe) and by less than 1% for Ar, $H_2$.

Kennard (1938, p330) derived an equation predicting a pressure

maximum to occur at around the plug centre. Gilliland et al (1962)

using this equation found a pressure maximum which exceeded the external

pressure $p_\ell$, by 0.5% for non-sorbed gases and by less than 1.5% for

sorbed gases.

It is interesting to note that Hill (1956) derived a pressure gradient

for the thermo-osmotic steady-state which departed from linearity. He

plotted $[(p_o-p)/x - (p_o-p_\ell)/\ell]$ as a function of $x/\ell$ (with $p_o/p_\ell = 2$) and

and predicted a maximum to occur close to $x/\ell = 0.5$.

CHAPTER 3

EXPERIMENTAL TECHNIQUE

## 3.1   MATERIALS USED

### 3.1.1 *Carbon*

The membranes used in this study have been constructed from

Graphon, a graphitised carbon black supplied by the Cabot Corporation,

Massachusetts, U.S.A.   The carbon is formed initially by burning

natural gas in an oxygen deficient atmosphere adjacent to a system of

steel channels in which the carbon is deposited.

This 'channel black' so produced (designated Spheron 6) is then

heated in an induction furnace in the absence of air to 2700-3200°C.

This has the effect of burning off any chemisorbed oxygen and residual

hydrogen and partially ordering the carbon crystallites into

approximately spherical capsules.   A uniform carbon surface with a

high degree of homogeneity is produced.   The preparation is described

in more detail by Schaeffer, Smith and Polley, 1953.

X-ray studies (Biscoe and Warren, 1942;   Houska and Warren, 1954)

and electron microscopy (Hall, 1948) have been used to investigate the

microscopic nature of carbon blacks, and the process of graphitisation.

Spheron 6 consists of crystallites of approximate dimension 1.3 nm by

2.0 nm by 2.0 nm.   These parallel layer groups have a graphite-type

structure with parallel, equidistant layers.   The layers are randomly

oriented around the layer normal and the layer separation is slightly

larger than in graphite.   Individual particles of Spheron 6 are about

30 nm in diameter and consist of clusters of parallel layer groups.

On heating to about 900°C the layers in the crystallites begin to grow.

If heating is continued to 3000°C the layers become sufficiently mobile

that they can rotate with respect to one another and thus take up the

true graphite structure, but with ABC... as well as ABA... layer

sequences. This rearrangement and partial ordering, known as graphitisation, is accompanied by a sharp change in the X-ray diffraction pattern from the broad, inextensive pattern in Spheron 6 to the true graphite pattern which occurs in Graphon.

The principal characteristics for several samples of Graphon are summarised in table 3.1. Graphon was chosen for this work (Ash, Baker & Barrer, 1967) because of its energetic homogeneity, its uniform and non-porous surface, large surface area and high surface fluxes.

TABLE 3.1

*Physical characteristics for 2 batches of Graphon*

| Property | Units | S6-D4 | S6-D5 |
|----------|-------|-------|-------|
| Area, $N_2$ B.E.T. | $m^2 g^{-1}$ | 89.7 | 87.4 |
| Helium density | $g\ cm^{-3}$ | 1.97 | 1.97 |
| Crystallite height | nm | 4.3 | 5.6 |
| Crystallite width | nm | 8.7 | 7.6 |
| Ash | % | 0.08 | 0.08 |
| Volatiles | % | 0.06 | 0.13 |
| pH | – | 10.6 | 10.3 |

3.1.2 *Gases*

The hydrocarbons ($CH_4, C_2H_6, C_3H_8, n-C_4H_{10}$ and $neo-C_5H_{12}$) were 99.9% pure and supplied in $500cm^3$ glass bulbs by the National Physical Laboratory, Teddington. All other gases ($H_2, N_2$, He, Ne, Kr and Xe) were B.O.C. Grade X gases, of purity $> 99.99\%$, supplied in one-litre bulbs filled to atmospheric pressure and sealed with fragile glass septa. The gases were used without further purification.

3.1.3 *Membrane construction*

For thermo-osmotic transport to occur, the membrane should have a pore diameter, d, such that $\lambda > 10d$ where $\lambda$ is the mean free path of the gas. At pressures used in this study d should be less than 20 nm

(section 5.2), hence the membrane porosity, based on a theoretical pore diameter of 4 $\varepsilon$ /Å, should be in the region of $0.4_4$ (void volume per unit plug volume).

In these membranes the required porosity was achieved by compressing the uniform particles of Graphon in a stainless steel cylinder between close-fitting hardened-steel plungers (Barrer and Gabor, 1959). This resulted in a network of fine tortuous channels between points of contact of the smooth carbon particles.

A Denison T 42 press, capable of exerting a force of 15 000 lb. wt., was employed. The membranes were made in eight equal increments, each increment being compressed to the same pre-determined porosity (calculated from the density and weight of carbon, and the volume to which it was compressed). This incremental construction produced a membrane having uniform properties without severe variations in porosity and degree of compaction near the ends (Ash, Baker and Barrer, 1968). The force used to form the plug was in the vicinity of 3000 lbs. wt. spread over the cross-sectional area of the plug (a pressure of about $1.5 \times 10^9$ Pa), resulting in a membrane which was physically hard and had a complete and tenacious contact with the walls of the steel cylinder.

This same cylinder was then attached to the high-vacuum apparatus via glass-Kovar metal seals or Cajon Ultra Torr vacuum unions. Prior to this however, steel plungers were screwed up to the faces of the plug to prevent any swelling which might occur with strongly sorbed gases (Carman and Raal, 1951b). Thermocouples were mounted in the face of each plunger and the plug assembled as described in sections 3.5.1, 3.6.1 and elsewhere (Clint, 1966; Ash, Barrer, Clint, Dolphin and Murray, 1973).

Two plugs have been used in this study, designated N and O

with reference to Ash et al, 1968 and Ash et al, 1973. Plug N was also used by Clint (1966) and Dolphin (1971); plug O was constructed for this investigation. The characteristics of these microporous membranes are given in table 3.2.

Adsorption isotherms, which were needed to interpret the isothermal and non-isothermal data, were obtained using Graphon pellets of a porosity similar to that of the plug. The pellets were made by compression, as above,but in a split cylindrical holder (Barrer and Gabor, 1960). This could be dismantled after construction and various sections of plug placed in an adsorption bulb.

TABLE 3.2

*Membrane characteristics*

| Property | Units | Membrane N | O |
|---|---|---|---|
| Weight of carbon | g | 1.551 | 1.523 |
| Number of increments | - | 8 | 8 |
| Length, $\ell$ | cm | 4.21 | 4.19 |
| Cross-section area, $A_c$ | $cm^2$ | 0.324 | 0.327 |
| Porosity, $\varepsilon$ | $cm^3 cm^{-3}$ | 0.423 | 0.434 |
| Area, A | $m^2 cm^{-3}$ | 98.0 | 96.1 |
| $(\varepsilon/A)*$ | nm | 4.32 | 4.52 |

*A and $\varepsilon/A$ calculated using $A_g$ of 86.2 $m^2g^{-1}$(section 4.1.1)

## 3.2  GENERAL FEATURES OF THE APPARATUS

### 3.2.1 *Pumping systems*

Three distinct high vacuum rigs with four high vacuum pumping lines were employed. Although differing in some details, several features were common to each system.

All high vacuum apparatus was constructed from Pyrex glass with wide bore tubing (15-20 mm diameter) being used whenever possible to increase the pumping speed. Right-angled taps were used in preference to straight-through taps as they had a longer leak path. Apiezon N

grease was used throughout.

A high vacuum of $10^{-5}$ Torr was achieved by the use of a three-stage mercury diffusion pump backed by a two-stage gas-ballast rotary oil pump. The latter was generally an Edwards 2SC20A model, capable of an ultimate vacuum of $10^{-3}$ Torr (although a newer, direct drive model, the EDM2, was used on the non-isothermal rig). For the adsorption and isothermal transport rigs, the three- stage mercury diffusion pump was backing a large-scale, single-stage mercury pump to give a faster pumping speed.

A non-return valve and oil trap were incorporated above the oil pump to prevent oil being sucked back into the apparatus in the event of a power failure. Another safety feature was a 'Truflo' flow warning switch inserted in the water outlet from the diffusion pump condenser. This device would cut off the electricity supply to the diffusion pump heater if the water pressure fell below a pre-determined value. A 5 litre buffer volume on the low vacuum side of the mercury pump permitted pumping to be continued when the oil pump was switched off for maintenance.

The cold trap inserted between the high vacuum manifold and the pumps minimised mercury contamination of the system and helped achieve a better vacuum by reducing the vapour pressure of mercury, water vapour or other condensable vapours which might be present. The trap was designed to have maximum molecular conduction giving minimum reduction in pumping speed (Dushman and Lafferty, 1965, p200). In the non-isothermal flow apparatus two cold traps in series were used to ensure that any traces of mercury vapour, which could condense in the capacitance manometer, were excluded from the system.

A Pirani vacuum gauge was incorporated into the high vacuum manifold of each rig. This was an Edwards G5C-2 head with model 8-2

control unit covering the range $1-10^{-4}$ Torr. Calibration was carried out using a McLeod gauge (also incorporated into the adsorption and isothermal rigs).

The oil in the rotary pumps was renewed every six months, but to prevent undue oxidation and contamination of the oil an auxiliary rotary pump was used to lower McLeod gauges and manometers and for the initial evacuation of the apparatus.

A schematic diagram of the high vacuum pumping system is shown in figure 3.1.

### 3.2.2 *Room temperature control*

The laboratory was equipped with two Temkon air-conditioning units which maintained an ambient temperature of $23 \pm 1^{\circ}C$. Airflow within the laboratory was good, a regional variation of only $\pm 0.5^{\circ}C$ being found, despite many local sources of heat.

### 3.2.3 *Liquid thermostats*

The temperature of the adsorption sample and the isothermal plug were controlled by immersing the sample in a bath of silicone fluid, DC 550. Although differing in size, these baths were similar in construction (figure 3.2). The heating wire was controlled from a Variac so that its heat output could be adjusted to keep the bath several degrees below the required temperature. Fine temperature control was then obtained by the use of an auxiliary heater (a lamp bulb or low wattage immersion heater) operated through an electronic relay controlled by a contact thermometer regulator. Temperature control of $\pm 0.05^{\circ}C$ was obtained. For outgassing purposes the baths could be heated up to $200^{\circ}C$ without the oil smoking.

In the non-isothermal flow apparatus a bath of Shell Thermia Oil 23 was used as a heat sink to control the temperature at the cold end of the plug. Copper cooling coils attached to the cold water supply were used to maintain a temperature close to ambient temperature.

a  5 dm$^3$ Buffer

b  High Vacuum Manifold

c  Cold Trap

d  Dewar

e  3-Stage Diffusion Pump

f  Oil Trap

g  Non-Return Valve

h  Rotary Vacuum Pump

k  Neoprene Tubing

l  Pirani Gauge Head
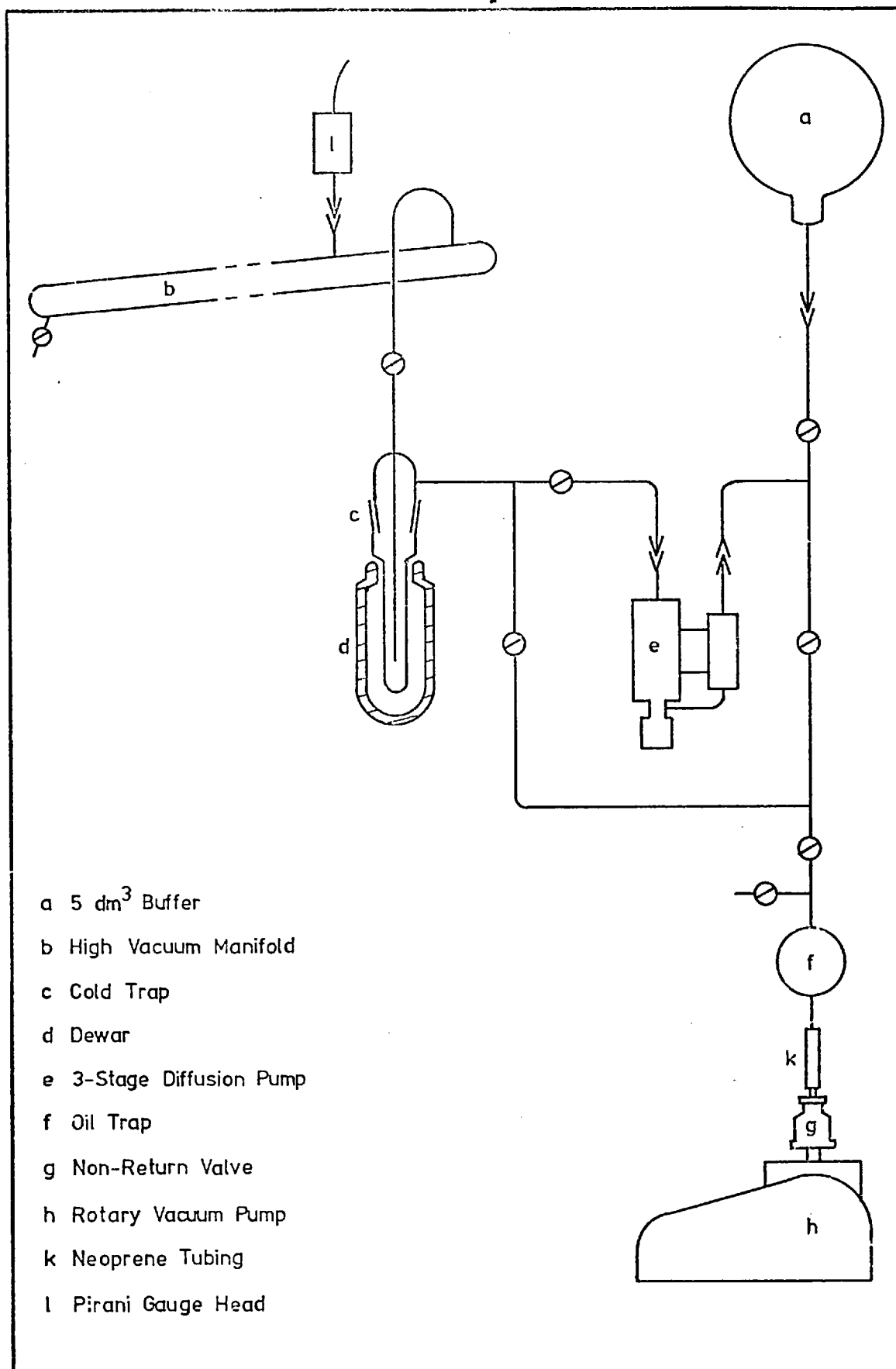
Figure 3.1            High Vacuum Pumping System

a  Aluminium Foil

b  Asbestos Rope

c  Pyrex Beakers

d  Electrothermal Heating Wire

e  Asbestos Wool

f  Asbestos Paper

g  Contact Thermometer Regulator

h  Calibrated Thermometer

k  Sample

l  Paddle Stirrer

m  Auxiliary Heater

n  Silicone Oil, DC 550
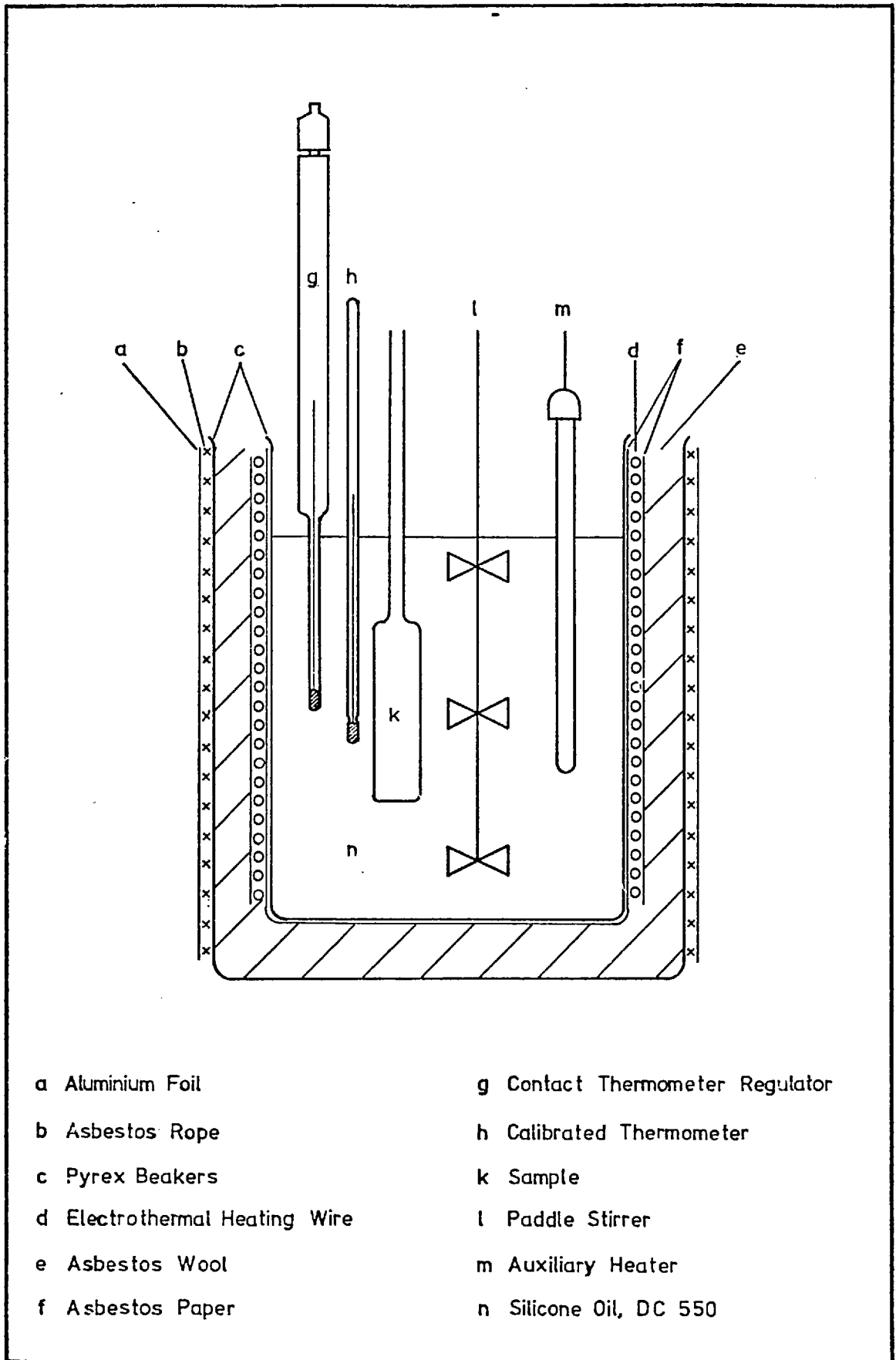
Figure 32          Silicone Oil Heating Bath

### 3.2.4 *Outgassing procedures*

The adsorption sample and plugs N and 0 were outgassed in a similar fashion. When the carbon had been in contact with the atmosphere, before being used again, it was pumped at room temperature until the pressure had fallen to $10^{-4}$ Torr. The temperature was then increased in $50^{o}C$ steps until $200^{o}C$ was reached. Pumping was continued for 12 hours at each temperature.

For adsorption and isothermal measurements, the sample was generally outgassed overnight at $200^{o}C$ between runs. However for the hydrocarbons $C_3H_8$ and above, outgassing for 24 to 36 hours at $200^{o}C$ was found to be necessary. In non-isothermal flow experiments the plug was only outgassed when the gas was changed.

### 3.3. THE CAPACITANCE MANOMETER

### 3.3.1 *Features*

During recent years, several high precision capacitance membrane manometers have become available. There is now a wide selection of such instruments covering the pressure range from ~0 to 1000 mmHg, and capable of measuring an absolute or a differential pressure. This type of manometer was used in the non-isothermal flow apparatus, replacing mercury manometers and McLeod gauges.

The advantages of these devices are many. A true pressure is measured, independent of the gas nature and composition. This pressure is the force per unit area on the diaphragm in the sensing head. The instrument is robust and the head can withstand an over-pressure of one atmosphere. Readings can be taken rapidly and are calibrated directly in mmHg. An output proportional to the pressure can be obtained and fed into a potentiometric recorder thus providing a continuous, instantaneous record of pressure. Sensing heads of an all-welded construction are available thus eliminating 'O' rings and

allowing corrosive gases to be handled. Contamination of the vacuum system is negligible and units are also available which can be baked at $450^{\circ}$C.

The manufacturers claim a high accuracy and linearity for their equipment with reproducibility of 0.005% and an accuracy of 0.03-0.1% of the reading.

Several papers have recently appeared in the literature where the performance of capacitance manometers has been compared favourably with conventional gauges. Utterback and Griffith (1966) were concerned with pressures in the range $10^{-4}$ to $3 \times 10^{-3}$ Torr and Bromberg (1969) covered the range $10^{-4}$ to 1 Torr. Both found capacitance manometers to be convenient and reliable with deviations from linearity of less than 0.3%. They were superior to a McLeod gauge which had an appreciable mercury streaming error to the cold trap and the range of gases for which it can be used is restricted. Gascoigne (1971) measured pressures in the range 0.1-500 Torr and checked the calibration of the instrument.

### 3.3.2 *Operating principle*

The pressure sensing head is in essence a transducer which relies on the pressure difference between two chambers to produce a deflection in the tensioned metal diaphragm separating them. This deflection causes a capacitance change to occur between the diaphragm and two fixed electrodes mounted in the chambers on either side, one capacitance being increased and the other decreased. These capacitances are incorporated into a bridge circuit, which is initially zeroed with both chambers connected to the same pressure. The bridge is balanced by a decade unit until a null out-of-balance signal is obtained.

Calibration of the instrument is such, that the decade reading gives the pressure in mmHg directly, and only minor calibration

corrections have to be applied. When the head is used as an absolute gauge, one chamber is connected to a high vacuum ($10^{-5}$ Torr) and the other chamber to the system whose pressure is to be determined.

### 3.3.3 *Equipment used*

The instrument chosen for this work was the MKS Baratron Type 170 Pressure Meter manufactured by MKS Instruments Inc. of Burlington, Massachusetts, U.S.A. This model was available in modular form and with many options. The following modules were chosen:

(i)    170M-7: *Electronics unit and power supply*

This provided excitation to the sensing head and power for the head heaters. It also converted the head signal to a proportional D.C. output of 10V full scale and by the use of a precision voltage divider circuit allowed four ranges of amplification to the signal (X1, X10, X100, X1000).

(ii)   170M-29: *Five-place, manual-balance digital offset unit*

This unit was used in the bridge balancing operation and consisted of three decade switches plus a vernier potentiometer. The decades were adjusted until the meter or D.C. output read zero (i.e. the bridge was balanced), whence the dial reading gave the pressure directly in mmHg.

(iii) 170M-26: *5-inch precision mirror scale meter*

The input to this meter was the out-of-balance signal taken from the electronics unit.

(iv) 170M-34: *Head-selector unit*

This allowed three heads to be used with the same electronics unit. It provided a power supply for the heaters in each head so that all three could be ready for immediate use. It also contained zero and quadrature adjustment potentiometers for each head. The zero control compensated for any capacitance changes of the head at zero differential

pressure, whilst the quadrature control allowed for any high

resistance or stray capacitance which was $90^{o}$ out of phase with the

bridge signal. The excitation signal was channelled from the electronics

unit to the head selected and the head signal fed back to the 170M-7

unit.

(v) *Head Sensor:* Type 145AH

This is an all-welded differential head and in use was thermostatted

at $50^{o}C$. The heads were attached to the vacuum system via Cajon VCR

couplings connected to $\frac{1}{4}$ inch outside diameter Kovar metal-glass seals.

The Cajon couplings incorporated an aluminium gasket seal.

A block diagram of the system is shown in figure 3.3.

Three heads were used; one, with a range of $10^{-5}$ to 1 mmHg,

for the isothermal flow studies; the remaining two, each with a range

of $10^{-2}$ to 1000 mmHg, to monitor pressures at the hot and cold sides

of the plug during thermo-osmotic runs.

The indicator module and heads were factory calibrated against

air dead-weight standards and were supplied with calibration data. In

addition a system check facility was also incorporated taking the form

of a relay in the head, operated from the electronics unit, which

shunted the sensor bridge circuit. When activated it simulated a test

pressure and the D.C. output obtained was a function of the head,

indicator module and interconnecting cables. This permitted a check

of the entire system.

### 3.3.4 *Operating technique*

In normal operation the reference port, $P_R$, of all three heads

was attached to a high vacuum line reserved solely for this purpose, so

that absolute pressures were measured. However, it was also possible

to use one of the 1000mm heads as a differential gauge to monitor the

pressure difference, $\Delta p$ (= $p_o - p_{\ell}$), between the hot and cold sides
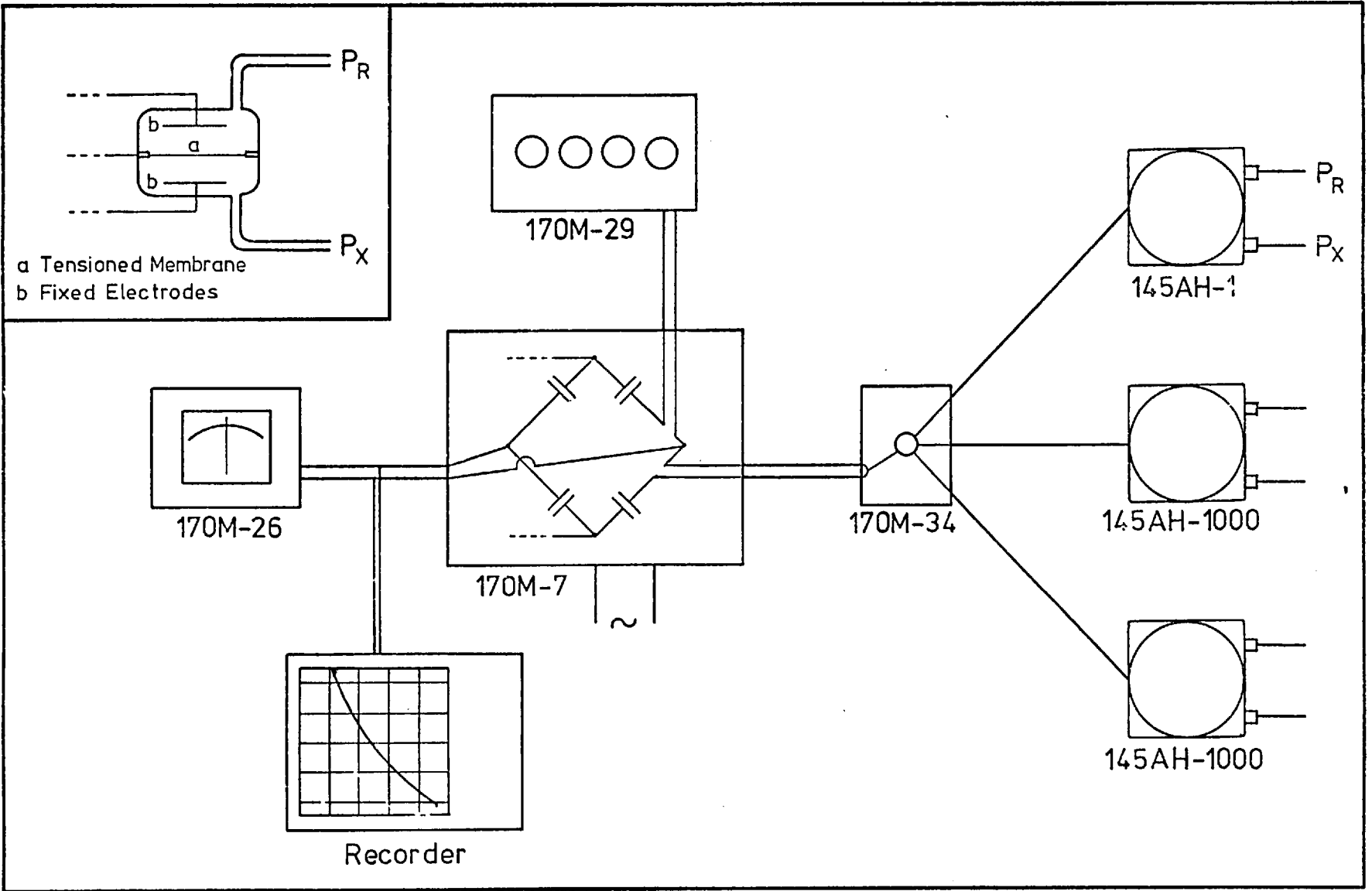
Figure 3.3    Schematic Diagram of Baratron
Equipment and Head (inset)

of the plug in thermo-osmotic experiments. Since the other 1000mm

head could still be used to measure $p_\ell$, then $p_o$ could also be obtained.

This had certain practical advantages to which reference will be made

below.

The 170M-7 unit furnished a D.C. output, which was linear with

pressure, of 0 to $\pm$ 10 volts full scale on each range selected. By

attaching this output to a potentiometric chart recorder, the build up

in pressure could be followed as a function of time for any one head.

By suitable range selection the pressure could be followed over 100%,

10%, 1% or 0.1% of the full head range.

When the digital offset unit was used in conjunction with the D.C.

output, by pre-setting a particular pressure on this unit, the pressure

build-up above a certain value could be followed, using a more sensitive

range. Also, by centre zeroing the recorder, pressure fluctuations

about a mean could be continuously monitored.

The digital offset unit balances the A.C. bridge by supplying a

voltage from an accurate voltage divider. The latter consists of

3 multi-tap ratio transformer decade switches and a vernier potentiometer

from which the last two figures in the pressure reading are obtained.

In practice it was found that at the top end of its range, the vernier

potentiometer gave readings about 2 to 4% lower than that expected

(by comparison with the next decade). It was thus found to be more

accurate in taking a pressure reading to interpolate the last two figures

from the recorder trace of the D.C. output, with the three decades

balanced and the range multiplier on the most sensitive range.

3.4 ADSORPTION APPARATUS

All adsorption isotherms were determined volumetrically on a rig

designed and constructed by Clint (1966). This was a standard

volumetric adsorption apparatus (see for example Young and Crowell, 1962,

p 284). It incorporated a twofold adsorption system and all connections between adsorption bulbs, gas burettes and manometers were constructed from 3 mm bore capillary tubing to keep the dead volume to a minimum. The sample of Graphon pellets used weighed 7.164 g.

Isotherms were determined at eight temperatures between 308.15 and 393.15 K and the dead volume in the sample bulb was calibrated at each temperature with helium (see Appendix B).

Water at 300K was circulated through the gas burette jacket and during a run the room temperature in the immediate region of the rig was monitored. Thus the volume of gas in the apparatus, parts of which were at three distinct temperatures, could be corrected to a standard temperature.

Manometers were constructed from Veridia 10. mm precision bore tubing and corrections made for: (i) fluctuations in mercury density with temperature and the corresponding changes in height of the mercury column; (ii) variation of capillary depression with pressure (Gould and Vickers, 1952).

To determine the surface area of the Graphon pellets used in these adsorption studies, a nitrogen isotherm was determined at liquid nitrogen temperature and a B.E.T. analysis performed. The dead space at this temperature was again calibrated with helium and corrections for the non-ideality of nitrogen applied (Emmett and Brunauer, 1937).

## 3.5. ISOTHERMAL FLOW APPARATUS

The plug assembly and high vacuum grid used in this part of the study were similar to those described in detail, elsewhere (Clint (1966); Dolphin (1971)).

### 3.5.1 *Plug assembly*

Isothermal permeability and time-lag studies were performed on plug N using the lower straight-chain paraffins. Minor modifications

were made to the assembly in an attempt to improve and resolve the temperature difference between the internal and external thermocouples (Clint, 1966). These included renewing the 34 s.w.g. copper-constantan thermocouples and inserting a layer of 40 mesh copper gauze between the plug and plunger. It was hoped that this would have the effect of improving the thermal conductivity between plug and plunger and at the same time allowing gas to circulate freely between them.

The temperature of the plug was controlled by immersion in a silicone oil bath which could be raised to $200^{\circ}C$ for outgassing. The external thermocouples and electrical windings were protected by using a silicone rubber compound to seal any gaps where oil could seep in.

3.5.2 *Experimental procedure for isothermal flow runs*

In the determination of isothermal fluxes and time-lags , gas at a known pressure, $p_o$, is admitted at time zero to one side of the outgassed membrane. The build-up of pressure, $p_{\ell}$, in a known volume at the other side of the membrane is measured as a function of time and hence the total flux can be obtained. So that the ingoing pressure, $p_o$, was essentially constant, a buffer volume of 3 $dm^3$ was used on the ingoing side. In order that the pressure difference across the plug may be approximated to the ingoing pressure, a large calibrated buffer volume was used on the outgoing side and the pressure measured on a McLeod gauge. This buffer could be varied from 1954 $cm^3$ to 9645 $cm^3$ to cope with widely differing fluxes.

In practice the fall in $p_o$ was less than 0.5% during a run and the final value of $p_{\ell}$ was less than 0.3% of $p_o$, so that $\Delta p \simeq p_o$ to within 0.8%, and in a plot of $\Delta p$ versus t no detectable deviation from linearity was found. The time scale of the experiments, over which measurements were made to obtain a significant linear portion of the $\Delta p$ - t plot, varied from 90 minutes for helium to over 6 hours for n-butane.

a  Outgoing Buffer Volumes
b  Ingoing Buffer Volume
c  Plug Assembly
d  McLeod Gauge, D2
e  Manometer
HV  High Vacuum Line
LV  Low Vacuum Line
⊘  2-way Tap
⊗  3-way Tap
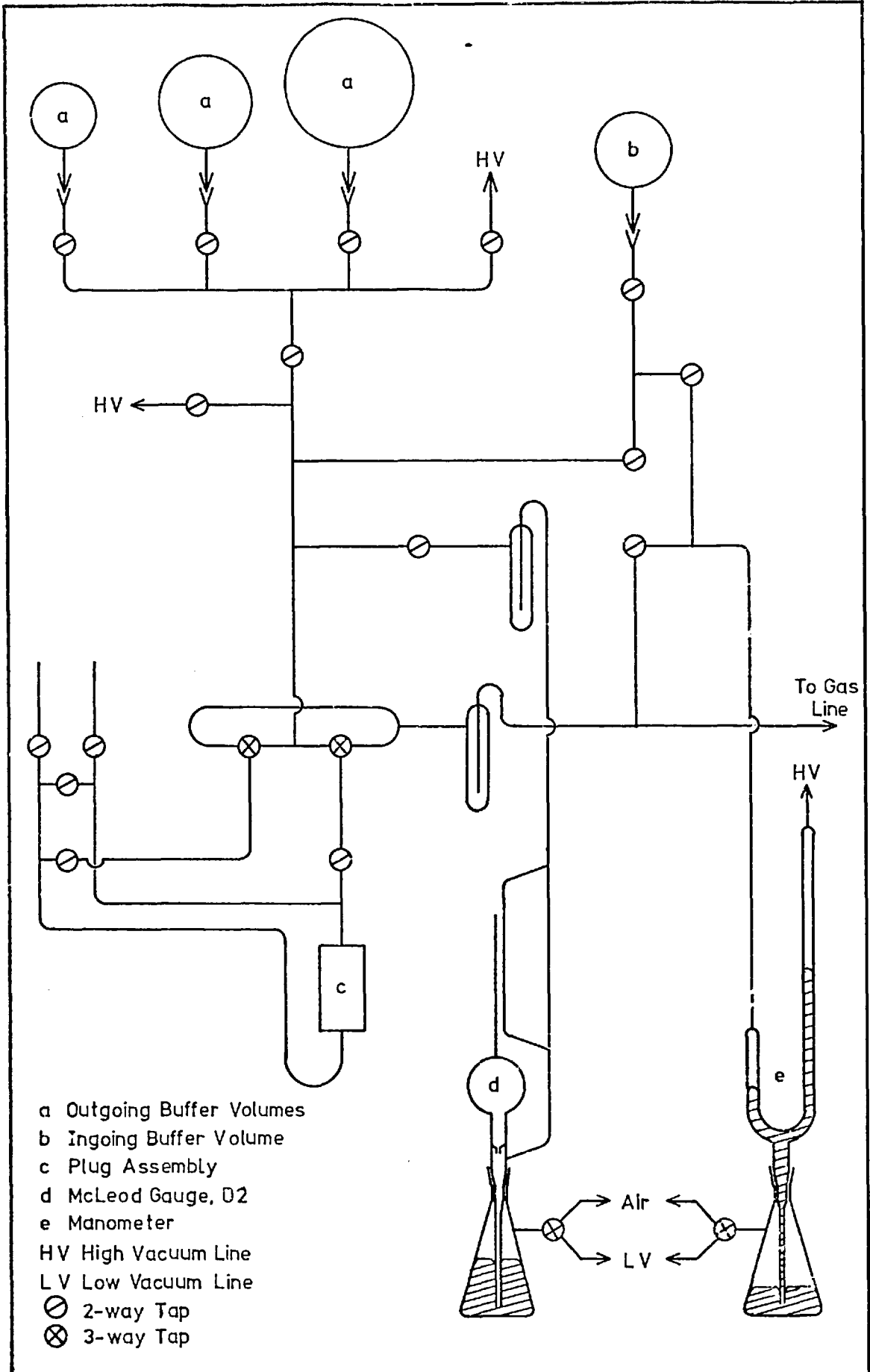
*Figure 3.4*          *Isothermal Flow Apparatus*

The essential features of the apparatus are shown in figure 3.4. A gas line (not shown) was also required and a Toepler pump was used to control the admission of gas. to the ingoing buffers.

## 3.6   NON-ISOTHERMAL FLOW APPARATUS

For this section of the work, a new plug, O, was constructed having a porosity similar to plug N, but with a thermocouple arrangement of slightly different design. The apparatus was novel in that capacitance membrane manometers were used in place of McLeod gauges and mercury manometers.

### 3.6.1 *Plug assembly*

The plug holder and heating coils were as described by Clint (1966). The heat source was an electrical winding set into an annular groove in a copper block which was screwed onto the top of the plug holder. Temperature control of this block (and hence of the hot face of the plug) was achieved using a thermistor (Type F23, supplied by I.T.T. Electronics) mounted in a hole in the block. This was incorporated into an A.C. bridge circuit in which the resistance of the thermistor was balanced by a decade resistance box. The off-balance current was amplified and used to activate a relay which shunted a series resistance in the heater circuit. Another copper block was screwed onto the bottom of the plug holder and acted as a heat sink when immersed in a constant temperature bath.

A double layer of Electrothermal heating wire was wound onto the plug holder and was used to heat the plug during outgassing. Two co-axial steel cylinders were enclosed between the top and bottom copper blocks and asbestos wool insulation was packed between them. These cylinders acted as guard-ring insulation for the flow of heat from top to bottom blocks. External thermocouples were not incorporated into this assembly since experience with plug N had shown that, provided

there was sufficient asbestos rope lagging around the assembly, an apparent linear temperature gradient was readily obtained.

Hardened steel plungers were again used to constrain the plug . Two thermocouples were mounted in the face of each plunger, one in the centre and one at the edge. These were sheathed and insulated thermocouples specially constructed by Spembly Ltd., Andover, Hants. The conductors were 0.09 mm diameter nickel chromium - nickel aluminium with mineral insulation enclosed in a stainless steel sheath of external diameter 0.5 mm. The hot junction was exposed and supported in a bed of silicone rubber. Compensation leads and incorporated cold junction were also supplied. The assembled plug is shown in figure 3.5.

Feedthrough of the thermocouples into the vacuum system was achieved by soft soldering the stainless steel sheath into small holes drilled in the upper flange of a miniature vacuum fitting as shown in figure 3.6. The fitting was constructed in stainless steel and was silver soldered onto the end of the plug holder. Argon arc welding was used to attach the side-arm, also of stainless steel ($\frac{3}{8}$ inch O.D.; $\frac{1}{8}$ inch I.D.). Vacuum-tight seal of the flange was effected by knife edges biting into a copper gasket.

The whole assembly was attached to the vacuum system via Cajon Ultra Torr unions forming a vacuum-tight seal between the stainless steel side-arm and the glass tubing of the vacuum line (figure 3.6).

The principal advantages of this design of system over that of Clint (1966) are:-

(i)    Two thermocouples, mounted directly in the face of the plug, are used. Hence any radial temperature gradient could be observed.

(ii)    The hot junctions were of very small dimensions, so that the temperature over a very small region could be measured. In Clint's

a Copper Blocks

b Steel Plug Holder

c Porous Carbon Plug

d Steel Plungers

e Steel Cylinders

f Outgassing Heater Coil

g Asbestos Wool

h Top Heater Coil

k Thermistor Hole

l Thermocouple Leads
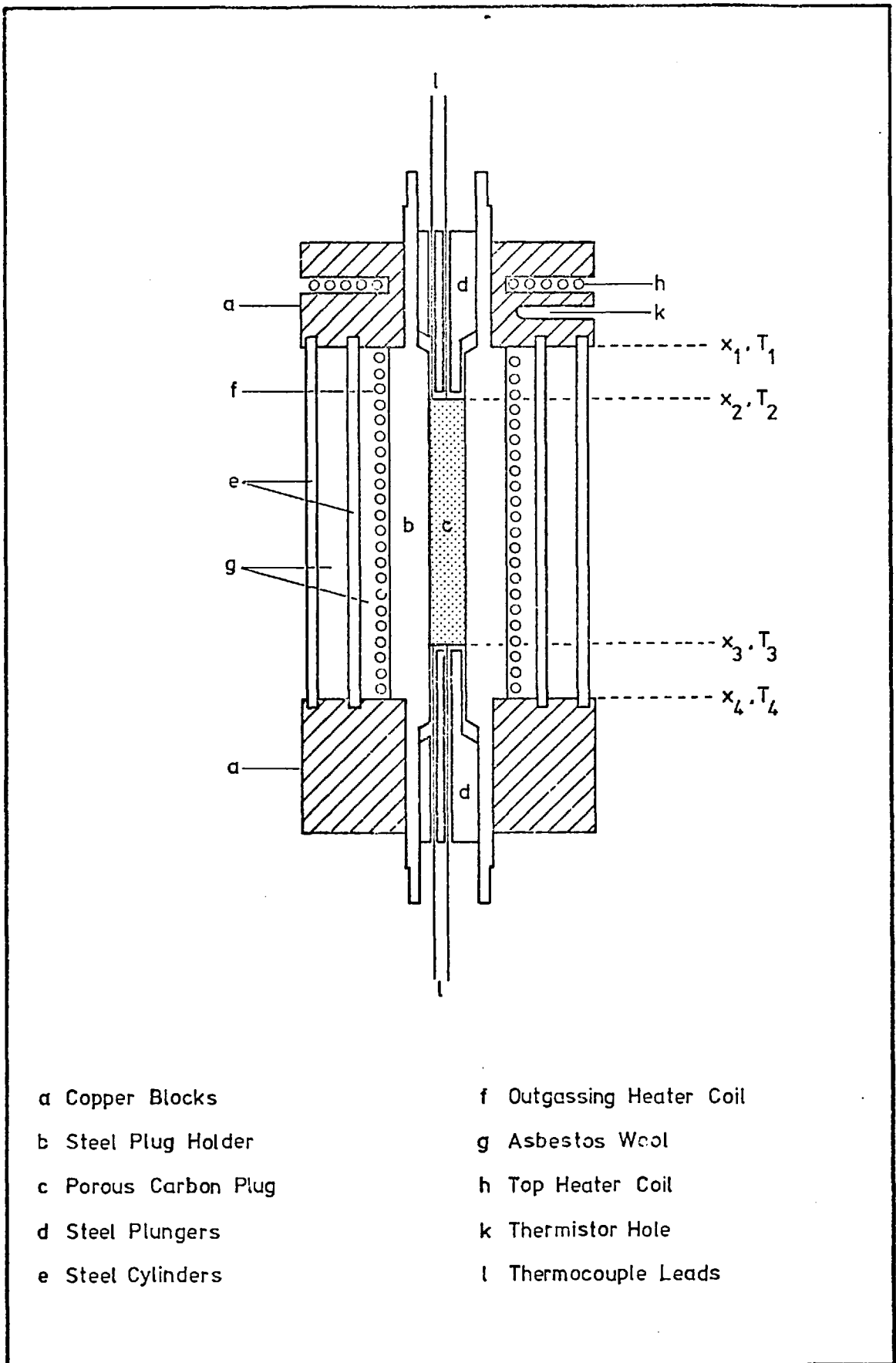
*Figure 3.5*          *Thermo-osmotic Plug Assembly*

a  Pyrex Tubing 3/8" O.D.

b  S/Steel Tubing 3/8" O.D.
      1/8" I.D.

c  Cajon Ultra Torr Union

d  Argon Welded Joint

e  Silver-Soldered Joint

f  Plug Assembly

g  Upper Flange

h  Lower Flange

k  Copper Gasket

l  Nut, Bolt and Washer

m  Thermocouple Leads

n  Soft-Soldered Vacuum
   Feedthrough
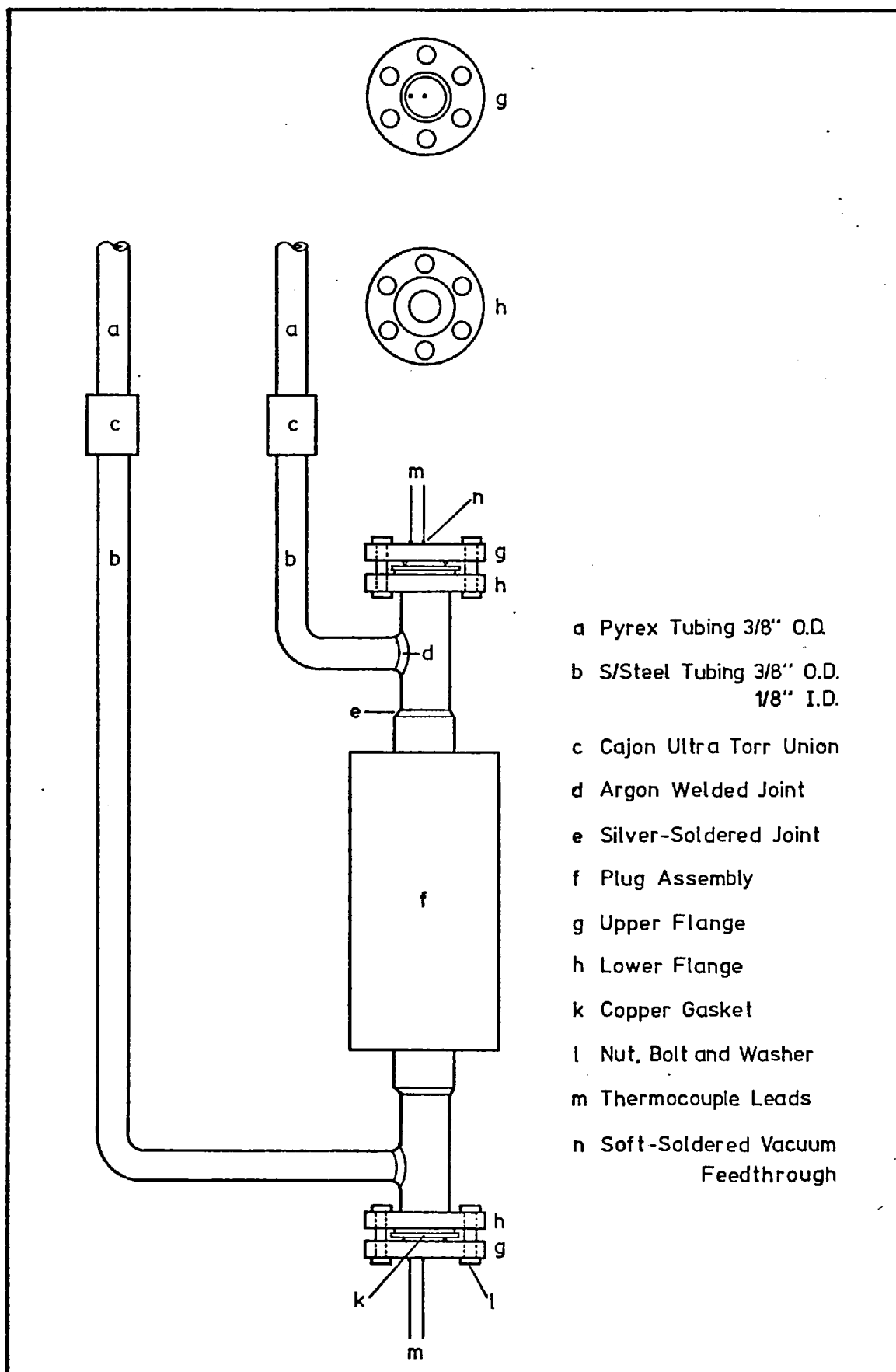
Figure 3.6  Miniature Flange Arrangement and

     Connection of Plug Assembly to Vacuum System

design the temperature measured was probably an average over the face of the plunger.

(iii) The sheathed thermocouples were relatively robust and the sheath could withstand the temperatures involved in soft soldering. Also the sheath was electrically insulated, so no electrical shorting occurred and the delicate glass bead insulation of Clint's design avoided.

(iv) By simply unscrewing the Cajon unions, the whole plug assembly could be removed, complete with thermocouples. If another plug assembly was made, this could be attached in a matter of minutes.

### 3.6.2 *Experimental procedure for thermo-osmotic runs*

Gas was admitted from the gas line to both sides of the plug. The required temperature gradient was then set up by adjustment of (i) the bridge resistance balancing the hot block thermistor; and (ii) the temperature of the heat sink bath. The degree of temperature control was optimised by suitable choice of the top-block heater voltage and buffer resistance (for $T_o$), and for $T_\ell$, the oil bath heater voltage and rate of flow of water through the cooling coils. The pressure of gas in the system was carefully adjusted by expansion of gas from the calibrated expansion volume and by the use of freezing limbs to transfer gas from the gas line to the bulb. A schematic diagram of the rig is shown in figure 3.7.

The pressure was monitored (usually overnight, using the Baratron D.C. output fed into a recorder) until sorption equilibrium had been obtained (indicated by a constant pressure). This could take up to 12 hours especially with n-butane.

At zero time the hot and cold sides were isolated and the pressures of each side, $p_o$ and $p_\ell$, were monitored as a function of time. For the Graphon membrane 0, a steady value of $(p_o/p_\ell)_\infty$ was achieved

HV2

HV1

HV1

Gas Line

a  Baratron Head, 1mm

b  Baratron Head, 1000mm

c  Calibration Volume, X

d  Plug Assembly

e  Cajon Couplings

HV1  Reference High Vacuum

HV2  System High Vacuum

⊘  2-way Tap

⊗  3-way Tap
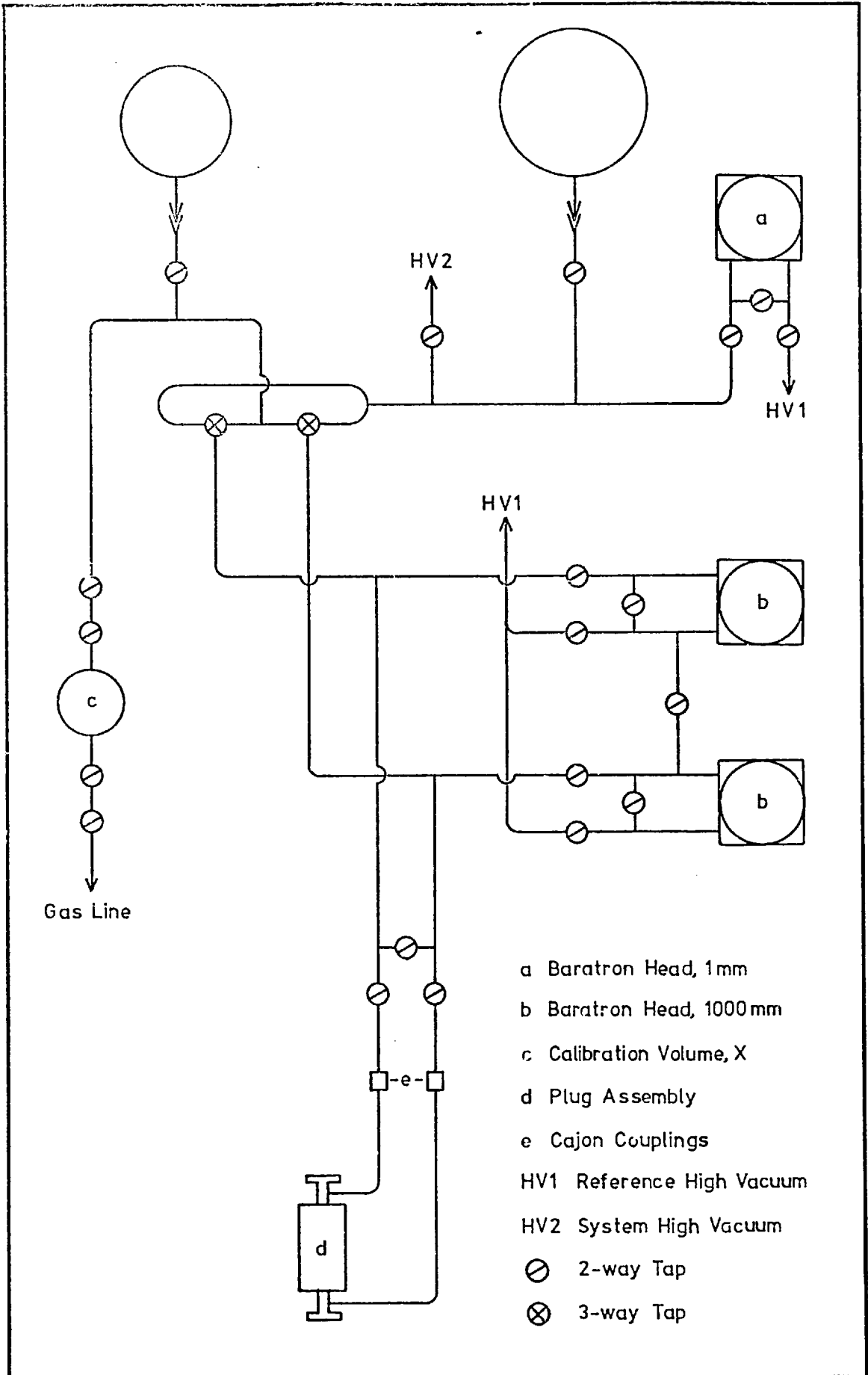
*Figure 3.7*     *Non-isothermal Flow Apparatus*

after about 60-70 hours. To ensure an accurate value of $(p_o/p_\ell)_\infty$
the ratio was monitored for a further 50 hours and the equilibrium
values averaged.

As a variation of this technique it was possible to monitor
$\Delta p$ $(= p_o - p_\ell)$ on one head and $p_\ell$ on the other. $(p_o/p_\ell)$ could still
be calculated, but between manual readings following $\Delta p$ on the recorder
permitted a visual check on the approach curve to equilibrium.

### 3.6.3 *Experimental procedure for isobaric flow runs*

A further advantage of being able to monitor $\Delta p$ was that it
enabled an isobaric permeability to be calculated. It was observed
that initially, over the first hour of a thermo-osmotic run, the plot
of $\Delta p$ versus t was approximately linear. $\Delta p$ is initially so small that flow
through the plug is very nearly isobaric. During this time the change
in $p_\ell$ was between 0.5 and 2.0% (being dependent upon the gas), hence
from the initial slope of this plot, $d\Delta p/dt$, the flux, $dn/dt$, and
hence an isobaric permeability, could be obtained. The optimum chart
speed and recorder range settings depended on the flowing gas, pressure
and temperature gradient, but for each such set of conditions, 3 to
5 isobaric plots were obtained and the limiting slopes averaged to
obtain the isobaric flux. This isobaric run was performed immediately
prior to starting a thermo-osmotic run, when sorption equilibrium had
been established in the plug.

### 3.7 CALIBRATION AND ACCURACY

### 3.7.1 *Mercury manometers*

The mercury used was triple-distilled, treated with acidified
dilute potassium permanganate solution and then with dilute nitric
acid. It was thoroughly washed with distilled water until the washings
were neutral and was then dried by heating to $80^\circ C$ on a sand bath in a
fume cupboard.

Precision bore tubing of the manometer was cleaned prior to filling by washing with a strong detergent (Decon 90) then with distilled water and finally with redistilled AnalaR acetone. The tubing diameter and surface tension of clean mercury were used in calculating the capillary depression correction (Gould and Vickers, 1952).

The height of the mercury column was measured to an accuracy of $\pm$ 0.004 cmHg using a cathetometer supplied by Precision Instruments Ltd.

### 3.7.2 *McLeod Gauges*

Veridia precision tubing of 2 mm bore was used for the capillary. It was checked for uniformity of diameter by measuring the length of a weighed mercury slug at various sections of the capillary. Both capillary limbs of the gauge were constructed from the same length of Veridia tubing.

Volumes of the McLeod gauge bulbs were calculated from the weight of water the bulb contained at a known temperature and water density. Before assembly the gauges were cleaned and filled with clean mercury as described in section 3.7.1. A cathetometer was used to measure the height of the mercury column and the estimated accuracy in pressure was $\pm$ 0.5%.

Calibration data for the gauges used in this work are given in Appendix B. Gauge D2 was used to measure outgoing pressure in the isothermal flow work, while D1 and D3 were used as reference gauges.

### 3.7.3 *The capacitance manometer*

The sensing heads and control unit were furnished complete with calibration data. To avoid possible mercury contamination of the heads no calibration reference manometer was employed. If a cold-trapped McLeod gauge had been used, this itself would have introduced errors due to mercury streaming (Carr, 1964; Utterback and Griffith,

1966; Bromberg, 1969). The accuracy of the Baratron has been established by these workers and the 1 mm head has been shown to be superior to a McLeod gauge.

However evidence has been produced to indicate that a thermal transpiration error can occur for the 1 mm head due to a difference in temperature between the thermostatted head and the vacuum system (Bromberg, 1969; Baldwin and Gaerttner, 1973). It was concluded that the thermal transpiration error was dependent upon the geometry of each installation. In this work the 1 mm head was used only for monitoring purposes and since thermal transpiration will not occur at the higher pressures measured by the 1000 mm heads, then no error will be introduced. When the 1 mm head is used at a later date for isothermal studies, this possible source of error should be investigated.

Gascoigne (1971) has investigated the calibration of Baratron instruments. The heads he used were found to be out of calibration when received and on re-calibration he found drifts in sensitivity and linearity of 0.3 to 1.0% due to temperature fluctuations. However the heads used in this work were thermostatted, unlike Gascoigne's, and so temperature fluctuations would not be expected to be important. Fluctuations in pressure with temperature changes were observed, but these were commensurate with pressure changes expected due to temperature fluctuations in a closed system.

Since the two 1000 mm heads agreed with one another within 0.2%, then Gascoigne's evidence on calibration is not applicable in our case. In use the heads were calibrated against one another to improve accuracy and reproducibility.

It is also worth considering the zero-drift over a long period, which with the Baratron model 77 was appreciable. However the 170 system with 145 model head was much more stable. A drift of $\pm$ 0.05 mmHg

over a week was typical. To improve the accuracy of the measurements, the zero and quadrature controls were adjusted every week or at the start of a run. It was observed that due to different outgassing rates of the chambers in the head, the zero position at nil differential pressure changed noticeably with absolute pressure. To avoid introducing errors when a head was used as a differential gauge, the zero and quadrature were adjusted at the pressure at which the measurements were to be made.

The manufacturers quoted accuracy, including non-linearity and drift of head and control unit was about $\pm$ 0.2%.

### 3.7.4 *Buffer volumes*

These were calibrated by weighing the amount of water at known temperature required to fill them, and were known with an accuracy of $\pm$ 0.2 cm$^3$. Volumes of small sections and gas burettes were calibrated similarly, but using mercury. Appendix B gives the volumes of buffers and standard volumes used in this work.

### 3.7.5 *Internal volumes*

Volumes of internal sections of the apparatus were determined by helium expansion from known calibrated volumes, such as a gas burette, buffer volume or McLeod gauge bulb. In the adsorption apparatus the sample bulb dead volume was calibrated at the temperature of each isotherm.

The Baratron was used as the pressure measuring device in the non-isothermal flow apparatus. This gave noticeably more reproducible calibrations than did the mercury manometer in the isothermal flow apparatus.

### 3.7.6 *Thermometers*

A set of thermometers, (0-50; 50-100; 100-150 and 150-200$^\circ$C) were supplied by Messrs Sugden Powell Ltd. These were of the total

immersion type with $0.1^O$ divisions and were furnished with a works

certificate (calibrated against N.P.L. thermometers). This set of

thermometers was used as a laboratory standard to calibrate thermometers

used elsewhere in the laboratory which could be read to $\pm$ $0.05^O$C.

### 3.7.7 *Thermocouples*

The laboratory standard thermometers were used to obtain the

temperatures corresponding to the thermocouple e.m.f.'s, when immersed

side by side in a constant temperature oil bath (Barber, 1971).

Calibration points were taken every $5^O$ in the range 25–120$^O$C. A curve

of e.m.f. differences between observed e.m.f.'s and those calculated

from standard tables (British Standards Institute, 1952 and 1961) was

plotted. To obtain the temperature corresponding to an observed e.m.f.,

the difference plot was used in conjunction with the standard tables.

E.m.f.'s were measured to $\pm$ 1 μV on a Precision Potentiometer,

model P10–7 manufactured by the Croydon Precision Instrument Company.

It was used with a 2 volt stabilised power supply and an electronic

null detector, both supplied by the same company. A Tinsley standard

cadmium cell was used to standardise the instrument. The potentiometer

had a resolution of 0.1 μV, although this accuracy was not required in

practice.

CHAPTER 4

ADSORPTION : RESULTS AND DISCUSSION

Adsorption isotherms for the gases used in this study and the calculation therefrom of Henry law constants, and of heats and energies of adsorption are required to enable the isothermal flow and non-isothermal flow measurements, described in subsequent chapters, to be fully interpreted. Whenever a gas is in contact with an active surface (such as Graphon) there exists the possibility of physical adsorption occurring, the extent of which depends on the gas and the surface and distribution of material between them. This distribution, represented in certain cases by the Henry law constant, in turn depends on the temperature and pressure of the gas, and is of importance where surface flow occurs, as in this work. The extent of sorption will give information on the degree of filling of pore space which, in turn, can give an indication of possible pore blockage.

Isotherms were measured using a conventional volumetric adsorption apparatus (Clint, 1966), constructed so as to keep dead volumes to a minimum. For the majority of isotherms a sample of Graphon of weight 7.164 g was used, but for the very weakly sorbed gases, $H_2$ and Ne, a 24.274 g sample was used.

In the results which follow v, the uptake of gas by the adsorbent is expressed in $cm^3$ S.T.P. $g^{-1}$ and p, the equilibrium pressure, in cmHg reduced to 273.15K. The temperature of the isotherm, T, is given in Kelvin and $A_g$, the surface area per gram of adsorbent, in $m^2 g^{-1}$. These are units conveniently employed in dealing with volumetric apparatus involving relatively small gas uptakes and using mercury manometers.

## 4.1    EXPERIMENTAL RESULTS

### 4.1.1 *Surface area determination of Graphon*

A nitrogen isotherm was determined at 77.4K, the normal boiling point of liquid nitrogen. This was fitted to the B.E.T. equation (Brunauer, Emmett and Teller, 1938) using the commonly accepted value for the surface area of the nitrogen molecule viz 0.162 $nm^2$ (Emmett and Brunauer, 1937; Davis, DeWitt and Emmett, 1947).

The overall isotherm was of type II in the Brunauer classification, with a sharp 'knee' near monolayer coverage and is shown in figure 4.1, (experimental data points are tabulated in Appendix C). Absence of capillary condensation and of hysteresis, indicated a non-porous adsorbent. Data were fitted to the B.E.T. isotherm, equation (4.1), by plotting $p/(p_o-p)v$ against relative pressure, $p/p_o$.

$$\frac{p}{(p_o-p)v} = \frac{1}{v_m \cdot c} + \frac{(c-1)}{v_m \cdot c} \cdot \frac{p}{p_o} \qquad (4.1)$$

Here $v$ and $v_m$ are uptake and monolayer uptake respectively; $p$ and $p_o$ are the vapour pressure and saturated vapour pressure respectively, and $c$ is a constant, related to the heat of adsorption. The B.E.T. plot was a good straight line in the $p/p_o$ range 0.01 to 0.18 and had a slope of 0.0505 $(cm^3 \text{ S.T.P. } g^{-1})^{-1}$ with intercept, $1/v_m \cdot c$, of $4.58 \times 10^{-5}$ $(cm^3 \text{ S.T.P. } g^{-1})^{-1}$. From these figures a value of 19.80 $cm^3$ S.T.P. $g^{-1}$ was calculated for $v_m$ and the surface area, $A_g$, was found to be 86.2 $m^2 g^{-1}$.

These results compare favourably with the previously published data on this system. Literature values for $A_g$ determined by the B.E.T. procedure cover the range 78.3 to 89.7 $m^2 g^{-1}$ (table 4.1) and the value determined in this work is within this range. That the surface area varies from batch to batch can be seen from the manufacturers'

Figure 4.1    Nitrogen Isotherm at 77.4K
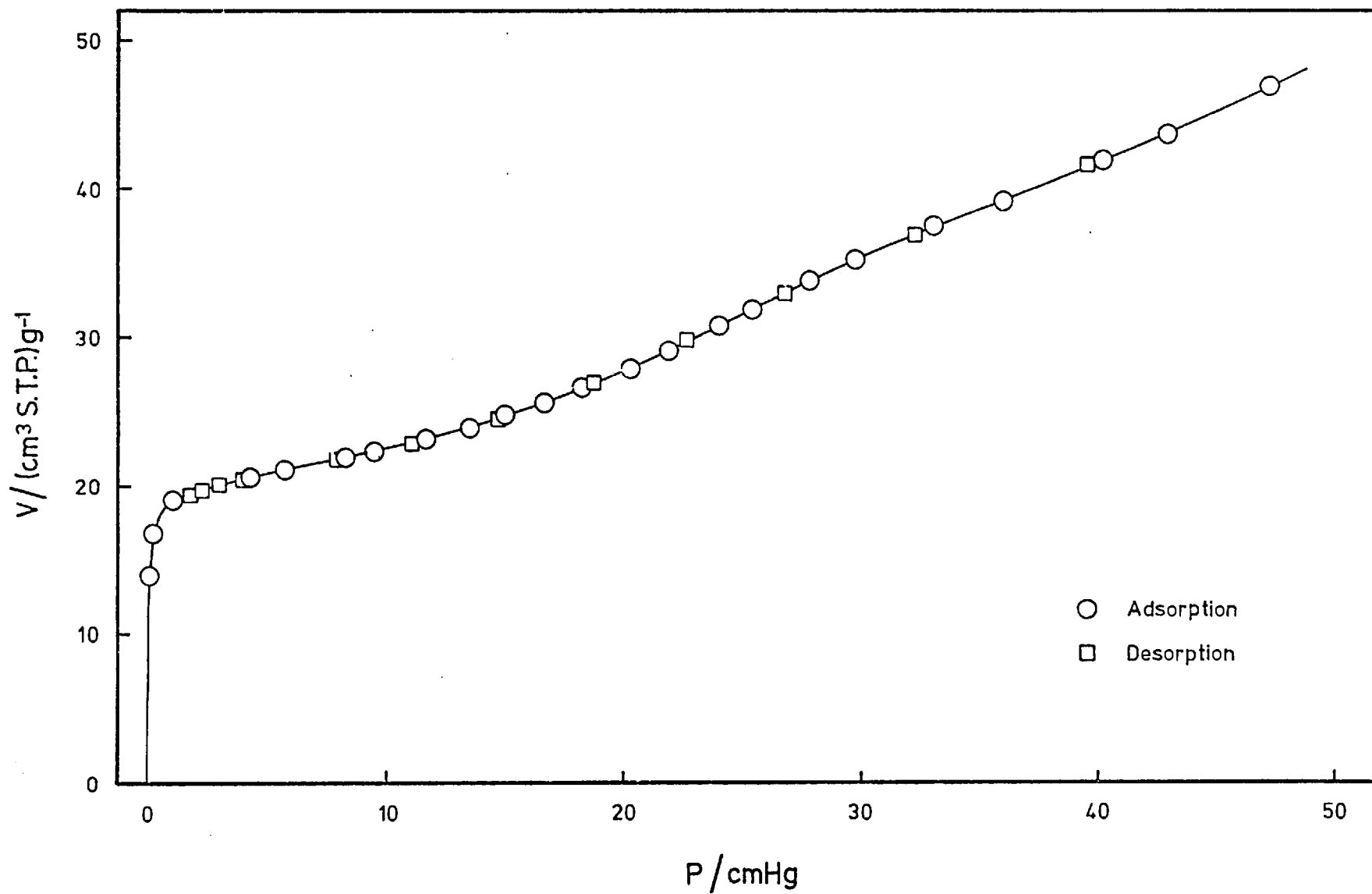
TABLE 4.1

$A_g$ *Values for Graphon*

| Adsorbate | Temperature K | $\frac{A_g}{m^2 g^{-1}}$ | References |
|-----------|---------------|--------------------------|------------|
| Ar | 90.0 | 78.9 | Plug ⎫ |
| Ar | 90.0 | 79.7 | Powder ⎬ Ash, Baker and Barrer, 1967 |
| Ar | 77.4 | 78.3 | Powder ⎭ |
| $N_2$ | 77.4 | 80.3 | Joyner and Emmett, 1948 |
| $N_2$ | 77.4 | 82.2 | Isirikyan and Kiselev, 1962 |
| $N_2$ | 77.4 | 84.0 | Schaeffer, Smith and Polley, 1953 |
| $N_2$ | 77.4 | 85.0 | Beebe, Polley, Smith and Wendell, 1947 |
| $N_2$ | 77.4 | 85.9 | Corrin, 1951 |
| $N_2$ | 77.4 | 86.2 | This work |
| $N_2$ | 77.4 | 87.4 | Cabot technical data sheet sample S6D5 |
| $N_2$ | 77.4 | 89.0 | Pope, 1967 |
| $N_2$ | 77.4 | 89.4 | Atkins, 1964 |
| $N_2$ | 77.4 | 89.7 | Cabot technical data sheet, sample S6D4 |

quoted areas for samples S6D4 and S6D5. Variation amongst experimenters

might also be expected owing to variations in temperature and adsorbate,

values of $N_2$ area etc.

It is known that areas obtained by the B.E.T. procedure using

argon tend to give low $A_g$ values and so it may be thought that the true

area is larger than that determined by Ash, Baker and Barrer (1967). These

workers did demonstrate, however, that no significant difference in

surface area was found between powder and compressed plug. This justified

the assumption that no change in particle shape occurred on compression

and that the Graphon particles behaved as hard, inelastic particles.

The value of $A_g$ is clearly dependent on the chosen area of the

adsorbate molecule, the value of $0.162nm^2$ for $N_2$ being that calculated

for a spherical molecule in a close-packed liquid. Corrin (1951), using

this area for $N_2$ at 77.4K, calculated the surface area of a standard

anatase sample. He then proceeded to evaluate the apparent area occupied

by an Ar molecule at 77.4K and by a pentane and a pent-1-ene molecule at 293K by carrying out B.E.T. measurements for each adsorbate on the same anatase sample. $A_g$ for several carbon blacks was then determined by adsorption of each adsorbate and using the apparent area per molecule based on the anatase area. Internal consistency of better than 2% was found between Ar, $N_2$ and pentane, and it is interesting to note that the area used for the Ar molecule was 0.166 $nm^2$ as opposed to 0.144 $nm^2$ based on a close-packed liquid. This supports the view that areas determined by Ar adsorption tend to be low.

More recently, Pierce and Ewing (1964) have suggested that areas of graphites determined by $N_2$ adsorption are also too low. They measured the surface area of a uniform graphite and found that while the areas determined by adsorption of benzene, n-hexane, and ethyl chloride agreed with one another, agreement with $N_2$ areas could only be obtained when a value of 0.20 $nm^2$ was taken for the $N_2$ cross-section. They postulated that the $N_2$ molecules were localised, being centred over a hexagonal graphite lattice site. Thus the nitrogen molecules are not close-packed but each molecule occupies four hexagonal units, giving a theoretical area of 0.21 $nm^2$.

Inspection of the nitrogen isotherm reveals a hump between v values of 28 and 42 $cm^3$ S.T.P. $g^{-1}$, i.e. between monolayer and second layer coverage, centred at approximately $v = 34$ $cm^3$ S.T.P. $g^{-1}$ ($\theta = v/v_m = 1.7_2$) and $p/p_o = 0.37$. This behaviour has been reported in the literature (Beebe, Millard and Cynarski, 1953; Joyner and Emmett, 1948; Corrin, 1951) for $N_2$ and Ar on Graphon at low temperatures. It occurs just before the theoretical completion of the second molecular layer and has been attributed to lateral interactions between adsorbed molecules in the second layer. Beebe et al (1953) and Joyner et al (1948) investigated the hump in more detail and found peaks in a plot of the differential heat of adsorption against coverage, occurring just before

completion of the first and second layers. While both peaks are attributed to lateral adsorbate - adsorbate interactions, only the second shows in the isotherm since the first peak occurs in a very steep section of isotherm. Beebe et al (1953) also found some evidence for a third peak, close to the completion of a third layer.

4.1.2 *Isotherms above room temperature*

Isotherms for hydrogen, neon, krypton, xenon, methane, ethane and propane were determined at each of eight temperatures in the range 308.15K to 393.15K and at equilibrium pressures up to 50 cmHg. n-Butane isotherms were determined at 308.15K, 373.15K and 393.15K. The experimental data are given in Appendix C and individual isotherms are plotted in figures 4.2 to 4.9. The isotherms of $H_2$ and Ne are not very reliable since uptakes involved were very small, in some cases being within the limits of experimental error. Isotherms for $H_2$ and the inert gases were determined primarily to allow isothermal and non-isothermal flow data collected by Dolphin (1971) to be more fully interpreted. The hydrocarbon isotherms were measured for this investigation since comprehensive isotherm data at the temperatures used in the flow experiments were not available in the literature. From the limiting slope of the isotherm at low coverage $(dv/dp)_{p \to o}$, Henry law constants $k_s$, were determined:

$$k_s = \frac{\text{Gibbs excess surface concentration (mol cm}^{-2})}{\text{gas phase concentration (mol cm}^{-3})} = \frac{c'_s}{c'_g} \quad (4.2)$$

$$= \left(\frac{dv}{dp}\right) \cdot \frac{76}{A_g} \cdot \frac{T}{273.15} \cdot 10^{-4} \quad (4.3)$$

where $k_s$ is in cm and units of other parameters are as previously stated.

Sorption of hydrogen, neon, krypton and methane did not depart measurably from Henry's law over the pressure range investigated, while
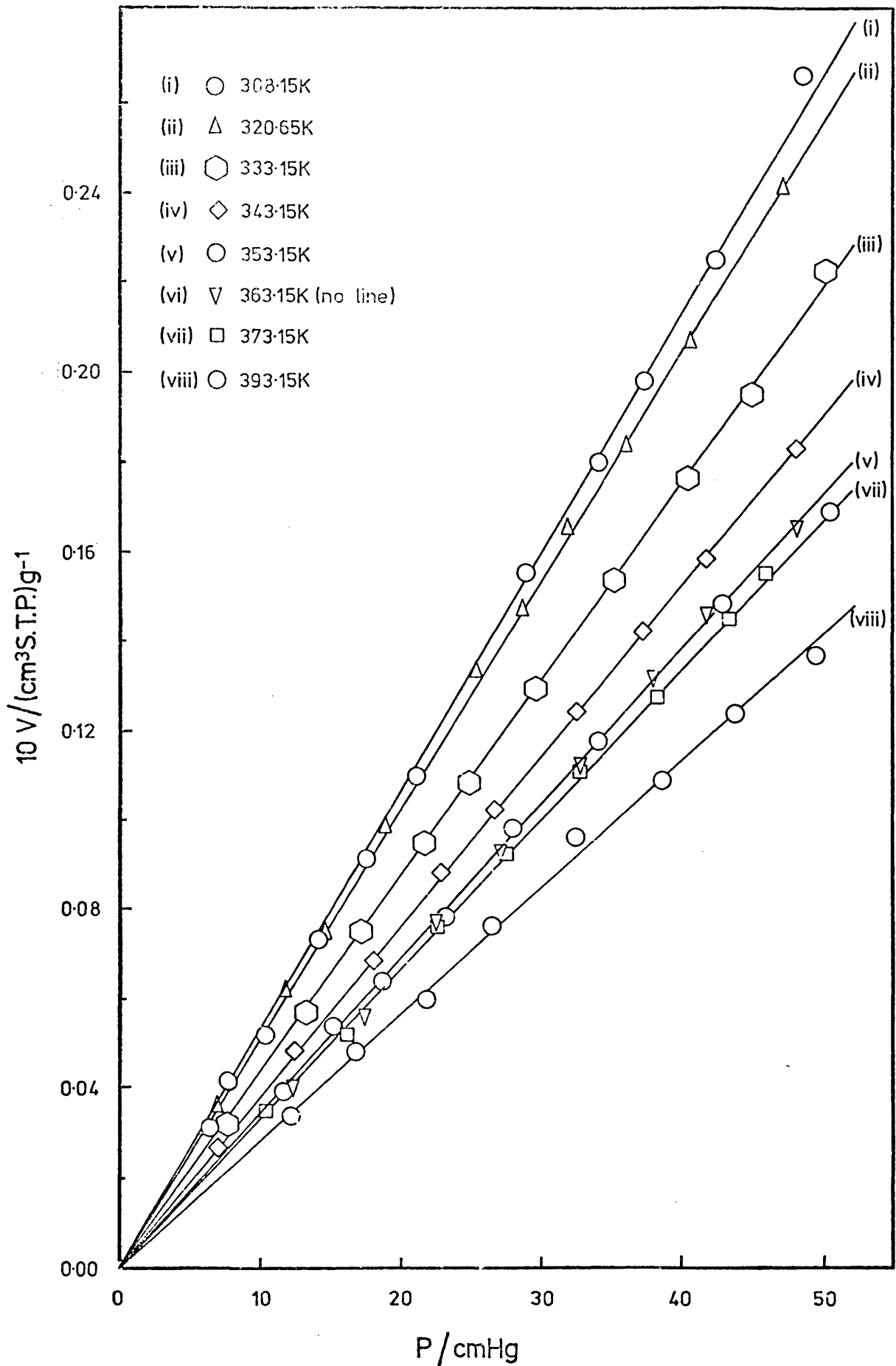
Figure 4.2          Hydrogen Isotherms
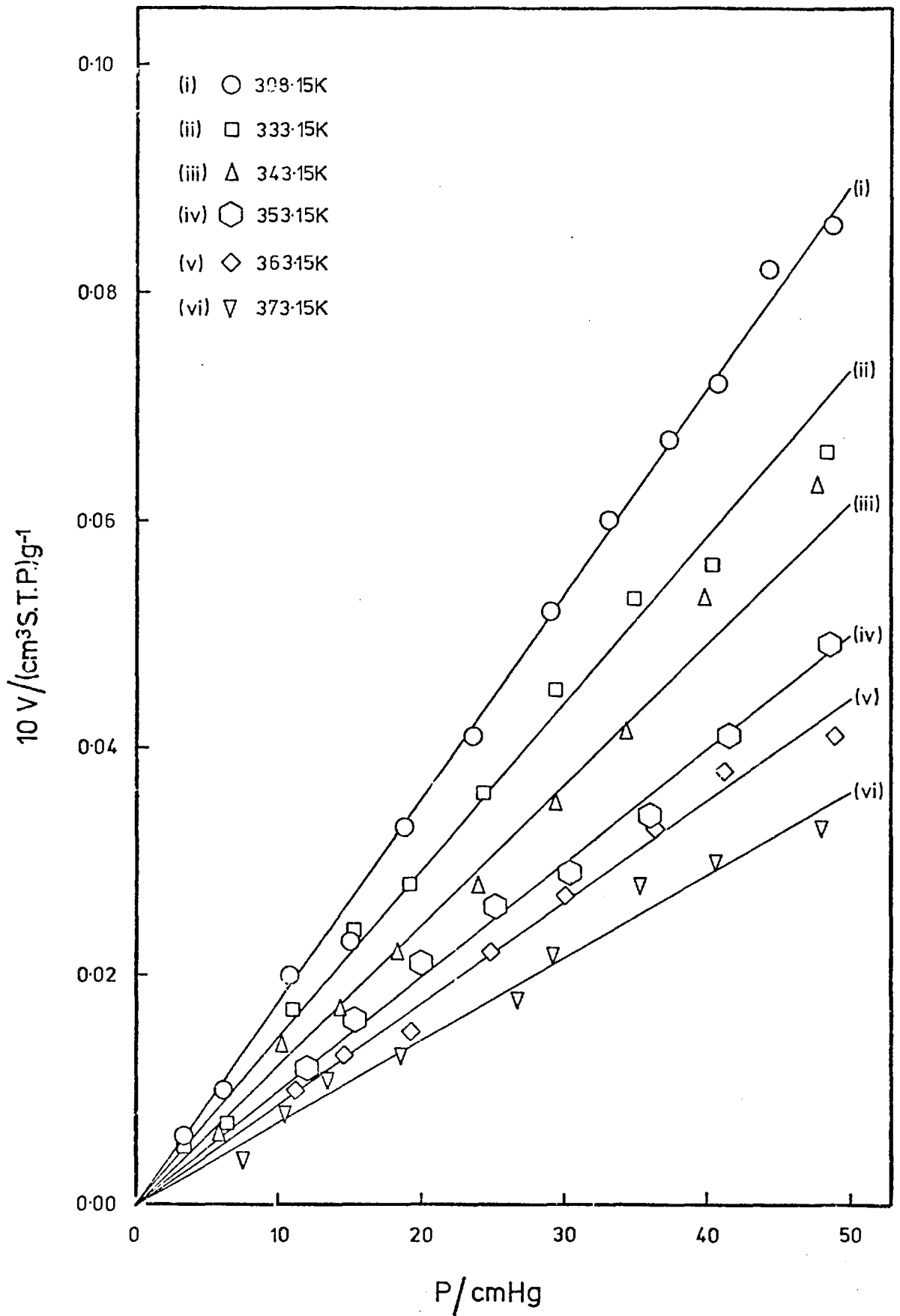
Figure 4.3          Neon Isotherms
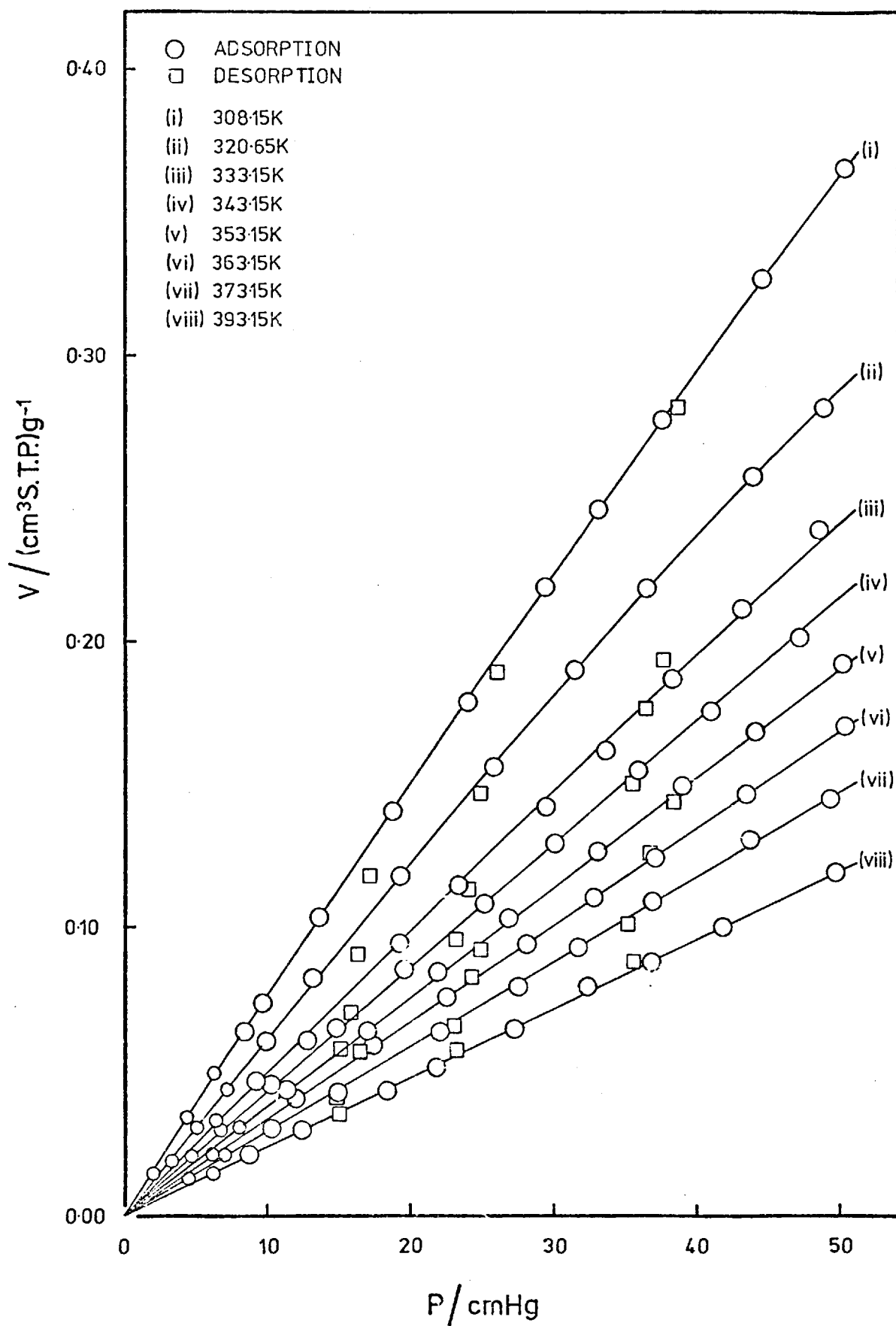
Figure 4.4     Krypton Isotherms
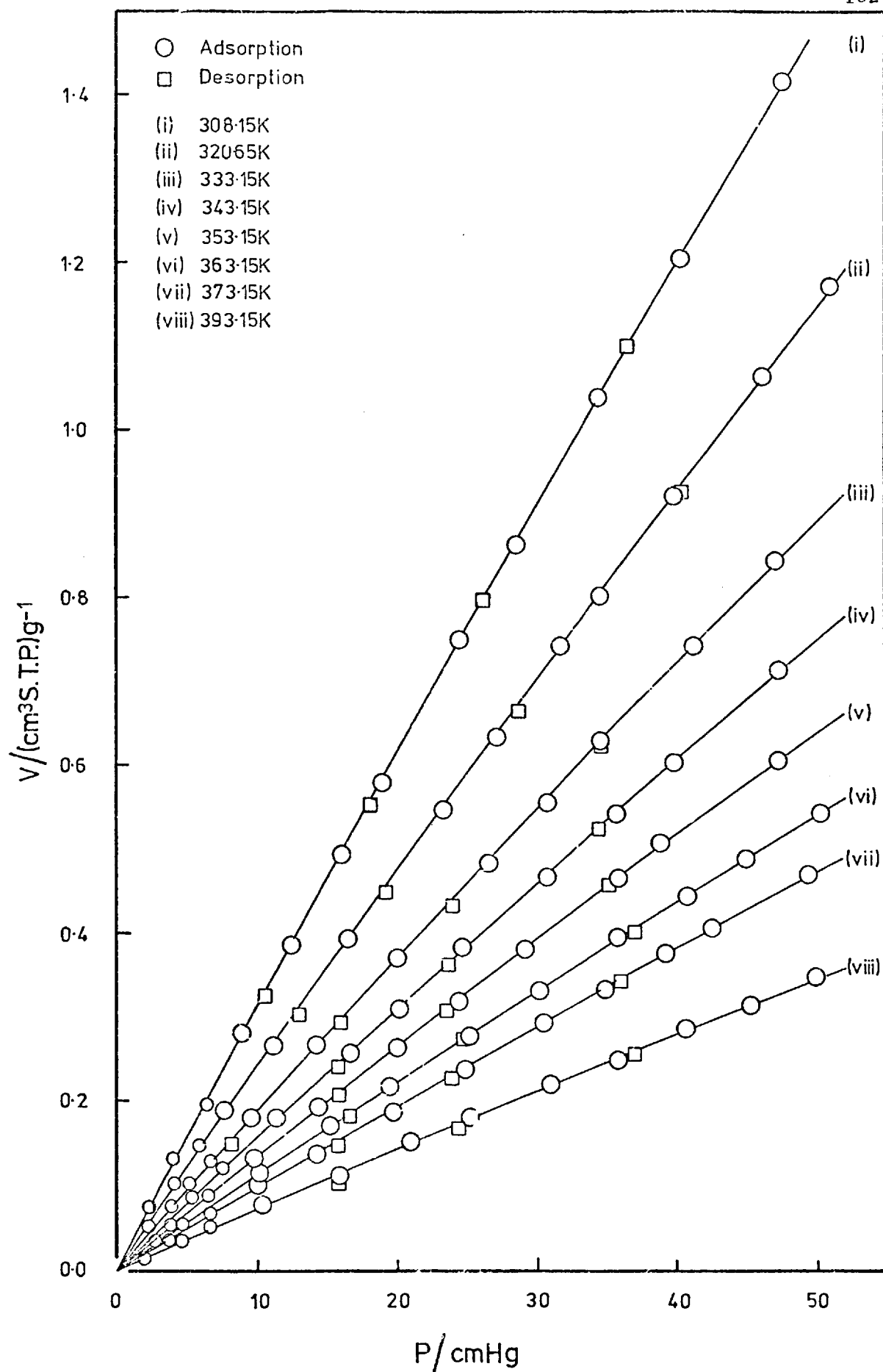
Figure 4.5    Xenon Isotherms
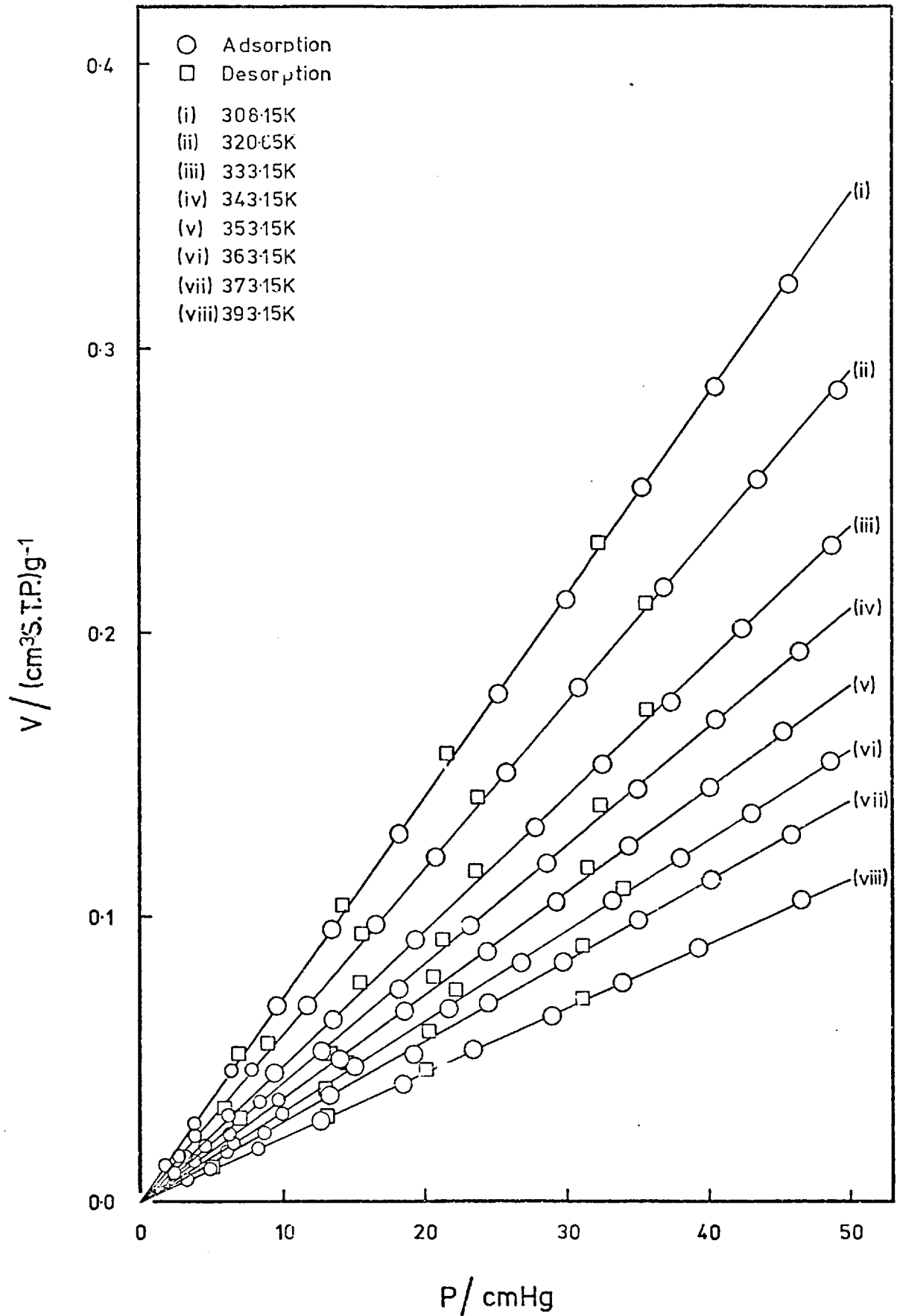
Figure 4.6          Methane Isotherms
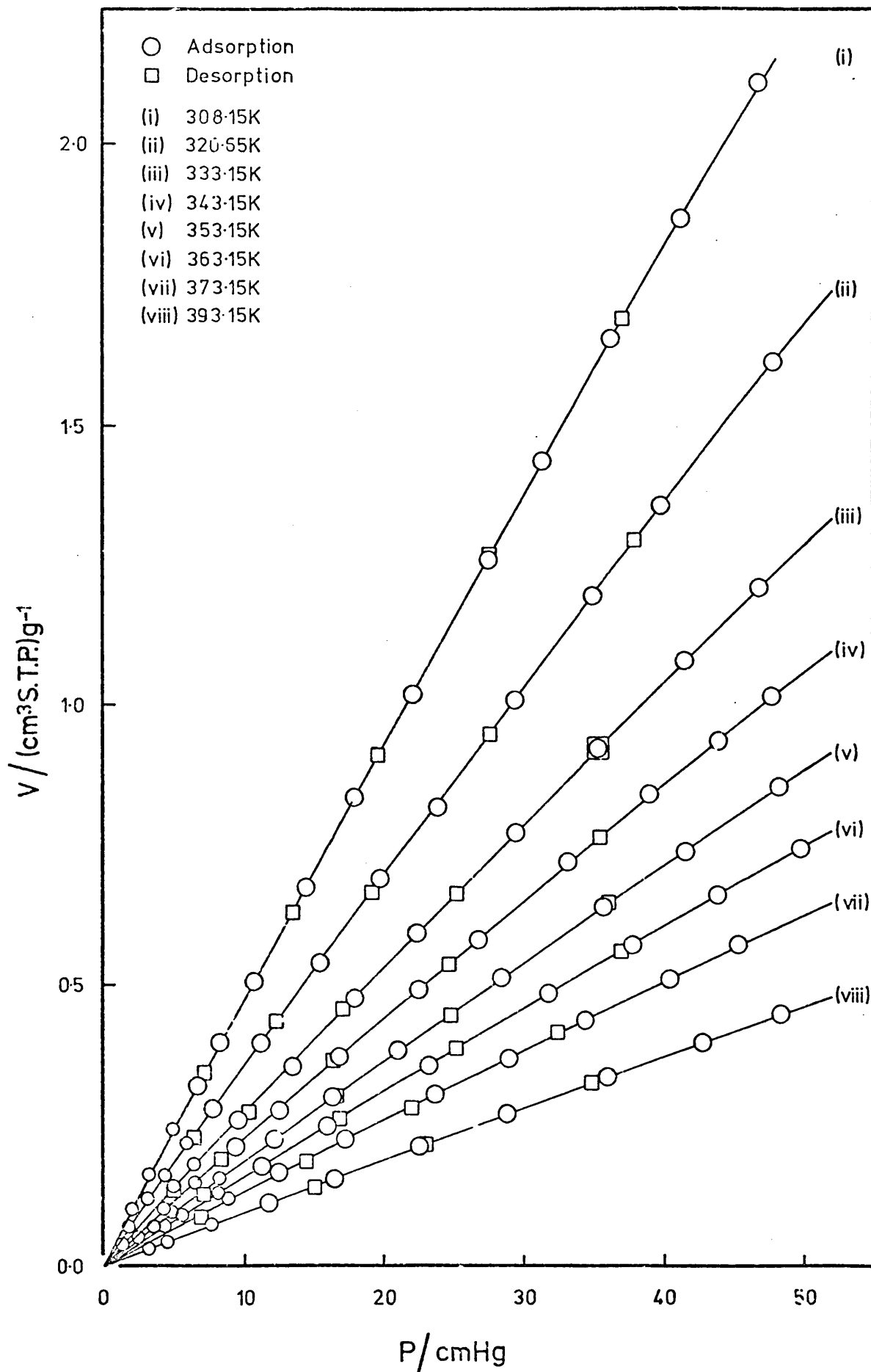
Figure 4.7        Ethane Isotherms
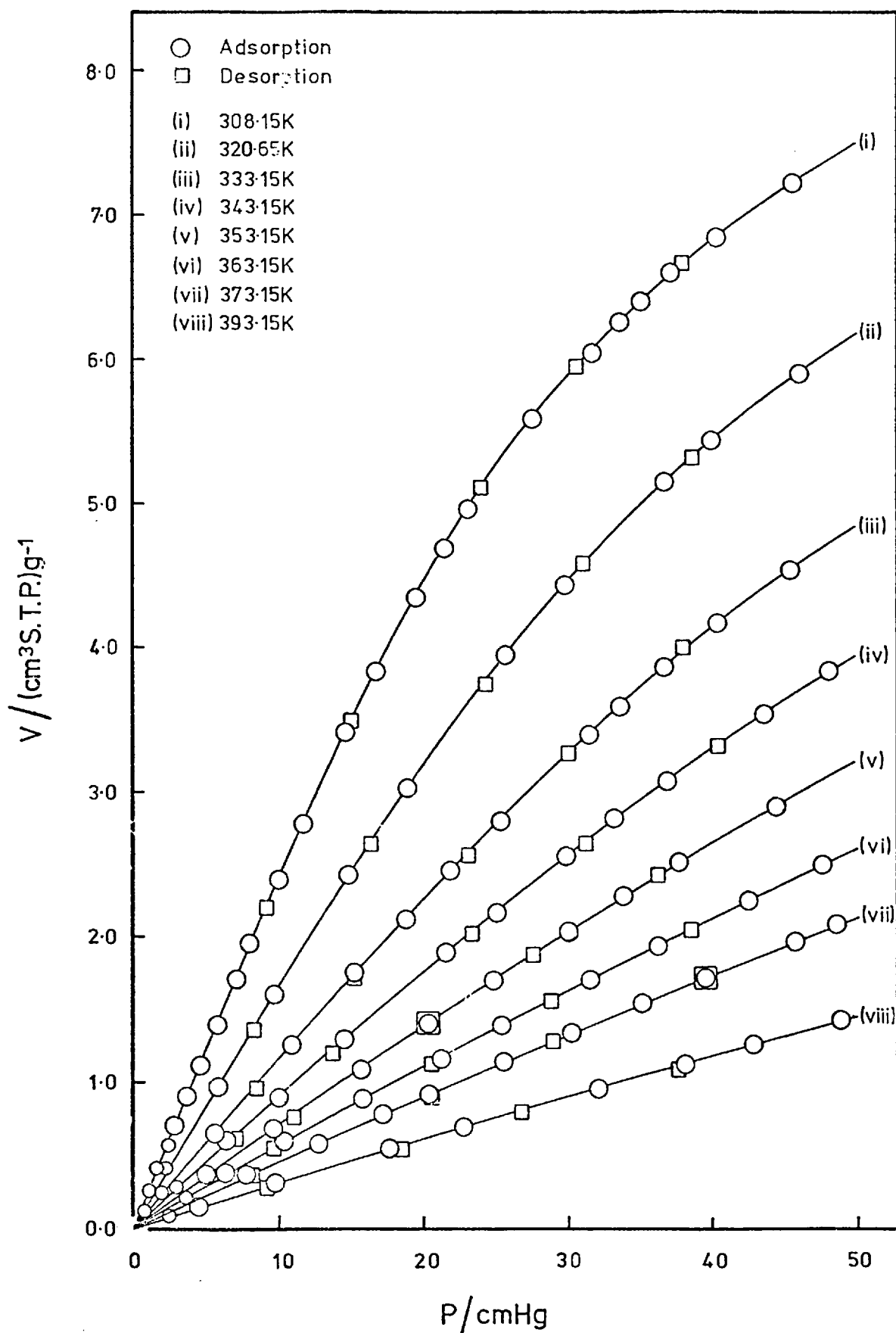
*Figure 4.8*          *Propane Isotherms*
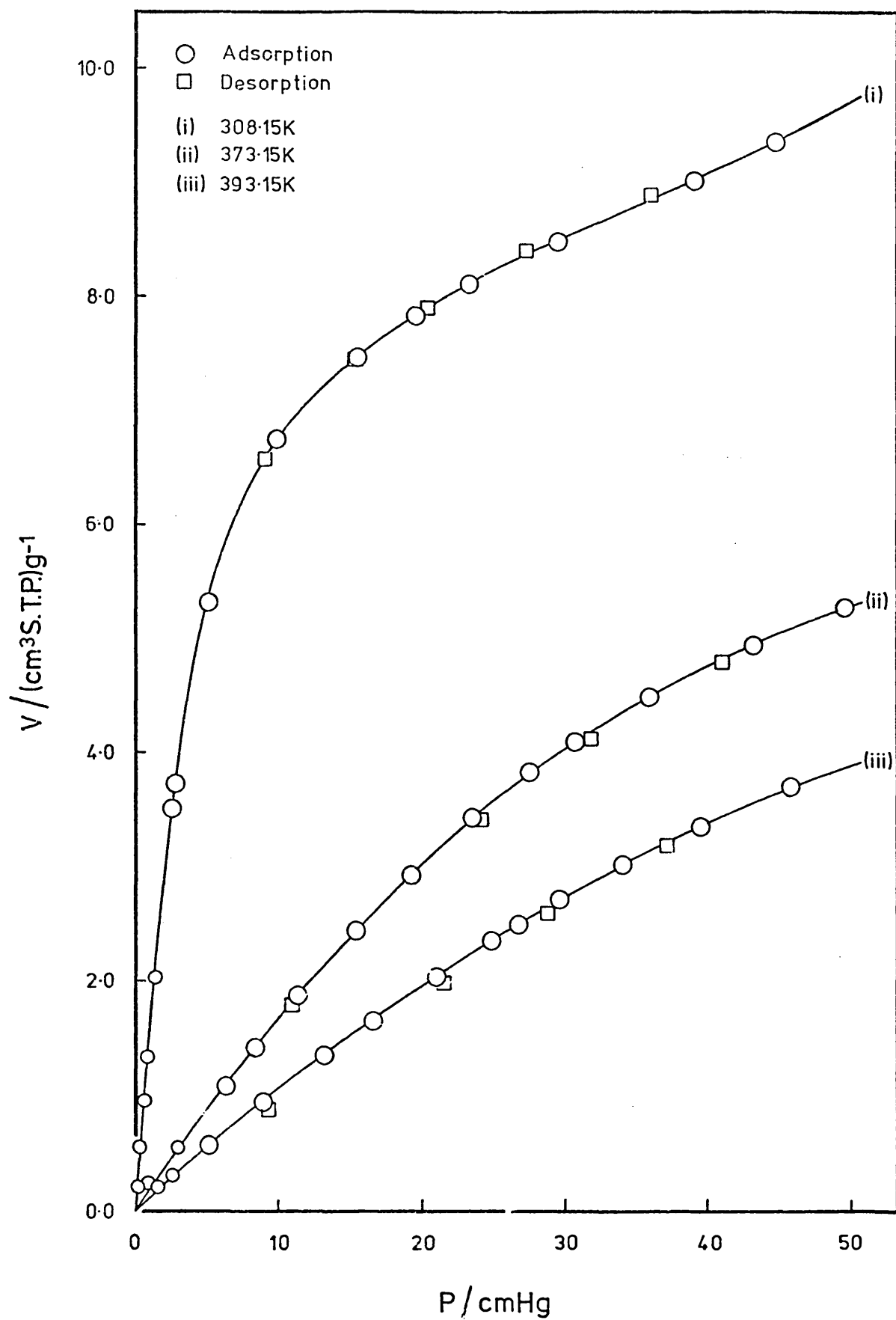
Figure 4.9        n-Butane Isotherms

departure for xenon and ethane was only slight. Propane and n-butane on the other hand, gave isotherms which were noticeably concave towards the pressure axis.

Given in table 4.2 are the values of $A_g k_s$ and of $k_s$ (taking $A_g$ as 86.2 $m^2 g^{-1}$), those for xenon and ethane being obtained from the limiting slope of the isotherm below 5 cmHg. The propane values were obtained using that portion of the isotherm below 2 cmHg and are consequently of low precision. n-Butane gave isotherms having no detectable Henry law region.

$k_s$ values for $H_2$ and Ne were erratic and so, for the purpose of comparison, smoothed values have also been presented in table 4.2. These were interpolated from the best straight line plot of $\log_{10} A_g k_s$ versus $1/T$.

### 4.1.3 *Isotherms of n-butane*

At 308.15K n-butane gave a type II isotherm with a fairly rounded 'knee', but was well suited to B.E.T. analysis (figure 4.9). Apparent monolayer uptake was found to be 7.88 $cm^3$ S.T.P. $g^{-1}$ and assuming an $A_g$ of 86.2 $m^2 g^{-1}$ (nitrogen B.E.T.) the area occupied by the n-butane molecule was found to be 0.407 $nm^2$. This compares well with the value of 0.397 $nm^2$ obtained by Beebe, Biscoe, Smith and Wendell (1947) at 273K, but is somewhat lower than the area suggested by Wynne-Jones(1958) of 0.47 $nm^2$ at 273.15K. The $v_m$ value agrees well with Beebe's value of 7.83 $cm^3$ S.T.P. $g^{-1}$ and with the determination of Ross and Good (1956) which gave 7.57 and 7.75 $cm^3$ S.T.P. $g^{-1}$.

### 4.1.4 *Experimental heats and energies of adsorption*

When Henry's law was obeyed, a heat of adsorption ($\Delta H'$) and an energy of adsorption ($\Delta E'$), defined in equations (4.4) and 4.5), could

## TABLE 4.2

*Henry Law Coefficients,* $k_s/cm$ *and* $A_g k_s/cm^3 \; g^{-1}$

| | T/K | 308.15 | 320.65 | 333.15 | 343.15 | 353.15 | 363.15 | 373.15 | 393.15 |
|---|---|---|---|---|---|---|---|---|---|
| **Adsorbate** | | | | | | | | | |
| Expt | $10^2.A_g k_s$ | 4.6 | 4.6 | 4.0 | 3.7 | 3.4 | 3.5 | 3.5 | 3.1 |
| | $10^8. k_s$ | 5.3 | 5.3 | 4.7 | 4.2 | 3.9 | 4.0 | 4.0 | 3.6 |
| **H₂** Smooth | $10^2.A_g k_s$ | $4.6_3$ | $4.3_0$ | $4.0_2$ | $3.8_2$ | $3.6_4$ | $3.4_8$ | $3.3_3$ | $3.0_8$ |
| | $10^8. k_s$ | $5.3_7$ | $4.9_9$ | $4.6_6$ | $4.4_3$ | $4.2_2$ | $4.0_4$ | $3.8_7$ | $3.5_7$ |
| Expt | $10^2.A_g k_s$ | 1.5 | 1.7 | 1.4 | 1.2 | 1.0 | 0.9 | 0.8 | 1.1 |
| | $10^8.k_s$ | 1.8 | 1.9 | 1.6 | 1.4 | 1.2 | 1.0 | 0.9 | 1.3 |
| **Ne** Smooth | $10^2.A_g k_s$ | $1.6_1$ | $1.4_3$ | $1.2_8$ | $1.1_6$ | $1.1_0$ | $1.0_3$ | $0.9_6$ | $0.8_5$ |
| | $10^8. k_s$ | $1.8_6$ | $1.6_6$ | $1.4_8$ | $1.3_5$ | $1.2_7$ | $1.1_9$ | $1.1_1$ | $0.9_8$ |
| **Kr** | $10.A_g k_s$ | $6.4_1$ | $5.4_1$ | $4.5_7$ | $4.1_7$ | $3.8_0$ | $3.4_4$ | $3.0_3$ | $2.6_3$ |
| | $10^8. k_s$ | $74._4$ | $62._7$ | $53._0$ | $48._3$ | $44._1$ | $39._9$ | $35._2$ | $30._5$ |
| **Xe** | $10.A_g k_s$ | $28._4$ | $22._4$ | 18.0 | 16.0 | $13._7$ | $11._8$ | $10._6$ | $8.0_3$ |
| | $10^8..k_s$ | 330. | 260. | 209. | 186. | 159. | 137. | 122. | $93._2$ |
| **CH₄** | $10.A_g k_s$ | $6.1_0$ | $5.2_3$ | $4.4_3$ | $3.9_8$ | $3.5_8$ | $3.1_2$ | $2.9_5$ | $2.5_3$ |
| | $10^8. k_s$ | $70._8$ | $60._7$ | $51._4$ | $46._2$ | $41._5$ | $36._2$ | $34._2$ | $29._3$ |
| **C₂H₆** | $10.A_g k_s$ | $43._8$ | $34._1$ | $26._5$ | $22._0$ | $18._8$ | $16._3$ | $13._8$ | $10._3$ |
| | $10^8. k_s$ | 508. | 396. | 307. | 256. | 218. | 189. | 161. | 119. |
| **C₃H₈** | $A_g. k_s$ | $22._8$ | $16._2$ | $12._1$ | $9.4_7$ | $7.9_2$ | $6.2_2$ | $5.2_3$ | $3.6_5$ |
| | $10^6. k_s$ | $26._5$ | $18._8$ | $14._0$ | $11._0$ | $9.1_9$ | $7.2_2$ | $6.0_7$ | $4.2_4$ |

be calculated from plots of $\ln (v/p)$ and $\ln (A_g.k_s)$ against $T^{-1}$.

$$\Delta H' = -R \left( \frac{\partial \ln (v/p)}{\partial T^{-1}} \right)_V = RT^2 \left( \frac{\partial \ln (v/p)}{\partial T} \right)_V \qquad (4.4)$$

$$\Delta E' = -R \frac{d \ln (vT/p)}{dT^{-1}} = RT^2 \frac{d \ln(A_g k_s)}{dT} = RT^2 \frac{d\ln k_s}{dT} \qquad (4.5)$$

Where it has been possible to determine $k_s$, then $\Delta H'$ and $\Delta E'$ have been calculated in this way and are given in table 4.3. Good straight lines were obtained and the slopes $(\partial \ln (v/p)/\partial T^{-1})_V$ and $(d\ln(A_g k_s)/dT^{-1})$ were evaluated by a least mean squares analysis. However in the case of $H_2$ there was a considerable scatter of results, and with Ne, the points were so scattered that no reliable values of $\Delta E'$ or $\Delta H'$ could be determined.

TABLE 4.3

$\Delta H'$, $\Delta E'$ and $q'_{st}$ *for sorption by Graphon*

| Adsorbate | $\dfrac{-\Delta H'}{kJ\ mol^{-1}}$ | $\dfrac{-\Delta E'}{kJ\ mol^{-1}}$ | $\dfrac{q'_{st}}{kJ\ mol^{-1}}$ | $\dfrac{(-\Delta E')^{*}}{kJ\ mol^{-1}}$ |
|---|---|---|---|---|
| $H_2$ | 7.7 | 4.8 | – | – |
| Kr | 13.5 | 10.5 | – | – |
| Xe | 17.6 | 14.7 | $18.0_5$ | 15.2 |
| $CH_4$ | 13.5 | 10.7 | 13.6 † | – |
| $C_2H_6$ | 20.0 | 17.1 | 20.6 | 17.7 |
| $C_3H_8$ | 24.7 | 21.7 | 25.0 | 22.1 |
| $n-C_4H_{10}$ | – | – | 30.7 | 27.8 |
| * – $\Delta E'$ obtained from $q'_{st}$ using eqn.(4.9) | | | | |
| † $q'_{st}$ obtained from – $\Delta E'$ using eqn.(4.9) | | | | |

TABLE 4.4

*Literature Values of $q_{st}'$ for Sorption of Hydrocarbons by Graphon* $(kJ \, mol^{-1})$

| Adsorbent | Adsorbate | | | | Method | References |
|---|---|---|---|---|---|---|
| | $CH_4$ | $C_2H_6$ | $C_3H_8$ | $n\text{-}C_4H_{10}$ | | |
| Graphon | 13.6 | 20.6 | 25.0 | 30.7 | Adsorption Isotherms | This work |
| " | – | – | – | 36.0 | | Beebe, Biscoe et al, 1947 |
| " | – | – | – | 34.3 | | Ross and Good, 1956 |
| " | – | – | – | 33.0 | Chromat-ography | Chirnside and Pope, 1964 |
| " | – | 23.5 | 35.1 | 51.0 | | Di Corcia and Samperi, 1973 |
| $H_2$-treated Graphon | – | 19.7 | 24.7 | 30.7 | | Di Corcia and Samperi, 1973 |
| Theoretical | 14.6 | 20.1 | 27.2 | 34.4 | | Lal and Spencer, 1974 |

With the more strongly adsorbed gases, Xe, $C_2H_6$, $C_3H_8$ and $n\text{-}C_4H_{10}$, it was possible to evaluate the isosteric heat of adsorption, $q_{st}'$, defined by equation (4.6).

$$q_{st}' = -R \left( \frac{\partial \ln p}{\partial T^{-1}} \right)_v = RT^2 \left( \frac{\partial \ln p}{\partial T} \right)_v \tag{4.6}$$

This is derived at constant uptake or surface coverage, and the limiting value of $q_{st}'$ as v tends to zero can serve to evaluate $\Delta E'$ where the isotherm is too curved, even at low uptakes, to evaluate Henry law constants. Thus from equation (4.3).

$$\ln A_g . k_s = \ln v + \ln T - \ln p + \text{Constant} \tag{4.7}$$

therefore $\quad RT^2 \left( \frac{\partial \ln A_g k_s}{\partial T} \right)_v = RT - RT^2 \left( \frac{\partial \ln p}{\partial T} \right)_v \tag{4.8}$

or $\quad \Delta E' = RT - q_{st}' \tag{4.9}$

Values of $\Delta E'$ calculated in this way, as well as the limiting value of $q'_{st}$, are given in table 4.3 for those gases where deviation from the Henry law was found. The mean of the isotherm temperatures, 348.5K, was used in this expression.

When Henry's law is obeyed it can be shown from equation (4.4) that $q'_{st} = -\Delta H'$. Examination of table 4.3 shows that this was observed to within 2.5%.

In the series of hydrocarbons studied there was found to be a linear relationship between $-\Delta E'$, or $q'_{st}$, and n, the number of carbon atoms in the molecule, as shown in figure 4.10. From this plot the average increment in $q'_{st}$, per $-CH_2-$ unit was found to be 5.4 kJ $mol^{-1}$. This behaviour agrees approximately with the theoretical treatment of Lal and Spencer (1974), where interaction energies between various hydrocarbon molecules and the surface of a graphite lattice were calculated by a Monte Carlo method. They found $q'_{st}$ to be linear with n in the range 2 to 6 and the theoretical increment in $q'_{st}$ per $-CH_2-$ unit was 7.3 kJ $mol^{-1}$ within this range. Experimental values have been obtained in the range 4 to 8 kJ $mol^{-1}$ and span the increment found in this work. Elkington and Curthoys (1969) for example found an increment per carbon atom of 4.6 kJ $mol^{-1}$ on Sterling MTD4.

Values of limiting isosteric heats of adsorption compared with those given in the literature are shown in table 4.4. Reasonably good agreement is found, especially with the values obtained by Di Corcia and Samperi for hydrogen-treated Graphon, and the theoretical heats calculated by Lal and Spencer.

4.1.5 *Variation of* $q'_{st}$ *with coverage*

Additional information concerning the adsorbent surface can be obtained by evaluating $q'_{st}$ at various degrees of surface coverage. In
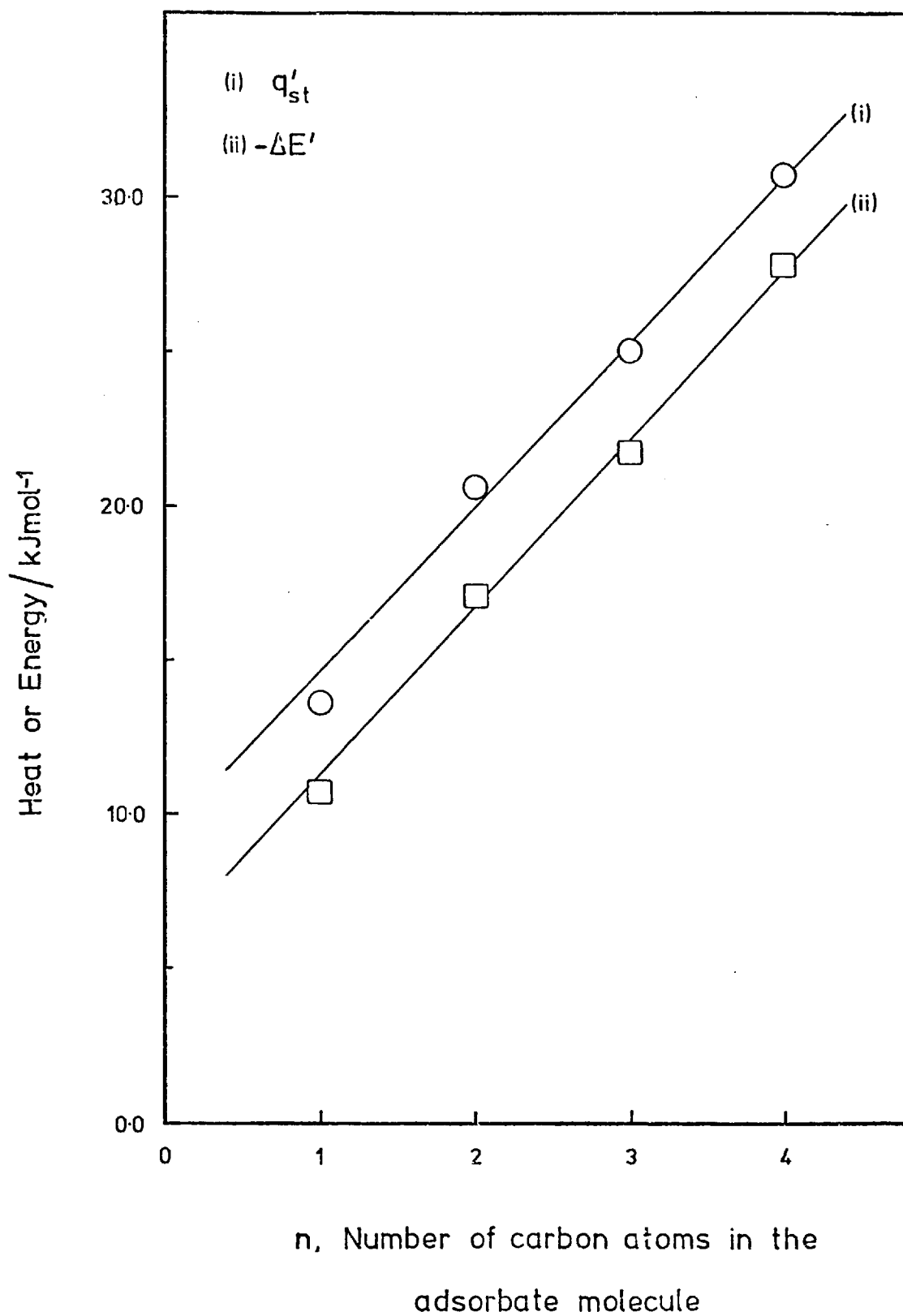
*Figure 4.10*     *Variation of* $q'_{st}$ *and* $-\Delta E'$ *with* n
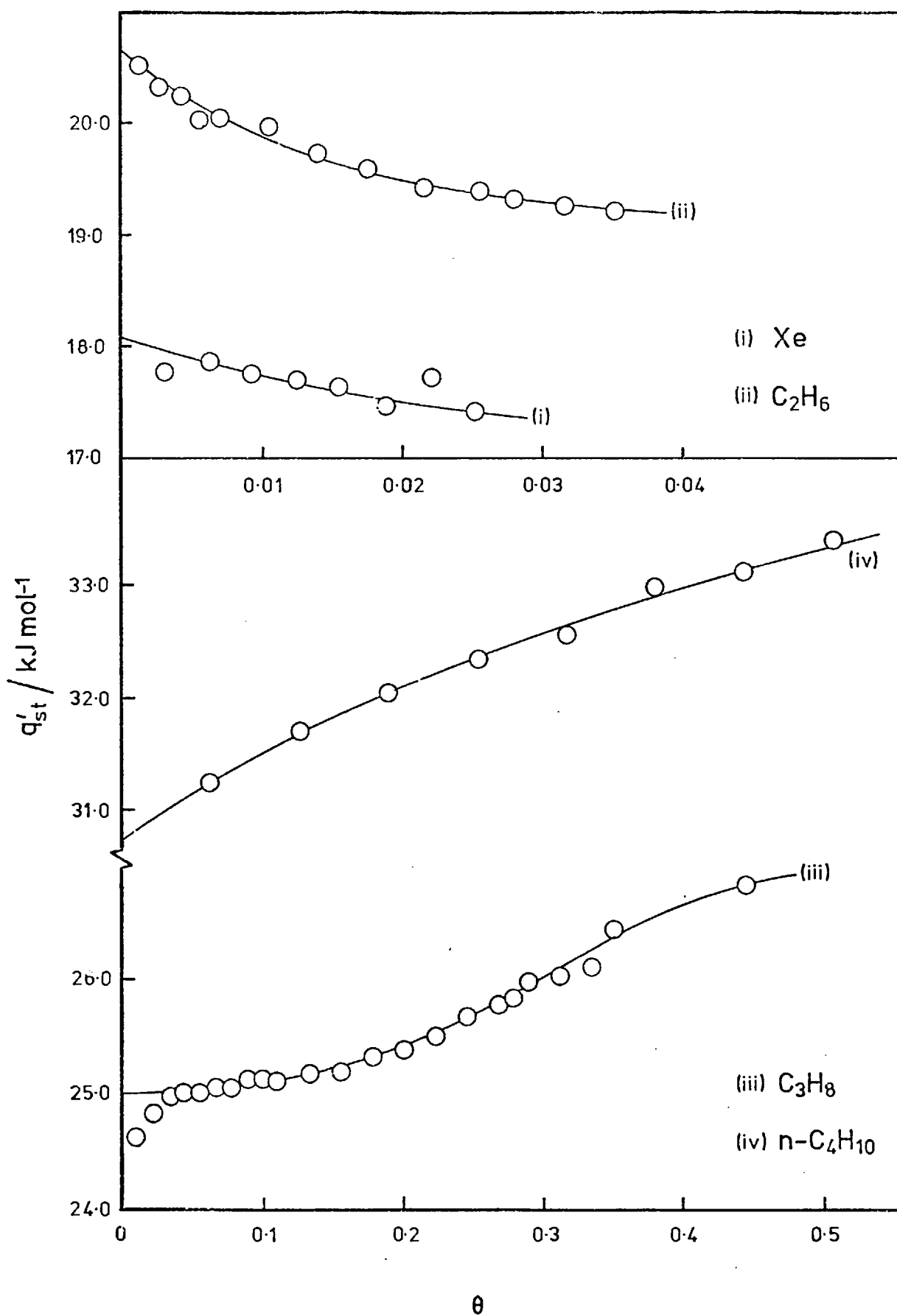
*Figure 4.11*        $q'_{st}$ *as a function of coverage,* $\theta$

figure 4.11 $q'_{st}$ has been plotted against $\theta \; (= v/v_m)$, the fraction of

monolayer coverage. $v_m$ was based upon a carbon area of 86.2 $m^2 \; g^{-1}$

and experimental areas per molecule of 0.202, 0.225, 0.357 and 0.407 $nm^2$

for Xe, $C_2H_6$, $C_3H_8$ and $n-C_4H_{10}$ respectively.

$q'_{st}$ for xenon and, more noticeably, for ethane is found to decrease

with increasing coverage. This can be attributed to initial preferential

uptake on more energetically sorbing surface sites, followed by adsorption

on less energetically sorbing sites. $q'_{st}$ thus falls and indicates some

degree of energetic heterogeneity of the Graphon surface.

As $\theta$ for Xe and $C_2H_6$ is very small (less than 0.05), each adsorbate

molecule is effectively isolated from its neighbours and energetic

heterogeneity can readily be detected. However, with the larger, more

strongly adsorbed molecules, $C_3H_8$ and $n-C_4H_{10}$, $\theta$ is much greater. The

ad-molecules approach one another more closely and lateral interactions

become possible, thus tending to increase $q'_{st}$. Figure 4.11 reveals

an increase in $q'_{st}$ for $C_3H_8$ and $n-C_4H_{10}$ and from the propane results

it would appear that lateral interactions begin to occur after $\theta = 0.1$.

Any heterogeneity in the region up to $\theta = 0.04$ would not be noticed since

this corresponds to part of the isotherms at very low pressure where few

data points are available. The apparent sharp rise in $q'_{st}$ to $\theta = 0.02$

is likewise explained by the inadequate precision of measurements at

low p. The $n-C_4H_{10}$ results are less accurate, $q'_{st}$ being determined from

isotherms at only three temperatures. Ross and Good (1956) detected

adsorbate – adsorbate interactions by a rise in $q'_{st}$ for $C_3H_8$ on Graphon

reaching a maximum at $\theta \approx 0.7$ and falling to a value corresponding to

the heat of liquefaction at $\theta = 1.0$. However they detected little

increase in $q'_{st}$ below $\theta = 0.4$.

Although Graphon is commonly taken to be a graphitised carbon

black having a substantially energetically homogeneous surface, there

is evidence in the literature as well as in this work, of a small

amount of energetic heterogeneity. From adsorption measurements with

$N_2$ and Ar, Beebe et al (1953) also suggested some physical heterogeneity

of the surface, and Graham (1957) likewise deduced a small amount of

geometric heterogeneity from $N_2$ isotherms at 77.5 and 90.3K and at very

low coverage. By measurement of the initial curvature of the isotherm

he found that strong adsorption took place on 1.25% of the surface sites,

and suggested that these sites occurred where an ad-molecule was in

contact with a geometric irregularity eg a step or kink site. $q'_{st}$ for

such sites was calculated to be 16.7 kJ $mol^{-1}$ as opposed to 8.3 kJ $mol^{-1}$

for the bulk of sites. This suggested two-fold bonding eg. an ad-molecule

located between two parallel sheets. From the $N_2$ isotherm at 77.5K he

calculated $v_m$ to be 18.80 $cm^3$ S.T.P. $g^{-1}$, composed of $v_m$ (strong) of

$0.23_4$ and $v_m$ (weak) of $18.5_7$ $cm^3$ S.T.P. $g^{-1}$. (Compare $v_m$ of 19.80

$cm^3$ S.T.P. $g^{-1}$ found in this work). He also pointed out that approximately

1% of surface sites on Graphon were involved in hydrogen bonding (due to

the presence of OH groups): these sites were less energetic than normal

and so did not affect the isotherm. Isirikyan and Kiselev (1962) also

deduced some heterogeneity of Graphon from isotherms and $q'_{st}$ of nitrogen,

benzene and n-hexane.

More recently Di Corcia and Samperi carried out adsorption studies

on several carbon blacks, including Graphon, at very low surface coverage,

using gas-solid chromatography. They worked principally with the lower

alkanes and found that treating the carbon with hydrogen at $1000^{o}C$, besides

removing chemical impurities, such as chemisorbed oxygen, also removed

geometric irregularities. This was manifest by a decrease in $q'_{st}$ after

treatment.

## 4.2    THERMODYNAMICS OF ADSORPTION

In order to derive exact and useful heats of adsorption and

thermodynamic quantities from adsorption isotherms, a model must first be assumed for the adsorbate – adsorbent system.

Three treatments have been proposed (Young and Crowell, 1962):

(i) Equilibrium is considered to exist between the gaseous adsorbate, the adsorbent and the adsorbed particles. Exact thermodynamic quantities are obtained, but they are of limited usefulness.

(ii) Solution thermodynamics (Everett, 1950; Hill, 1952). The adsorbent atoms and the adsorbed particles are considered to form a single, independent phase, having the properties of a solution; equilibrium exists between this phase and the gas phase.

(iii) Inert adsorbent (Everett, 1950). The solid adsorbent is considered to be thermodynamically inert and equilibrium is established between gaseous adsorbate and an adsorbed phase.

Solution and inert adsorbent (or adsorption) thermodynamics are the most frequently used, and the thermodynamic relationships derived from each are identical. However the physical interpretation of the quantities involved differs and depends on the assumptions made in the treatment.

Clint (1966) has reviewed solution and adsorption thermodynamics with particular reference to adsorption in the Henry law and sub-monolayer range. Essential points in the solution thermodynamic treatment will now be given.

4.2.1 *Solution thermodynamics*

Equilibrium is assumed to exist between the solution, having a mole fraction of adsorbate $x_s = n_s/(n_s + n_a)$ ($n_s$ and $n_a$ are the number of moles of sorbate and adsorbent respectively), and the pure gas phase. Changes in temperature, pressure and composition are considered to bring about infinitesimal changes in chemical potential of sorbate in the condensed phase (d $\mu_s$) and in chemical potential of the pure gas phase (d $\mu_g$).

Since the system is at equilibrium, then $d\,\mu_g = d\,\mu_s$ and it can be shown that

$$- \tilde{S}_g dT + \tilde{V}_g dp = - \bar{S}_s dT + \bar{V}_s dp + \left(\frac{\partial \mu_s}{\partial x_s}\right)_{p,T} dx_s \qquad (4.10)$$

where S represents entropy and V, volume, subscripts $_g$ and $_s$ refer to gas phase and adsorbed phase, and $-$ and $\sim$ denote partial and total molar quantities.

At constant composition $dx_s = 0$ and it follows that a Clausius Clapeyron type of equation can be deduced:

$$\left(\frac{\partial p}{\partial T}\right)_{x_s} = \frac{\bar{S}_s - \tilde{S}_g}{\bar{V}_s - \tilde{V}_g} = \frac{\bar{H}_s - \tilde{H}_g}{T(\bar{V}_s - \tilde{V}_g)} = \frac{\Delta \bar{H}'}{T(\bar{V}_s - \tilde{V}_g)} \qquad (4.11)$$

where H represents enthalpy and $\Delta\bar{H}$ is a partial molar heat of adsorption, regarded as the partial molar heat of solution of a gas in a solution of composition $n_s + n_a$.

In applying equation (4.11) to adsorption isotherms, difficulties arise in (i) deciding the meaning of constant $x_s$ and (ii) in interpreting $\bar{V}_s$.

Assuming $n_a$ to be constant, then constant $x_s$ implies constant $n_s$, the number of moles of sorbate in the condensed phase. A physical interpretation of the condensed phase is now required. If it consists solely of the adsorbent and the experimentally measured surface excess, $A_s c_s'$ (where $c_s'$ is the Gibbs excess number of moles of sorbate per unit area arising as a result of adsorption and $A_s$ is the surface area of $n_a$ moles adsorbent), then $n_s = A_s \cdot c_s' = n_s'$. Hence we obtain

$$\left(\frac{\partial p}{\partial T}\right)_{x_s} = \left(\frac{\partial p}{\partial T}\right)_{n_s} = \left(\frac{\partial p}{\partial T}\right)_{c_s'} = \frac{\Delta \bar{H}}{T(\bar{V}_s - \tilde{V}_g)} \qquad (4.12)$$

However, a more realistic interpretation of the condensed phase is

obtained by considering it to comprise the $n_a$ moles of adsorbent and the number of moles of sorbate in a uniform layer surrounding it. $n_s$ will now consist of the surface excess, $A_s \, c_s'$, and also the number of moles of gaseous adsorbate which would be included in this surrounding layer if the gas phase was continued unchanged right up to the adsorbent surface. If $V_s$ is the volume of this surface phase then

$$n_s = A_s \, c_s' + V_s/\tilde{V}_g = n_s' + V_s/\tilde{V}_g \qquad (4.13)$$

When sorption occurs to any appreciable extent ($\theta > 0.1$, say) then $A_s \, c_s'$ is large compared with $V_s/\tilde{V}_g$ and it is then usually a good approximation to neglect this term and hence $n_s = n_s'$.

Where the extent of adsorption is small, however, e.g. $H_2$ and Ne at room temperature, the extra moles occurring in $V_s$ due to sorption will be so small as to be commensurable with $V_s/\tilde{V}_g$ and so must be allowed for in calculating $n_s$. An estimate must thus be made of the sorption volume, $V_s$. One simple approximation (Clint 1966; Dolphin 1971; Ash, Barrer, Clint, Dolphin and Murray, 1973) has been to consider this sorption volume as consisting of a layer, one molecular diameter in thickness, $\delta$, surrounding the adsorbent. i.e. $V_s = A_s \delta$.

We must now consider the meaning of $\bar{V}_s$ defined by (4.14).

$$\bar{V}_s = \left( \frac{\partial V_c}{\partial n_s} \right)_{T,p,n_a} \qquad (4.14)$$

where $V_c = V_s + V_a$ = volume of the condensed phase. If $V_c$ is considered to be constant, then at any submonolayer coverage, addition of sorbate to the sorption volume will increase its concentration but $V_s$ and $V_c$ will remain constant. Hence $\bar{V}_s = 0$ and equation (4.11) can be written as

$$\left( \frac{\partial p}{\partial T} \right)_{x_s} = \left( \frac{\partial p}{\partial T} \right)_{n_s} = - \frac{\Delta \bar{H}}{T \bar{V}_g} \qquad (4.15)$$

For a perfect gas $\tilde{V}_g = RT/p$ and so

$$\left(\frac{\partial p}{\partial T}\right)_{n_s} = -p\frac{\Delta\bar{H}}{RT^2} \quad \text{or} \quad \left(\frac{\partial \ln p}{\partial T}\right)_{n_s} = -\frac{\Delta\bar{H}}{RT^2} \tag{4.16}$$

This can be compared with $q'_{st}$ $(= RT^2 (\partial \ln p/\partial T)_{n'_s})$. When $n_s = n'_s$, then $q'_{st} = -\Delta\bar{H}$.

However, without making any assumptions about $\bar{V}_s$, from equation (4.12) we can define an isosteric heat for absolute sorption as

$$q_{st} = RT^2\left(\frac{\partial \ln p}{\partial T}\right)_{n_s} = -\frac{\Delta\bar{H}}{(1 - \bar{V}_s/\bar{V}_g)} \tag{4.17}$$

$q_{st}$ refers to the absolute adsorption of $n_s$ moles whereas $q'_{st}$ refers to the adsorption of the Gibbs excess uptake, $n'_s$. Barrer and Papadopoulos (1972) derived a relationship between $q_{st}$ and $q'_{st}$ as :

$$\frac{q'_{st}}{q_{st}} = \frac{(\partial n'_s/\partial T)_p \cdot (\partial n_s/\partial p)_T}{(\partial n_s/\partial T)_p \cdot (\partial n'_s/\partial p)_T} \tag{4.18}$$

For an ideal gas this becomes:

$$\frac{q'_{st}}{q_{st}} = \left\{1 + \frac{V_s}{RT}\left(\frac{\partial p}{\partial n'_s}\right)_T\right\} \div \left\{1 - \frac{pV_s}{RT^2}\left(\frac{\partial T}{\partial n'_s}\right)_p\right\} \tag{4.19}$$

Using the relations $n'_s = A_s \cdot c'_s$ and $V_s = A_s \cdot \delta$ this can be rearranged to :

$$\frac{q'_{st}}{q_{st}} = \left\{1 + \frac{\delta}{RT}\left(\frac{\partial p}{\partial c'_s}\right)_T\right\} \div \left\{1 - \frac{p\delta}{RT^2}\left(\frac{\partial T}{\partial c'_s}\right)_p\right\} \tag{4.20}$$

By manipulation it can be shown that in the Henry law range

$$\left(\frac{c'_s}{T}\right) \cdot \left(\frac{\partial T}{\partial c'_s}\right)_p = -\frac{RT}{q'_{st}} \tag{4.21}$$

and by substituting this relationship into equation (4.20) we obtain

$$q_{st} = \frac{q'_{st} \cdot k_s + RT\delta}{k_s + \delta} \tag{4.22}$$

This expression can be used to evaluate a heat of adsorption, $\Delta E$, referring to absolute sorption. By analogy with equation (4.9) we can define $\Delta E$ as $\Delta E = RT - q_{st}$, hence we obtain the relation

$$\Delta E = \left(\frac{k_s}{k_s + \delta}\right) . \Delta E' = RT^2 \frac{\partial \ln(k_s + \delta)}{\partial T} \tag{4.23}$$

A study of equations (4.22) and (4.23) will reveal that, in magnitude, $q'_{st} \geqslant q_{st}$ and $\Delta E' \geqslant \Delta E$, equality occurring when $k_s \gg \delta$. This corresponds with strong adsorption in which the number of sorbed molecules is far greater than the number of sorbate molecules which would have been present in the sorption volume in the absence of sorption.

## 4.3. APPLICATION OF ADSORPTION THERMODYNAMICS TO EXPERIMENTAL DATA

### 4.3.1 $q_{st}$ and $\Delta E$ for absolute sorption

Experimental data (tables 4.2 and 4.3) can be used to demonstrate the effect of finite sorption volume and to obtain energies for absolute sorption, $\Delta E$. In table 4.5 $\Delta E$ has been calculated at the highest and lowest temperatures used in this study. For $H_2$ the smoothed $k_s$ values have been used and the values chosen for $\delta$ were the molecular diameters which have been assumed to be independent of temperature. The ratio $\Delta E'/\Delta E$ is also given and data for Ar and $N_2$ measured by R J Dolphin (1971) are included for comparison purposes.

It can be seen that for the least strongly adsorbed gas, hydrogen, and to a lesser extent, Ar, $\Delta E$ is significantly different from $\Delta E'$. The same behaviour should be observed with Ne if sufficiently accurate data were available; this has been demonstrated on Carbolac (Ash et al 1973). Although $\Delta E'$ is an average, applicable to the temperature range 308.15 to 393.15K, from the isotherms $\log(v/p)$ versus $T^{-1}$ was a straight line in all cases and revealed no detectable curvature which would indicate temperature dependence. The effect of temperature on $\Delta E$ can be considered by evaluating $\Delta E$ at the extremes of the temperature range.

TABLE 4.5

ΔE and ΔE'/ΔE at 308.15 and 393.15K

| Adsorbate | $10^8 \delta$ cm | $-\Delta E'$ kJ mol$^{-1}$ | 308.15K $10^8 k_s$ cm | $-\Delta E$ kJ mol$^{-1}$ | $\dfrac{\Delta E'}{\Delta E}$ | 393.15K $10^8 k_s$ cm | $-\Delta E$ kJ mol$^{-1}$ | $\dfrac{\Delta E'}{\Delta E}$ |
|---|---|---|---|---|---|---|---|---|
| $H_2$ | $2.50^{(1)}$ | 4.8 | $5.3_7$ | $3.2_5$ | $1.4_8$ | $3.5_7$ | $2.8_3$ | $1.7_0$ |
| $N_2$ [4] | $4.0$ [1] | 8.9 | $29._4$ | $7.8_3$ | $1.1_4$ | $13._9$ | $6.9_1$ | $1.2_9$ |
| $Ar$ [4] | $3.8_2$ [2] | 7.8 | $26._8$ | $6.8_3$ | $1.1_4$ | $13._6$ | $6.1_0$ | $1.2_8$ |
| $Kr$ | $4.0_4$ [2] | 10.5 | $74._4$ | $9.9_6$ | $1.0_5$ | $30._5$ | $9.2_8$ | $1.1_3$ |
| $Xe$ | $4.5_6$ [2] | 14.7 | 330. | 14.5 | $1.0_1$ | $93._2$ | 14.0 | $1.0_5$ |
| $CH_4$ | $4.2_9$ [2] | 10.7 | $70._8$ | 10.1 | $1.0_6$ | $29._3$ | $9.3_3$ | $1.1_5$ |
| $C_2H_6$ | $4.9_6$ [3] | 17.1 | 508. | 16.9 | $1.0_1$ | 119. | 16.4 | $1.0_4$ |
| $C_3H_8$ | $5.6_8$ [3] | 21.7 | 2650. | 21.7 | $1.0_0$ | 424. | 21.4 | $1.0_2$ |

(1)  Barrer and Ruzicka, 1962.

(2)  Parsonage and Staveley, 1959.

(3)  Hirschfelder, Curtiss and Bird, 1964.

(4)  Data from Ash et al, 1973, but using $A_g = 86.2$ m$^2$ g$^{-1}$.

Owing to the decrease of $k_s$ with increasing temperature, $\Delta E'/\Delta E$ departs more from unity at higher temperatures where $\delta$ is a larger fraction of $k_s$. This is again more noticeable for weakly sorbed molecules where $\Delta E'$ is smallest.

Dolphin (1971) attempted to calculate the volume of the adsorbed layer more rigorously by identifying $\delta$ with $\bar{z}$ , the average perpendicular distance from the centre of the sorbed molecule to the centre of the surface layer of sorbent atoms. $\bar{z}$ was calculated at each of the isotherm temperatures and an increase of 1% for $H_2$ and 4% for Xe was detected from 308.15 to 393.15K. Although more refined, the assumptions made are equally arbitrary and the results no more useful than those obtained here. This treatment gave very little distinction between different

gases, $\bar{z}$ at 308.15 being 0.45 nm for $H_2$ and 0.48 nm for Xe.

### 4.3.2 *Free energy and entropy of absolute sorption*

An equilibrium constant, $K_c$, can be obtained for the adsorption process, equilibrium existing between adsorbed molecules in the sorption volume and those in the gas phase. Since the total concentration of molecules in the adsorption volume is $c_s' + \delta c_g'$ moles cm$^{-3}$ or $(c_s' + \delta c_g')/\delta$ moles per unit sorption volume (see Appendix A), then $K_c$ is given by

$$K_c = \frac{c_s' + \delta c_g'}{\delta} \cdot \frac{1}{c_g'} = \frac{k_s + 1}{\delta} \tag{4.24}$$

As we are concerned with the dilute (Henry law) range, then activity coefficients are unity and $K_c$ can be identified with the thermodynamic equilibrium constant. Hence, if $\delta$ is assumed independent of temperature, we can write:

$$\Delta E^{\ominus} = RT^2 \frac{d\ln K_c}{dT} = RT^2 \frac{d\ln(k_s + \delta)}{dT} \tag{4.25}$$

On comparing this with equation (4.23), one can see that

$$\Delta E^{\ominus} = \Delta E \tag{4.26}$$

The following standard thermodynamic relationships will also hold

$$\left.\begin{array}{l} \Delta A^{\ominus} = -RT\ln K_c \\ \Delta S^{\ominus} = (\Delta E^{\ominus} - \Delta A^{\ominus})/T \end{array}\right\} \tag{4.27}$$

Thus from a knowledge of $k_s$ and $\delta$ (and hence $\Delta E$), the standard thermodynamic free energies and entropies for absolute sorption can be calculated at a given temperature.

Values of these properties, evaluated at 308.15 and 393.15K are shown in table 4.6. The standard free energies and entropies can be seen to increase in magnitude with increasing molecular weight in the series of inert gases or paraffins. At higher temperatures $-\Delta S^{\ominus}$ is smaller, presumably owing to a greater degree of mobility of the adsorbed species.

Further information on the nature of the adsorbed species may be obtained by comparing $\Delta S^{\ominus}$ with calculated entropies based on statistical thermodynamics. When a freely rotating gas molecule possessing three modes of translational energy becomes adsorbed on a surface, an accompanying entropy change will occur owing to loss of translational modes and gain of vibrational modes. If the adsorbed molecule has the properties of a two dimensional gas i.e. if it has two translational modes and one vibrational mode relative to the adsorbent surface, then in the Henry law range the entropy change, $\Delta S_I^{\ominus}$, will be given by (Barrer and Rees, 1961):

TABLE 4.6

*Energy, Free Energy and Entropy of Absolute Sorption*

| Gas | 308.15K | | | 393.15K | | |
|---|---|---|---|---|---|---|
| | $\dfrac{-\Delta E^{\ominus}}{kJ\ mol^{-1}}$ | $\dfrac{-\Delta A^{\ominus}}{kJ\ mol^{-1}}$ | $\dfrac{-\Delta S^{\ominus}}{J\ mol^{-1}K^{-1}}$ | $\dfrac{-\Delta E^{\ominus}}{kJ\ mol^{-1}}$ | $\dfrac{-\Delta A^{\ominus}}{kJ\ mol^{-1}}$ | $\dfrac{-\Delta S^{\ominus}}{J\ mol^{-1}K^{-1}}$ |
| $H_2$ | $3.2_5$ | $2.9_2$ | 1.1 | $2.8_3$ | $2.9_2$ | (-0.2) |
| $N_2$ * | $7.8_3$ | $5.4_4$ | 7.7 | $6.9_1$ | $4.9_1$ | 5.1 |
| $Ar$ * | $6.8_3$ | $5.3_4$ | 4.8 | $6.1_0$ | $4.9_3$ | 3.0 |
| $Kr$ | $9.9_6$ | $7.6_1$ | 7.6 | $9.2_8$ | $7.0_2$ | 5.7 |
| $Xe$ | 14.5 | 11.0 | 11.3 | 14.0 | 10.0 | 10.2 |
| $CH_4$ | 10.1 | $7.3_4$ | 8.9 | $9.3_3$ | $6.7_3$ | 6.6 |
| $C_2H_6$ | 16.9 | 11.9 | 16.3 | 16.4 | 10.5 | 15.0 |
| $C_3H_8$ | 21.7 | 15.8 | 19.1 | 21.4 | $14.1_4$ | 18.5 |
| * Data from Ash et al (1973) | | | | | | |

$$\Delta S_I^{\ominus} = R \ln \left[ \left( \frac{10^3 . RT}{2 \pi M} \right)^{\frac{1}{2}} . \frac{e^{\frac{1}{2}}}{\nu \delta} \right] + \frac{1}{2} R \qquad (4.28)$$

Here $e = 2.30259$, M is the molecular weight of the sorbate and $\nu$ is a mean vibration frequency of the adsorbed molecule. $\nu$ can be estimated empirically using the expression (Hill,1952):

$$\frac{\nu}{\nu^*} = \left( \frac{\Delta E . M^*}{\Delta E^* . M} \right)^{\frac{1}{2}} \qquad (4.29)$$

where * denotes a reference molecule of assigned frequency, an argon atom having $\nu^* = 1.0 \times 10^{12}$ s$^{-1}$ and $\Delta E^* = -6.27$ kJ mol$^{-1}$ being chosen.

More localised adsorption could occur, with the loss of two translational modes and the gain of two vibrational modes ($\Delta S_{II}^{\ominus}$) or complete localisation could take place with loss of all translational energy and gain of three vibrational modes ($\Delta S_{III}^{\ominus}$). These entropies will be related according to:

$$\Delta S_I^{\ominus} = \frac{1}{2} \Delta S_{II}^{\ominus} = \frac{1}{3} \Delta S_{III}^{\ominus} \qquad (4.30)$$

## TABLE 4.7

*Comparison of calculated and experimental entropies* (J mol$^{-1}$ K$^{-1}$)

| Gas | 308.15K | | | | 393.15K | | | |
|-----|---------|---------|----------|---------------------------------------------------------------|---------|---------|----------|---------------------------------------------------------------|
| | $-\Delta S_I^{\ominus}$ | $-\Delta S_{II}^{\ominus}$ | $-\Delta S_{III}^{\ominus}$ | $\dfrac{\Delta S_{II}^{\ominus} - \Delta S^{\ominus}}{\Delta S^{\ominus} - \Delta S_I^{\ominus}}$ | $-\Delta S_I^{\ominus}$ | $-\Delta S_{II}^{\ominus}$ | $-\Delta S_{III}^{\ominus}$ | $\dfrac{\Delta S_{II}^{\ominus} - \Delta S^{\ominus}}{\Delta S^{\ominus} - \Delta S_I^{\ominus}}$ |
| $N_2^*$ | $4.7_7$ | $9.5_5$ | 14.2 | 0.6 | $3.2_3$ | $6.4_7$ | $9.7_0$ | 0.7 |
| $Ar^*$ | $3.7_6$ | $7.5_1$ | $11.2_7$ | 2.7 | $2.3_3$ | $4.6_5$ | $6.9_8$ | 2.5 |
| Xr | $5.7_5$ | $11.5_0$ | 17.3 | 2.2 | $4.5_3$ | $9.0_6$ | 13.6 | 2.8 |
| Xe | $8.4_1$ | 16.8 | 25.2 | 1.9 | $7.2_6$ | 14.5 | 21.8 | 1.5 |
| $CH_4$ | $6.3_8$ | 12.8 | 19.1 | 1.5 | $5.0_7$ | $10.1_5$ | 15.2 | 2.4 |
| $C_2H_6$ | $9.7_3$ | 19.5 | 29.2 | 0.5 | $8.5_9$ | 17.2 | 25.8 | 0.3 |
| $C_3H_8$ | $11.9_2$ | 23.8 | 35.8 | 0.7 | $10.8_3$ | 21.7 | 32.5 | 0.4 |

\* Data from Ash et al (1973)

In table 4.7 these entropies have been tabulated for 308.15K and 393.15K. No figures are given for $H_2$, since $\Delta E$ was insufficiently accurate to determine a reliable value of $\nu$. Comparison can be made with the experimental entropies, $\Delta S^{\ominus}$, given in table 4.6. It can be seen that adsorption is largely mobile since $\Delta S^{\ominus}$ for all sorbates lies between $\Delta S^{\ominus}_{I}$ and $\Delta S^{\ominus}_{II}$.

The quotient $(\Delta S^{\ominus}_{II} - \Delta S^{\ominus})/(\Delta S^{\ominus} - \Delta S^{\ominus}_{I})$ allows comparison to be made between the sorbates, which fall into two groups. Ar, Kr, Xe, $CH_4$ (spherical, non-polar molecules) are more mobile than $C_2H_6$, $C_3H_8$ and $N_2$ (linear or dumbell-shaped molecules). $C_2H_6$ and $C_3H_8$ are more strongly sorbed, while $N_2$ possesses a quadrupole, and these factors could contribute to a reduced surface mobility. However, part of this increase in $-\Delta S^{\ominus}$ for dumbell-shaped molecules could be due to loss of rotational modes.

Similar calculations have been carried out for Carbolac (Ash et al 1973) where it was found that $\Delta S^{\ominus}$ lay between $\Delta S^{\ominus}_{II}$ and $\Delta S^{\ominus}_{III}$ indicating more localised adsorption with adsorbates behaving as oscillators. This behaviour reflects the greater energetic heterogeneity of the Carbolac surface, whilst Graphon is more energetically homogeneous and has greater mobility of ad-molecules.

### 4.3.3 *Relationships between* $K_c$, $\Delta E^{\ominus}$, $\Delta S^{\ominus}$ *and polarizability*

It has been established that the Henry law constant increases rapidly with gas properties related to the condensability of the adsorbate (Dolphin, 1971). Hence the equilibrium constant for absolute sorption, $K_c$, might be expected to show similar trends. Figure 4.12 shows the dependence of $\log k_s$ and $\log K_c$ (at 308.15K) on the polarizability, $\alpha$ (values of $\alpha$ are shown in table 4.8). It would appear that, with the exception of $C_3H_8$, there is a linear relationship between $\log k_s$ or $\log K_c$ and $\alpha$ at temperatures in the region of 300K and for the limited range of gases studied. In the case of $H_2$, where $k_s$ is
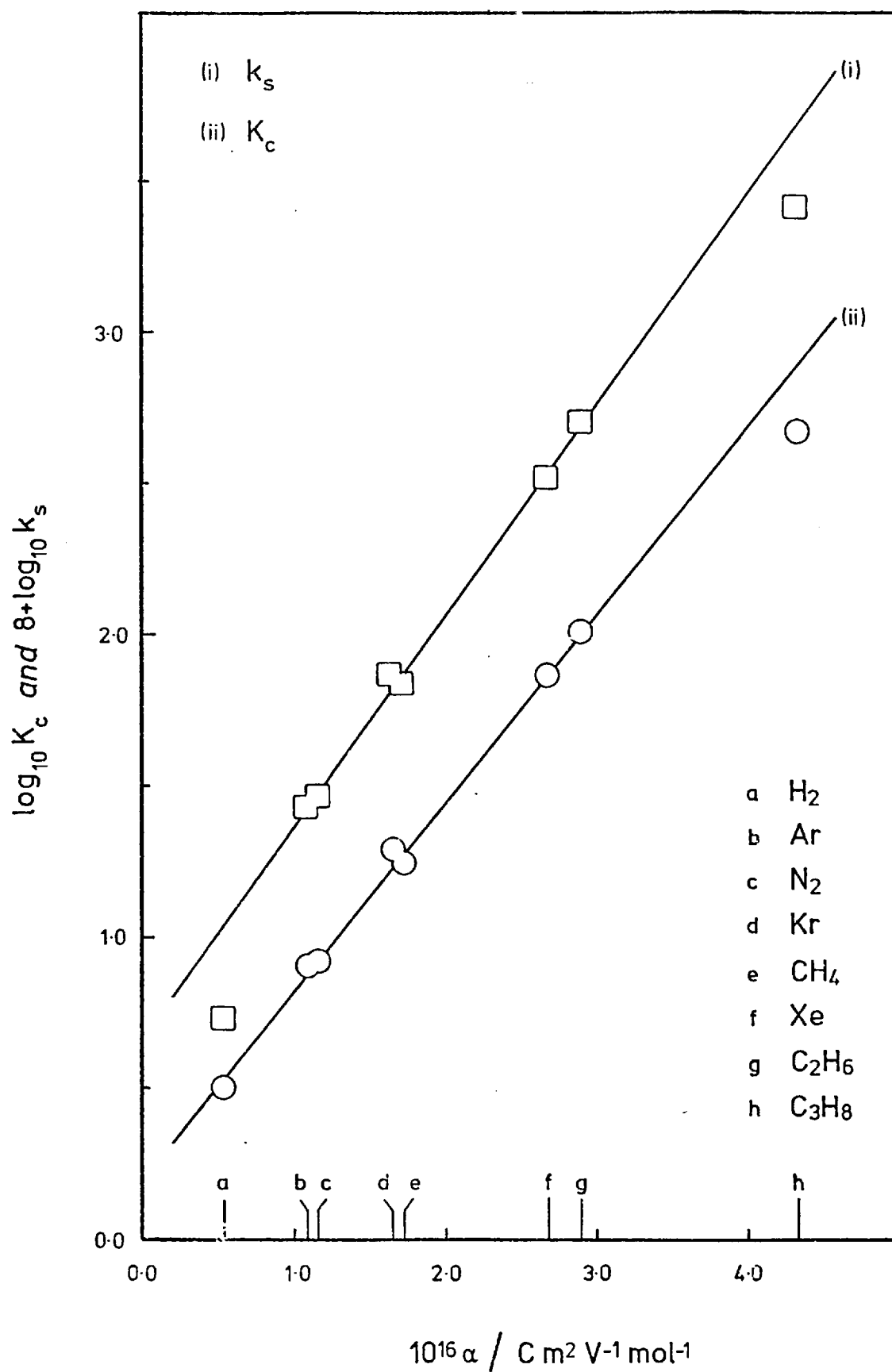
*Figure 4.12*     *Variation at 308·15K of $k_s$ and $K_c$*

*with polarizability, $\alpha$*

substantially different from $k_s + \delta$, $\log K_c$ (referring to absolute sorption) gives a better fit than $\log k_s$ (concerned with Gibb's excess sorption) thus demonstrating the importance of correcting for sorption volume when dealing with weakly sorbed gases.

As a linear relationship was also found between $-\Delta E^{\ominus}$ and $\alpha$ (figure 4.13) then from equation (4.27) it follows that $\Delta A^{\ominus}$ can be expressed as a linear function of $\Delta E^{\ominus}$ (through the dependence of $\log K_c$ and $\Delta E^{\ominus}$ on $\alpha$). Hence at constant temperature a linear relationship should exist between $\Delta S^{\ominus}$ and $\Delta E^{\ominus}$. Similar behaviour has been observed in other systems (Frank, 1945; Everett, 1950; Barrer and Rees, 1959, 1961) and is again demonstrated here (figure 4.14).

## 4.4 CORRELATION WITH INTERACTION ENERGY

The interaction energy, $\varphi(r)$, between a sorbate molecule and an atom of sorbent has frequently been expressed using the Lennard-Jones 6-12 potential:

$$\varphi(r) = - A_{12} \left[ \frac{1}{r^6} - \frac{r_o^6}{2r^{12}} \right] \qquad (4.31)$$

where r is the distance between centres of sorbate and sorbent atoms, $r_o$ being the value at equilibrium (when $\partial \varphi(r)/\partial r = 0$). $A_{12}$ is the dispersion energy constant.

To obtain the total energy of interaction, E, of one adsorbate molecule with the entire surface (an infinite, plane solid), a de Boer and Custers (1934) integration is performed with the result:-

$$E = - \frac{\pi A_{12} N}{6} \left[ \frac{1}{z^3} - \frac{r_o^6}{15z^9} \right] \qquad (4.32)$$

N is the number of adsorbent atoms per unit volume of solid and z is the perpendicular distance from the centre of the gas molecule to the plane containing the centres of the first layer of adsorbent atoms.
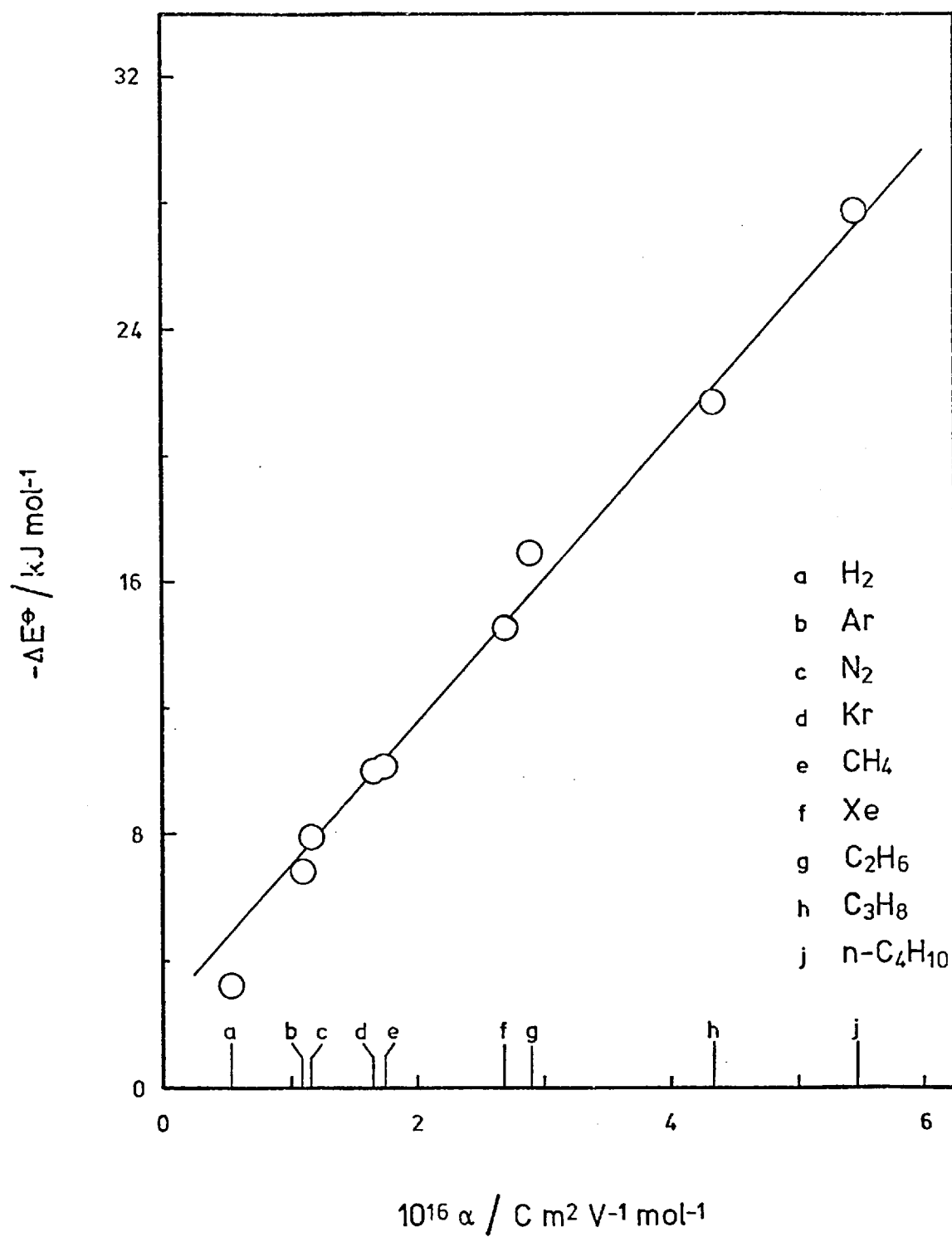
Figure 4.13     Relation between $-\Delta E^{\ominus}$ and $\alpha$

at 308·15K
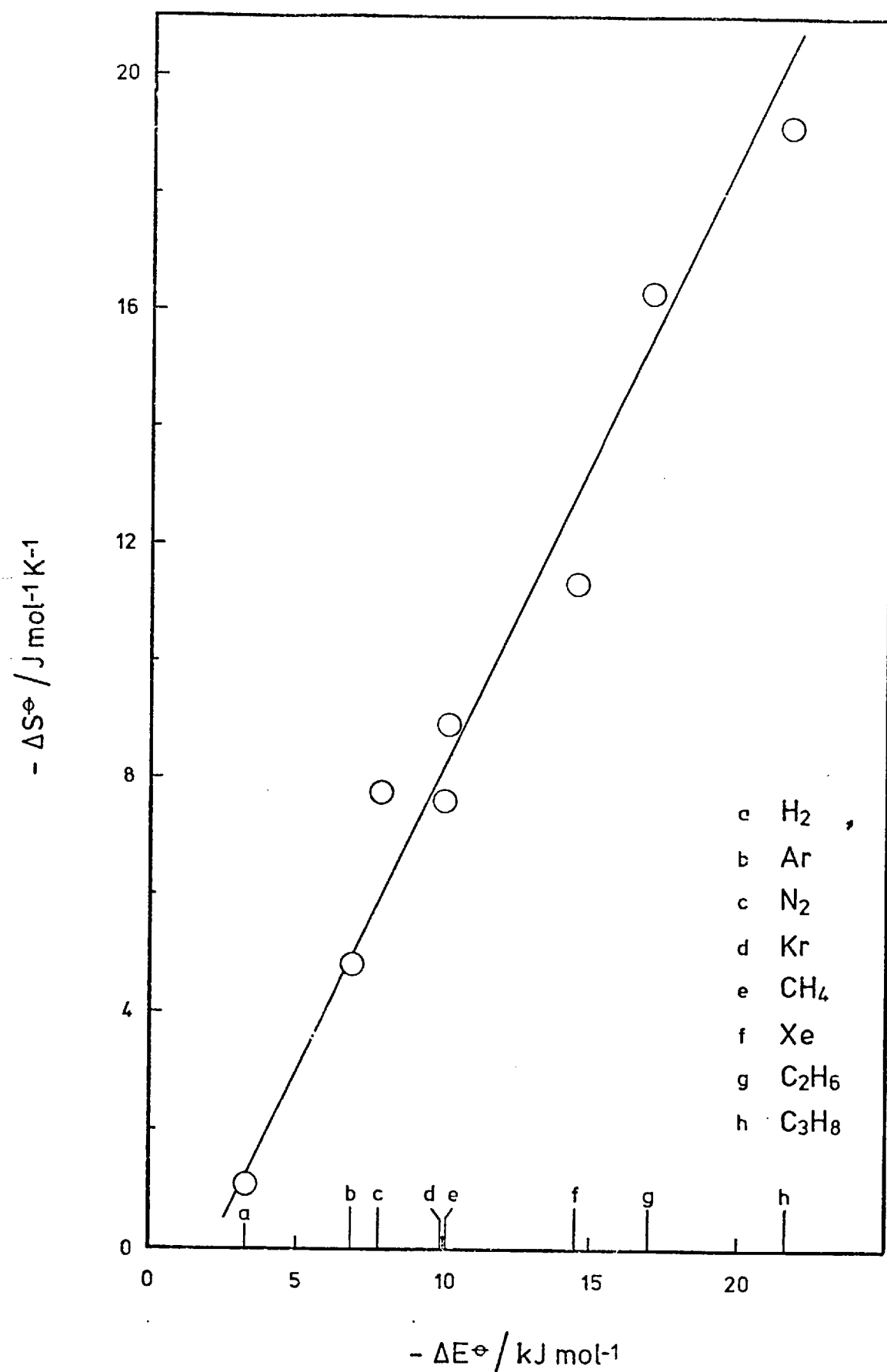
Figure 4.14    Relation between -ΔS$^\ominus$ and -ΔE$^\ominus$ at 308·15K

$z_o$ is the value of z at the minimum of the potential energy well at $E = E_{min}$, when $\partial E / \partial z = 0$, and can be shown to be

$$z_o = \sqrt[6]{(0.2)}\ r_o = 0.7647\ r_o \tag{4.33}$$

Hence $\quad E = -\dfrac{\pi A_{12}\ N}{6} \left[ \dfrac{1}{z^3} - \dfrac{z_o^6}{3\ z^9} \right] \tag{4.34}$

and $\quad E_{min} = -\dfrac{\pi A_{12} N}{9\ z_o^3} \tag{4.35}$

$r_o$ can be obtained from the expression $r_o = r_1 + r_2$ where $r_1$ and $r_2$ are the van der Waals radii of carbon atom and sorbate molecule respectively. $r_1$ was taken to be half the graphite interlamellar spacing ($r_1 = 0.167_5$nm) and half the molecular diameter (table 4.5) was used for $r_2$.

Several expressions have been proposed for $A_{12}$ by London (1930), Slater and Kirkwood (1931) and Kirkwood and Müller (Kirkwood, 1932; Müller, 1936) which are given by equations (4.36), (4.37) and (4.38) respectively.

$$A_{12}^{L} = \frac{3}{32\ \pi^2\ \varepsilon_o^2} \cdot \frac{\alpha_1\ \alpha_2}{(1/I_1 + 1/I_2)} \tag{4.36}$$

$$A_{12}^{SK} = \frac{3}{64\ \pi^3\ \varepsilon_o^2} \cdot \frac{eh}{m^{\frac{1}{2}}} \cdot \frac{\alpha_1\ \alpha_2}{(\alpha_1/n_1)^{\frac{1}{2}} + (\alpha_2/n_2)^{\frac{1}{2}}} \tag{4.37}$$

$$A_{12}^{KM} = -\frac{3\ mc^2}{8\ \pi^2\ \varepsilon_o} \cdot \frac{\alpha_1\ \alpha_2}{(\alpha_1/\chi_1 + \alpha_2/\chi_2)} \tag{4.38}$$

Where $\varepsilon_o$ is the permittivity of a vacuum, c is the velocity of light in a vacuum, h is Planck's constant, e and m are the charge and mass of an electron; $\alpha$, $\chi$ and I represent polarizability, diamagnetic susceptibility and ionisation potential, subscripts 1 and 2 referring

to the carbon sorbent atom and gas molecule respectively. The quantities used should be expressed in S.I. units.

To test the validity of equation (4.35) as a model for the energy of adsorption, $\Delta E$, the ratio $R$,

$$R = -\frac{\Delta E \; z_o^3}{A_{12}} \propto -\frac{\Delta E}{E_{min}} \qquad (4.39)$$

was calculated for some of the gases used in this study from the three expressions for $A_{12}$ given above. If $E_{min}$ is a good approximation to $\Delta E$, then $R$ will remain substantially constant and independent of the gas. The ratios $R_1$, $R_2$ and $R_3$ shown in table 4.9 were obtained using the London, Slater-Kirkwood and Kirkwood-Müller expressions respectively, the relevant gas parameters being given in table 4.8, and $\Delta E$ at 308.15K being used.

Using the Kirkwood-Müller expression, $R_3$ is approximately constant for the gases $H_2$, $N_2$, Ar, Kr, Xe and $CH_4$, but shows a large scatter. However, $C_2H_6$ and higher paraffins gave significantly larger values of $R$. Similarly, anomalous behaviour of hydrocarbons was observed in $R_1$ and $R_2$, but $R_2$ showed a slight, and $R_1$ a pronounced, tendency to increase with molecular weight. This behaviour is illustrated graphically in figure 4.15 where $R$'s are plotted against $\Delta E$ (the data for Ar and $N_2$ being taken from Dolphin, 1971). The relative constancy of $R$, especially for Kirkwood-Müller, supports the model and indicates that physical or chemical heterogeneity is essentially absent from the carbon. This contrasts with the behaviour of Carbolac (Ash et al, 1973) where $R$ increased several-fold from $H_2$ to Xe. This was attributed to energetic heterogeneity of the carbon surface, giving rise to anomalously high energies of adsorption with strongly sorbed molecules, thus ensuring $\Delta E > E_{min}$ for molecules such as xenon.
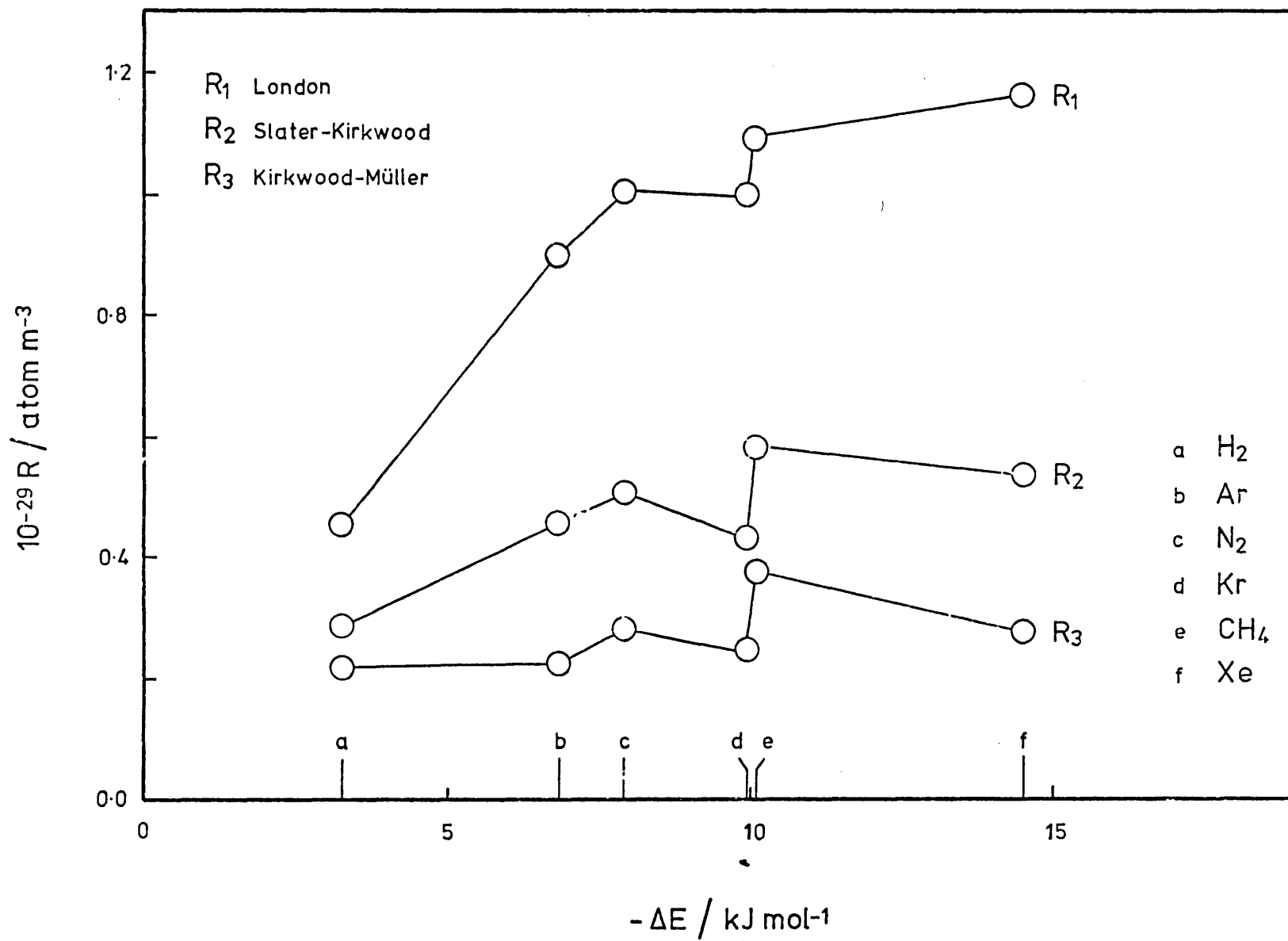
Figure 4.15 Variation of $R \left(=-\Delta E z_o^3 / A_{12}\right)$ with $-\Delta E$

## TABLE 4.8

*Parameters Used in Evaluating* $R_1$, $R_2$ *and* $R_3$

| Species | n | $\dfrac{z_0}{nm}$ | $\dfrac{10^{16}\,\alpha}{Cm^2 V^{-1} mol^{-1}}$ | $\dfrac{10^{18}\,I}{J\,(molecule)^{-1}}$ | $\dfrac{-10^{10}\,\chi}{m^3 mol^{-1}}$ |
|---|---|---|---|---|---|
| $H_2$ | 2 | 0.224 | 0.538 | 2.63 | 0.50 |
| $N_2$ | 10 | 0.281 | 1.162 | 2.50 | 1.51 |
| Ar | 8 | 0.274 | 1.090 | 2.53 | 2.45 |
| Kr | 18 | 0.283 | 1.647 | 2.24 | 3.52 |
| Xe | 18 | 0.302 | 2.681 | 1.94 | 5.41 |
| $CH_4$ | 8 | 0.292 | 1.73 | 2.10 | 2.19 |
| $C_2H_6$ | 14 | 0.318 | 2.900 | 2.05 | 3.44 |
| $C_3H_8$ | 20 | 0.346 | 4.34 | 1.78 | 5.09 |
| $n\text{-}C_4H_{10}$ | 26 | 0.381 | 5.49 | 1.70 | 7.22 |
| Carbon | 8 | – | 0.684 | 1.80 | 2.87 |

## TABLE 4.9

*Values of* $-\Delta E.z_0^{\,3}$, $A_{12}$ *and* $R$

| Gas | $\dfrac{-10^{25}\,\Delta E.z_0^{\,3}}{J\,m^3}$ | $10^{54}\,A_{12}$ in $Jm^6(mol)^{-1}(atom\ carbon)^{-1}$ | | | $10^{-29}\,R$ in $(atom\ carbon)\,m^{-3}$ | | |
|---|---|---|---|---|---|---|---|
| | | $A_{12}^L$ | $A_{12}^{SK}$ | $A_{12}^{KM}$ | $R_1$ | $R_2$ | $R_3$ |
| $H_2$ | 0.37 | 0.79 | 1.25 | 1.63 | 0.46 | 0.29 | 0.22 |
| $N_2$ | 1.75 | 1.67 | 3.47 | $4.6_0$ | 1.05 | 0.51 | 0.38 |
| Ar | 1.41 | 1.58 | 3.11 | $6.3_7$ | 0.90 | 0.46 | 0.22 |
| Kr | 2.25 | 2.26 | 5.23 | $9.3_1$ | 1.00 | 0.43 | 0.24 |
| Xe | 4.00 | 3.44 | $7.4_6$ | 14.6 | 1.16 | 0.54 | 0.27 |
| $CH_4$ | 2.52 | 2.31 | $4.3_1$ | $6.7_2$ | 1.09 | 0.58 | 0.38 |
| $C_2H_6$ | 5.43 | 3.82 | $7.3_4$ | 10.7 | 1.42 | 0.74 | 0.51 |
| $C_3H_8$ | $8.9_7$ | $5.3_5$ | 10.8 | 15.8 | 1.67 | 0.83 | 0.57 |
| $n\text{-}C_4H_{10}$ | 15.4 | 6.60 | 13.7 | 21.9 | 2.33 | 1.12 | 0.70 |

Several limitations are, however, imposed on this treatment.

(i) Since no allowance has been made in the calculation of A's for

adsorption of asymmetric molecules (with non-isotropic $\alpha$'s), spherically

symmetrical molecules should be chosen, ic Ar, Kr, Xe and $CH_4$. No allowance is likewise made for the quadrupole moment of $N_2$ which might cause favoured orientations of the admolecule thus increasing $-\Delta E$. R is therefore likely to be too high.

(ii) The calculated $E_{min}$ will be greater than $\Delta E$ by $E_o$, the zero-point energy of the adsorbed molecule. This effect will increase with temperature as the adsorbed molecule acquires more vibrational energy.

(iii) The deBoer and Custers integration assumes an infinite plane solid. This clearly does not exist in a real adsorbent where crevices, steps etc occur on the surface. These surface defects can give rise to very high energies of adsorption and account, in part, for energetic heterogeneity. $E_{min}$ would not be a good approximation to $\Delta E$ in such a case. Since a small amount of heterogeneity has been detected on Graphon (section 4.1.5) then $\Delta E$ might be expected to be larger than predicted by the model especially for smaller molecules which could penetrate the crevices. Since this behaviour is not observed, then the heterogeneity must be too small to manifest itself in this treatment.

CHAPTER 5

ISOTHERMAL TRANSPORT

## 5.1  EXPERIMENTAL RESULTS

Isothermal flow measurements of He, $CH_4$, $C_2H_6$, $C_3H_8$ and $n-C_4H_{10}$

through Graphon membrane N have been made in the temperature range

308.15 to 393.15K. The effect of varying the ingoing pressure, $p_o$, from

5 to 20 cmHg for the hydrocarbons and from 5 to 50 cmHg for helium has

also been investigated.

In chapter 3 the experimental procedure to measure flow through

the membrane from $d\,p_\ell/dt$, the rate of build up of pressure in a fixed,

known volume, V, was described. Plots of $p_\ell$ versus t, with V kept constant,

are shown in figure 5.1 for n-butane at 308.15K and several values of

$p_o$. Extrapolation of the straight line part of the curve to cut the

t axis gives the outgoing adsorption time-lag, L. It can be seen that L

varies with $p_o$, but this behaviour is not typical of all gases. The

more weakly sorbed gases He, $CH_4$ and $C_2H_6$ show no change in L with $p_o$ and

for a given gas the extrapolated curves of $p_\ell$ versus t cut the t axis

coincidentally.

The permeability, $K$, is obtained from $d\,p_\ell/dt$ using equations

(2.9) and (2.10). If p is expressed in cmHg, t in minutes, $\ell$ in metres,

$A_c$ in $m^2$ and V in $m^3$, then the flux is given by:

$$J = \left(\frac{d\,p_\ell}{dt}\right) \cdot \frac{1}{10^2} \cdot \frac{V}{R}\,\frac{1.354 \times 10^4 \times 9.81}{T_R\,60} \qquad (5.1)$$

or

$$G = \left(\frac{d\,p_\ell}{dt}\right) \cdot \frac{1}{10^2} \cdot \frac{V\,1.354 \times 10^4 \times 9.81}{60} \cdot \frac{T}{T_R} \qquad (5.2)$$

where $J$ is the total molar flux (mole $s^{-1}$) and G is the corresponding
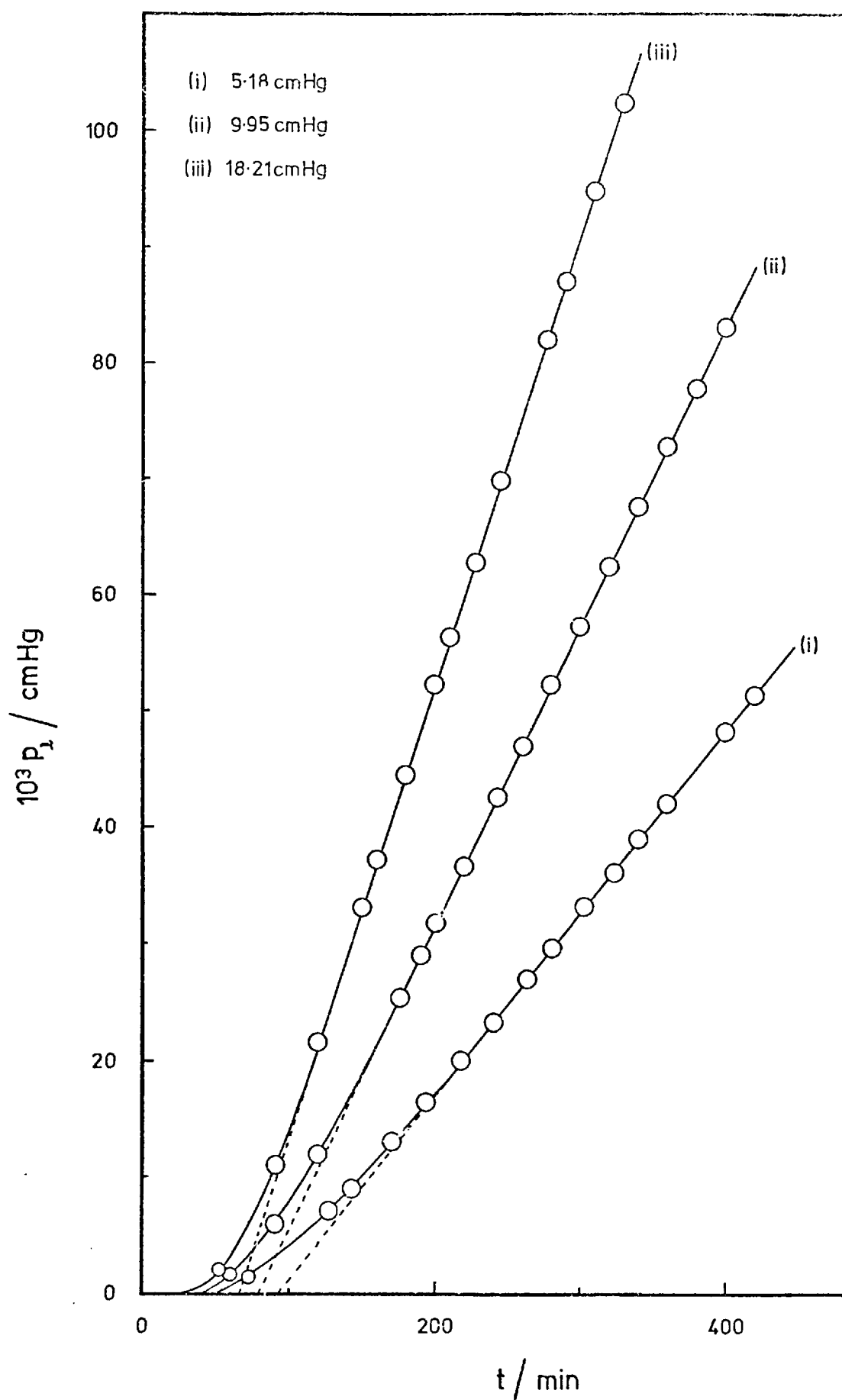
*Figure 5.1* P$_1$ *as a function of* t *at several values of* P$_0$ *for n-butane at* 308·15K

energy flux (J s$^{-1}$) reduced to the membrane temperature, T. $T_R$ is

ambient temperature. The permeability $K$ (m$^2$s$^{-1}$) is thus given by

$$K = \left(\frac{d\ p_\ell}{dt}\right) \cdot \frac{1}{60} \cdot \frac{\ell}{p_o} \cdot \frac{V}{A_c} \cdot \frac{T}{T_R} \qquad (5.3)$$

Values of L, G and $K$ are tabulated in Appendix D for each gas at every

temperature and pressure used, and are presented graphically in figures

5.2 to 5.6.

In the absence of a viscous flow component it has been suggested

that the gas phase permeability, $K_g$, can be obtained from that of

helium, $K^{He}$, using the relationship for Knudsen flow of an ideal gas:

$$K_g = K^{He} (M_{He}/M)^{\frac{1}{2}} \qquad (2.12)$$

Helium is assumed to be non-adsorbed and thus has no surface flow

component, $K_s$. For a sorbed gas in the absence of pore blockage $K_s$ can

be obtained from

$$K = K_s + K_g \qquad (2.11)$$

Using equations (2.12) and (2.11) the $K_s$ and $K_g$ components of $K$

have been obtained and these, together with the ratio $K_s/K_g$, are

tabulated in Appendix E.

## 5.2   HELIUM DATA AND THE KNUDSEN REGIME

In the analysis above we have assumed that Knudsen flow conditions

prevail in the gas phase and that helium can be used as a non-sorbed

calibrating gas. This must now be shown.

The average pore diameter, d, based on the hydraulic radius of

the membrane, was 17.0 nm (section 3.1.3). The commonly accepted

criterion for Knudsen flow is that λ, the mean free path of gas molecules,

be greater than 10d, ie in this case λ> 170 nm. In figure 5.7 λ has

been evaluated at 308.15K (the least favourable temperature) and plotted
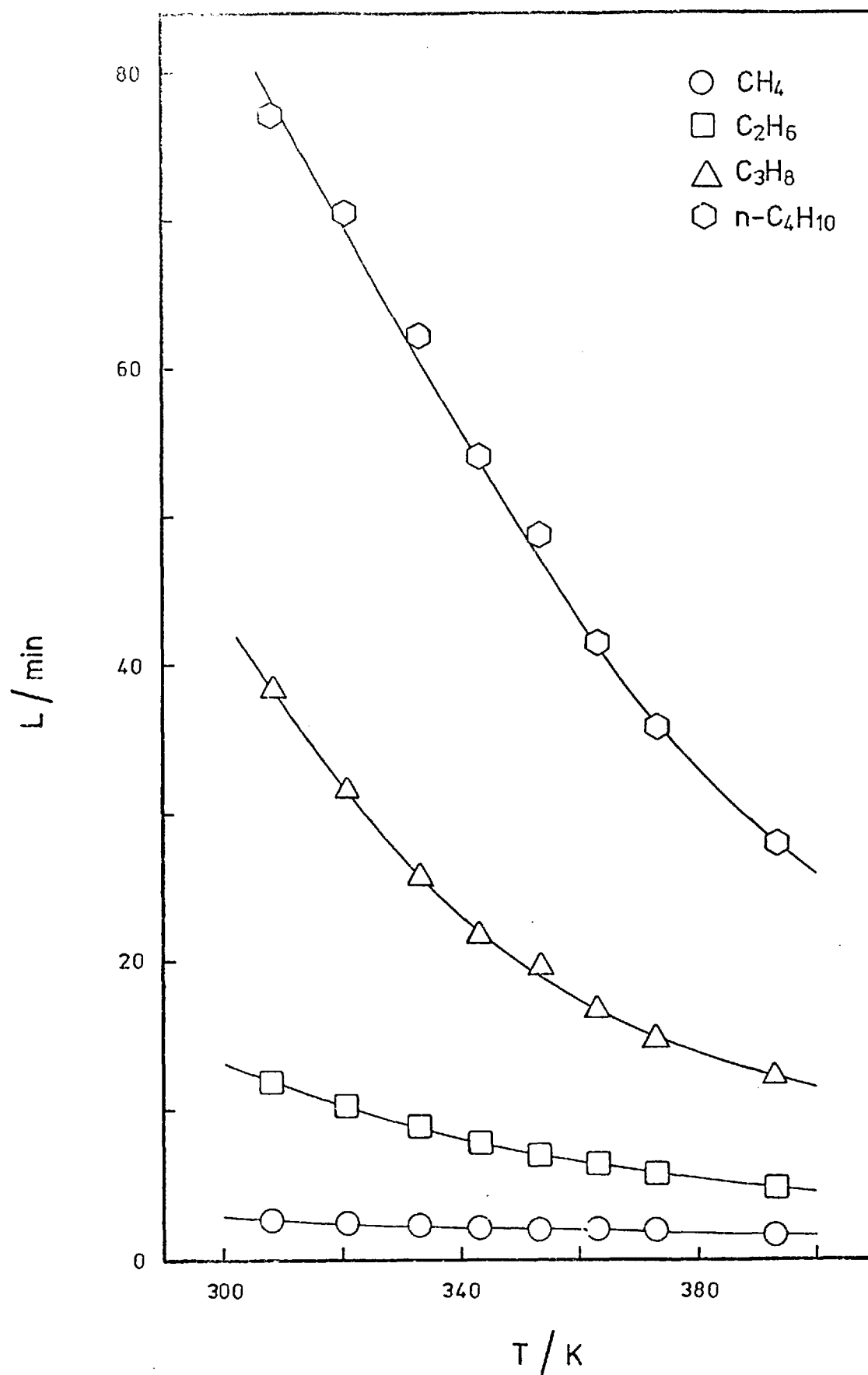
*Figure 5.2*     *Temperature dependence of time-lags*

*at* $p_o \cong 10 \ cm \ Hg$
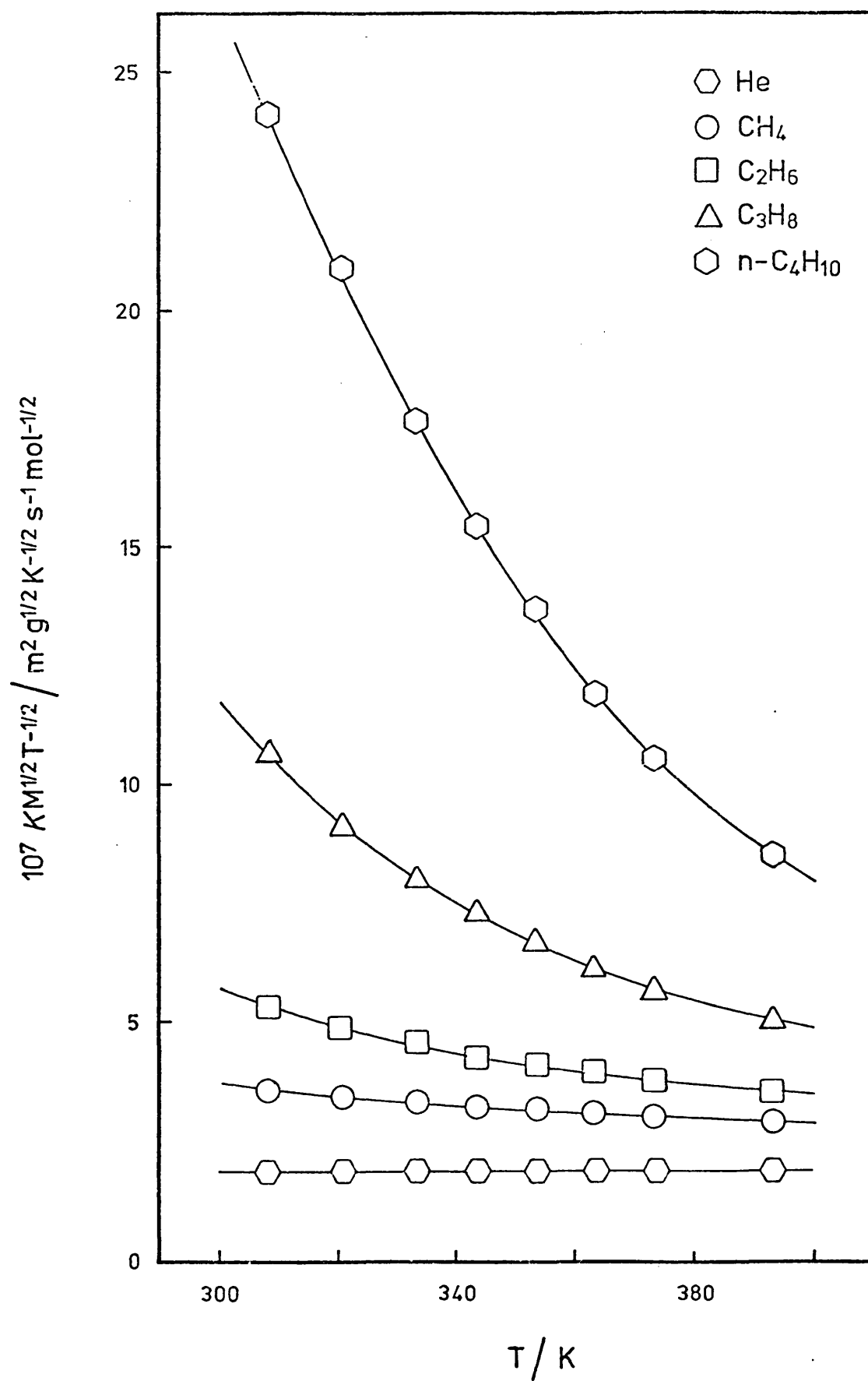
*Figure 5.3* Temperature dependence of permeabilities

*at* $p_o \cong 10$ cm Hg
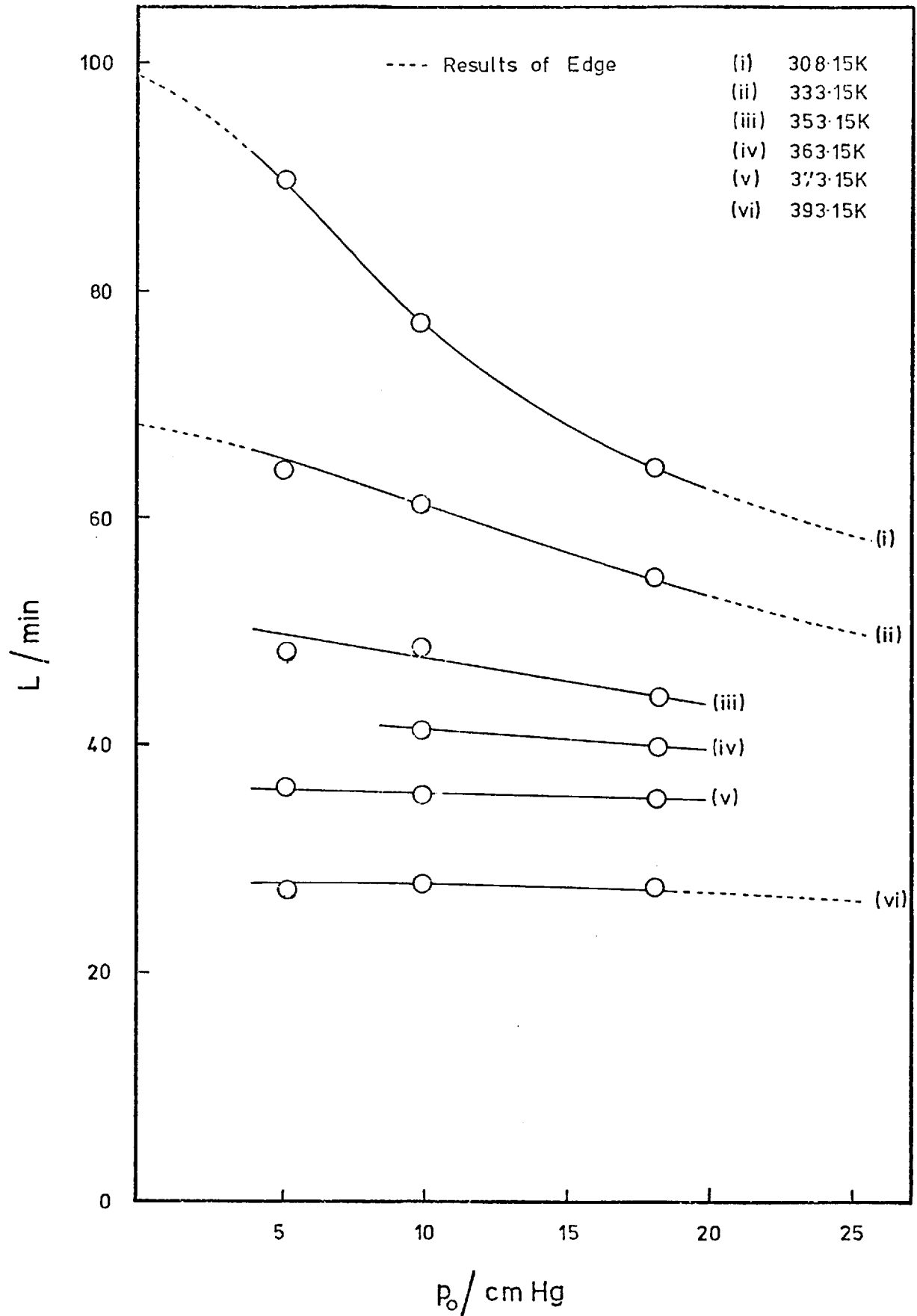
Figure 5.4    Pressure dependence of time-lags for

$n-C_4H_{10}$ at several temperatures
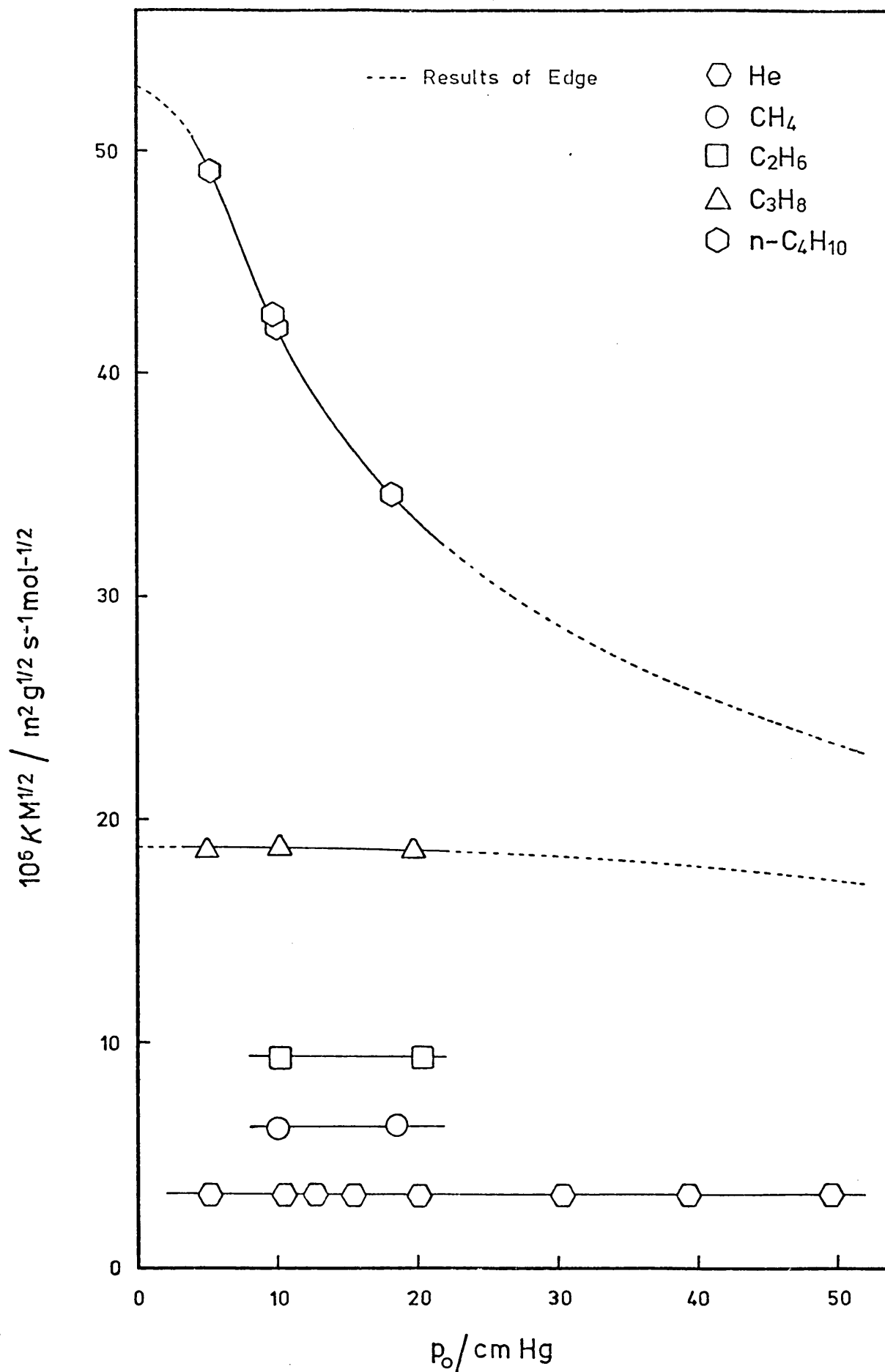
*Figure 5.5*     *Pressure dependence of permeabilities at* 308·15K
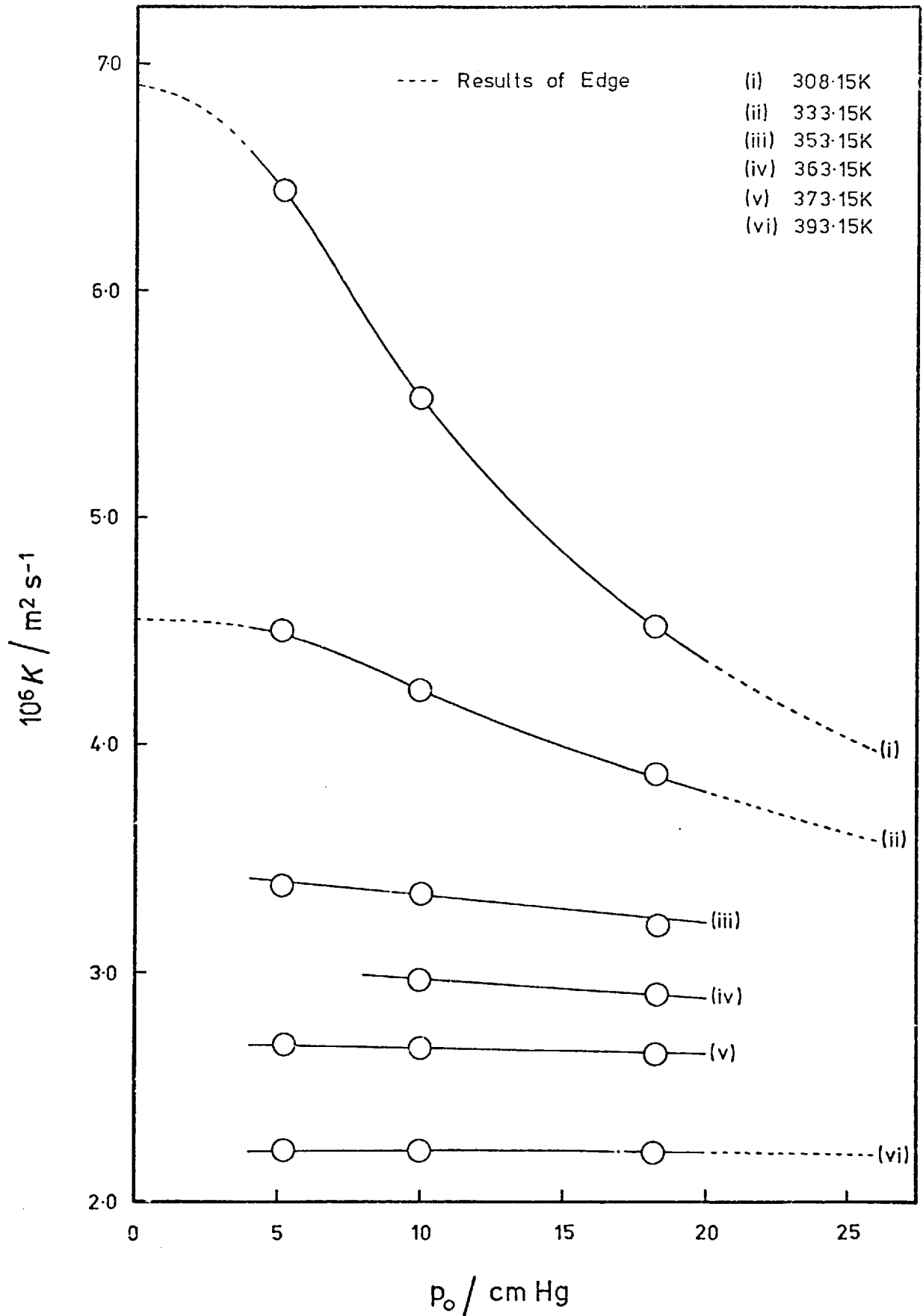
*Figure 5.6*    *Pressure dependence of permeabilities for*
*n-butane at several temperatures*

against pressure, p, for each gas studied using the expression

$$\lambda = \frac{kT}{2^{\frac{1}{2}} \cdot \pi \cdot \delta^{2} \cdot p} \qquad (5.4)$$

Here $\delta$ is the molecular diameter given in table 4.5, 0·289 nm being

taken for He and 0.659 nm for $n\text{-}C_4H_{10}$ (Parkinson and Gray, 1972) and

k is Boltzmann's constant. The condition $\lambda = 10d$ is shown on figure

5.7 and it can be seen that the criterion $\lambda > 10d$ is met for He at

pressures of up to 50 cmHg and for the paraffins at 10 cmHg or below.

As the majority of measurements were made at a $p_o$ value of 10 cmHg then

the criterion is met. If the average pressure $(p_o + p_{\ell})/2$ is used to

characterise the membrane then the situation is even more favourable.

A further check on the absence of viscous flow was obtained by

determining $K^{He}$ for several pressures in the range 5 to 50 cmHg (plotted

as $KM^{\frac{1}{2}}$ versus $p_o$ in figure 5.5). No significant pressure dependence of

$K^{He}$ in this range was found, which accords with the predictions of the

Knudsen equation. Thus in the gas phase, Knudsen flow is likely to

prevail.

Now if helium is to be used as a non-sorbed calibrating gas, then

$K(M/T)^{\frac{1}{2}}$ must be a constant as predicted by equation (2.5) for pure gas

phase Knudsen flow. The presence of adsorption and flow of the mobile

adsorbed phase leads to an increase in $K$ and consequently in $K(M/T)^{\frac{1}{2}}$,

which is more pronounced at lower temperatures ie at greater adsorption.

Figure 5.3 shows $K(M/T)^{\frac{1}{2}}$ versus T for helium as well as for the

hydrocarbons. It will be seen that for helium, $K(M/T)^{\frac{1}{2}}$ is substantially

constant, whereas for all the hydrocarbons adsorption and surface flow

occur since $K(M/T)^{\frac{1}{2}}$ increases with decreasing temperature, the deviation

being more pronounced for the larger molecules.

Careful examination of the helium results shows a very slight

increase in $K(M/T)^{\frac{1}{2}}$ with temperature (table 5.1). From a logarithmic plot

(i) He
(ii) $CH_4$
(iii) $C_2H_6$
(iv) $C_3H_8$
(v) $n-C_4H_{10}$

$\lambda > 10\,d$

$\lambda = 10\,d$

$\lambda < 10\,d$
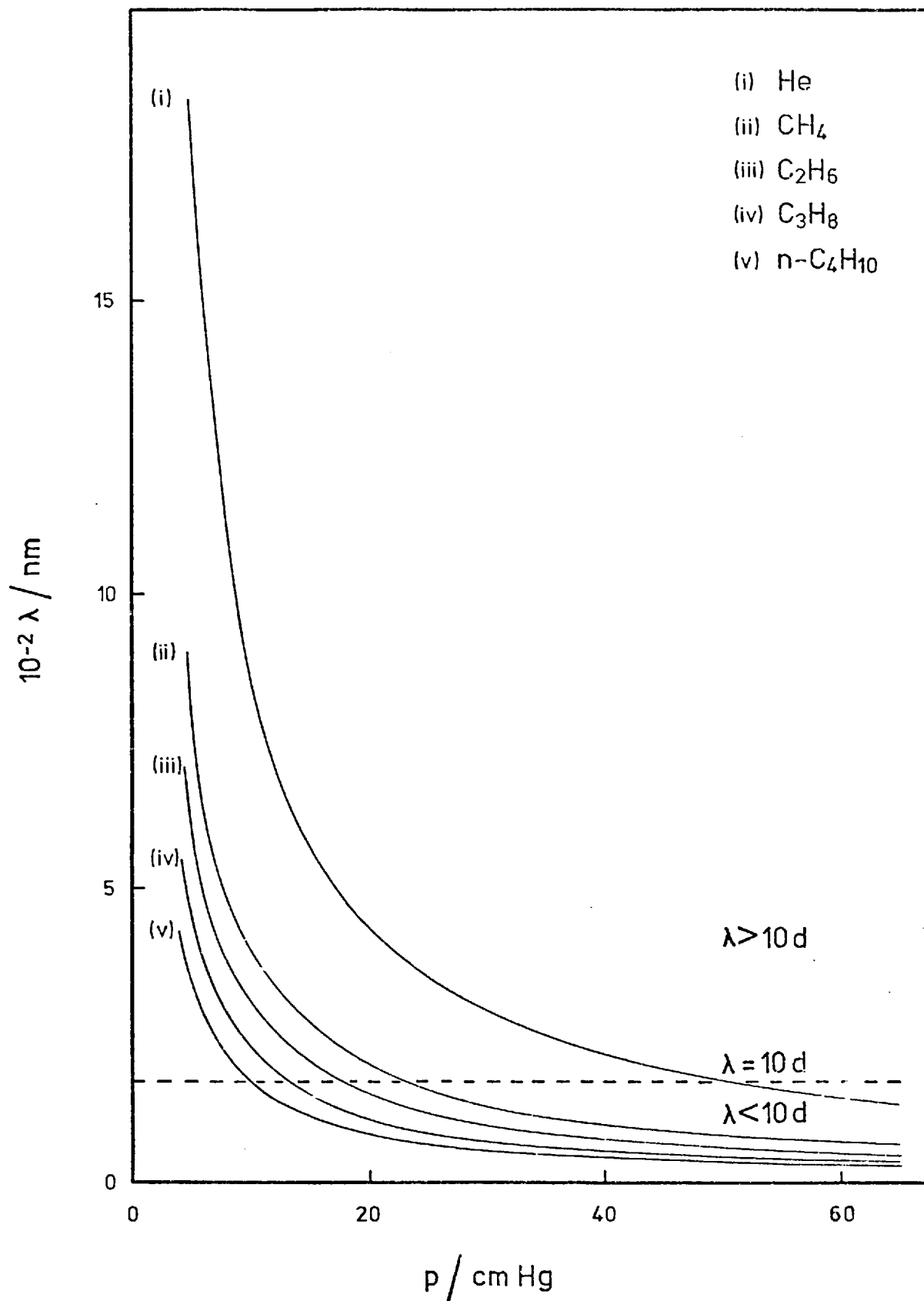
*Figure 5.7*     *Mean free paths, $\lambda$, as a function of pressure at 308·15K*

$K$ was found to be proportional to $T^{0.57}$. This behaviour is similar to that found by Ash, Barrer and Lowson (1970) and the effect is in the opposite direction to that expected of surface flow due to adsorption ie $K'(M/T)^{\frac{1}{2}}$ is found to increase with temperature. Consequently it was concluded that no adsorption or surface flow of helium occurs. In subsequent evaluations of $K_g$, the $K^{He}$ values used were 'smoothed' ones obtained from a plot of $K$ versus $T^{\frac{1}{2}}$ or log $K$ versus log T evaluated by a statistical least mean squares analysis. Both approaches gave the same smoothed values, $<K>$ in table 5.1.

TABLE 5.1

$K$ and $K(M/T)^{\frac{1}{2}}$ for Helium

| T/K | 308.15 | 320.65 | 333.15 | 343.15 | 353.15 | 363.15 | 373.15 | 393.15 |
|---|---|---|---|---|---|---|---|---|
| $10^6 \dfrac{K}{m^2 s^{-1}}$ | $1.61_1$ | $1.64_1$ | $1.68_1$ | $1.70_7$ | $1.74_4$ | $1.76_9$ | $1.79_7$ | $1.84_7$ |
| $10^7 \dfrac{K M^{\frac{1}{2}} T^{-\frac{1}{2}}}{g^{\frac{1}{2}} m^2 s^{-1} mol^{-\frac{1}{2}} K^{-\frac{1}{2}}}$ | $1.83_5$ | $1.83_3$ | $1.84_2$ | $1.84_3$ | $1.85_6$ | $1.85_7$ | $1.86_1$ | $1.86_3$ |
| $10^6 \dfrac{<K>}{m^2 s^{-1}}$ | $1.60_8$ | $1.64_6$ | $1.68_2$ | $1.71_1$ | $1.73_9$ | $1.76_7$ | $1.79_5$ | $1.85_0$ |

Sandler (1972a) proposed that slight deviations of helium from the Knudsen permeability model could be attributed to the neglect by that model of any interaction between an impinging gas molecule and the surface, where rigid sphere collision was assumed. The interaction will modify the scattering pattern which in turn will vary with the kinetic energy of the impinging molecule ie with temperature. Using the Lennard-Jones 6-12 potential for interactions between atoms and the Dusty Gas Theory expression for $K$, Sandler derived the temperature dependence of $K$ given by equation (5.5)

$$K = C_1 \frac{T^{7/6}}{S + T^{1/2}} \qquad (5.5)$$

where S is a generalised Sutherland constant and $C_1$ is a proportionality constant.

A plot of $T^{7/6}/K$ versus $T^{1/2}$ was made and proved to be a good straight line. From the slope and intercept of this line $C_1$ was calculated as $2.94_4 \times 10^{-8} \ m^2 \ s^{-1} \ K^{-4/6}$ and S as $-2.9 \ K^{1/2}$. Interpolated values of $K$ were identical with those given in table 5.1.

## 5.3 HYDROCARBON PERMEABILITY DATA

Experimental permeability results obtained for the hydrocarbons are tabulated in Appendices D and E. Selected results are also shown in figures 5.2 to 5.6, demonstrating the dependence of L and $K$ on membrane temperature and on ingoing pressure, $p_o$. In figures 5.4 to 5.6 the curves for $C_3H_8$ and $n-C_4H_{10}$ are based on subsequent experimental work carried out by Dr A V J Edge of the Physical Chemistry Laboratories, Imperial College. He used the same experimental apparatus but made measurements down to 1 cmHg and up to 60 cmHg. The results of the present work coincide with his findings and provide the justification for the curves drawn, whereas based solely on the results of this investigation less extensive lines could be drawn.

From Appendix E it will be observed that the surface flow component of permeability, $K_s$, ranges from being comparable to the theoretical gas phase permeability, $K_g$, ($CH_4$ and $C_2H_6$) to being an order of magnitude greater (n-butane at 308.15K). The ratio of surface flux to gas phase flux is represented by $K_s/K_g$ and is tabulated in Appendix E.

### 5.3.1 *Temperature dependence of* L *and* K

Both L and $K$ are affected by temperature, diminishing with increasing membrane temperature (figures 5.2 and 5.3). At constant temperature and pressure they also depend on the adsorbate, increasing very rapidly with the molecular weight of the species. For the weakly

sorbed gases, $CH_4$ and $C_2H_6$, the percentage fall in L from 308.15K to 393.15K is much larger than that in $K$, indicating perhaps a greater temperature sensitivity of L than $K$. However, for $C_3H_8$ and, more especially, $n-C_4H_{10}$, the temperature dependence is much greater, both $K$ and L encountering a fall in magnitude of 50-70% between 308.15K and 393.15K.

The time-lag, L, arises because of the finite time required for gas to permeate through the membrane. When gas is first admitted to the membrane the pores are free of adsorbate. Hence the initial flux of gas is used up in filling the pore space, including dead-end pores, and establishing adsorption equilibrium with the surface. At higher temperatures the diffusing gas molecules will be more mobile and have a higher kinetic energy. Less gas will also be required to establish sorption equilibrium and hence a reduction in L can be expected. This has been observed in this work and elsewhere (Clint, 1966; Dolphin, 1971).

For a Knudsen gas $K(M/T)^{\frac{1}{2}}$ should be constant and $K$ would be expected to increase slowly with temperature. As figure 5.3 shows $K(M/T)^{\frac{1}{2}}$ is always greater than the helium value, hence for all the hydrocarbons studied some sorbed phase flow occurs, the magnitude of which increases with decreasing temperature. This temperature dependence of $K$ is entirely due to the surface flow component, $K_s$, and reflects the influence of temperature on sorption equilibrium as found in the isotherm measurements. At higher temperatures there will be a lower adsorbate concentration on the membrane surface and thus the $K_s$ component, due to transport by hopping of adsorbed molecules, will be reduced.

### 5.3.2 *Pressure dependence of L and K*

Figures 5.4 and 5.5 show the pressure variation of L and $K$, where observed, in the range 5 to 20 cmHg. Both parameters gave similar behaviour and the following general observations can be made.

No significant change in $K$ or L was observed for the slightly sorbed gases, $CH_4$ and $C_2H_6$, where sorption is within the Henry law range. The constancy of $K$ also indicates the absence of any viscous flow. At higher pressures propane appears to show a slight decrease in both $K$ and L at 308.15K (this observation being reinforced by Dr Edge's measurements) but at higher temperatures variations in $K$ and L were too small to ascribe any significance to them.

Horiguchi, Hudgins and Silveston (1971) investigated diffusion in the $C_2H_6$/Graphon system. At $50^{\circ}$C $K_s$ was substantially constant up to 30 cmHg but at $25^{\circ}$C and $0^{\circ}$C a slight but noticeable decrease in $K_s$ with increasing pressure was observed. At $0^{\circ}$C $K_s$ decreased linearly by 22% when the mean pressure was increased from 0 to 70 cmHg. The limiting values of $K_s$ at zero pressure were found to be $2.10 \times 10^{-6}$, $1.45 \times 10^{-6}$ and $1.07 \times 10^{-6}$ $m^2$ $s^{-1}$ at 0, 25 and $50^{\circ}$C respectively. That no significant pressure dependence of $K_s$ at 308.15K was observed in this work is compatible with Horiguchi's work as here we investigated a change in mean pressure only from 5 to 10 cmHg which would give an extremely small change in $K_s$.

n-Butane, however, exhibits a marked increase in $K$ and L at diminishing pressure, tending to a flat maximum close to p = 0. This effect is most noticeable at lower temperatures (figure 5.6) and could not be observed at 393.15K. Dr Edge has found similar behaviour with iso-butane and also with propane at a lower temperature (273.15K) while Horiguchi observed this behaviour with propylene at 273.15 and 298.15K. Ash, Barrer and Sharma (1976) in a study of hydrocarbon flow between 195 and 373K through a Carbolac membrane, obtained permeabilities for $C_2H_6$, $C_3H_8$, $n$-$C_4H_{10}$ and $neo$-$C_5H_{12}$ which were found to decrease with increasing equilibrium uptake and hence with increasing pressure. For the more weakly sorbed $CH_4$, $K$ was independent of uptake.

The behaviour of L can be understood by considering the
adsorption isotherms. Within the Henry law range equal pressure
increments give rise to equal increments in the amount of gas adsorbed
and so L might be expected to be independent of p. This would correspond
with low pressures and high temperatures. Outside the Henry law range,
adsorbents with isotherms having curvature towards the p-axis (as
encountered in this work) will require progressively less adsorbate, per
unit pressure increment, until the isotherm flattens out close to
monolayer coverage. Thus in regions of isotherm curvature, less sorbate
is required to establish equilibrium with the membrane surface than would
be required if the Henry law was obeyed, and hence L decreases.

The pronounced pressure dependence of the n-butane permeability was
an unexpected result in this work. From the magnitude and temperature
dependence of $K$ we have already ascertained that a substantial part of
$K$ is due to surface flow. It is again this component, $K_s$, which is
responsible for the pressure dependence. Any pressure dependence of $K_g$
is more likely to lead to an increase in $K$ owing to the onset of
Poiseuille and conduction flow at higher pressures as predicted by Weber
(equation 2.6). It is conceivable that $K_g$ could be reduced or eliminated
completely by the presence of extensive adsorption causing pore blockage
in the region of pore constrictions within the membrane. However n-butane
at 308.18K shows a 29.6% drop in $K$ between $5.1_8$ and $18.2_1$ cmHg. Since
the theoretical value of $K_g$ represents only 6.6% of $K$ at the initial
pressure, then it is clear that even complete blockage cannot explain all
this fall in $K$. Ash et al (1976) investigated flow of a binary gas
mixture (helium and a hydrocarbon) through a Carbolac membrane. They
found that the membrane was very substantially blocked to helium flow
as sorption of the hydrocarbon approached monolayer coverage.

However, permeability here is defined as the molar flux per unit

cross-section per unit gradient in gas phase concentration, $c_g'$. A

permeability could equally well be defined in terms of a gradient in

surface concentration, $c_s'$ , or total adsorbate concentration, c

$(= Ac_s' + \varepsilon c_g')$.

Figure 5.8 demonstrates the dependence of flux, $J$, on the

concentrations $c_g'$, $c_s'$ and c, all at x = 0, for propane and n-butane at

308.15K. $CH_4$ and $C_2H_6$, obeying the Henry law, showed a linear dependence

on concentration and so are not plotted here. It can be seen that

departure of $J$ from linearity is very slight for $C_3H_8$. n-Butane on

the other hand, whilst showing a decrease in $dJ/dc_g'$ with increasing

$c_g'$, exhibits a pronounced increase in $dJ/dc_s'$ and $dJ/dc$ with increasing

$c_s'$ and c. Thus a permeability defined in terms of $c_s'$ or c is found to

increase rapidly with increasing surface coverage, whereas $K$ in terms of a

$c_g'$ gradient decreases. This behaviour can be related to the marked

isotherm curvature in this pressure region, and the similarity between

the dependence of $J$ on $c_s'$ and on c is due to the major contribution by

adsorbed molecules to c.

The permeability $(K)^S$ defined by equation (5.6) has been evaluated

for n-butane at 308.15K and is shown in figure 5.9.

$$(K)^S = \frac{J_s}{A_c} \cdot \frac{\ell}{\Delta c_s'} \tag{5.6}$$

where $\qquad J_s = J - K_g \dfrac{\Delta c_g' \cdot A_c}{\ell}$

It will be observed that $(K)^S$ is approximately constant up to $\theta$ = 0.3,

but then increases rapidly in an exponential fashion.

It is perhaps relevant at this stage to consider the mechanism

by which surface diffusion occurs, (in section 2.1.6 several mechanisms

were discussed). Whilst no single mechanism can be universally applied,

151



Figure 5.8    Flux as a function of concentration at 308·15K
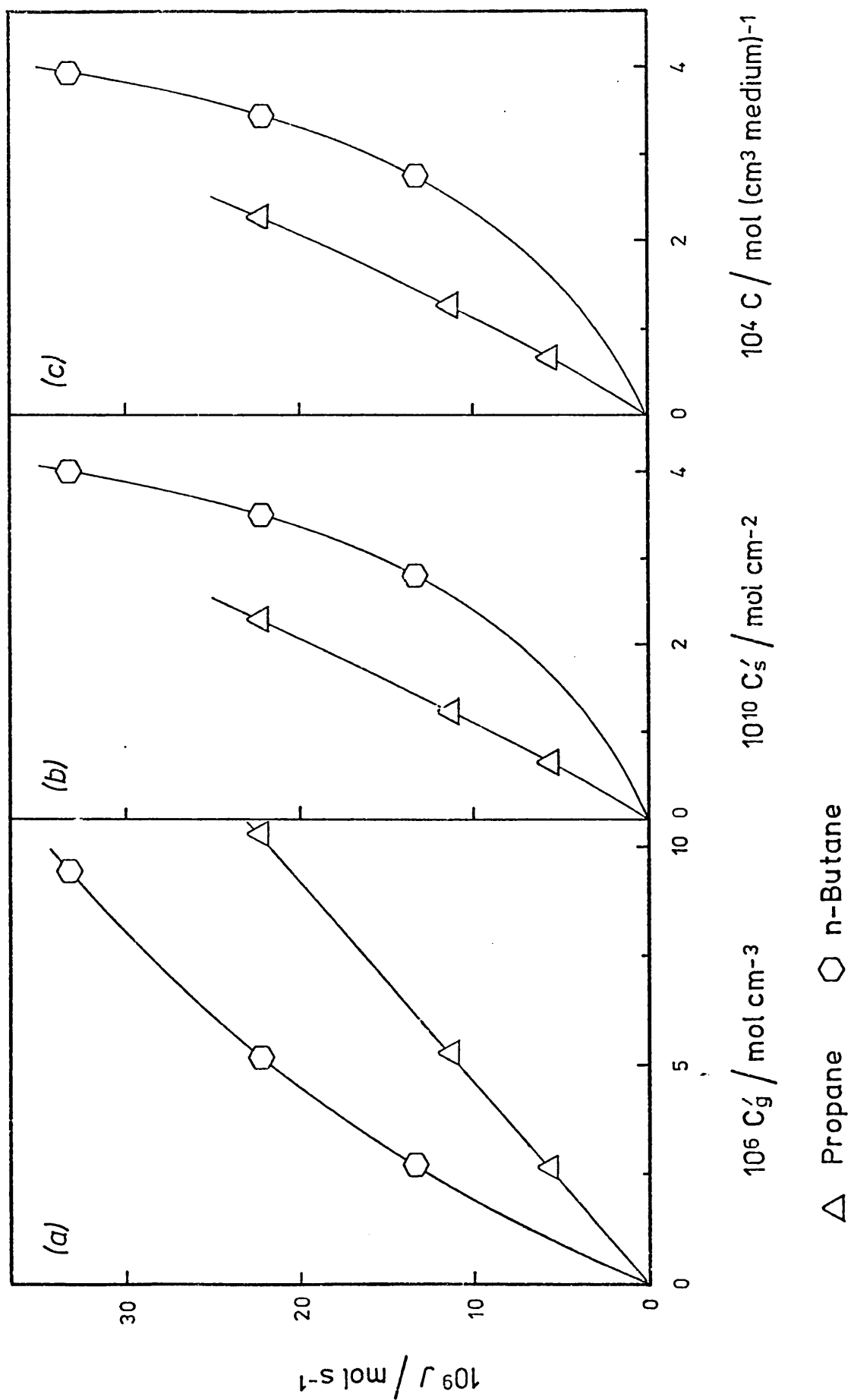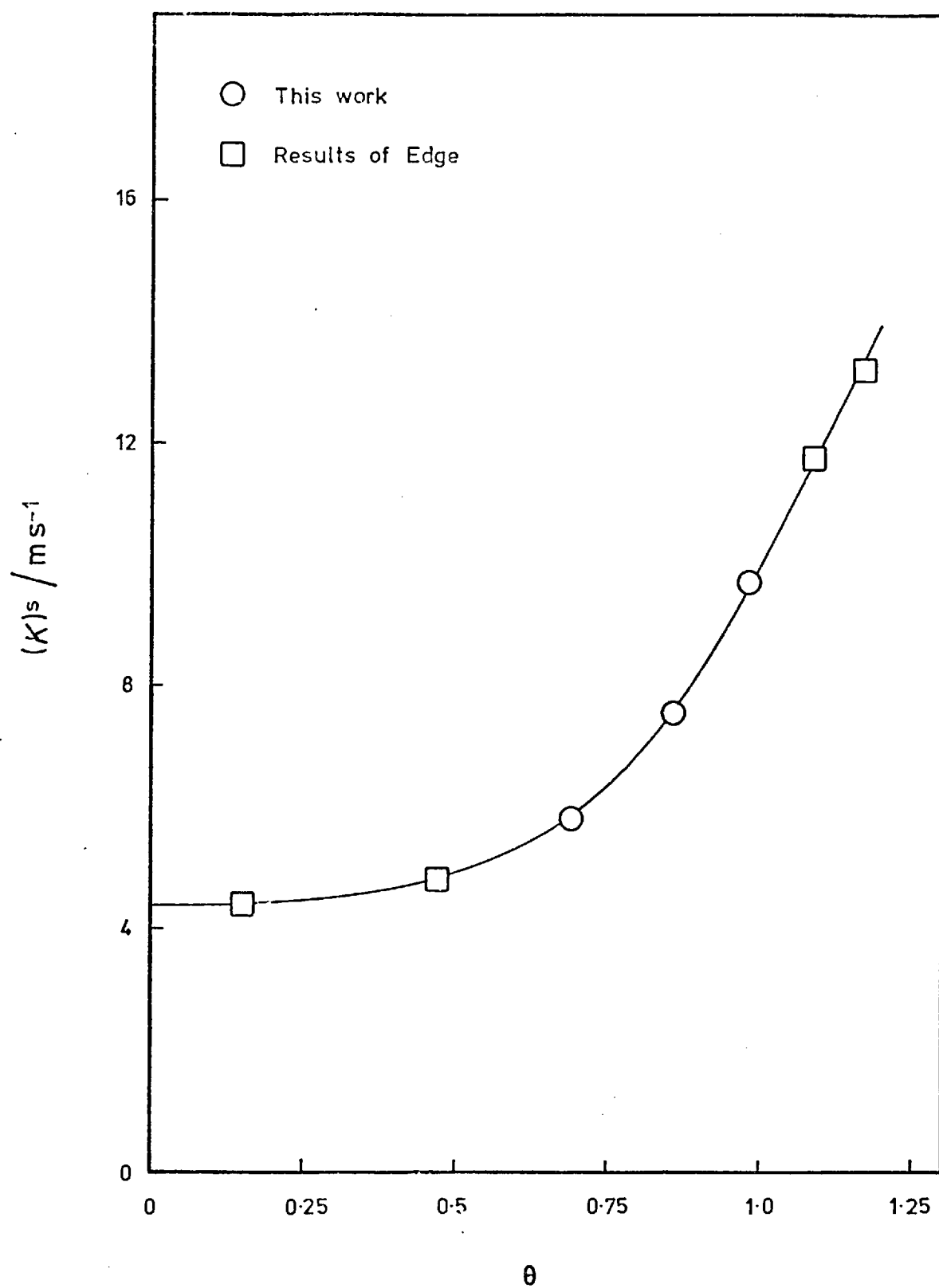
*Figure 5.9*    $(K)^s$  *as  a  function  of*  $\theta$  *for  n-butane*
*at*  308·15K

it is thought that at low sorption ($\theta \ll 1$) flow behaviour is best explained by a process of activated diffusion whereby transport occurs by a series of adsorption/desorption steps. Under conditions of higher sorption, as monolayer coverage is approached and exceeded, the hydrodynamic mechanism prevails with flow of a 'condensed' film across the surface.

Table 5.2 gives values of $\theta$ at several temperatures and pressures derived from adsorption data (chapter 4). Adsorption for $CH_4$ and $C_2H_6$ is clearly small and so the adsorbed layer will be very dilute. Activated diffusion will operate, diffusion being by a series of random jumps. Because of the diluteness of the film, there will be no hindrance to diffusion by neighbouring ad-atoms and the mean free path for ad-atom collisons ($\lambda_s$) will be much greater than the active site spacing. Thus in this dilute Henry law region suface flux will be proportional to the surface concentration gradient and hence proportional to the pressure gradient. Since $K$ is flux per unit pressure gradient, then it will remain constant with respect to pressure as is observed with $CH_4$ and $C_2H_6$.

TABLE 5.2

*Fractional surface coverage at several* T *and* p

| Adsorbate | $\frac{T}{K}$ | $\theta$ at | | |
| --- | --- | --- | --- | --- |
| | | 1 cmHg | 10 cmHg | 20 cmHg |
| $CH_4$ | 308.15 | 0.0004 | 0.0038 | 0.0077 |
| | 393.15 | 0.0001 | 0.0012 | 0.0024 |
| $C_2H_6$ | 308.15 | 0.0035 | 0.033 | 0.065 |
| | 393.15 | 0.0006 | 0.0065 | 0.013 |
| $C_3H_8$ | 308.15 | 0.029 | 0.27 | 0.50 |
| | 320.65 | 0.020 | 0.18 | 0.35 |
| | 393.15 | 0.0037 | 0.035 | 0.072 |
| $n-C_4H_{10}$ | 308.15 | 0.19 | 0.86 | 1.00 |
| | 373.15 | 0.024 | 0.21 | 0.38 |
| | 393.15 | 0.015 | 0.13 | 0.25 |

When adsorption approaching a monolayer occurs on the membrane surface (as was found here with n-butane at 308.15K) the surface density of ad-atoms will be high, $\lambda_s$ will be much smaller and few empty sites will be available to accommodate molecules migrating by a series of hops. Self encounters of migrating molecules will occur reducing surface mobility and transport by activated diffusion will be severely restricted. Thus a sharp drop in flux due to activated diffusion might be expected as the surface becomes filled and $\theta$ increases, although the activity correction and isotherm shape may mitigate the reduction in flux (Barrer and Jost, 1949).

However, as the monolayer is formed, it is likely that a hydrodynamic mechanism begins to take over, whereby a concerted flow of the first ad-layer occurs as a 2-dimensional liquid.

The behaviour of n-butane found here indicates that the pressure range ~0 to 1.5 cmHg (or $\theta < 0.3$) corresponds to a dilute film where $K$ and $(K)^s$ are approximately constant. Limiting values can be obtained as $\theta$ tends to zero. Above 5 cmHg $K$ falls corresponding to a curved section of the adsorption isotherm and $(K)^s$ begins to rise. This latter effect must be due to formation of a loosly bound highly mobile layer. Since no sharp discontinuity in $K$ is observed at $\theta = 1$ then a gradual change in diffusive mechanism must take place from site hopping in a dilute film ($\theta$ very small) to liquid-type diffusion in the first monolayer.

The sensitivity of the pressure dependence of $K$ upon temperature (figure 5.6) can readily be rationalised in terms of site coverage. At higher temperatures $\theta$, for a given pressure, becomes smaller (table 5.2) and so a higher pressure is required to observe a fall in $K$. Since the relative magnitude of $K_s$ is smaller and isotherm curvature less pronounced, then the fall in $K$ is less steep. Higher pressures than were used in this work must be employed to observe a significant fall in $K$ at the

higher temperatures. However at such high pressures the condition $\lambda > 10d$ will begin to break down and Poiseuille flow could occur in the gas phase leading to an increase in $K$.

Throughout this discussion the gas pressure and surface concentration have been related through isotherm data using the ingoing pressure, $p_o$, as being characteristic of the entire membrane. Clearly some pressure profile must exist within the membrane between the faces $x = 0$ and $x = \ell$, respectively at $p_o$ and nearly zero pressure. In the Henry's law range the pressure will fall in a linear manner between these faces. However, one may enquire whether the choice of $p_o$ to characterise the membrane is correct. $p_o/2$ (the average pressure within the membrane) has been suggested by Weber (1954). The choice of $p_o$ represents the most adverse condition, ie if $\lambda > 10d$ for $p_o$, then this condition is valid within the entire membrane. The use of $p_o$ is also suggested by analogy with the presence of bottlenecks. Since a narrow bottleneck can reduce flow through the entire membrane, then the region of greatest adsorption, causing greatest resistance to gas phase migration, will affect the flux throughout the membrane. Since this region corresponds to the ingoing surface, then $p_o$ is a reasonable characteristic pressure.

Ash, Baker and Barrer (1967) have suggested that $K$ remains independent of p so long as $dc_g'/dx$ is constant with x, ie if a linear pressure gradient is maintained within the membrane, even if $p_o$ lies outside the Henry law. This theory was tested in the following manner.

From the experimentally measured $J$ values at various pressures a master plot of $J$ against c (at $x = 0$) was constructed using isotherm data to evaluate c (the total concentration per unit volume of porous medium). This has been done in figure 5.8c. Values of c as a function of $x/\ell$ were then obtained when D is a function of concentration only using the relation:

$$\left(\frac{x}{\ell}\right)_c = \frac{J(c^*) - J(c)}{J(c^*)} \tag{5.7}$$

where $J(c^*)$ is the flux corresponding to $p_o$ and $J(c)$ is the interpolated

flux at another value of p and c ($<c^*$). Isotherm data were then used

to relate p to c and hence to $x/\ell$. Plots of pressure and total

concentration profile within the membrane could then be constructed.

In this work profiles were virtually linear except for n-butane

(figure 5.10) where significant deviations from linearity can be observed.

### 5.3.3 *Correlation of K with other parameters*

(i) Dolphin (1971) and Ash, Barrer, Clint, Dolphin and Murray

(1973) demonstrated that inert gases and other slightly sorbed adsorbates

gave smooth correlation curves when $KM^{\frac{1}{2}}$ (at constant temperature) was

plotted against properties related to the condensability of the gas such

as boiling point, $T_B$, and polarizability, $\alpha$. The plot of $KM^{\frac{1}{2}}$ versus

$\alpha T_B$ also proved to be a straight line in their work. In this study a

smooth curve was obtained for each relationship, but the curves for these

appreciably sorbed gases did not agree with those of Dolphin who used

the same adsorbent. Also the $\alpha T_B$ plot was not a straight line. The

least sorbed hydrocarbon, $CH_4$, did however fall on the correlation curves

obtained by Dolphin.

(ii) Similar poor agreement was found when the data from this

work were fitted to the plot of $KM^{\frac{1}{2}} T^{-\frac{1}{2}}$ versus $k_s$ (Ash et al, 1973).

Although methane came close to the reported curve, the points for $C_2H_6$

and $C_3H_8$ fell well below it; no $k_s$ values were determined for $n-C_4H_{10}$.

This poor agreement could be due to :-

(a) the difficulty of obtaining $k_s$ values for these hydrocarbons

since the isotherms were appreciably curved except at very low uptakes

where few data points were available.

(b) the increasing amount of surface flow (especially for $C_3H_8$)
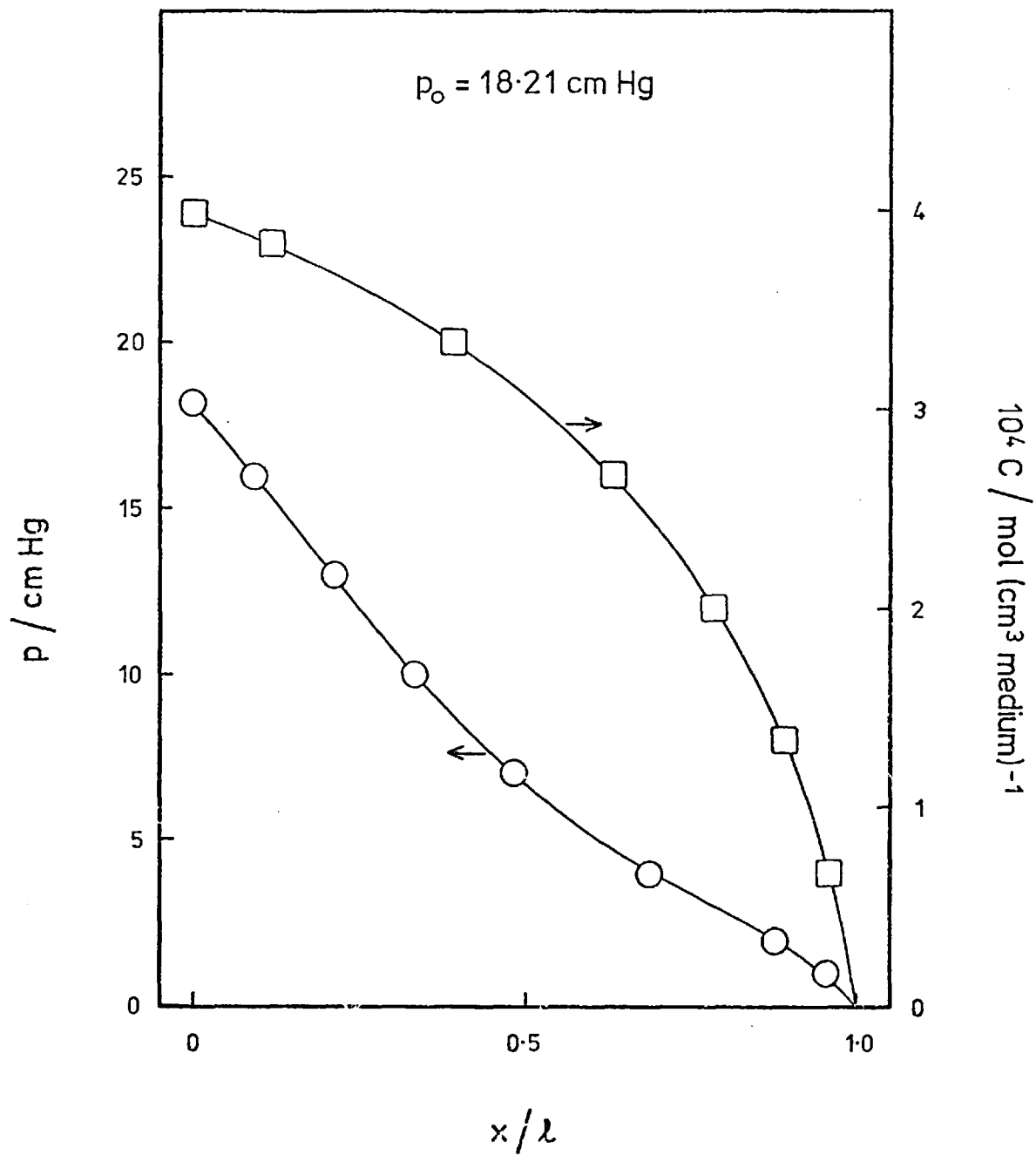
*Figure 5.10*      *Pressure and total concentration profiles*

*within the membrane for n-butane*

and the departure from Henry's Law adsorption in the pressure range used.

(iii)  Good correlations have been obtained between the product $KL$ and $A_g k_s$, and the straight line obtained agrees well with that reported for the inert gases by Ash et al (1973). There it was shown theoretically that $KL$ and $k_s$ are related for gases sorbed according to the Henry law by:-

$$KL = \frac{1}{6} \ell^2 \left[ (\varepsilon - 3\varepsilon_b) + k_s (A - 3A_b) \right] \qquad (2.30)$$

where $\varepsilon_b$ and $A_b$ are the porosity and area associated with blind-pore character and $A = A_g (1 - \varepsilon)\rho$. This correlation is shown in figure 5.11.

(iv)  It is of interest to compare the permeability results of Graphon, a substantially energetically homogeneous carbon, with those of Carbolac, a carbon having a degree of energetic heterogeneity. Some permeability data for $CH_4$, $C_2H_6$ and $C_3H_8$ on Carbolac have been reported (Ash et al 1973) and are here compared with the results on Graphon.

Table  5.3 compares $K_s$ and $K_s/A$ for the two carbons at 333.15K. $K_s$ values are several times greater on Graphon than on Carbolac and the extra flux generated per unit area of surface (as given by $K_s/A$) is at least an order of magnitude greater on Graphon. However $K_s/K_g$ is greater on Carbolac because of the very much smaller gas phase permeability and greater sorption.

TABLE 5.3

*$K_s$ and $K_s/A$ for Graphon and Carbolac at 333.15K*

| Adsorbate | Graphon | | | Carbolac | | |
|---|---|---|---|---|---|---|
| | $10^6 \dfrac{K_s}{m^2 s^{-1}}$ | $10^{15} \dfrac{K_s A^{-1}}{m^3 s^{-1}}$ | $\dfrac{K_s}{K_g}$ | $10^7 \dfrac{K_s}{m^2 s^{-1}}$ | $10^{16} \dfrac{K_s A^{-1}}{m^3 s^{-1}}$ | $\dfrac{K_s}{K_g}$ |
| $CH_4$ | $0.64_7$ | $6.6_0$ | 0.77 | $1.18_6$ | $1.1_3$ | 2.40 |
| $C_2H_6$ | $0.89_0$ | $9.0_8$ | 1.45 | 2.95 | $2.8_0$ | 8.17 |
| $C_3H_8$ | $1.70_0$ | $17.3_5$ | 3.35 | 6.63 | $6.3_0$ | 22.3 |

Figure 5.11 $\quad$ $KL$ as a function of $A_g k_s$
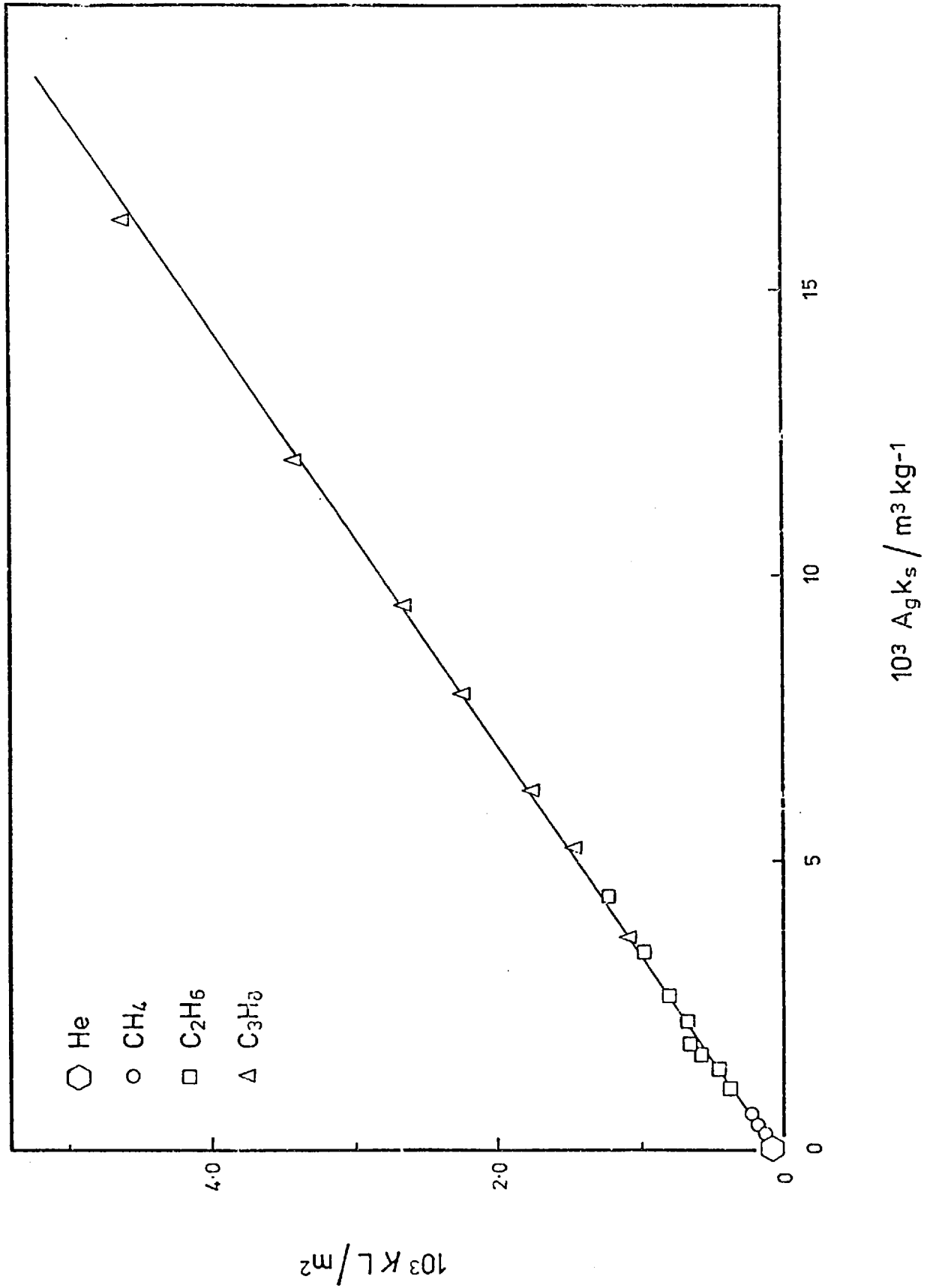
The smaller mobility of adsorbed atoms on a heterogeneous surface, Carbolac, compared with this mobility on a homogeneous surface could be due to the energetically sorbing sites on the Carbolac surface. These bind ad-atoms very strongly and retard progress of a molecule diffusing by a series of adsorption-desorption steps since a greater activation energy is required. Other factors, such as pore size and surface irregularities, are also involved. Gilliland et al (1974) and Horiguchi et al (1971) have also compared permeabilities of energetically homogeneous and heterogeneous materials (Graphon and Vycor glass). They found $K_s$ to be much greater for the homogeneous sorbent even though the membranes were of similar surface area, had a similar extent of adsorption and energy of activation for surface diffusion.

Onset of pressure dependence in $K$ occurs more readily for Carbolac than Graphon, marked pressure dependence on Carbolac occurring for $C_3H_8$ at 320.65K (compare with figure 5.5). This arises from the stronger sorption on Carbolac (owing to highly energetic surface sites), isotherms of $C_3H_8$ having a high degree of curvature and departing from the Henry law.

## 5.4. DIFFUSION COEFFICIENTS

In chapter 2 the following diffusion coefficients for gas phase and surface phase flow in the steady-state were defined

$$D_{gs} = \frac{K_g}{\varepsilon} = D_{gs}^{He} \left( \frac{M_{He}}{M} \right)^{\frac{1}{2}} \qquad (2.13 \; ; \; 2.14)$$

$$D_{ss} = \frac{K_s}{A. \, k_s} \qquad (2.15)$$

These coefficients are only valid within the Henry law range and rely on the values of $K_g$ obtained for helium, used as a non-sorbed calibrating gas.

Diffusion coefficients, $D_g$ and $D_s$, characteristic of the transient flow can be obtained from:

$$D_g^{He} = \frac{\ell^2}{6 L_{He}} \quad ; \quad D_g = D_g^{He} \left( \frac{M_{He}}{M} \right)^{\frac{1}{2}} \qquad (2.17)$$

and

$$D_s = \frac{\ell^2}{6A \, k_s/\varepsilon} \cdot \left[ \frac{(1 + A \, k_s/\varepsilon)}{L} - \frac{(M_{He}/M)^{\frac{1}{2}}}{L_{He}} \right] \qquad (2.19)$$

Both $D_g$ and $D_s$ depend on the accuracy of the time-lags for helium and the gas. Since the $L_{He}$ obtained in this work were too small to be measured accurately, the $L_{He}$ used in calculating $D_g$ and $D_s$ were those obtained by Dolphin (1971) using the same membrane but a different experimental rig where he took great care to measure $L_{He}$ as accurately as possible. The $K^{He}$ values were those of this determination.

Comparison can be made with $D_g^{cyl}$, the diffusion coefficient for gas phase, Knudsen flow for a cylindrical capillary model.

$$D_g^{cyl} = \frac{8}{3} \frac{\varepsilon}{A} \left( \frac{2RT}{\pi M} \right)^{\frac{1}{2}} \qquad (2.7)$$

The structure factors $\kappa_g$ and $\kappa_{gs}$, equation (2.20), then give an indication of the closeness of D for gas phase flow in the real, tortuous medium to D in the straight cylindrical channel having $\varepsilon/A$ equal to $\varepsilon/A$ in the actual medium:

$$\kappa_g = \frac{D_g}{D_g^{cyl}} \quad ; \quad \kappa_{gs} = \frac{D_{gs}}{D_g^{cyl}} \qquad (2.20)$$

The diffusion coefficients are given in table 5.4; $\kappa_g$ was found to be 0.73 and $\kappa_{gs}$ was 0.52. Slight differences in D's for helium from those reported by Ash et al, 1973 arose from the different value of $A_g$ (and hence A) obtained in this work. It did not prove possible to obtain $k_s$ values for n-butane and so no $D_s$ or $D_{ss}$ values could be obtained by this analysis.

## TABLE 5.4

*Diffusion coefficients in* $m^2 s^{-1}$

| Gas | Property | T/K | | | | | | | |
|-----|----------|-----|-----|-----|-----|-----|-----|-----|-----|
| | | 308.15 | 320.65 | 333.15 | 343.15 | 353.15 | 363.15 | 373.15 | 393.15 |
| He | $10^6 D_g^{cyl}$ | 7.35 | 7.50 | 7.65 | 7.76 | 7.87 | 7.98 | 8.09 | 8.31 |
| | $10^6 D_g$ | 5.40 | 5.51 | 5.61 | 5.69 | 5.78 | 5.86 | 5.94 | 6.10 |
| | $10^6 D_{gs}$ | 3.80 | 3.89 | 3.98 | 4.05 | 4.11 | 4.18 | 4.24 | 4.37 |
| $CH_4$ | $10^6 D_g^{cyl}$ | 3.67 | 3.75 | 3.82 | 3.88 | 3.93 | 3.99 | 4.04 | 4.15 |
| | $10^6 D_g$ | 2.70 | 2.75 | 2.80 | 2.84 | 2.89 | 2.93 | 2.97 | 3.04 |
| | $10^6 D_{gs}$ | 1.90 | 1.94 | 1.99 | 2.02 | 2.05 | 2.09 | 2.12 | 2.19 |
| | $10^6 D_s$ | 1.39 | 1.63 | 1.67 | 1.81 | 2.00 | 2.18 | 2.15 | 2.89 |
| | $10^6 D_{ss}$ | 1.08 | 1.16 | 1.29 | 1.37 | 1.47 | 1.60 | 1.62 | 1.74 |
| $C_2H_6$ | $10^6 D_g^{cyl}$ | 2.68 | 2.74 | 2.79 | 2.83 | 2.87 | 2.91 | 2.95 | 3.03 |
| | $10^6 D_g$ | 1.97 | 2.01 | 2.05 | 2.08 | 2.11 | 2.14 | 2.17 | 2.22 |
| | $10^6 D_{gs}$ | 1.39 | 1.42 | 1.45 | 1.48 | 1.50 | 1.52 | 1.55 | 1.60 |
| | $10^7 D_s$ | 2.78 | 3.09 | 3.43 | 3.87 | 4.30 | 4.62 | 5.09 | 5.78 |
| | $10^7 D_{ss}$ | 2.24 | 2.55 | 2.96 | 3.26 | 3.58 | 3.86 | 4.26 | 5.13 |
| $C_3H_8$ | $10^6 D_g^{cyl}$ | 2.22 | 2.26 | 2.30 | 2.34 | 2.37 | 2.41 | 2.44 | 2.50 |
| | $10^6 D_g$ | 1.63 | 1.66 | 1.69 | 1.72 | 1.74 | 1.77 | 1.79 | 1.84 |
| | $10^6 D_{gs}$ | 1.15 | 1.17 | 1.20 | 1.22 | 1.24 | 1.26 | 1.28 | 1.32 |
| | $10^7 D_s$ | 1.07 | 1.23 | 1.45 | 1.66 | 1.80 | 2.07 | 2.29 | 2.64 |
| | $10^7 D_{ss}$ | $0.89_8$ | 1.07 | 1.24 | 1.40 | 1.51 | 1.72 | 1.86 | 2.27 |
| $n\text{-}C_4H_{10}$ | $10^6 D_g^{cyl}$ | 1.93 | 1.97 | 2.01 | 2.04 | 2.07 | 2.10 | 2.12 | 2.18 |
| | $10^6 D_g$ | 1.42 | 1.45 | 1.47 | 1.49 | 1.52 | 1.54 | 1.56 | 1.60 |
| | $10^6 D_{gs}$ | $0.99_7$ | 1.02 | 1.04 | 1.06 | 1.08 | 1.10 | 1.11 | 1.15 |

All diffusion coefficients are found to increase with increasing temperature. This can readily be ascribed to increasing mobility of ad-atoms when they possess greater thermal energy. As would be expected D is found to decrease with increasing molecular size. The structure factors are both less than unity implying that tortuosity and bottlenecks play an important part in regulating the values of the diffusion coefficients.

Some comparisons with literature values can be made. Horiguchi et al (1971) obtained limiting $D_{ss}$ of $2.8 \times 10^{-7}$, $4.1 \times 10^{-7}$ and $5.1 \times 10^{-7}$ $m^2 s^{-1}$ at 273.15K, 298.15K and 323.15K respectively for ethane on a Graphon membrane ($A_c = 0.709$ $cm^2$, $\ell = 1.47$ cm, $\varepsilon = 0.51$, $\kappa_{gs} = 0.31$). From table 5.4 it would appear that these values are approximately twice as great as would be expected from this work. Horiguchi's work however covered the mean pressure range 5 to 700 Torr and in his calculation of $D_{ss}$ (expressed as $D_{ss}$ $\varepsilon/\kappa_{gs}$) used the isotherm slope rather than the limiting slope, $k_s$. He also found a slight pressure dependence of $D_{ss}$ even at $50^{\circ}C$.

### 5.4.1 *Temperature dependence of* $D_s$ *and* $D_{ss}$

In chapter 2 we saw that energies of activation for surface diffusion in the transient and the steady-state can be obtained from Arrhenius plots in accordance with:

$$D_s = D_o \exp(-E_s/RT) \quad ; \quad D_{ss} = D_{os} \exp(-E_{ss}/RT) \qquad (2.21)$$

Plots of $\log_{10} D_s$ and $\log_{10} D_{ss}$ versus $T^{-1}$ can therefore yield $E_s$ and $E_{ss}$ from the slope and $D_o$ and $D_{os}$ from the intercept. Table 5.5 presents activation energies and standard diffusion coefficients obtained in this way. The energy of adsorption for each adsorbate is also given (chapter 4).

TABLE 5.5

*Arrhenius activation energies and pre-exponential factors*

| | $E_s$ | $E_{ss}$ | $10^6 D_o$ | $10^6 D_{os}$ | $-\Delta E'$ |
|---|---|---|---|---|---|
| | $kJ\ mol^{-1}$ | $kJ\ mol^{-1}$ | $m^2\ s^{-1}$ | $m^2\ s^{-1}$ | $kJ\ mol^{-1}$ |
| $CH_4$ | 7.3 | 6.0 | 23.$_3$ | 11.2 | 10.7 |
| $C_2H_6$ | 9.2 | 9.7 | 9.9 | 9.8 | 17.1 |
| $C_3H_8$ | 11.6 | 10.9 | 9.5 | 6.1$_7$ | 21.7 |

It can be seen that for all adsorbates the activation energy is at least twice the thermal energy available (RT) but less than $-\Delta E'$. The surface molecules are therefore quite stongly bound and activated diffusion must take place for surface phase migration. Adsorption does not lead to two-dimensional gas behaviour, which would imply temperature insensitive diffusion coefficients, and sorption is too small for the hydrodynamic flow model of Babbitt (1950, 1951) to operate.

Recent papers by Horiguchi (1971) and Gilliland (1974) have examined the hydrodynamic model and the activated diffusion model for surface diffusion using published experimental data for a variety of adsorbate/ adsorbent systems. Only for strong adsorption ($\theta \geq 1$) could agreement be obtained between experimental results and the hydrodynamic model. However the activated diffusion model (equation (2.21)) gave a reasonable fit of the experimental data where $\theta < 1$.

The activation energy $E_{ss}$ was interpreted as bq where q is a heat of adsorption. b was found to be about $\frac{1}{2}$ for most gases on carbon blacks (Sladek (1974) found 0.45 and Horiguchi 0.57) when correlated against the isosteric heat. In this investigation the correlation gave b as 0.44, 0.47 and 0.44 for $CH_4$, $C_2H_6$ and $C_3H_8$ respectively. Both Horiguchi and Gilliland assumed that the correlation

$$D_{ss} = D_{os} \exp \left( -\frac{bq}{RT} \right) \tag{5.8}$$

was valid for all gases on a given surface ie that $D_{os}$ and b are

universal constants. In this work it was found that b was approximately

constant but that $D_{os}$ varied considerably in the $q'_{st}$ correlation.

However if $\Delta E'$ was used in the correlation, a smooth curve was obtained

when log $D_{ss}$ or log $D_s$ was plotted against $- \Delta E'/RT$ (figure 5.12) for

methane, ethane and propane.

### 5.4.2  *Concentration dependence of* $D_{ss}$

In cases where the Henry law was not obeyed, even in the very low

pressure region of the isotherm, the analysis which leads to $D_{ss} = K_s/Ak_s$

is no longer valid. It can be shown that

$$K = \varepsilon \left( \frac{\ell}{\Delta c_g} \right) \left[ - D_{ss} \left( \frac{\partial c_s}{\partial c_g} \right)_T - D_{gs} \right] \left( \frac{\partial c_g}{\partial x} \right)_T \qquad (5.9)$$

and assuming a linear gas phase concentration gradient

$$\frac{K}{\varepsilon} = D_{ss} \left( \frac{\partial c_s}{\partial c_g} \right)_T + \frac{K^{He}}{\varepsilon} \left( \frac{M_{He}}{M} \right)^{\frac{1}{2}} \qquad (5.10)$$

Now $(\partial c_s/\partial c_g)_T$ can be obtained from isotherm data and so we get

$$D_{ss} = \frac{273.15}{\rho (1-\varepsilon) 76} \frac{\left[ K - K^{He}(M_{He}/M)^{\frac{1}{2}} \right]}{T} \left( \frac{\partial p}{\partial v} \right)_T \qquad (5.11)$$

$D_{ss}$ can now be determined as a function of v at each temperature for which

$K$, $K^{He}$ and isotherm data are known. This analysis can also allow for any

variation in $K$ with pressure (and v) by interpolation of $K$ from a plot of

$K$ versus v.

It has been pointed out (Ash et al, 1973) that for permeability data

where extensive adsorption occurs, partial or total blockage of pore

space might take place resulting in a complete absence of a $K_g$ component.

Hence $K_s$ ($= K - K^{He} (M_{He}/M)^{\frac{1}{2}}$) in equation (5.11) should be replaced by $K$

when complete gas phase blockage occurs. Internal calibration with

helium in the presence of the adsorbed gas should be carried out to

estimate the precise degree of blockage, but in the absence of such data
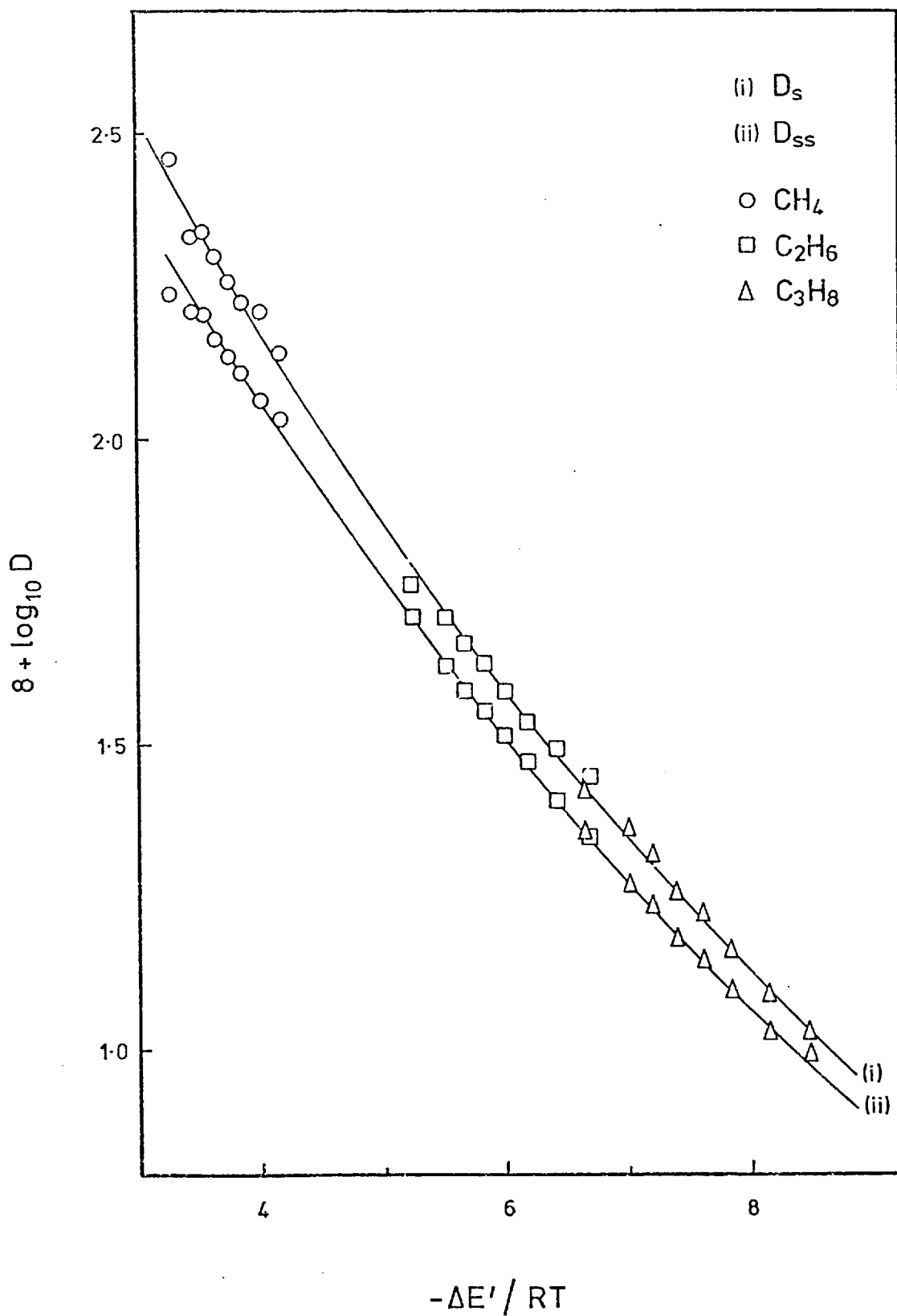
Figure 5.12 · Correlation of $D_s$ and $D_{ss}$ with $-\Delta E'/RT$

maximum and minimum values of $D_{ss}$ can be obtained by using $K$ and $K_s$ respectively. In practice, owing to the large value of $K_s/K_g$ for gases where this analysis is necessary, maximum and minimum values differ by only 5-10%.

The above analysis was carried out for n-butane at 308.15K, taking account of the variation of $K$ with v and with calculation of maximum and minimum $D_{ss}$ values. The resulting curves of $D_{ss}$ versus v are displayed in figure 5.13. Permeability data at 373.15 and 393.15K were also analysed using $K_s$ and taking account of the very slight pressure dependence of $D_{ss}$ (figure 5.14). As θ was less than 0.4, no blockage was thought to occur, and so $K_s$ was used in equation (5.11). Analysis at intermediate temperatures was not possible as isotherm data was not available.

A similar analysis was attempted for propane. However above 320.65K the isotherms were nearly straight lines in the pressure region concerned so that accurate values of changes in the tangential slope were difficult to obtain and the slopes were nearly constant. $D_{ss}$ versus v at 308.15 and 320.65K is shown in figure 5.14; no pressure dependence of $K$ was detected and as θ was less than 0.5, $K_s$ was used.

Limiting values of $D_{ss}$ at v = 0 were obtained by extrapolation in figures 5.13 and 5.14, and are quoted in table 5.6. The values obtained for propane were found to be higher than those obtained from the limiting Henry law coefficient, the discrepancy being caused by a relatively sharp isotherm curvature at low pressure. Limiting values obtained for n-butane required the use of permeability data obtained by Dr Edge to calculate $D_{ss}$ at low values of v (and hence p).
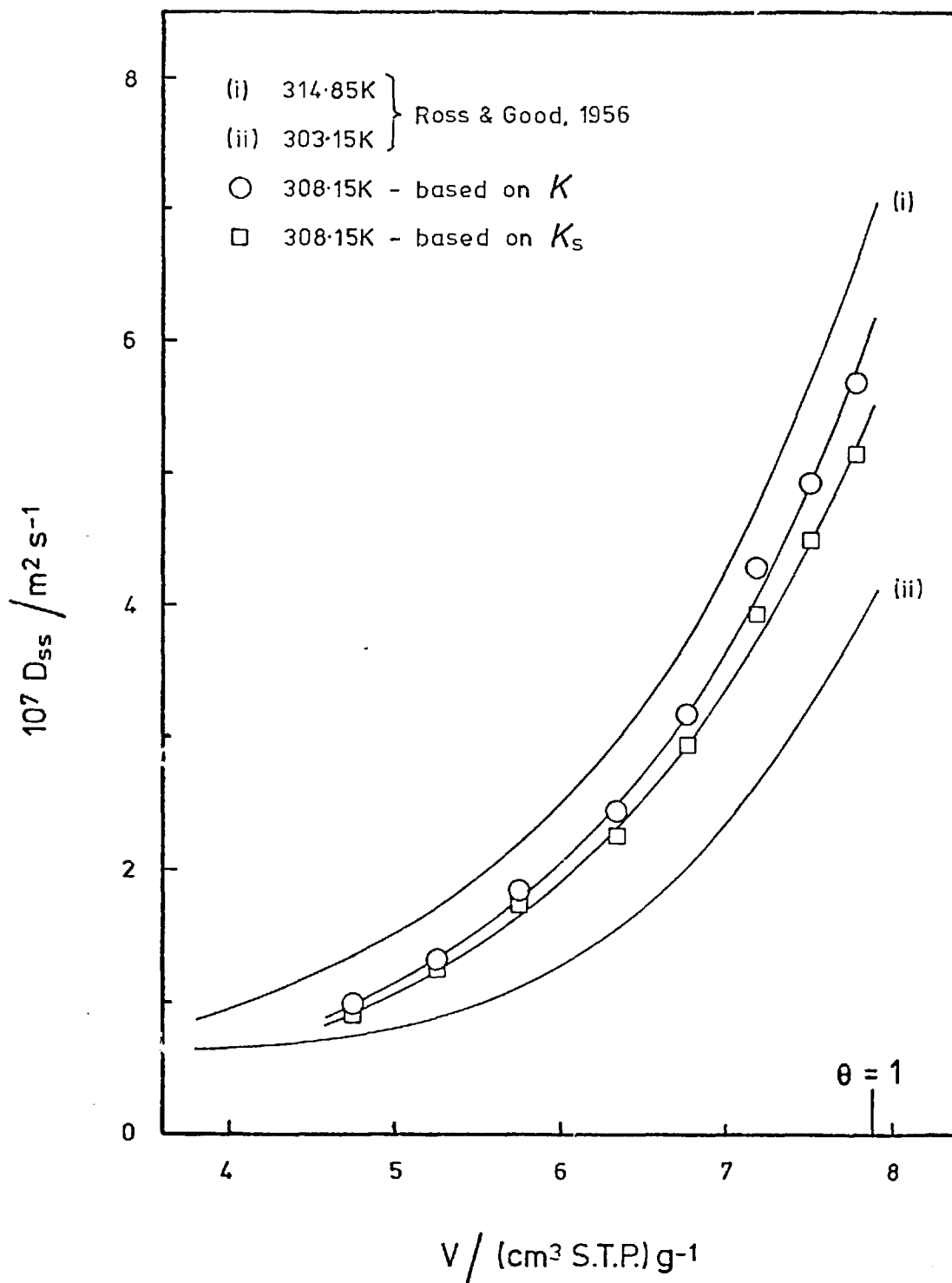
*Figure 5.13*   $D_{ss}$ *as a function of adsorption uptake*

*for n-butane*
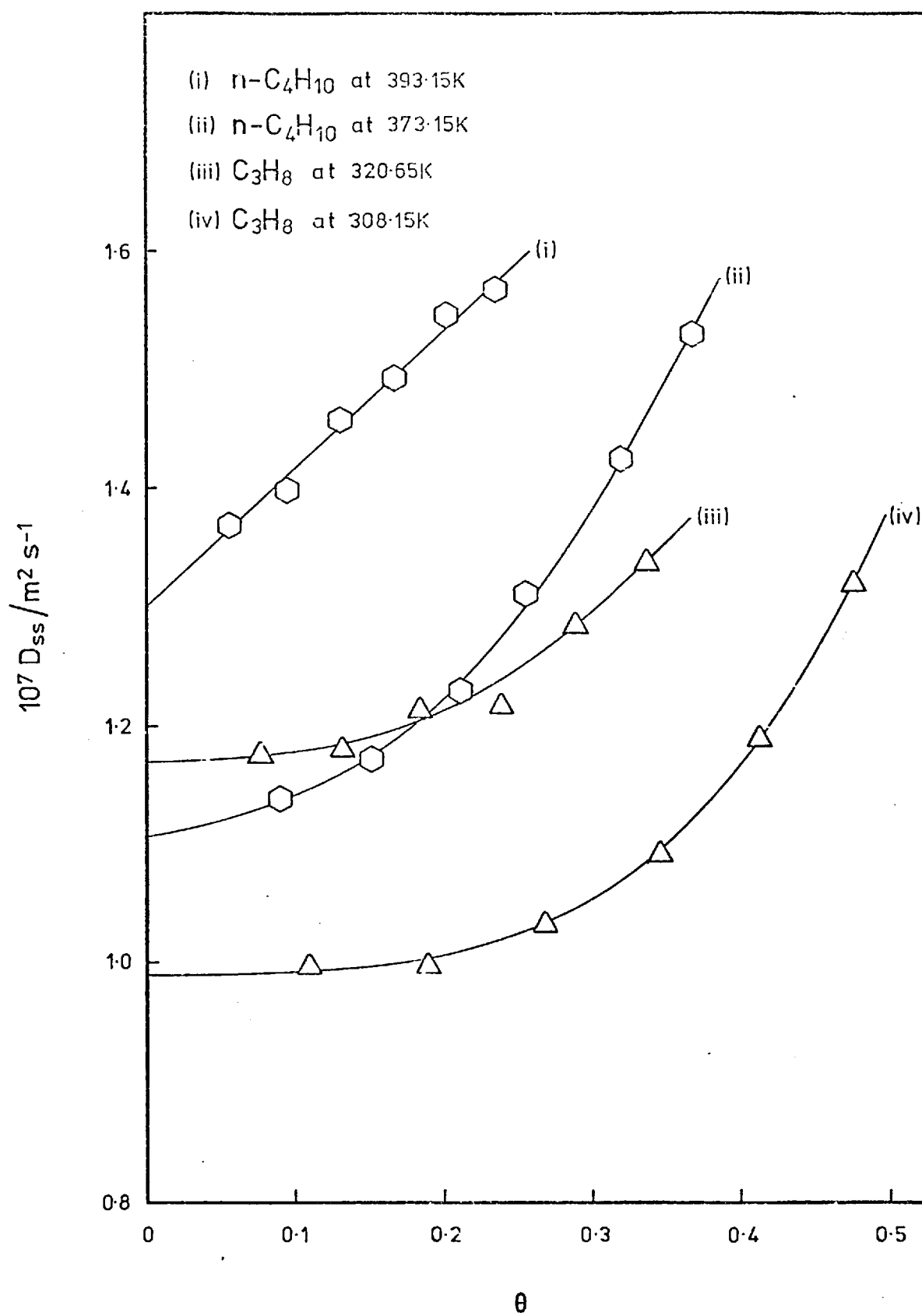
Figure 5.14            $D_{ss}$ as a function of $\theta$

TABLE 5.6

*Limiting values of* $10^7 \ D_{ss} \ (m^2 \ s^{-1})$

|  | T/K | | | |
|---|---|---|---|---|
|  | 308.15 | 320.65 | 373.15 | 393.15 |
| $C_3H_8$ | 0.99 | 1.17 | – | – |
| $n-C_4H_{10}$ | 0.45 | – | 1.10 | 1.30 |

In general the $D_{ss}$ versus v curve is of a near exponential form implying increased surface diffusion at greater surface concentration. At low $\theta$ the adsorbed species are strongly bound but become much more mobile as $\theta$ approaches unity. This behaviour is more pronounced on a heterogeneous surface where mobility increases very rapidly as the weaker adsorption sites become occupied (eg propane on Carbolac, Ash et al 1973). The behaviour found in figures 5.13 and 5.14, using equation (5.11), arises largely because the isotherm slope decreases with increasing v. When monolayer coverage is approached the isotherm might be expected to flatten out, possibly exhibiting a broad point of inflection and having a sigmoidal shape. If this were the case, then (dp/dv) would reach a high constant value in the flat inflection region before decreasing sharply as a second molecular layer begins to form. $D_{ss}$ would then exhibit a sharp maximum close to $\theta = 1$ when plotted against v.

Ross and Good (1956) studied the surface diffusion of n-butane on a Graphon membrane ($\epsilon = 0.54$) at 303.15 and 314.85K at surface coverages up to $\theta = 1.3$. They found a steady increase in $D_{ss}$, as observed here, reaching a maximum value at $\theta = 1$ after which $D_{ss}$ became constant or had a slight tendency to decrease. $D_{ss}$ values obtained by Ross and Good are illustrated in figure 5.13 and give excellent agreement with the diffusion coefficients obtained in this work.

As in the previous section equation (5.8) can be used to correlate $D_{ss}$ and $q'_{st}$ by plotting log $D_{ss}$ against $q'_{st}/RT$ but now, because of the

variation of both $D_{ss}$ and $q'_{st}$ with $\theta$ or $p$, a set of data points occurs at each temperature. Gilliland et al (1974) did this for $CO_2$ and $SO_2$ on Vycor, as well as correlating the data of Pope (1961) for $SO_2$ on Carbolac and of Carman and Raal (1951a) for $CF_2Cl_2$ on silica. Good linear relationships were obtained.

The adsorbents described by Gilliland were energetically heterogeneous and consequently $q'_{st}$ decreased markedly with increasing $\theta$. When a more homogeneous adsorbent is used, as in this work, $q'_{st}$ is approximately constant, increasing slightly at high $\theta$ where lateral interactions are possible, and the correlation is less good. Figure 5.15 demonstrates this - a series of curves, approximately perpendicular to the main log $D_{ss}$ versus $q'_{st}/RT$ line, occurs. This increase in $D_{ss}$ at constant temperature reflects the dependence of $D_{os}$ on $\theta$. On a heterogeneous sorbent this behaviour is masked by the simultaneous decrease in $q'_{st}$ at larger $\theta$ which compensates for the increase in $D_{ss}$ and enables a straight line to be drawn through the experimental points. Horiguchi attempted to correlate a very wide range of published data in this way, including $C_2H_6$ on a Graphon membrane at 273.15, 298.15 and 323.15K. He found similar behaviour to that shown in figure 5.15.

Several models have been proposed to allow for a gradual change in flow mechanism from activated diffusion (valid at low coverage where $D_{ss}$ is independent of $\theta$) to one where $D_{ss}$ varies with $\theta$ as the monolayer is approached.

Barrer and Jost (1949) showed how $D_{ss}$ could remain independent of $\theta$ at relatively high surface concentrations. They obtained an expression for $D_{ss}$ as :

$$D_{ss} = D_{os} (1 - \theta) \cdot \frac{d\ln p}{d\ln\theta} \tag{5.12}$$

$D_{os}$ is the diffusion coefficient at $\theta = 0$ and $(1 - \theta)$ is the probability that there is a vacant site available for the diffusing molecule to
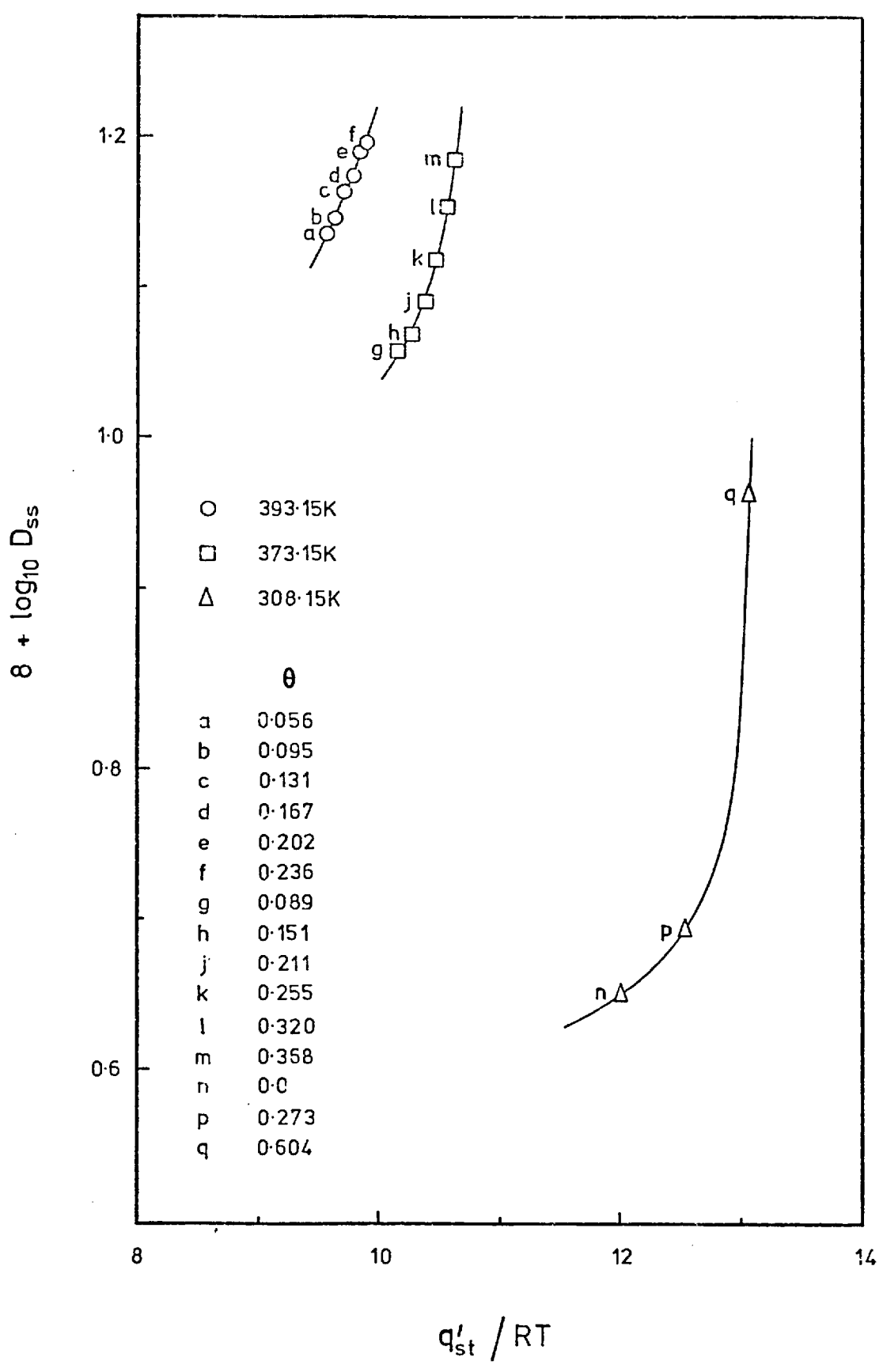
Figure 5.15    Correlation of D$_{ss}$ with q$'_{st}$/RT
for n-butane

jump into. $d\ln p/d\ln\theta$ is the activity correction which allows for the effect of the sorption isotherm on surface concentration. For a Langmuir-type isotherm $d\ln p/d\ln\theta = 1/(1 - \theta)$ hence the two opposing effects of surface concentration and isotherm shape cancel out and $D_{ss}$ is predicted to be constant.

In this work a marked increase in $D_{ss}$ occurs as $\theta \rightarrow 1$. Higashi et al (1964) attempted to explain this type of behaviour using the random walk diffusive model. He assumed that when a diffusing molecule encountered an occupied site it immediately bounced off and continued its journey until it found an unoccupied site where it was re-adsorbed. Thus, in this model, the effective mean jump distance appears to be lengthened by the presence of neighbouring ad-atoms and the diffusion coefficient is thereby increased. He obtained the relation (cf equation (5.8)):

$$D_{ss} = \frac{D_{os}}{1 - \theta} \exp\left(- \frac{E_{ss}}{RT}\right) \qquad (5.13)$$

$D_{os}$ is independent of $\theta$.

Horiguchi fitted this equation to literature data on Graphon and found fair agreement up to $\theta = 0.6$. At higher values of $\theta$, $D_{ss}$ is predicted to be larger than the experimental values, and the relationship clearly breaks down at $\theta = 1$, since $D_{ss}$ is then predicted to become infinite.

Figure 5.16 tests equation (5.13) for propane and butane when $\theta$ - dependence of $D_{ss}$ was found. In all cases the Higashi model provided for a more rapid increase in $D_{ss}$ with $\theta$ than was found by experiment.

Yang et al (1973) suggested a modification to allow for interaction between a sorbed molecule and an impinging one and for a finite residence time of the molecule on an occupied site. Their suggestion replaces $1 - \theta$ in equation (5.13) by :

$$1 - \theta + \theta \cdot \frac{\nu_1}{\nu_2} \cdot \exp\left[\frac{- (\Delta E_1 - \Delta E_2)}{RT}\right] \qquad (5.14)$$
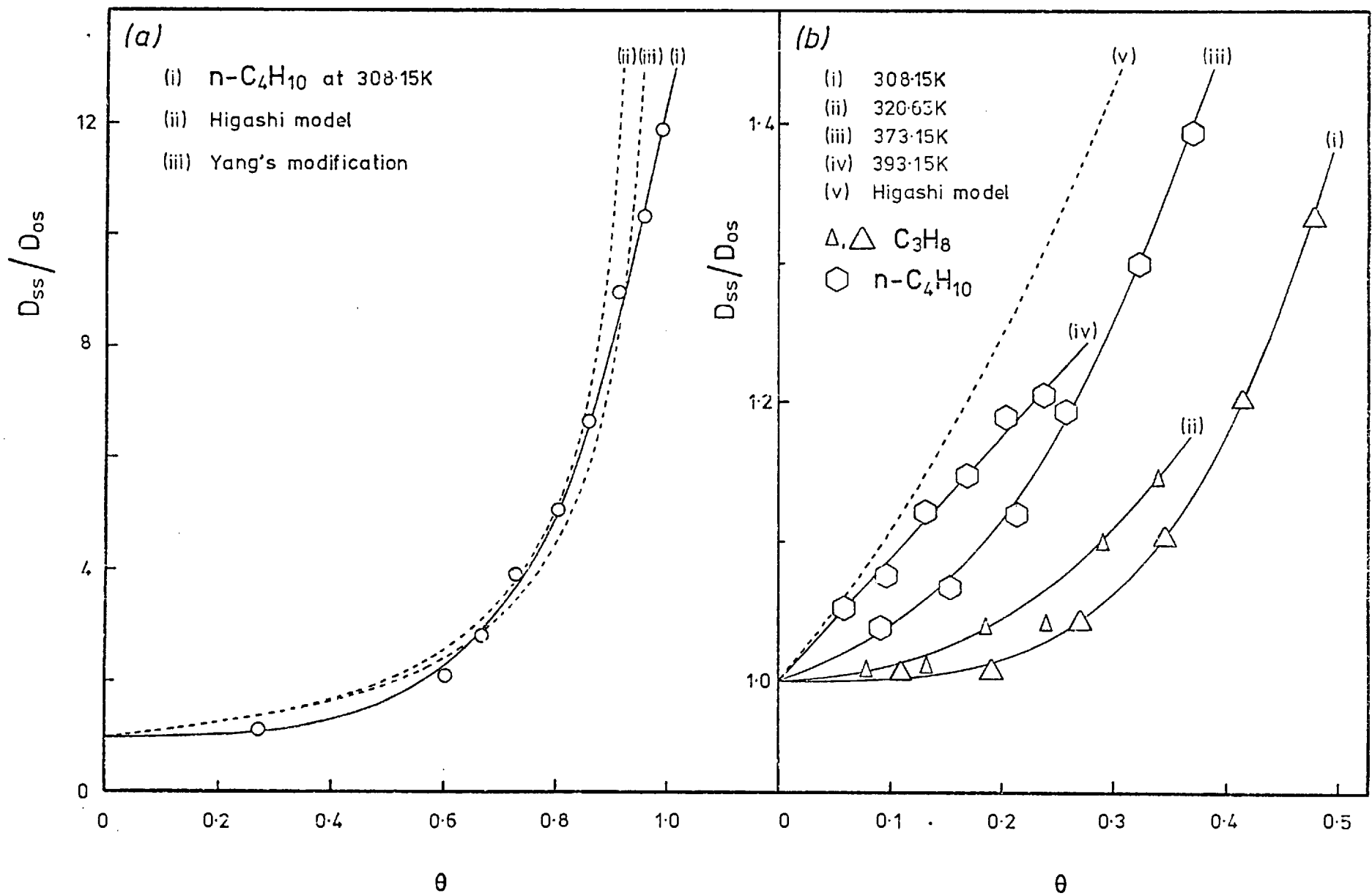
Figure 5.16 Comparison of $D_{ss}$ with the Higashi model

(a)

(i)   n-$C_4H_{10}$ at 308·15K

(ii)  Higashi model

(iii) Yang's modification

(b)

(i)   308·15K

(ii)  320·63K

(iii) 373·15K

(iv)  393·15K

(v)   Higashi model

$\triangle, \triangle$  $C_3H_8$

$\hexagon$  n-$C_4H_{10}$

where $\Delta E$ is an activation energy and $\nu$ is the oscillation frequency of

an adsorbed molecule. Subscripts 1 and 2 refer to molecules adsorbed on

unoccupied and occupied sites respectively. This relation provides for

finite values of $D_{ss}/D_{os}$ at $\theta = 1$.

Using $\Delta E_1 - \Delta E_2 = 8.8$ kJ/mol and $\nu_1/\nu_2 = 1.5$ (314.85K) or

1.0 (303.15K) Yang fitted the n-butane/Graphon data of Ross and Good.

Reasonable agreement appears to be obtained, but this model merely

shifts the point at which $D_{ss}$ becomes infinite to a slightly larger value

of $\theta$, which will be both gas and temperature dependent. No attempt at

allowing for an alternative surface diffusion mechanism above $\theta = 1$

was made.

In figure 5.16a the theoretical curves of the Higashi model and

the Yang modification are shown, the latter using $\Delta E_1 - \Delta E_2 = 8.8$ kJ mol$^{-1}$

and $\nu_1/\nu_2 = 1.0$. Both models correctly predict the general shape of the

$D_{ss}/D_{os}$ versus $\theta$ curve for n-butane at 308.15K and a good fit is obtained

between $\theta = 0.6$ and $\theta = 0.9$. However, both models break down above $\theta = 0.92$

and at low $\theta$ there is a discrepancy between theoretical curve and

experimental data which is larger at lower temperatures (figure 5.16b).

CHAPTER 6

THERMO-OSMOTIC TRANSPORT

## 6.1 EXPERIMENTAL RESULTS

The thermo-osmotic investigations employed a membrane of similar

shape and porosity to that used in the isothermal flow studies, but

a temperature gradient was maintained between the membrane faces.

The membrane was exposed to gas at a constant pressure and when

sorption equilibrium had taken place then the gas reservoirs either

side of the membrane were isolated. Since the condition $\lambda > 10d$ was met,

then some thermo-osmotic transport occurred and a pressure difference

began to build up between the membrane faces.

From the initial build-up of pressure an isobaric permeability

was determined. The approach to a constant pressure gradient was

followed and from the steady-state pressure ratio, a heat of transport

was determined.

### 6.1.1 *Preliminary work concerning thermocouples*

The previous membrane design used in these laboratories (Clint,

1966; Dolphin, 1971) employed thermocouples set into the face of the

restraining plungers to record face temperatures, $T_o$ and $T_\ell$. Since

these plungers were in light contact with the plug, an insulating layer

of gas probably existed between thermocouple junction and plug face.

Clint investigated the effect of varying the gas pressure on the

response of these thermocouples. Whilst thermocouple output remained

constant at pressures in excess of 10 cmHg, at low pressures (ca. 1 cmHg)

$T_o$ (the hot face temperature) increased significantly and $T_\ell$ (the cold

face temperature) fell. This behaviour was attributed to a reduction in

the gas thermal conductivity at low pressures.

The plug assembly in this work (Graphon membrane O, see section

3.6.1) was designed to reduce, and to allow estimates of,

the uncertainties in $T_o$ and $T_\ell$ by (i) using thermocouples with hot

junctions actually pressing into the plug faces and (ii) recording

any temperature variation across the face by having a thermocouple at

the centre and edge of each face. Four temperatures were therefore

measured : $T_o^c$, $T_o^e$, $T_\ell^c$, $T_\ell^e$, superscripts c and e referring to centre and

edge respectively.

Propane is typical of the gases used in the thermo-osmotic work

in having a low thermal conductivity (table 6.1). A careful study was

therefore made of the thermocouple outputs for constant temperatures of

heat source and sink when the propane pressure was increased from high

vacuum to 30 cmHg. Thermocouple output was found to remain constant

above 2 cmHg, an improvement on Clint's findings where with He and Ne,

gases of greater thermal conductivity than $C_3H_8$, a constant output was

not obtained below 5 cmHg and experiments were only conducted at

pressures considerably in excess of this value.

### TABLE 6.1

*Thermal conductivities, k, at 300K for gases and*

*materials used in the membrane assembly*

| Material | k $Wm^{-1} K^{-1}$ | Ref |
|---|---|---|
| Porous carbon ($\varepsilon=0.47$) | 1.75 | 1 |
| Copper | 400. | 2 |
| Stainless steel | 25. | 1 |
| Helium | $0.15_1$ | 2 |
| Neon | $0.04_8$ | 2 |
| Methane | $0.03_4$ | 2 |
| Ethane | $0.02_1$ | 2 |
| Propane | $0.01_8$ | 2 |
| n-Butane | $0.01_6$ | 2 |
| (1) Perry and Chilton, 1973 | | |
| (2) Weast, 1970 | | |

Figure 6.1 Thermocouple outputs as a function of pressure
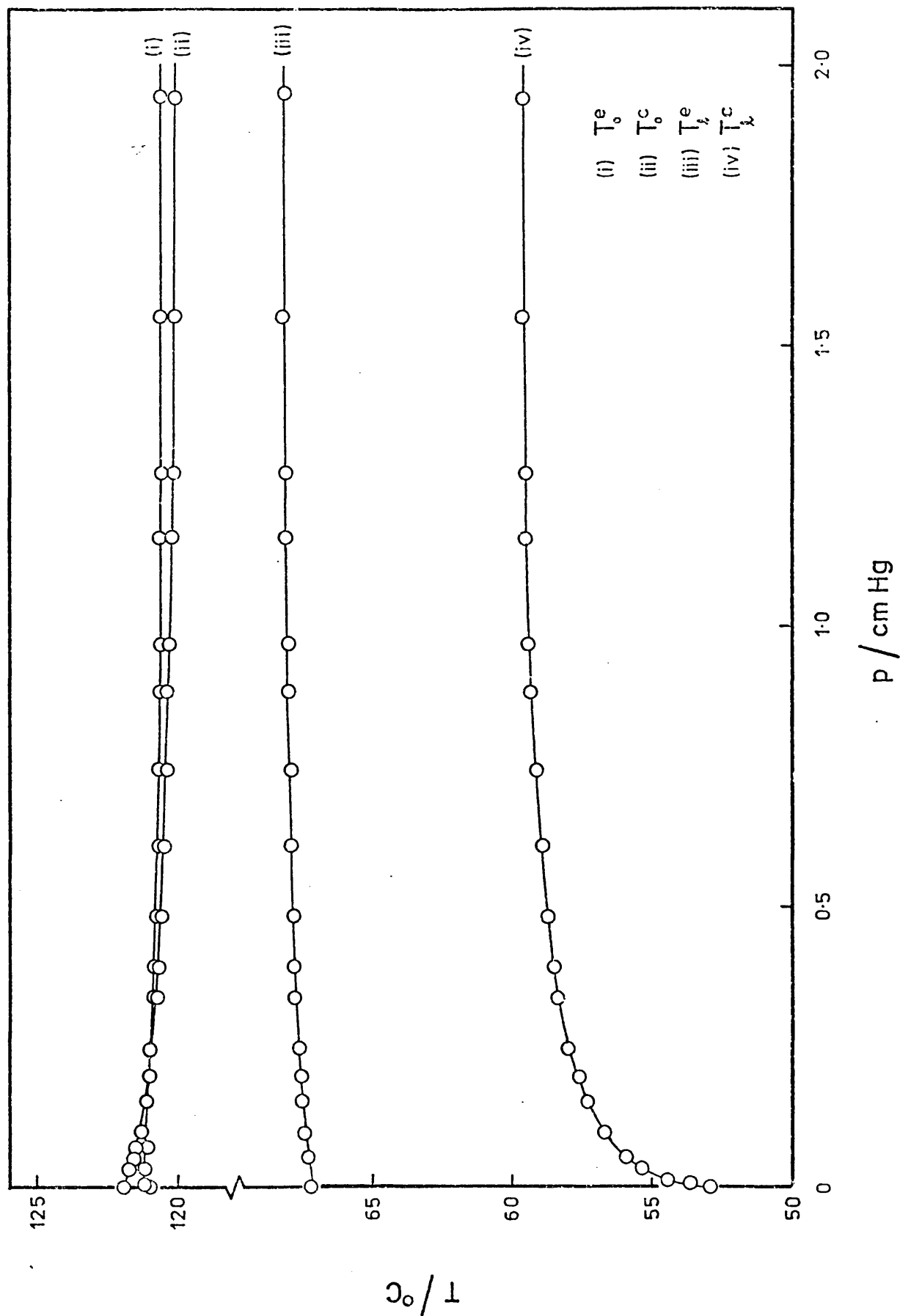
Figure 6.1 shows the pressure variation below 2 cmHg : $T_o^c$ and $T_o^e$ are reasonably constant being within 1 degree of one another and increasing by less than 2 degrees in the pressure range studied. $T_\ell^e$ is also substantially constant, decreasing by about 1 degree between 30 cmHg and vacuum. However $T_\ell^c$ decreases by 7 degrees in this range and differs from $T_\ell^e$ by 8 degrees or more.

The behaviour of $T_o^c$, $T_o^e$ and $T_\ell^e$ is a substantial improvement over Clint's thermocouples where $T_o$ could rise by 20 degrees and $T_\ell$ fall by 10 degrees between 10 cmHg and vacuum, and this improvement can be attributed to the more intimate contact of thermocouple with plug face. In the former design, as the gas pressure becomes small the number of thermally conducting species is reduced and so the plunger-mounted thermocouple becomes progressively more insulated from the plug. Heat loss from the upper plunger and heat transmission to the lower plunger will be reduced thus accounting for the apparent temperature changes. In practice the actual face temperature will not change to the same extent since lateral heat transmission will occur from the steel plug holder; in the present design the actual face temperature is measured.

The output from $T_\ell^c$ was at variance with the other thermocouples since (i) it recorded a lower temperature than $T_\ell^e$ and (ii) its pressure dependence resembled the Clint system. A possible explanation for this would be provided if the thermocouple had not been mounted correctly but had 'lodged' at some point in the plunger before it made contact with the membrane face. It would thus be surrounded by gas and susceptible to the same low pressure effects as found by Clint.

### 6.1.2 *Heat flow patterns*

Consideration of the pattern of heat flow within the plug is instructive. The membrane system can be thought of as an insulating material (the Graphon membrane) embedded in a conducting matrix (the steel plug holder and plungers, and the copper blocks acting as heat

source and sink). In a steady-state of temperature, heat flow lines must run parallel to the plug axis in the end blocks and, away from the plug ends, in the holder/plug combination. Near the plug ends, however, heat flow lines tend to diverge, more heat per unit cross-section passing through the plug holder (a good conductor) than through the plug (a poor conductor - see table 6.1).

A hypothetical visualisation of this is shown in figure 6.2a whilst in figure 6.2b the corresponding equal temperature contours are shown. In these diagrams the plug diameter has been exaggerated, gas pockets have been ignored and the steel/copper assembly has been considered as a uniform matrix.

The implication of this is that within the body of the plug a linear temperature gradient will exist parallel to the axis, but near the plug ends this axial temperature gradient will not be linear and the plug will also possess a radial temperature gradient. The effect of this radial gradient predicts that $T_o^c > T_o^e$ and $T_\ell^c < T_\ell^e$, and this is observed at very low pressures.

An estimate of the magnitude of this effect can be made by comparing at various points the temperatures in the plug holder with those within the plug at the same point. To simplify the calculation we assume that (i) a constant heat flow rate per unit cross section exists within the holder and the plug; (ii) a linear temperature gradient exists in the plug holder and (iii) no radial heat transfer occurs between holder and plug.

We consider a 'composite plug' composed of the Graphon membrane and those sections of the plungers between the bottom of the heat source and the top of the heat sink ie the 'plug' runs from $x_1$ to $x_4$ in figure 3.5. For a steady heat flow

$$- \left( \frac{Q}{t} \right) = \left( \frac{dT}{dx} \right)_i \cdot k_i = \text{Constant} \qquad (6.1)$$

Figure 6.2   Heat flow lines and isothermal contours
within the plug assembly

(b)

$T_o^c$  $T_o^e$                    $T_\ell^e$  $T_\ell^c$

Isothermal Contours

Heat Flow Lines

Conducting
Matrix

Insulation

Carbon
Plug

(a)
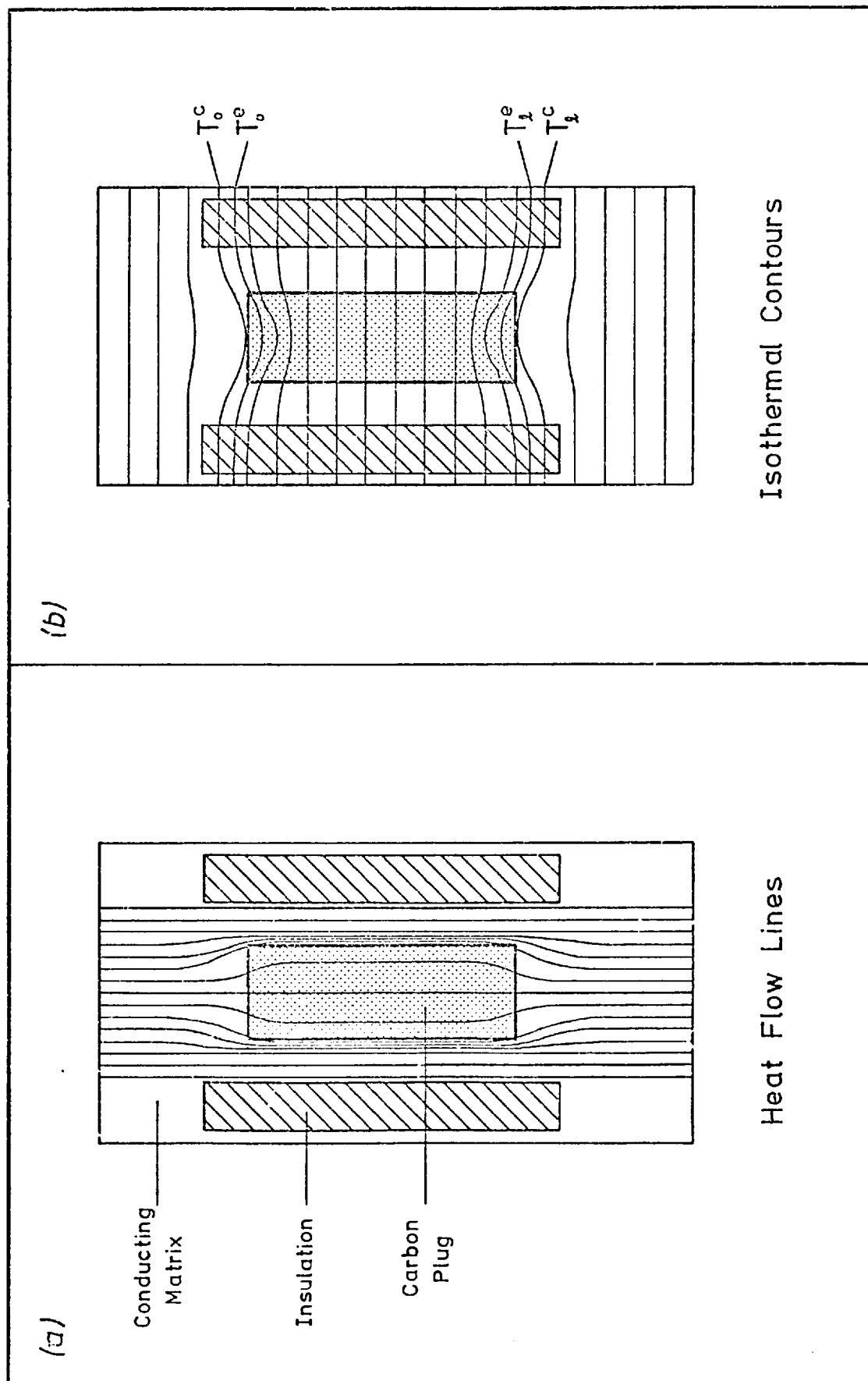
where $Q$ is the quantity of heat per unit cross-section conducted
in time t through the 'composite plug'; $k_i$ is the thermal conductivity
of the $i^{th}$ component and $(dT/dx)_i$ is the temperature gradient across
this component. Ignoring any gas layers present the 'composite plug'
is in three sections, viz steel/carbon membrane/steel.

Using the data in table 6.1 and the following temperatures and
distances :-

$$x_2 - x_1 = 0.846 \text{ cm} \qquad T_2 = 120^{\circ}C$$

$$x_3 - x_2 = 4.17_7 \text{ cm} \qquad T_3 = 65^{\circ}C$$

$$x_4 - x_3 = 0.94_0 \text{ cm}$$

simultaneous equations were set up which gave $T_1 = 120.7_8{}^{\circ}C$ and
$T_4 = 64.1_3{}^{\circ}C$. If these temperatures at $x_1$ and $x_4$ were the same in the
plug holder, then with the linear gradient, temperatures corresponding
to $x_2$ and $x_3$ in the plug holder will be $T_2 = 112.7_4{}^{\circ}C$ and $T_3 = 73.0_6{}^{\circ}C$.

This simple calculation predicts that at the hot face the plug
holder will be $7.2_6$ degrees below the membrane temperature and $8.0_6$ degrees
above it at the cold face. This type of behaviour was in fact observed by
Clint when he attached thermocouples to the outside of the plug holder;
Gilliland et al (1962) have also found similar discrepancies.

Some radial heat flow must occur and this will reduce the size of
the effect but there is a tendency for the centre of the membrane face
to differ in temperature from the edge in contact with the steel holder.
However the similarity of $T_o^c$ and $T_o^e$ indicates that such an effect is much
smaller than predicted by these calculations.

6.1.3 *The temperature gradient*

Previous non-isothermal measurements on Graphon (Clint, 1966;
Dolphin, 1971) involved inert gases with $T_\ell$ maintained at 308.15K whilst
$T_o$ varied from 320.65K to 393.15K, and at a pressure of approximately
20 cmHg.

In this work, because of the slightly different plug construction, $T_\ell$ could not be maintained as low as 308.15K hence 333K was used. All runs were conducted with $T_o$ of 393K to observe a large thermo-osmotic flow. The pressure dependence of the thermo-osmotic steady-state pressure ratio and isobaric permeabilities were also determined.

The face temperatures were taken to be averages of centre and edge values. For $T_o$ very little uncertainty is involved since $T_o^c$ and $T_o^e$ agreed within 0.5 degrees, but, as previously discussed, $T_\ell^c$ was lower than $T_\ell^e$. Since $T_\ell^c$ was not correctly located, then $T_\ell^e$ may be a better choice to characterise $T_\ell$. However in the following calculations average temperatures have been used. Any radial gradient which may exist across the membrane face has been shown to have a minimal effect on the steady-state pressure ratio (Ash, Barrer, Clint, Dolphin and Murray, 1973) for long membranes such as were used here.

### 6.1.4 *The approach to the thermo-osmotic steady-state*

The experimental technique employed in obtaining steady-state pressure ratios, $(p_o/p_\ell)_\infty$, was described in section 3.6.2. Typical approach curves to the steady-state are shown in figure 6.3 for $C_3H_8$, n-$C_4H_{10}$ and neo-$C_5H_{12}$. Also shown is the theoretical steady-state pressure ratio for a Knudsen gas, $(T_o/T_\ell)^{\frac{1}{2}}$. Pressure ratios achieved for these strongly sorbed gases are greater than this limit, demonstrating the influence of transport involving the sorbed phase.

Several workers have fitted this approach curve to an equation of the form:

$$\frac{m_\infty - m_t}{m_\infty - m_o} = \exp(-kt) \qquad (6.2)$$

m has been variously interpreted as

(i) $\ln(p_o/p_\ell)$ ; Denbigh and Raumann (1952a)

(ii) $p_o - p_\ell (= \Delta p)$ ; Crowe (1963); Knudsen (1910b).

(iii) $(p_o/p_\ell)$ ; Clint (1966).
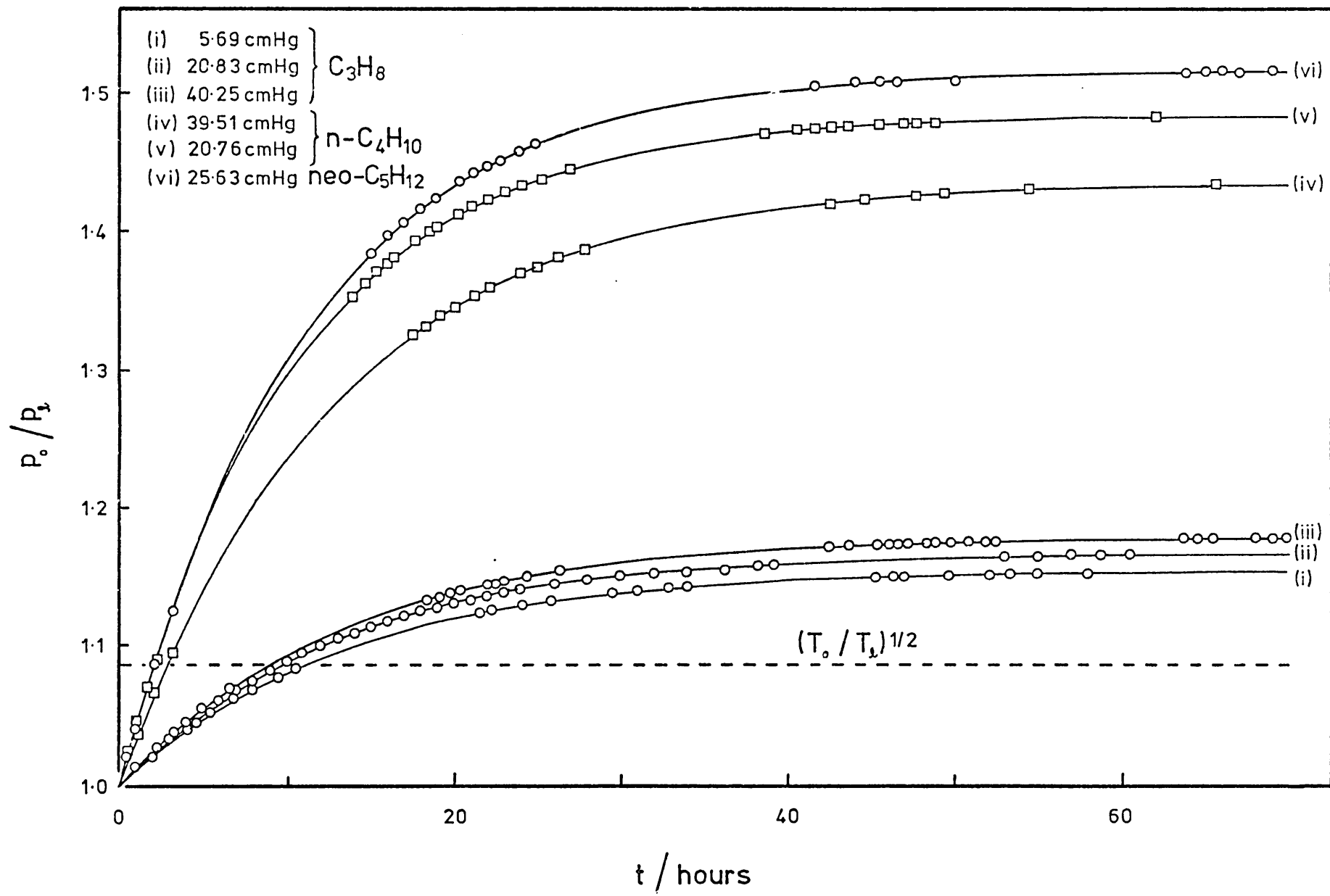
Figure 6.3   The approach to the steady-state

The legend shown in the figure:

(i)    5.69 cmHg  
(ii)   20.83 cmHg  } $C_3H_8$  
(iii)  40.25 cmHg  

(iv)  39.51 cmHg  } $n-C_4H_{10}$  
(v)   20.76 cmHg  
(vi)  25.63 cmHg  neo-$C_5H_{12}$

Axis labels: $P_o / P_l$ (vertical), $t$ / hours (horizontal)

$(T_o / T_l)^{1/2}$

A detailed study of the approach curve has been made for

$C_3H_8$ at 20 cmHg, where $p_o$ and $p_\ell$ were continuously monitored for 40 hours. Each interpretation of m was tested and found to fit the approach curve in its initial stages. However at large t deviations tended to occur such that log $[(m_\infty - m_o)/(m_\infty - m_t)]$ was larger than predicted from the linear initial stage. $Ln(p_o/p_\ell)$ gave the best fit, being valid up to 30 hours, followed by $\Delta p$ (up to 20 hours) and $(p_o/p_\ell)$ (up to 10 hours). These findings contradict Clint's work where $p_o/p_\ell$ gave the best fit and where a deviation at low t was found, analogous to a 'time lag'.

However there are several important differences between the experimental methods of Clint and this work. (i) Clint used Guggenheim's method to predict a value of $m_\infty$, whereas it was directly measured in this work. (ii) The time required to establish $(p_o/p_\ell)_\infty$ was much shorter using a Graphon membrane and most of the approach curve was continuously monitored. (iii) Baratron sensors of high accuracy and stability were used in this work. They entailed smaller dead volumes and no volume changes were involved.

### 6.1.5 *Thermo-osmotic pressure ratios and heats of transport*

Thermo-osmotic steady-state pressure ratios $(p_o/p_\ell)_\infty$ were obtained for He, $C_3H_8$, $n-C_4H_{10}$ and $neo-C_5H_{12}$ at a nominal $T_o$ of 393K and $T_\ell$ of 333K; they are given in table 6.2, together with the pressures at which they were obtained.

TABLE 6.2

*Thermo-osmotic results,* $(p_o/p_\ell)_\infty$ *and* $Q_m$

| Initial Pressure cmHg | $T_o/K$ | | | $T_\ell/K$ | | | $\left(\dfrac{p_o}{p_\ell}\right)_\infty$ | $\dfrac{-Q_m}{kJmol^{-1}}$ |
|---|---|---|---|---|---|---|---|---|
| | $T_o^c$ | $T_o^e$ | $<T_o>$ | $T_\ell^c$ | $T_\ell^e$ | $<T_\ell>$ | | |
| **Helium** | | | | | | | | |
| 49.38 | $391._2$ | $392._3$ | $391._8$ | $330._6$ | $336._7$ | $333._6$ | $1.056_5$ | 1.03 |
| 23.23 | $391._7$ | $393._3$ | $392._5$ | $321._3$ | $328._4$ | $324._9$ | $1.066_8$ | 1.02 |
| **Propane** | | | | | | | | |
| 5.69 | $393._0$ | $393._6$ | $393._3$ | $328._5$ | $337._5$ | $333._0$ | $1.155_2$ | 2.61 |
| 20.83 | $393._0$ | $393._6$ | $393._3$ | $328._7$ | $337._7$ | $333._2$ | $1.167_5$ | 2.81 |
| 20.94 | $393._0$ | $393._7$ | $393._4$ | $328._7$ | $337._7$ | $333._2$ | $1.167_4$ | 2.80 |
| 40.25 | $393._0$ | $393._6$ | $393._3$ | $328._5$ | $337._5$ | $333._0$ | $1.179_1$ | 2.98 |
| 61.30 | $392._7$ | $393._3$ | $393._0$ | $328._5$ | $337._5$ | $333._0$ | $1.183_3$ | 3.05 |
| 19.33 | $392._4$ | $393._0$ | $392._7$ | $318._9$ | $329._4$ | $324._2$ | $1.209_5$ | 2.94 |
| **n-Butane** | | | | | | | | |
| 2.42 | $392._5$ | $392._8$ | $392._7$ | $327._7$ | $336._9$ | $332._3$ | $1.473_4$ | 6.97 |
| 11.33 | $392._5$ | $392._9$ | $392._7$ | $327._8$ | $336._9$ | $332._4$ | $1.516_2$ | 7.49 |
| 20.21 | $392._7$ | $393._1$ | $392._9$ | $328._9$ | $338._0$ | $333._5$ | $1.484_4$ | 7.23 |
| 20.76 | $392._5$ | $393._0$ | $392._8$ | $328._5$ | $337._7$ | $333._1$ | $1.484_2$ | 7.20 |
| 39.51 | $392._2$ | $392._8$ | $392._5$ | $327._8$ | $336._9$ | $332._4$ | $1.434_1$ | 6.51 |
| **neo-Pentane** | | | | | | | | |
| 25.63 | $393._0$ | $393._2$ | $393._1$ | $327._8$ | $337._1$ | $332._5$ | $1.515_0$ | 7.45 |

An integral heat of transport, $Q_m$, can be derived from a single steady-state pressure ratio as described in chapter 2, from the relation:

$$R \ln \left( \frac{p_o}{p_\ell} \right)_\infty = - Q_m \left[ \frac{1}{T_\ell} - \frac{1}{T_o} \right] = - Q_m \frac{\Delta T}{T_o \cdot T_\ell} \qquad (2.72)$$

Values of $Q_m$ calculated in this way are also tabulated in table 6.2.

6.1.6 *Isobaric permeabilities*

In chapter 2 $B(T_o)$ was defined as the energy flow through the membrane at constant pressure, p, caused by unit temperature gradient through unit cross-section in unit time.

ie $\qquad B(T_o) = R T_o \cdot \frac{J\ell}{\Delta T} \qquad (6.3)$

where $J$ is the flux in mol s$^{-1}$ per unit cross-section in the + x-direction. The ratio $B(T_o)/p_o$ can therefore be obtained while $p_o$ and $p_\ell$ are still nearly equal, and plotted against pressure. It has been found in this work that if a sufficiently sensitive diaphragm gauge is used to record $\Delta p$ $(= p_o - p_\ell)$ as a function of time in thermo-osmotic measurements, then in the initial stages $\Delta p$ is linear with t. Flux $J$ (and hence $B(T_o)/p_o$) can therefore be evaluated from the limiting rate of increase of pressure difference ie from $(d \Delta p/dt)_{t \to o}$ (see section 3.6.3). The only previous measurements of $B(T_o)/p_o$ have involved the use of a lubricated mercury slug in a horizontal capillary connecting both sides of the membrane, where an isobaric flux was obtained from the rate of travel of the slug (Gilliland et al, 1962).

If the reservoirs at the hot and cold sides of the plug have volumes $V_o$ and $V_\ell$, and contain gas at a pressure of $p_o$ and $p_\ell$ at time t, then

$$p_o = p + n. \frac{RT_R}{V_o} \quad \text{and} \quad p_\ell = p - n. \frac{RT_R}{V_\ell} \qquad (6.4)$$

where p is the initial pressure, ($= p_o = p_\ell$) at isobaric equilibrium before isolating the reservoirs at the hot and cold sides, $T_R$ is the reservoir temperature and n is the number of moles which have passed from cold to hot side after t seconds. The pressure difference , $\Delta p$, will be given by:

$$\Delta p = p_o - p_\ell = n\, RT_R \left[ \frac{V_o + V_\ell}{V_o \cdot V_\ell} \right] \tag{6.5}$$

Hence by differentiation with respect to t and substitution in (6.3) we get:

$$\left. \begin{array}{l} J = -\dfrac{dn}{dt} \cdot \dfrac{1}{A_c} = -\dfrac{1}{A_c} \cdot \dfrac{V_o\, V_\ell}{V_o + V_\ell} \cdot \dfrac{1}{RT_R} \cdot \dfrac{d\Delta p}{dt} \\[3mm] B(T_o) = -\dfrac{T_o}{T_R} \cdot \dfrac{\ell}{\Delta T} \cdot \dfrac{1}{A_c} \cdot \dfrac{V_o\, V_\ell}{V_o + V_\ell} \cdot \dfrac{d\Delta p}{dt} \\[3mm] \dfrac{B(T_o)}{P_o} = -\dfrac{T_o}{T_R}\cdot\dfrac{1}{P_o}\cdot\dfrac{\ell}{\Delta T} \cdot \dfrac{1}{A_c} \cdot \dfrac{V_o\, V_\ell}{V_o + V_\ell} \cdot \dfrac{d\Delta p}{dt} \end{array} \right\} \tag{6.6}$$

If $p_o$ (the initial equilibrium pressure, $= p_\ell$) is expressed in cmHg, $\ell$ in m, $A_c$ in $m^2$, V in $m^3$ and t in minutes, then $J$ ($mol\ s^{-1}\ m^{-2}$), $B(T_o)$ ($N\ s^{-1}\ K^{-1}$) and $B(T_o)/p_o$ ($m^2\ s^{-1}\ K^{-1}$) are given by:

$$\left. \begin{array}{l} J = -\dfrac{V_o \cdot V_\ell}{V_o + V_\ell} \cdot \dfrac{22.138}{A_c \cdot R \cdot T_R} \cdot \dfrac{d\Delta p}{dt} \\[3mm] B(T_o) = -\dfrac{V_o \cdot V_\ell}{V_o + V_\ell} \dfrac{T_o}{T_R}\dfrac{\ell}{\Delta T}\dfrac{22.138}{A_c} \cdot \dfrac{d\Delta p}{dt} \\[3mm] \dfrac{B(T_o)}{P_o} = -\dfrac{V_o \cdot V_\ell}{V_o + V_\ell}\dfrac{T_o}{T_R}\dfrac{1}{P_o}\dfrac{\ell}{\Delta T}\dfrac{1}{A_c}\dfrac{1}{60}\cdot\dfrac{d\Delta p}{dt} \end{array} \right\} \tag{6.7}$$

For the present membrane (plug O) the physical parameters in the working equation, (6.7), are :

$\ell = 0.0418_7$ m; $A_c = 3.27 \times 10^{-5} m^2$; $V_o = 81.4 \times 10^{-6} m^3$; $V_\ell = 153.9 \times 10^{-6} m^3$.

The parameters $J$, $B(T_o)$ and $B(T_o)/p_o$ were determined for He, $C_3H_8$, $n$-$C_4H_{10}$ and neo-$C_5H_{12}$ in the pressure range 1 to 60 cmHg for the fixed values of $T_o$ and $T_\ell$ used in the thermo-osmotic work. Results obtained are tabulated in table 6.3; each value of $J$ (and hence of $B(T_o)$ and $B(T_o)/p_o$) represents the average of between 3 and 5 determinations at each pressure.

TABLE 6.3

*Isobaric fluxes and permeabilities*

| Initial pressure cmHg | $<T_o>$ K | $<T_\ell>$ K | $-10^5 J$ mol s$^{-1}$ m$^{-2}$ | $-10^4 B(T_o)$ N s$^{-1}$ K$^{-1}$ | $-10^8 B(T_o)/p_o$ m$^2$ s$^{-1}$ K$^{-1}$ |
|---|---|---|---|---|---|
| **Helium** | | | | | |
| * | 391.8 | 333.6 | – | – | $0.21_5$ |
| **Propane** | | | | | |
| 2.45 | $393._0$ | $333._0$ | $0.64_8$ | $0.14_8$ | $0.45_2$ |
| 5.69 | $393._3$ | $333._0$ | 1.53 | $0.34_8$ | $0.46_0$ |
| 12.09 | $393._0$ | $333._0$ | 3.43 | $0.77_9$ | $0.48_6$ |
| 20.51 | $392._8$ | $333._0$ | $6.0_7$ | 1.38 | $0.50_7$ |
| 31.56 | $393._0$ | $333._0$ | $9.5_8$ | 2.18 | $0.52_0$ |
| 40.31 | $393._3$ | $333._0$ | 12.3 | 2.80 | $0.52_4$ |
| 61.67 | $392._8$ | $333._0$ | 19.2 | 4.38 | $0.53_4$ |
| **n-Butane** | | | | | |
| 2.41 | $392._8$ | $332._4$ | 2.98 | $0.67_5$ | 2.11 |
| 11.09 | $392._7$ | $332._3$ | 14.1 | 3.19 | 2.16 |
| 20.89 | $392._8$ | $333._1$ | 23.9 | $5.4_6$ | 1.97 |
| 40.04 | $392._8$ | $332._3$ | 33.3 | $7.4_5$ | 1.41 |
| **neo-Pentane** | | | | | |
| 25.70 | $393._4$ | $332._9$ | 28.6 | $6.4_9$ | 1.90 |
| * $B(T_o)/p_o$ is the average of 8 permeabilities in the range 25–50 cmHg | | | | | |

## 6.2  DISCUSSION OF THERMO-OSMOTIC RESULTS

The thermo-osmotic steady-state pressure ratios of table 6.2 are quite different from the ratio $(T_o/T_\ell)^{\frac{1}{2}}$ expected for Knudsen flow of an ideal gas.  For $T_o$ of 393 K and $T_\ell$ of 333 K, $(T_o/T_\ell)^{\frac{1}{2}}$ is 1.086. Hydrocarbon ratios are well above this figure and tend to vary with pressure, whilst the helium ratio is below it and independent of pressure.  For the helium result the considerations given in chapter 5 concerning the Knudsen pressure regime are equally valid here, since the plug used, O, is of very similar pore dimensions to N.  Hence we are still concerned with a pressure region where the mean free path of the gas is large compared with the mean pore diameter $(4\epsilon/A)$.

### 6.2.1 *The helium result*

The low value of $(p_o/p_\ell)_\infty$ obtained here accords with the findings of other workers.  Ash et al (1973) found consistently low values for non-sorbed and weakly sorbed gases (He, Ne, Ar, Kr and $H_2$) through membranes of Graphon and Carbolac with $T_o$ between 320 and 393 K.  They also calculated heats of transport, $Q_o$, from equation (2.71) which were found to be less than the value of $-\frac{1}{2}RT_o$ predicted for an ideal gas transported by molecular streaming (Kennard, 1938).  This led them to propose the empirical relationship

$$Q_o = \beta \left(- \tfrac{1}{2}RT_o\right) \tag{6.8}$$

where $\beta$ was found to vary with the gas and membrane, but was independent of $T_o$ and $T_\ell$.

On both Graphon and Carbolac Ash et al found $\beta$ to be 0.72.  In this work, based on the single point determination of an integral $Q_m$, $\beta$ was found to be 0.63 for each of the helium results.  It is instructive at this point to consider the values of $Q_o$ obtained from equations (2.71) and (2.72) to see how closely they will agree with $-\frac{1}{2}RT_o$ for an ideal gas.  With $T_\ell$ of 333 and $T_o$ adopting several values between 343

and 393 K, $Q_o$ and $Q_m$ were calculated from (2.71) and (2.72) assuming that $(p_o/p_\ell) = (T_o/T_\ell)^{\frac{1}{2}}$. It was found that the heat from (2.71) agreed with $-\frac{1}{2}RT_o$ within 20 J mol$^{-1}$, the experimental error arising from the accuracy of the tangents which must be drawn. For the integral heat $Q_m$ however, systematic deviations will always occur, which will be larger at high values of $\Delta T$ ($= T_o - T_\ell$). The approximate relationship (6.9) was derived

$$Q_o = Q_m - 2.2 \, \Delta T \qquad (6.9)$$

where $Q_o$ is the differential heat (J mol$^{-1}$) from (2.71) and $Q_m$ is the integral heat. Thus even at $T_o$ of 393K the deviation from $Q_o$ is only 132 J mol$^{-1}$, whereas $Q_m$ is 604 J mol$^{-1}$ lower than the Knudsen value of $-\frac{1}{2}RT_o$ ($= -1634$ J mol$^{-1}$).

### 6.2.2 *Deviations from the Knudsen limit*

Several papers have recently been published, pointing out the limitations of the kinetic theory in treating thermal transpiration and attempting to explain why ideal gas values of $(p_o/p_\ell)_\infty$ and $Q_o$ are not obtained, even for helium, in capillaries and porous media.

Edmonds and Hobson (1965) obtained the Knudsen thermal transpiration limit of $(T_o/T_\ell)^{\frac{1}{2}}$ for apertures under high vacua and with $T_o = 295$K and $T_\ell = 77.4$K. However with capillary tubes $(p_o/p_\ell)_\infty$ was always less than the limit, but most closely approached it at small tube diameters and with heavier gas molecules.

They applied the following elementary transmission probability theory to thermal transpiration to account for the discrepancies. Assuming a Maxwellian distribution of velocities in the gas phase, then the number of molecules incident on the capillary or membrane entrance, per unit area and in unit time, will be given by (Knudsen 1910a):

$$Z = \frac{1}{4} \rho \bar{c} \qquad (6.10 \text{ cf } 2.37)$$

where $\rho$ is the molecular density (= p/kT) and $\bar{c}$ is the average molecular velocity, $(8 \ kT/\pi m)^{\frac{1}{2}}$.

Because of differing temperatures and molecular velocities at $T_o$ and $T_\ell$, Z will have different values at x = 0 and x = $\ell$, $Z_o$ and $Z_\ell$ respectively.

$$
\left.
\begin{aligned}
Z_o &= \frac{1}{4} \rho_o \bar{c}_o = \frac{P_o}{(2\pi mkT_o)^{\frac{1}{2}}} \\[2em]
Z_\ell &= \frac{1}{4} \rho_\ell \bar{c}_\ell = \frac{P_\ell}{(2\pi mkT_\ell)^{\frac{1}{2}}}
\end{aligned}
\right\} \quad (6.11)
$$

Transmission probabilities, W, (Clausing, 1932) are now introduced. These represent the fraction of molecules striking one face which eventually leave the capillary (or membrane) at the other. $W_o$ indicates molecules travelling from 0 to $\ell$ and $W_\ell$ those from $\ell$ to 0.

In an isothermal situation $W_o = W_\ell$ but for the steady-state in thermal transpiration $Z_o . W_o = Z_\ell . W_\ell$. Substituting from (6.11) we get, for the steady-state condition:

$$
\left( \frac{P_o}{P_\ell} \right)_\infty = \left( \frac{T_o}{T_\ell} \right)^{\frac{1}{2}} . \frac{W_\ell}{W_o} \qquad (6.12 \ cf \ 2.45)
$$

$W_\ell/W_o$, which we call $\alpha$ is a measure of the departure from the Knudsen gas limit. It can be related to the factor $\beta$ proposed by Ash et al (1973), in the following way. We substitute for $(P_o/P_\ell)_\infty$ from (6.12) into equation (2.68) and using the relation (2.69), differentiate w.r.t. $T_o$ at constant $T_\ell$. Then writing $Q_o$ as $\beta \ (-\frac{1}{2}RT_o)$ we get

$$
\frac{d\ln\alpha}{d\ln T_o} = \frac{\beta - 1}{2} \qquad (6.13)
$$

Thus, it is the *temperature dependence* of the departure of the steady-state pressure ratio from the Knudsen expression which accounts for

the non-ideal value of $Q_o$. Since $\beta$ is constant and independent of $T_o$, then on these carbon membranes departure from $(T_o/T_\ell)^{\frac{1}{2}}$ is more marked at higher $T_o$, and the size of the temperature dependence of $\alpha$ determines the departure of $Q_o$ from $-\frac{1}{2}RT_o$.

In table 6.4 values of $\alpha$ obtained on several porous membranes and capillary tubes are presented, together with $\lambda/d$ and the temperatures used. It can be seen that even for tubes having a high $\lambda/d$, $\alpha$ is less than unity and is smaller for wider tubes. The value of $\alpha$ obtained in this work is compatible with that obtained by Clint on Carbolac and agrees with the observation that both carbon plugs have very similar $\beta$ values. It can also be observed from Clint's work that $\alpha$ decreases as $\Delta T$ or $T_o$ increases and that $\alpha$ is in the order $H_2 > He > Ne$ ie $H_2$ is most nearly ideal. Berman and Lund (1958) obtained isothermal transmission probabilities ($W_{\ell\ell}$ and $W_{oo}$) through capillaries, porous metal and sintered glass. For $T_o$ of 300K, $T_\ell$ of 100K, $W_{\ell\ell}/W_{oo} = 0.971$ is obtained for Ne and $H_2$, a value comparable with empirical $\alpha$ values (see table 6.4).

Edmonds and Hobson went on to consider the effect of the nature of the reflections within a capillary on the transmission probabilities. They proposed that if each wall collision took place by complete specular reflection (forward velocity retained after reflection), by complete diffuse or cosine reflection (random re-emission after collision) or by a fixed proportion of both (independent of molecular velocity), then $W_\ell = W_o$. However they postulated that 'hot' molecules striking a colder surface had a greater degree of specular reflection than a 'cold' molecule striking a warmer surface. Hence $W_o > W_\ell$ and so $\alpha < 1$, as is experimentally observed.

Miller and Buice (1966) advanced a model for thermal transpiration, involving transmission probabilities from Monte Carlo calculations and varying degrees of specular reflection. $\alpha$ was predicted to be nearer

## TABLE 6.4

*Transmission probability ratios (α) for several systems*

| System | Gas | $\lambda/d$ | $\dfrac{T_o}{K}$ | $\dfrac{T_\ell}{K}$ | $\alpha$ | Ref |
|---|---|---|---|---|---|---|
| Porous Plug | Air | — | 373 | 290 | $0.97_4$ | (1) |
| Magnesia Plug | $H_2$ | $6.4 \times 10^1$ | $521._7$ | $295._1$ | $0.99_2$ | (2) |
| Graphon Plug | He | $7.8_3 \times 10^1$ | $391._7$ | $333._6$ | $0.97_5$ | (3) |
| $\varepsilon/A = 4.52$ rm | He | $1.6_5 \times 10^2$ | $392._5$ | $324._9$ | $0.97_1$ | (3) |
| | He | $1.7_0 \times 10^3$ | 352.9 | 308.2 | $0.98_1$ | (4) |
| | $H_2$ | $1.2_7 \times 10^3$ | 352.9 | 308.2 | $0.99_4$ | (4) |
| Carbolac Plug | Ne | $7.3_2 \times 10^2$ | 320.7 | 308.2 | $0.99_1$ | (4) |
| $\varepsilon/A = 0.471$ nm | Ne | $7.4_4 \times 10^2$ | 333.2 | 308.2 | $0.98_3$ | (4) |
| | Ne | $7.9_5 \times 10^2$ | 352.9 | 308.2 | $0.97_0$ | (4) |
| | Ne | $8.2_3 \times 10^2$ | 378.0 | 308.2 | $0.95_6$ | (4) |
| Glass tube, | He | $1.1_5 \times 10^5$ | 295. | 77.4 | $0.96_6$ | (5) |
| 2.1 mm diameter | Ne | $2.5_2 \times 10^3$ | 295. | 77.4 | $0.95_5$ | (5) |
| Glass tube, | He | $1.3_9 \times 10^4$ | 295. | 77.4 | $0.87_7$ | (5) |
| 19 mm diameter | Ne | $2.7_9 \times 10^2$ | 295. | 77.4 | $0.87_7$ | (5) |

(1) Reynolds, 1879

(2) Knudsen, 1910a

(3) This work

(4) Clint, 1966

(5) Edmonds and Hobson, 1965

unity for shorter tubes (small length/diameter ratios) and for small

degrees of specular reflection. As specular reflection increases, then

$W_o$ and $W_\ell$ diverge more. They postulated that it was the *initial*

reflection of the molecule from the reservoir into the tube which largely

determined W. Hence it was $T_o$ and $T_\ell$ which were important in governing

$p_o/p_\ell$, whereas any gradients within the tube were of minor significance.

The work of Hobson et al (1963) supports this view since $(p_o/p_\ell)_\infty$ was found

to be sensitive to the position of the temperature discontinuity ie to

small changes in entrance geometry. Edmonds et al (1965), by having

very wide reservoirs at the tube entrance, removed these variations and

obtained values of $\alpha$ closer to unity.

Wu (1968) considered that the classical kinetic theory of Maxwell and Knudsen when applied to thermal transpiration was only valid for near-Maxwellian distributions; it does not allow for a microscopic description of the system. He developed an identical expression to equation (6.12) but W was replaced by I, a geometric factor measuring the deviation of the velocity distribution from classical theory. If I is constant throughout the system then the Knudsen limit is obtained. In practice it varies with the geometric arrangement eg the capillary entrance.

Several workers have proposed mathematical models for thermal transpiration which derive the result:

$$\left(\frac{P_o}{P_\ell}\right)_\infty = \left(\frac{T_o}{T_\ell}\right)^\gamma \qquad\qquad \text{(6.14 cf 2.44)}$$

$\gamma$ has been interpreted as follows:-

(i)  $\dfrac{1}{2} - \dfrac{0.56\sigma}{1 + 0.1\sigma}$  :  Siu, 1973

(ii)  $\dfrac{1}{2} - \dfrac{3\pi}{16}.\sigma$  :  McCormick and Kuščer, 1972.

(iii)  $\dfrac{1}{2} - \dfrac{\sigma}{1 + \sigma}$  :  Cha and McCoy, 1972.

The parameter $\sigma$ pertains to the nature of the gas-surface collision. For complete diffuse reflection (or perfect energy accommodation) $\sigma = 0$ and the Knudsen limit is obtained. In (ii) and (iii) $\sigma = 1 - \alpha$ where $\alpha$ is a tangential momentum accommodation coefficient. Equation (6.14) was developed for long tube models ie where $\ell \gg \lambda \gg d$, and as the amount of specular reflection increases $(p_o/p_\ell)_\infty$ diverges from the Knudsen limit, but is predicted to be independent of $\ell$. $\gamma$ can be related to the $\beta$

measured by Ash et al (1973), by substituting (6.14) into (2.70) for $(p_o/p_\ell)_\infty$ and using $\beta(-\frac{1}{2}RT_o)$ for $Q_o$. When the differentiation is carried out w.r.t. $T_o$ we get

$$\gamma = \beta/2 \qquad\qquad (6.15)$$

We can thus evaluate $\alpha$, $\gamma$ and $\sigma$ of Siu, McCormick and Cha for lightly sorbed gases on carbon membranes. Table 6.5 presents data for He, $H_2$ and Ne on Graphon and Carbolac, the Graphon results being obtained in this work whilst the Carbolac results are the work of Clint (1966). For ideal Knudsen gas behaviour, $\alpha = 1$, $\gamma = 0.5$ and $\sigma = 0$.

TABLE 6.5

*Values of $\alpha$, $\gamma$ and $\sigma$ on carbon membranes*

| Gas | $\dfrac{T_o}{K}$ | $\dfrac{T_\ell}{K}$ | $\left(\dfrac{P_o}{P_\ell}\right)_\infty$ | $\alpha$ | $\gamma$ | $\sigma$ Siu | McCormick | Cha |
|---|---|---|---|---|---|---|---|---|
| Graphon | | | | | | | | |
| He | 391.7 | 333.6 | 1.056₆ | 0.975 | 0.342 | 0.29 | 0.27 | 0.19 |
| He | 392.5 | 324.9 | 1.066₈ | 0.971 | 0.342 | 0.29 | 0.27 | 0.19 |
| Carbolac | | | | | | | | |
| He | 320.7 | 308.2 | 1.012₇ | 0.993 | 0.317 | 0.34 | 0.31 | 0.22 |
| He | 333.2 | 308.2 | 1.027₈ | 0.988 | 0.352 | 0.27 | 0.25 | 0.17 |
| He | 352.9 | 308.2 | 1.049₆ | 0.981 | 0.357 | 0.26 | 0.24 | 0.17 |
| $H_2$ | 320.7 | 308.2 | 1.017₇ | 0.998 | 0.441 | 0.11 | 0.10 | 0.063 |
| $H_2$ | 333.2 | 308.2 | 1.036₃ | 0.997 | 0.457 | 0.077 | 0.073 | 0.045 |
| $H_2$ | 352.9 | 308.2 | 1.064₂ | 0.994 | 0.459 | 0.074 | 0.070 | 0.043 |
| $H_2$ | 378.0 | 308.2 | 1.098₈ | 0.992 | 0.461 | 0.070 | 0.066 | 0.040 |
| Ne | 320.7 | 308.2 | 1.011₃ | 0.991 | 0.283 | 0.40 | 0.37 | 0.28 |
| Ne | 333.2 | 308.2 | 1.021₈ | 0.983 | 0.277 | 0.42 | 0.38 | 0.29 |
| Ne | 352.9 | 308.2 | 1.038₆ | 0.970 | 0.279 | 0.41 | 0.38 | 0.28 |
| Ne | 378.0 | 308.2 | 1.058₈ | 0.956 | 0.280 | 0.41 | 0.37 | 0.28 |

$\sigma$, which can be considered to be the fraction of specular reflections, is less than 0.5 and for a fixed temperature gradient is in the order $Ne > He > H_2$, tending to decrease with increasing $T_o$. The order of $\gamma$ (and hence $\beta$) shows the opposite trends to $\sigma$ and the treatments of Siu, McCormick

and Cha give different values for $\sigma$, in the order

$$\sigma \text{ (Siu)} > \sigma \text{ (McCormick)} > \sigma \text{ (Cha)}.$$

An apparent contradiction occurs here, since $\gamma$ increases ($\sigma$ decreases) as $\alpha$ decreases. Now increasing $\gamma$ indicates a decreasing amount of specular reflection whilst decreasing $\alpha$ represents an increase in $W_o - W_\ell$ which Edmonds and Hobson attributed to differing degrees of specular reflection acting on $W_o$ and $W_\ell$. However it can be shown by manipulation that $d\gamma/dT_o$ can be positive or negative depending on the relative magnitude of

$\dfrac{1}{\alpha}\dfrac{d\alpha}{dT_o}$ and $\dfrac{\gamma-\frac{1}{2}}{T_o}$, both of which are negative. Siu pointed out that it was

the temperature dependence of $\sigma$, scattering being dependent on incident velocity or thermal energy, which was responsible for differing W's and departure from the Knudsen limit.

No account has so far been taken of back scattering, which has been found to be large for molecules impinging at low angles (Siu 1973). Back scattering would tend to decrease both $W_\ell$ and $W_o$. Siu's model could take account of preferential back scattering by allowing $\sigma$ to adopt negative values.

The microscopic nature of the reflecting surface, which would give rise to back scattering, has not been considered. Hobson (1969) leached a Pyrex capillary to produce a 'rough' surface and found that the ideal Knudsen limit could be obtained at low pressures. He concluded that atomic roughness forced all reflections to be diffuse with no specular reflection so $W_\ell = W_o$, $\sigma = 0$. Siu (1973) used a model having a rough interior surface but allowed specular reflection to take place.

We have thus seen that when $\lambda \gg d$ classical Knudsen gas behaviour is not necessarily to be expected, even for helium. Transmission probability theory has been advanced to account for the discrepancies, but calculation of W's will be a complex task involving gas temperature, surface temperature, the microscopic nature of the surface, nature of surface

reflections, impact angles and entrance geometry. Non-Maxwellian distribution of molecular velocities could also be important.

When we consider a porous carbon membrane, even more uncertainties are introduced. The precise microscopic nature of the capillary paths is uncertain, but they probably consist of 'long' capillaries ($\ell >> \lambda$) which link larger caverns or voids, and they will be extensively kinked. Entrance geometry is likely to be very irregular on a microscopic scale, a multitude of different entrance geometries existing. One might think that because of this rough and irregular nature, complete randomisation and diffuse reflection would occur, and the Knudsen limit be obtained. In practice this is not so as table 6.5 demonstrates. The most probable explanation is that of Edmonds & Hobson, viz that differing degrees of specular reflection occur for the initial reflections from the gas reservoirs at different temperatures. This will cause a deviation from the Knudsen limit, the magnitude of which increases with increasing $\Delta T$, as is experimentally observed.

The presence of an adsorbed film presents further complications, since this will modify any surface reflections and can itself exhibit a temperature gradient flow. Adsorption might be expected to lead to random re-emission and diffuse reflection since the impinging molecule has a finite residence time on the surface and will therefore lose any 'memory' of its incident direction. The presence of an adsorbed film will also present an irregular surface to any non-adsorbed species present.

In the present experimental arrangement the gas gaps which exist between the heat source and sink, and the membrane could be instrumental in reducing $\Delta T$ below that which is measured thereby reducing the actual value of $(T_o/T_\ell)^{\frac{1}{2}}$. The thermal conductivity of the gas could also be important (Gilliland, Baddour and Engel, 1962).

### 6.2.3 *Hydrocarbon results*

$(p_o/p_\ell)_\infty$ has been obtained for $C_3H_8$, $n-C_4H_{10}$ and $neo-C_5H_{12}$ on Graphon for a fixed temperature gradient (table 6.2). Information concerning temperature dependence of $(p_o/p_\ell)_\infty$ is not available, but such measurements have been made elsewhere for sorbed gases on Graphon and Carbolac membranes (Clint, 1966; Dolphin, 1971; Ash et al, 1973). There it was shown that sorbed gases exhibited a steady-state pressure ratio greater than the Knudsen limit, and they exceeded this limit to an extent which depended both on the gas and on $\Delta T$ $(= T_o - T_\ell)$. As $\Delta T$ increased (at constant $T_\ell$), then $(p_o/p_\ell)_\infty$ also increased owing to the greater mobility of the sorbed phase at higher temperatures.

In this work, however, the *pressure dependence* of the thermo-osmotic pressure ratio was examined and the results are shown in figure 6.4. All gases exhibited a greater $(p_o/p_\ell)_\infty$ than the Knudsen limit and at a constant pressure $(p_o/p_\ell)_\infty$ increased as the molecular weight of the hydrocarbon increased.

It is evident that a maximum occurs when $(p_o/p_\ell)_\infty$ is plotted against pressure, $p_o$, and that the position of this maximum is moved to progressively lower pressures as the gas becomes more strongly sorbed. Such behaviour has not been observed before on carbon membranes.

If we ignore the gas phase transport, then one might expect that the surface analogue of thermal transpiration (giving rise to $(p_o/p_\ell)_\infty$ $> (T_o/T_\ell)^{\frac{1}{2}}$) could be related to the surface concentration gradient, ie to part of the driving force for surface flow. $\theta$, the fraction of monolayer coverage obtained from adsorption isotherm data, can be considered to characterise the surface concentration. Now this will vary between $x = 0$ and $x = \ell$ due to (i) the temperature gradient and (ii) the pressure gradient. If we have the isotherm data then we can calculate $v$ (the adsorption uptake) and $\theta$ at each end of the plug, ie at $T_o$, $p_o$ and at
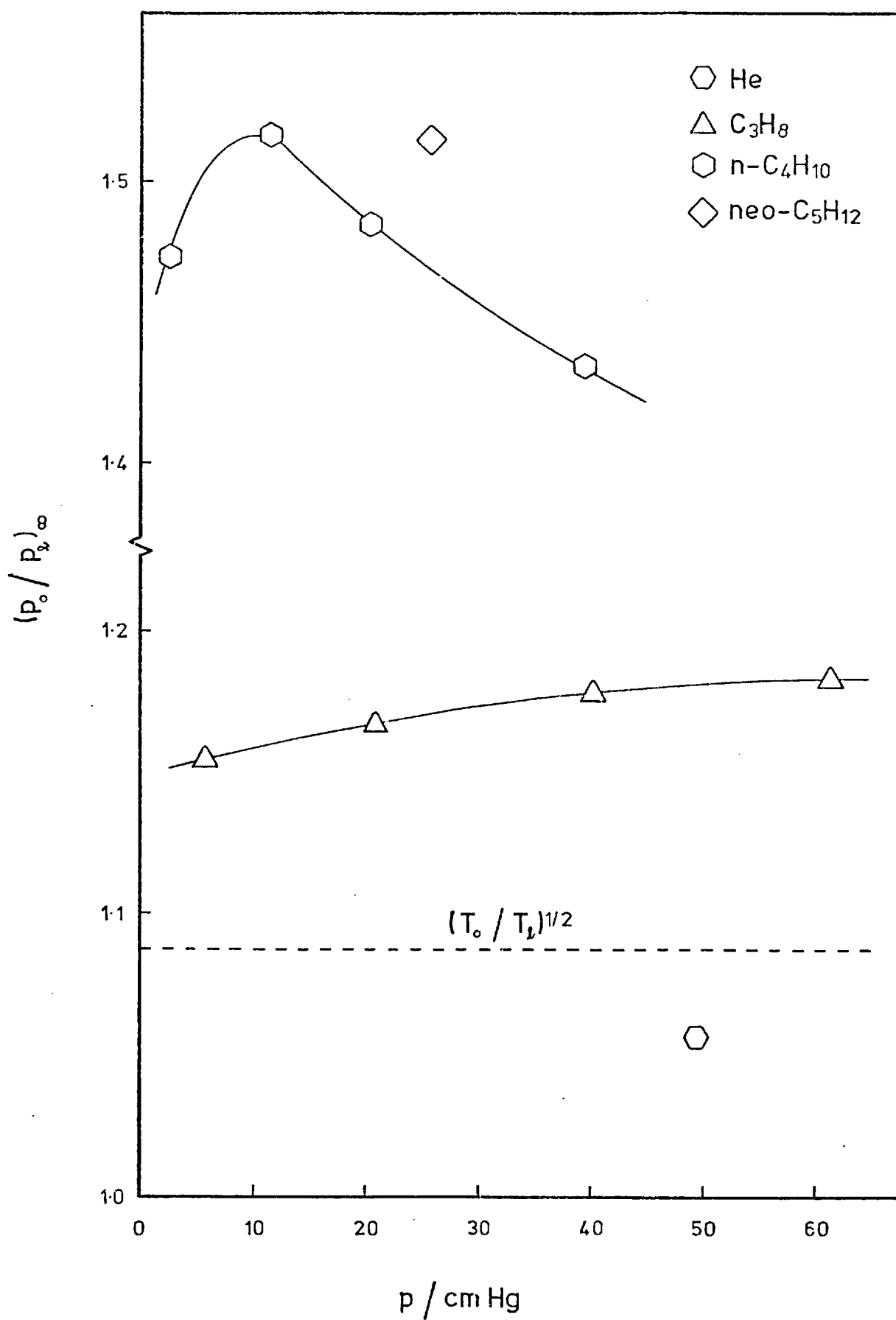
*Figure 6.4* $(p_o / p_l)_\infty$ *as a function of initial pressure*

$T_\ell$, $p_\ell$. Table 6.6 gives the values of p and $\theta$ at the plug faces in the steady-state for propane. Unfortunately n-butane isotherm data were not available at the required temperatures.

## TABLE 6.6

*Values of* p *and* $\theta$ *at the membrane faces for propane when* $T_o$ = 393 *and* $T_\ell$ = 333K.

| $\dfrac{P_o}{cmHg}$ | $\theta_{393}$ | $\dfrac{P_\ell}{cmHg}$ | $\theta_{333}$ | $\dfrac{\theta_{333}}{\theta_{393}}$ |
|---|---|---|---|---|
| $6.3_8$ | $0.02_3$ | $5.5_2$ | $0.07_4$ | $3.2_2$ |
| $22.5_7$ | $0.07_7$ | $19.3_3$ | $0.24_4$ | $3.1_7$ |
| $44.7_7$ | $0.14_6$ | $37.9_7$ | $0.44_1$ | $3.0_2$ |

It is clear that a considerable driving force is available for surface transport, since this elementary analysis reveals a 3.2-fold increase in surface concentration between 393 and 333K for propane: it is likely to be even greater for n-butane.

We can take this analysis a step further and speculate that the steady-state pressure ratio, $(p_o/p_\ell)_\infty$, may be a function of the ratio of surface concentrations at $x = \ell$ and $x = 0$, ie $v_\ell/v_o$. In figure 6.5 the ratio $v_\ell/v_o$ is plotted as a function of pressure, p, for propane and n-butane at several pairs of $T_o$ and $T_\ell$ for which isotherms had been measured (chapter 4). For simplicity $v_o$ and $v_\ell$ have been evaluated at the same pressure instead of taking actual pairs of $p_o$ and $p_\ell$.

The ratios obtained for $n-C_4H_{10}$ are found to fall very sharply with increasing pressure whilst a broad maximum is observed for $C_3H_8$. The very different behaviour of these two gases arises as a result of the isotherm shape and differences in shape between $T_o$ and $T_\ell$. Figure 6.5 parallels the experimental pressure dependence of $(p_o/p_\ell)_\infty$ (figure 6.4), while a gas obeying the Henry law is predicted to have a constant value of $v_\ell/v_o$.

It should be noted however that (i) no n-butane isotherm was
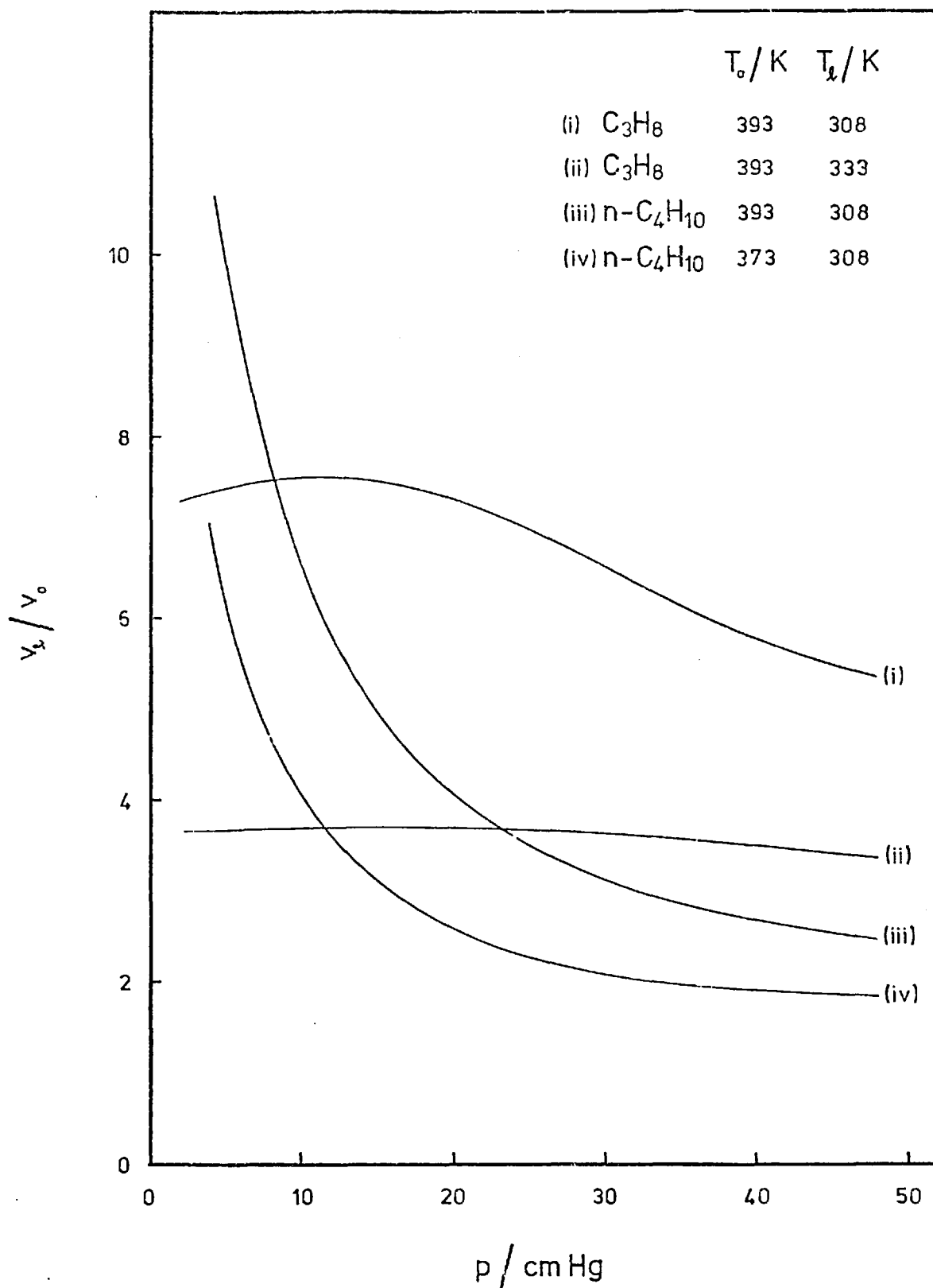
Figure 6.5    $v_\ell / v_o$  as a function of pressure

measured at 333K and so the isotherm used for $T_\ell$ in figure 6.5 was

at 308K, the nearest temperature available; (ii) $(p_o/p_\ell)_\infty$ also includes

a contribution from gas phase flow; (iii) actual values of $p_o$ and $p_\ell$

were not used, $v_o$ and $v_\ell$ being obtained at the same pressure.

The observation of a maximum in figure 6.4 for the n-butane result

but not for propane is attributable to the very much smaller degree of

adsorption in the case of $C_3H_8$. At a given temperature and pressure $\theta$

for $n-C_4H_{10}$ is about four times greater than for $C_3H_8$, thus any maximum

in $(p_o/p_\ell)_\infty$ will not be observed at the low pressures used here. In

the case of $n-C_4H_{10}$ the maximum occurs at about 11 cmHg; a similar degree

of surface coverage on propane would require a gas pressure of 40 - 50

cmHg. Figure 6.4 indicates that a shallow maximum could very well occur

around 60 cmHg.

On the basis of the simple argument presented here, one might

expect that when the steady-state is achieved the flux from $T_o$ to $T_\ell$

due to the pressure difference $p_o - p_\ell$, would be equal in magnitude to

the combined molecular fluxes from $T_\ell$ to $T_o$ caused by (i) gas-phase thermal

transpiration and (ii) sorbed-phase thermal transpiration coupled with a

surface concentration difference between x = 0 and x = $\ell$.

### 6.2.4 *Heats of transport,* $Q_m$

The calculation of $Q_m$ was described in section 6.1.5 and results

presented in table 6.2. The helium result has already been discussed in

detail.

The hydrocarbons considered here undergo extensive adsorption on

the membrane surface and so ideal Knudsen gas values of $Q_o$ are not to be

expected, and are considerably in excess of the $-\frac{1}{2}RT_o$ value of -1634

J mol$^{-1}$ and of the helium result of -1030 J mol$^{-1}$. This extra heat of

transport arises from the transport of adsorbed molecules and is

associated with the considerable heat of adsorption of the hydrocarbon.

$-Q_m$ exhibits a strong pressure dependence, in parallel with the
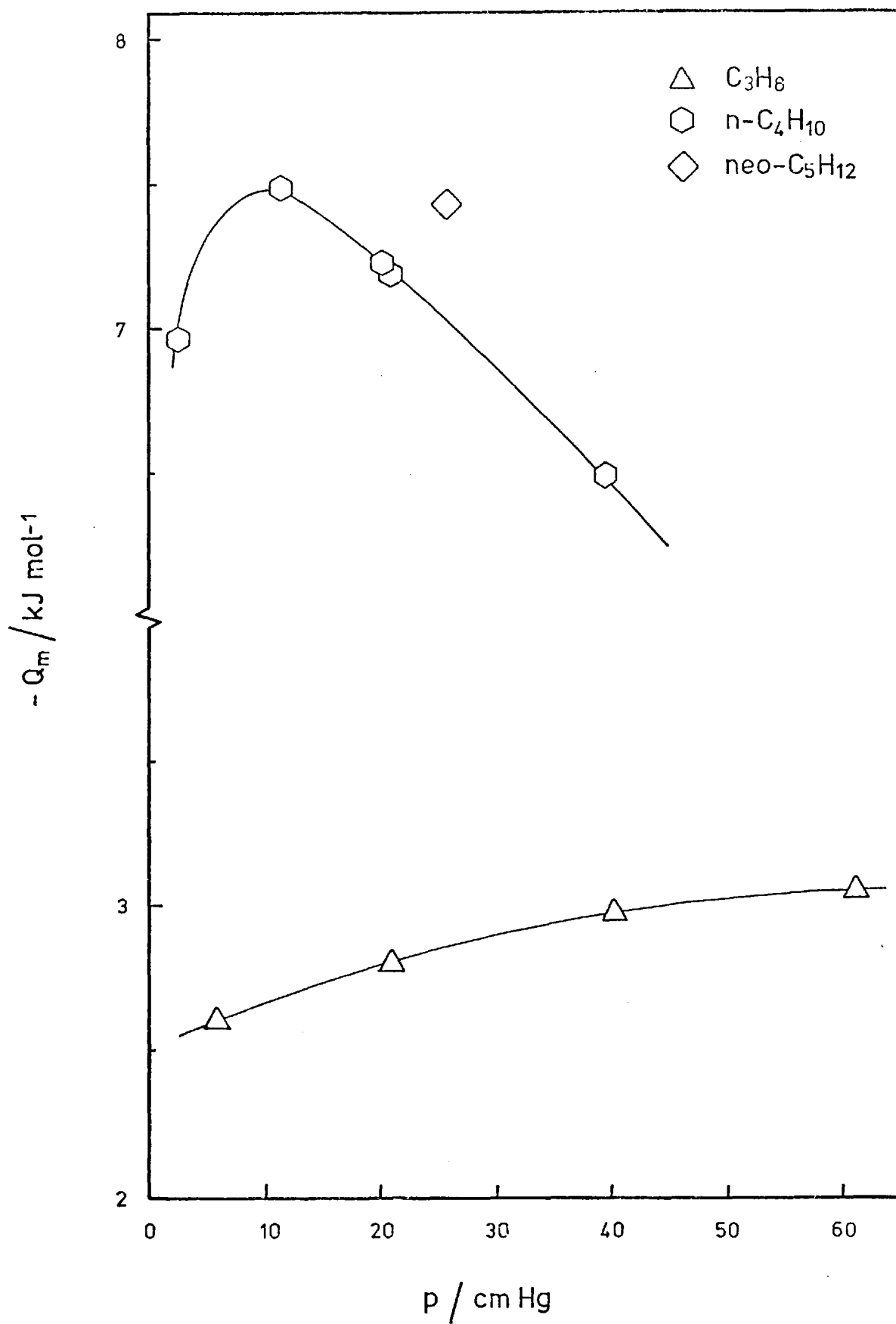
*Figure 6.6*     *Pressure dependence of* -$Q_m$

maximum in $(p_o/p_\ell)_\infty$ also observed, and this is depicted in figure 6.6. These maxima, at high surface concentrations (but still sub-monolayer) have not been observed under these conditions before. However maxima in $\Delta p$ ($= p_o - p_\ell$) and non-ideal values (generally low) of $(p_o/p_\ell)_\infty$ and $Q_o$ have been reported when transpiration has occurred in the intermediate pressure region where $\lambda/d$ is close to unity. Under such conditions transpiration occurred, but was accompanied by slip or viscous flow and the condition $\lambda > 10d$ (for Knudsen behaviour) was not met.

Examples of such work include the flow of inert gases through stainless steel tubes (Hanley and Steele, 1965; Steele and Hanley, 1971), through porous ceramics (Hanley, 1966; Hopfinger and Altman, 1969), Millipore filters (Hopfinger and Altman, 1969) and unglazed porcelain (Rastogi, Singh and Singh, 1969). These membranes had pore diameters of about 1000 nm and were investigated at between 2 and 10 cmHg.

In the slip regime ($\lambda/d \approx 4$) it was found that $Q_o$ was a function of pressure and temperature but as $\lambda/d \to \infty$ these dependencies disappeared. As p increased, $Q_o$ decayed asymptotically from $-\frac{1}{2}RT_o$ at p = 0. Steele and Hanley (1971) endeavoured to isolate $Q_o'$, the temperature and pressure independent part of $Q_o$ by postulating the relationship:

$$Q_o = Q_o' - \alpha \frac{\Delta p}{p} - \beta \frac{\Delta T}{T} \tag{6.16}$$

Bearman and Bearman (1966) working on rubber membranes found a temperature dependence of $Q_o$. However at constant $\Delta T, Q_o$ was independent of p, although the diffusion mechanism was partly by solution in the rubber.

Rastogi et al (1974) used a membrane of unglazed porous porcelain to investigate heats of transport for binary, ternary and quaternary systems. They found the heats to be additive, viz

$$Q_m = \sum c_i \left[ Q_m \right]_i \tag{6.17}$$

where $c_i$ is the mass fraction of the $i^{th}$ component and $\left[Q_m\right]_i$ is its

heat. Knudsen behaviour was not found for the individual components

$(O_2, CO_2, C_2H_4)$.

The question therefore arises, are the effects of slip flow being

manifested at the higher pressures in this work? From figure 5.7 we

can see that $\lambda/d = 10$ (the commonly accepted limit for pure thermal

transpiration) occurs close to 15 cmHg for propane and n-butane, so that

above this pressure one might expect a steady decrease in $Q_m$ or $p_o/p_\ell$.

However this is a gas-phase phenomenon whereas here values are obtained

for $(p_o/p_\ell)_\infty$ and $Q_m$ which are dominated by surface transport. If the

decay of gas phase thermal transpiration was significant, then we should

certainly have observed a reduction in $Q_m$ for $C_3H_8$ at 60 cmHg where

$\lambda/d = 2.2$, but in fact $Q_m$ is still tending to increase.

Gas phase thermal transpiration therefore makes a minor contribution

to $Q_m$ since no decrease is obtained where, with purely gas phase flow, we

would be entering the slip flow regime. The pronounced reduction in $Q_m$

for $n\text{-}C_4H_{10}$ is attributed to a reduction in the driving force for the

surface analogue of thermal transpiration. This could be due to the

adsorbate surface concentration difference between the membrane faces

actually decreasing as $\theta \to 1$. There is also a possibility of a changeover

to hydrodynamic flow (see section 5.3.2). Some fall in $Q_m$ may be observed

at very low pressures when gas phase transport could be comparable with

surface transport.

### 6.2.5 *Surface and gas phase heats of transport*

A treatment of non-isothermal transport in terms of non-equilibrium

thermodynamics has been derived by Ash and Barrer (1963) and Ash et al

(1973); this approach was outlined in chapter 2.

It was shown that the heat of transport can be analysed into

components pertaining solely to extra or surface flow $(Q_s)$ and to gas

phase flow $(Q_g)$, related by

$$Q_o = Q_s \frac{K_s}{K} + Q_g \frac{K_g}{K} \qquad\qquad (6.18)$$

$K$, $K_s$ and $K_g$ are the overall permeability, surface and gas phase

permeabilities under isothermal conditions at $T_o$. Further, the relations

(6.19) can also be derived:-

$$\left.\begin{aligned}
Q_g &= Q_g^* - H_g^{\ominus} \\
Q_s &= Q_s^* - H_g^{\ominus}
\end{aligned}\right\} (6.19)$$

where $Q_g^*$ and $Q_s^*$ are molar heats of transport under isothermal conditions

in the gas phase and by extra flow respectively. $H_g^{\ominus}$ is the ideal gas

enthalpy.

In chapter 5 $K$, $K_s$ and $K_g$ were given for $C_3H_8$ and $n\text{-}C_4H_{10}$ on plug N.

Although a different membrane (plug O) is used for the thermo-osmotic

measurements, they both have very similar porosities and other physical

parameters.

If the gas is only slightly sorbed, then $Q_g$ will adopt a value close

to that of a non-sorbed gas, but this will be less than the Knudsen limit

(see section 6.2.2). However for the hydrocarbons used in this study

extensive adsorption occurs, which could cause gas phase blockage at

constrictions within the membrane. This would decrease the gas phase

transport and therefore reduce the amount of heat transported by the gas.

If complete blockage occurred, then we would have no gas transport and

$Q_g = 0$. This situation is probably the case for strongly sorbed gases on

Carbolac membranes, where the pores are much narrower than in Graphon

(Ash et al, 1973). Thus, if $-\frac{1}{2}RT_o$ and zero are taken as upper and lower

limits for $Q_g$, the exact value being undetermined, then from the measured

$Q_o$ an estimate of the magnitude of $Q_s$ can be made.

$H_g^{\ominus}$ can be obtained from standard tables of gas enthalpies (Rossini,

et al, 1947) and so estimates of both $Q_s^*$ and $Q_g^*$ can be made. Values of

$H^{\ominus}_g$ as well as limiting values of $Q_g$ and $Q^*_g$ are given in table 6.7 for

$C_3H_8$ and $n-C_4H_{10}$ for $T_o$ of 393K. In table 6.8 $Q_s$ and $Q^*_s$ are given for a

$T_o$ of 393K and at several pressures, due account being taken of the

pressure dependence of isothermal permeabilities (Note: $Q_m$ values,

rather than precise $Q_o$ values, were used in the calculations). No analysis

was possible for $neo-C_5H_{12}$ since isothermal permeability data were not

available.

TABLE 6.7

$H^{\ominus}_g$, $Q_g$ and $Q^*_g$ for $C_3H_8$ and $n-C_4H_{10}$ at $T_o = 393K$

| Gas | $H^{\ominus}_g$ kJ mol$^{-1}$ | $-Q_g$ kJ mol$^{-1}$ | $+Q^*_g$ kJ mol$^{-1}$ |
|---|---|---|---|
| $C_3H_8$ | $22.5_9$ | $1.6_4$ | $20.9_5$ |
| " | " | 0 | $22.5_9$ |
| $n\ C_4H_{10}$ | $30.0_4$ | $1.6_4$ | $28.4_0$ |
| " | " | 0 | $30.0_4$ |

TABLE 6.8

$Q_s$, $Q^*_s$ and X for $C_3H_8$ and $n-C_4H_{10}$ at $T_o = 393K$

| p cmHg | $-Q_m$ kJ mol$^{-1}$ | $Q_g = -\frac{1}{2}RT_o$ | | $Q_g = 0$ | | X |
|---|---|---|---|---|---|---|
| | | $-Q_s$ kJ mol$^{-1}$ | $+Q^*_s$ kJ mol$^{-1}$ | $-Q_s$ kJ mol$^{-1}$ | $+Q^*_s$ kJ mol$^{-1}$ | |
| | | | Propane | | | |
| 5.69 | $2.6_1$ | $3.1_8$ | 19.4 | $4.1_5$ | 18.4 | $0.7_5$ |
| 20.83 | $2.8_1$ | $3.5_0$ | 19.1 | $4.4_7$ | 18.1 | $0.7_3$ |
| 40.25 | $2.9_8$ | $3.7_8$ | 18.8 | $4.7_5$ | 17.8 | $0.7_2$ |
| 61.30 | $3.0_5$ | $3.8_9$ | 18.7 | $4.8_6$ | 17.7 | - |
| | | | n-Butane | | | |
| 2.42 | $6.9_7$ | $8.4_7$ | 21.6 | $8.9_3$ | 21.1 | $0.5_7$ |
| 11.33 | $7.4_9$ | $9.1_3$ | 20.9 | $9.5_9$ | 20.5 | $0.5_5$ |
| 20.76 | $7.2_0$ | $8.7_6$ | 21.3 | $9.2_1$ | 20.8 | $0.5_7$ |
| 39.51 | $6.5_1$ | $7.8_4$ | 22.2 | $8.3_2$ | 21.7 | $0.6_2$ |

It can be seen that $-Q_s$ for $C_3H_8$ is twice $-Q_o$ for the ideal

Knudsen gas and for $n-C_4H_{10}$ it is five times as great, thus surface

transport clearly dominates the flow. The behaviour of $Q_s$ with pressure

parallels that of $Q_m$, as would be expected. $Q_s^*$ is positive and its

variation with pressure exhibits the opposite trends to $- Q_s$. It is

larger for $n-C_4H_{10}$ than for $C_3H_8$.

Barrer and Gabor (1960) considered extra isothermal flow to

occur by surface transport, accompanied by evaporative flights across

the crevices and side pores; during these flights the extra flow is in

the gas phase. Thus the surface flux, $J_s$, can be divided into the fraction

occurring in the gas phase, $XJ_s$, and that remaining on the surface, $(1 - X)J_s$

(Appendix A). $Q_s$ can be similarly expressed in terms of the heats due

to the extra flow in the gas phase and on the surface.

Ash et al (1973) analysed equation (6.18) in this way by expressing

$Q_s$ as :

$$Q_s = (1 - X) (\tilde{H}_m + \tilde{\Delta H}) + X Q_g \qquad (6.20)$$

where $\tilde{H}_m$ is the molar enthalpy required by adsorbed molecules for

surface migration, and $\tilde{\Delta H}$ is the integral heat of adsorption. By making

the approximation $\tilde{H}_m \simeq -\frac{1}{3} \tilde{\Delta H}$ and taking the limit where $Q_g = 0$ then

(6.20) becomes

$$Q_s = (1 - X) . \frac{2}{3} . \tilde{\Delta H} = Q_o \frac{K}{K_s} \qquad (6.21)$$

Hence X, the fraction of the extra flow in the gas phase can be very

approximately obtained and the values for 393K are included in table 6.8,

$-q'_{st}$ being used for $\tilde{\Delta H}$.

For $C_3H_8$, ~73% of the extra flow is estimated to occur by

evaporative flights in the gas phase. This compares well with the values

given by Ash et al (1973) on Graphon viz ~91 % (Ar), ~87% (Kr) and ~73%

(Xe). However one might have expected a value for $C_3H_8$ smaller than for

Xe in view of the much greater extent of sorption.

The butane fraction consisted of 55-60% in the gas phase and this

appears to have a minimum value at around 10 cmHg, in line with the

maximum in transport properties related to surface flow $(p_o/p_\ell,\ Q_o$ etc) which also occurs at approximately 10 cmHg.

### 6.2.6 *Surface thermal transpiration*

Several treatments of thermal transpiration through porous media have been advanced and extended to accommodate surface transport. These are reviewed in sections 2.2.2 and 2.2.3. The treatment due to Hill (1956) will now be considered further.

Clint (1966) extended an expression derived by Hill (equation (2.50)) for the steady-state transport due to surface flow (see section 2.2.3):

$$\dot{n} = -2\pi r.\ D_{ss}.\frac{dc'_s}{dx} - \pi r^2\ \frac{d(D_{gs}c'_g)}{dx} \qquad (6.22)$$

where $\dot{n}$ is the number of molecules per second passing through unit cross-section in the x direction.

If Fick's law is written as:

$$J = -\frac{\partial}{\partial x}\ (D_{ss}\ c'_s) - \frac{\partial}{\partial x}\ (D_{gs}c'_g) \qquad (6.23)$$

then Clint demonstrated that for this postulated equation, including $D_{ss}$ in the integration w.r.t. x, yields the result

$$Q_o = -\frac{1}{2}\ RT_o\left[\frac{K_g}{K}\right]_{T_o} + (\Delta H + E_{ss})\left[\frac{K_s}{K}\right]_{T_o} \qquad (6.24)$$

where $\Delta H$ is the heat of adsorption and $E_{ss}$ the activation energy for surface diffusion. $K$, $K_g$ and $K_s$ are the isothermal permeabilities at $T_o$. This expression allows for varying contributions to $Q_o$ from gas and surface transport.

Hill's treatment predicted that for a heat of transport due entirely to surface flow

$$Q_o = -\frac{1}{2}\ RT_o + \Delta E \quad - \text{ mobile adsorption} \qquad (6.25)$$

$$= +\frac{1}{2}\ RT_o + \Delta E \quad - \text{ localised adsorption} \qquad (6.26)$$

where $\Delta E$ is the energy of adsorption.

The equivalent expressions to equations (6.24) to (6.26) for the steady-state pressure ratio $(p_o/p_\ell)_\infty$ are respectively equations (6.27) to (6.29) as follows:

$$\ln\left(\frac{p_o}{p_\ell}\right)_\infty = \int_{T_\ell}^{T_o} \left\{ \frac{1}{2T}\left[1 + \frac{K_s}{K}\right] - \frac{K_s}{K}\frac{(\Delta E + E_{ss})}{RT^2}\right\} dT \quad (6.27)$$

$$\left(\frac{p_o}{p_\ell}\right)_\infty = \frac{\exp(-\Delta E/RT_\ell)}{\exp(-\Delta E/RT_o)} \cdot \left(\frac{T_o}{T_\ell}\right)^{\frac{1}{2}} \quad (6.28)$$

$$\left(\frac{p_o}{p_\ell}\right)_\infty = \frac{\exp(-\Delta E/RT_\ell)}{\exp(-\Delta E/RT_o)} \cdot \left(\frac{T_\ell}{T_o}\right)^{\frac{1}{2}} \quad (6.29)$$

Equation (6.27) may be evaluated from isothermal data (chapter 5) by a graphical integration.

Heats of transport and $(p_o/p_\ell)_\infty$ have been calculated by each of the three expressions for propane on Graphon, at $T_o = 393K$, $T_\ell = 333K$ and 10 cmHg pressure. Table 6.9 presents the values obtained, together with $-\frac{1}{2}RT_o$ and the experimental values. It can be seen that both surface transport models of Hill lead to a gross overestimate of $(p_o/p_\ell)_\infty$ and $-Q_o$, whereas Clint's model, allowing for varying proportions of surface and gas phase transport leads to a better approximation, but is still an overestimate.

TABLE 6.9

$Q_o$ *and* $(p_o/p_\ell)_\infty$ *for propane calculated by the theories of Hill and Clint*

| | $\left(\dfrac{p_o}{p_\ell}\right)_\infty$ | $\dfrac{-Q_o}{kJ\ mol^{-1}}$ |
|---|---|---|
| Knudsen gas flow | 1.09 | 1.64 |
| Experimental value | 1.16 | 2.67 |
| Clint | 1.75 | 9.11 |
| Hill; mobile adsorption | 3.69 | 23.7 |
| Hill; localised adsorption | 3.12 | 20.5 |

## 6.3 DISCUSSION OF ISOBARIC PERMEABILITY RESULTS

Isobaric permeabilities were determined at several pressures for the temperature gradient $T_o$ = 393K and $T_\ell$ = 333K (table 6.3); the pressure dependence is depicted in figure 6.7. The behaviour is similar to that observed for $(p_o/p_\ell)_\infty$ and $Q_o$ (see sections 6.2.3 and 6.2.4). Helium, undergoing only gas phase flow, has a constant value of $-B(T_o)/p_o$ while the value for $C_3H_8$ increases with pressure, flattening out at approximately 50 cmHg. n-Butane exhibits a high value initially, possibly reaching a maximum in the region of 5 cmHg, but falls rapidly above 15 cmHg to 60% of its initial value at 40 cmHg.

Dr A.V.J. Edge of these laboratories has studied the pressure dependence of $B(T_o)/p_o$ for $n-C_4H_{10}$ and $neo-C_5H_{12}$ in the pressure range 1 to 60 cmHg. The $n-C_4H_{10}$ and $neo-C_5H_{12}$ measurements of this work lie close to the curves he obtained. He found neo-pentane exhibited a maximum in $-B(T_o)/p_o$ of $3.2 \times 10^{-8}$ $m^2 s^{-1} K^{-1}$ at about 2 cmHg, but decreased more steeply than n-butane, reaching half its maximum value at 37 cmHg. iso-Butane was intermediate between $C_3H_8$ and $n-C_4H_{10}$, reaching an apparent maximum of about $1.14 \times 10^{-8}$ $m^2 s^{-1} K^{-1}$ at 15 cmHg, followed by a gradual decrease in $-B(T_o)/p_o$.

In this work no pressure dependence was observed for helium, although it was studied only between 25 and 50 cmHg. At low pressures the flux obtained was too small to be detected with any accuracy by the Baratron sensor, since background noise, caused by environmental temperature fluctuations, was severe. An average $-B(T_o)/p_o$ of $0.215 \times 10^{-8}$ $m^2 s^{-1} K^{-1}$ was obtained for He. This is very similar to the 'theoretical' value obtained from isothermal work (see below).

The pressure dependence of the isobaric permeability due largely to a 'surface' component can also be related to the driving force for thermo-osmotic flow. In section 6.2.3 this driving force was considered
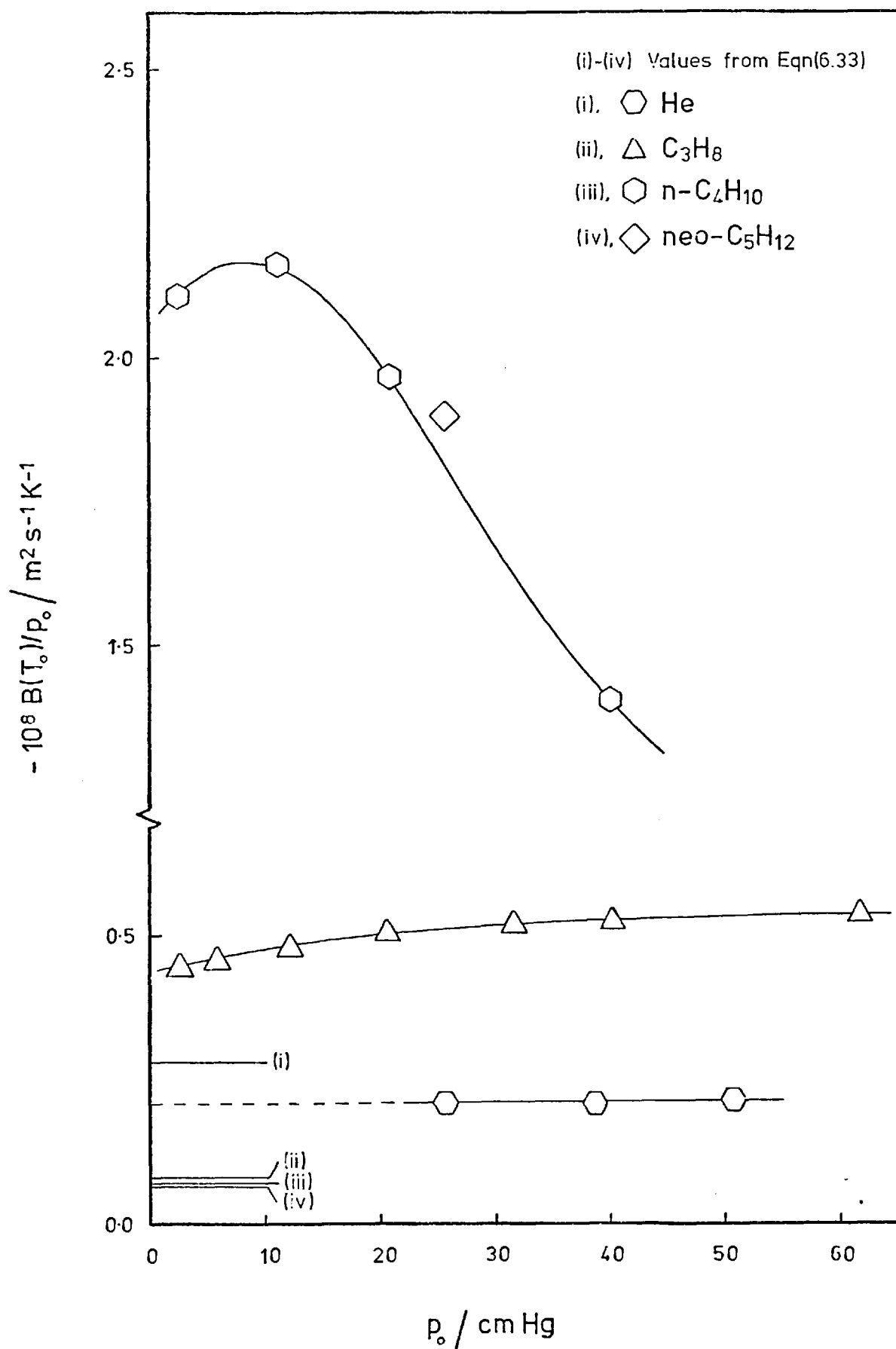
Figure 6.7    Pressure dependence of isobaric permeabilities

to be due to the surface concentration difference ($\Delta v = v_\ell - v_o$) between the membrane faces. In a steady-state of isobaric flow $\Delta v$ will be proportional to the isobaric flux and hence $\Delta v/p$ should be proportional to the isobaric permeability (equation 6.3).

Using the same isotherm data as before, figure 6.8 shows the dependence of $\Delta v/p$ on p. Comparison with the experimental findings depicted in figure 6.7 is favourable (although different values of $T_o$ and $T_\ell$ had to be used for n-$C_4H_{10}$ in figure 6.8 due to lack of isotherm data at 333K). A sharp fall in $\Delta v/p$ is observed for n-$C_4H_{10}$ whilst $C_3H_8$ has a much smaller variation with pressure.

Gilliland et al (1962) measured the isobaric permeability of ethylene and propylene on a Vycor membrane and found maxima with pressure as observed in this work. As the mean temperature was reduced, the magnitude of isobaric flow increased and the pressure dependence was more pronounced with the maxima being moved to lower pressures. Gilliland used a hydrodynamic mechanism for surface flow and derived an expression for the isobaric surface permeability which could predict the maximum observed.

### 6.3.1 *Derivation of* $B_g(T_o)/p_o$ *for a Knudsen gas*

An expression to derive an isobaric flux from limiting non-isothermal pressure ratios and isothermal permeabilities was derived by Ash et al (1973) and given in chapter 2, viz

$$J = \frac{p_o \exp\left(\displaystyle\int_{T_\ell}^{T_o} \frac{Q_o}{RT^2}\, dT\right) - p_\ell}{\displaystyle\int_0^\ell \left[\frac{RT}{K}\exp\left(\displaystyle\int_{T_\ell}^{T} \frac{Q_o}{RT^2}\, dT\right)\right] dx} \qquad (2.103)$$

| | | $T_o/K$ | $T_1/K$ |
|---|---|---|---|
| (i) | $C_3H_8$ | 393 | 308 |
| (ii) | $C_3H_8$ | 393 | 333 |
| (iii) | $n-C_4H_{10}$ | 393 | 308 |
| (iv) | $n-C_4H_{10}$ | 373 | 308 |
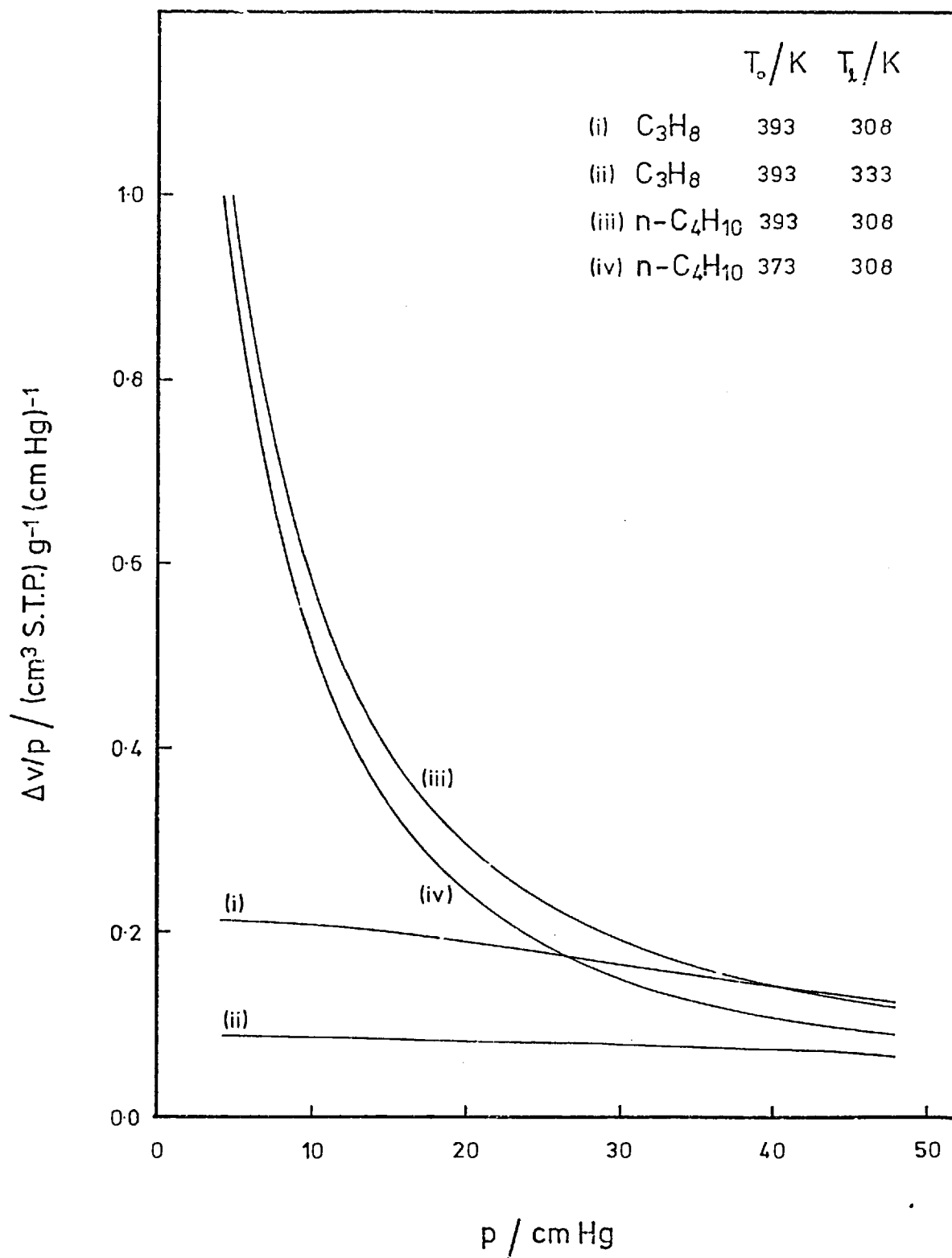
*Figure 6.8*      $\Delta v/p$ *as a function of pressure*

For solely gas phase flow we write $J = J_g$, and for weakly sorbed gases $Q_0 = \beta(-\frac{1}{2}RT_0)$. Substituting this relation in (2.103) and evaluating the integrals w.r.t. T we get :-

$$J_g = \frac{p_0 T_0^{-\beta/2} - p_\ell T_\ell^{-\beta/2}}{\int_0^\ell \left(\frac{RT}{K}^{1-\beta/2}\right) dx} \tag{6.30}$$

Now the isothermal permeability, $K$, can be obtained from $K = \kappa_{gs} D_g^{cyl} \epsilon$ where $D_g^{cyl}$ is given by equation (2.7). Hence the remaining integral can be evaluated , giving

$$J_g = \frac{8\epsilon^2 \kappa_{gs}}{3 \, A. \, \ell} \left(\frac{2}{\pi RM}\right)^{\frac{1}{2}} \frac{p_0 T_0^{-\beta/2} - p_\ell T_\ell^{-\beta/2}}{T_\ell^{\frac{1}{2}(1-\beta)}} \tag{6.31}$$

In isobaric flow $p_0 = p_\ell$, hence from equation (6.3) $B(T_0)/p_0$ becomes:

$$\frac{B_g(T_0)}{p_0} = \frac{8\epsilon^2 \kappa_{gs}}{3 \, A} \cdot \left(\frac{2R}{\pi M}\right)^{\frac{1}{2}} \cdot \frac{T_0}{\Delta T} \cdot \frac{T_0^{-\beta/2} - T_\ell^{-\beta/2}}{T_\ell^{\frac{1}{2}(1-\beta)}} \tag{6.32}$$

where $B_g(T_0)/p_0$ is the isobaric permeability due to gas phase flow only. Several simplifications are now possible. For an ideal Knudsen gas $\beta = 1$, hence we obtain:

$$\frac{B_g(T_0)}{p_0} = \frac{8\epsilon^2 \kappa_{gs}}{3 \, A} \left(\frac{2R}{\pi M}\right)^{\frac{1}{2}} \frac{T_0}{\Delta T} \left[\frac{1}{T_0^{\frac{1}{2}}} - \frac{1}{T_\ell^{\frac{1}{2}}}\right] \tag{6.33}$$

Equation (6.33) can be re-expressed in terms of $K_g(T_0)$, the isothermal gas phase permeability at $T_0$ :

$$\frac{B_g(T_0)}{p_0} = K_g(T_0). \, \frac{T_0^{\frac{1}{2}}}{\Delta T} \left[\frac{1}{T_0^{\frac{1}{2}}} - \frac{1}{T_\ell^{\frac{1}{2}}}\right] \tag{6.34}$$

This can be manipulated to give

$$\frac{B_g(T_0)}{p_0} = -\frac{1}{2} \frac{K_g(T_0)}{T_0} \left\{\frac{2 T_0}{(T_0^{\frac{1}{2}} + T_\ell^{\frac{1}{2}})} \frac{1}{T_\ell^{\frac{1}{2}}}\right\} \tag{6.35}$$

If $\Delta T$ is small, ie $T_o \simeq T_\ell$, then the term in brace brackets reduces to unity and so we get

$$- \frac{B_g(T_o)}{P_o} = \frac{1}{2} \frac{K_g(T_o)}{T_o} \tag{6.36}$$

Thus we have three expressions for $B_g(T_o)/P_o$, (6.32), (6.33) and (6.36), and we can apply these to helium. The values obtained are shown in table 6.10, the last column being based on the experimental helium value of -2.15 x $10^{-9}$ $m^2 s^{-1} K^{-1}$.

TABLE 6.10

*Values of* $10^9$ x $(- B_g(T_o)/P_o)$

| Gas | Eqn. (6.32) | Eqn. (6.33) | Eqn. (6.36) | Expt. |
|-----|-------------|-------------|-------------|-------|
| He | 2.09 | 2.86 | 2.35 | 2.15 |
| $C_3H_8$ | 0.63 | 0.86 | 0.71 | 0.65 |
| $C_4H_{10}$ | 0.55 | 0.75 | 0.62 | 0.56 |
| $C_5H_{12}$ | 0.49 | 0.67 | 0.55 | 0.51 |

Very good agreement is found between the experimental $B_g(T_o)/P_o$ for helium and that derived from equation (6.32). This equation makes use of experimental isothermal permeability data for a real tortuous medium but it should be noted that a different membrane (N) was used in that work although it had a very similar length, area and porosity to plug 'O'. Allowance is also made in (6.32) for departure from Knudsen gas behaviour in the form of $\beta$. When no allowance was made for $\beta$ (equation (6.33)) the ratio between experimental and calculated values was 0.75, very close to the value of $\beta$ (0.72). Equation (6.36) also gives an isobaric permeability close the experimental $B_g(T_o)/P_o$, even though the approximation, $\Delta T \to 0$, was not a good one ($\Delta T$ = 58.2K). This approximation has been used by Gilliland et al, 1962 .

6.3.2 *Isobaric flow for hydrocarbons*

It is now possible to divide $B(T_o)/p_o$ for the hydrocarbons $C_3H_8$ to neo-$C_5H_{10}$ into gas and 'surface' phase components (compare equation (2.11)):

$$\frac{B(T_o)}{p_o} = \frac{B_g(T_o)}{p_o} + \frac{B_s(T_o)}{p_o} \qquad (6.37)$$

The gas phase isobaric permeabilities, $B_g(T_o)/p_o$, given in table 6.10, rely on the relationship $B_g(T_o)/p_o \propto M^{\frac{1}{2}}$ (cf section 5.1), and can be derived from the helium values (obtained from equations (6.32), (6.33) and (6.36)). Using the $B_g(T_o)/p_o$ values given in the last column of table 6.10, then $B_s(T_o)/p_o$ and $B_s(T_o)/B_g(T_o)$ can be obtained from equation (6.37) and are presented in table 6.11. It is assumed that for gas phase flow in the absence of blockage $B_g(T_o)$ is independent of pressure.

TABLE 6.11

*Values of $B_s(T_o)/p_o$ and $B_s(T_o)/B_g(T_o)$ ratios*

| $\dfrac{p}{cmHg}$ | $\dfrac{-10^8.B(T_o)/p_o}{m^2\ s^{-1}\ K^{-1}}$ | $\dfrac{-10^8.B_s(T_o)/p_o}{m^2\ s^{-1}\ K^{-1}}$ | $\dfrac{B_s(T_o)}{B_g(T_o)}$ |
|---|---|---|---|
| | Propane | | |
| 2.45 | $0.45_2$ | $0.38_6$ | $5.9_6$ |
| 5.69 | $0.46_0$ | $0.39_5$ | $6.1_0$ |
| 12.09 | $0.48_6$ | $0.42_1$ | $6.5_0$ |
| 20.51 | $0.50_7$ | $0.44_2$ | $6.8_2$ |
| 31.56 | $0.52_0$ | $0.45_6$ | $7.0_3$ |
| 40.31 | $0.52_4$ | $0.45_9$ | $7.0_9$ |
| 61.67 | $0.53_4$ | $0.47_0$ | $7.2_5$ |
| 2.41 | 2.11 | n-Butane 2.06 | $36._5$ |
| 11.09 | 2.16 | 2.11 | $37._4$ |
| 20.89 | 1.97 | 1.91 | $33._9$ |
| 40.04 | 1.41 | 1.35 | $23._9$ |
| | neo-Pentane | | |
| 25.70 | 1.90 | 1.85 | $36._5$ |

$B_s(T_o)/B_g(T_o)$ represents the relative efficiency of surface

to gas phase transport for isobaric flow at a fixed pressure. For the

strongly sorbed gases, $n-C_4H_{10}$ and $neo-C_5H_{12}$, large values were found for

this ratio, especially at low pressures. However as the degree cf site

filling increases and a monolayer is approached, the effectiveness of

isobaric surface transport is reduced. Propane however has a much more

dilute surface film and $B_s(T_o)/B_g(T_o)$ is found to increase with increasing

pressure; here the surface concentration of adsorbate is small and so

increasing sorption merely increases the concentration of species

participating in isobaric transport.

Gilliland (1962) found that for $C_2H_4$ on Vycor, $B_s(T_o)/p_o$ and

$B_g(T_o)/p_o$ were of similar magnitude, however for $C_3H_6$, $B_s(T_o)/B_g(T_o)$ could

be as large as six. The values obtained here on Graphon can be

considerably greater than this owing to the more effective surface flow.

### 6.3.3 Isothermal and isobaric separation factors

The comparative effectiveness of isothermal transport and isobaric

transport as a means of gas separation can be observed by comparing, for

a given pair of gases at a fixed $T_o$, the ratios of isobaric and

isothermal permeabilities. Table 6.12 presents the permeability ratios

for $C_3H_8$ and $n-C_4H_{10}$ at 393.15K (isothermal) and $T_o$ of 393K and $T_\ell$ of

333K (isobaric). Figure 6.9 shows how the permeability ratios behave

with pressures up to 40 cmHg.

These ratios, predicted separation factors, indicate that in the

pressure/temperature range studied for this gas pair, isobaric flux is 2-3

times more effective than isothermal in gas separation. Very similar

behaviour was observed by Ash et al (1973) for various pairs of inert and

permanent gases on Graphon and, less effectively, on Carbolac. An

isothermal ratio of 1.7 and an isobaric ratio of 3.5 have been found by

Gilliland (1962) for $C_2H_4/C_3H_6$ on Vycor. However, it should be
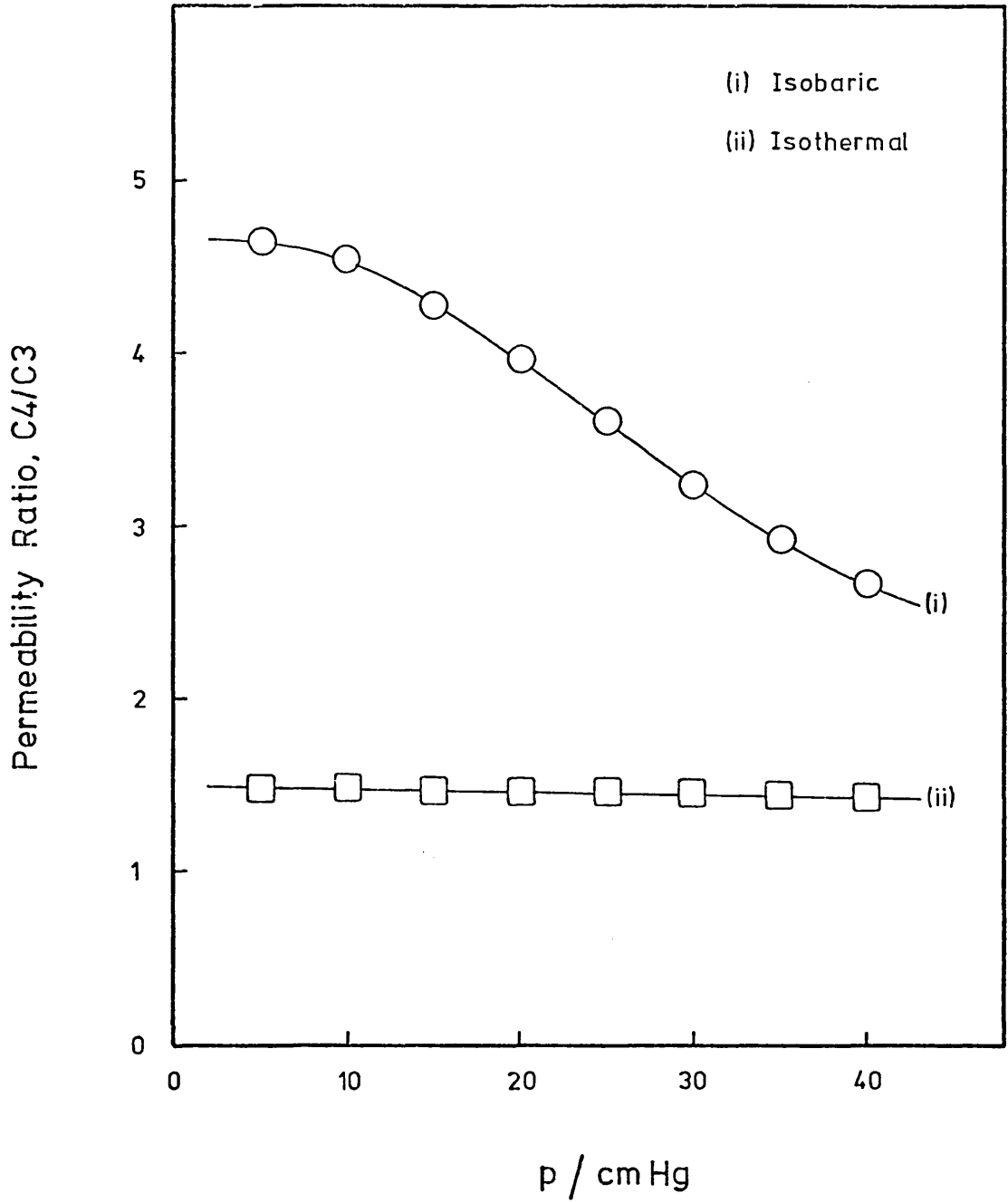
*Figure 6.9    Isobaric and isothermal permeability ratios between n-butane and propane*

remembered that these permeability ratios from single-gas studies

are only predicted separation factors. In a binary gas mixture cross-

coupling is likely to occur, ie the flow of gas A could be influenced

by the presence of gas B (and vica-versa), thus leading to quite

different separation factors.

TABLE 6.12

*Isothermal and isobaric permeability ratios*

| p $\overline{cmHg}$ | $10^6$ $K$ $\overline{m^2 s^{-1}}$ | | $-10^8$ $B(T_o)/p_o$ $\overline{m^2 s^{-1} K^{-1}}$ | | Permeability Ratio, $n\text{-}C_4H_{10}/C_3H_8$ | |
|---|---|---|---|---|---|---|
| | $C_3H_8$ | $n\text{-}C_4H_{10}$ | $C_3H_8$ | $n\text{-}C_4H_{10}$ | Isothermal | Isobaric |
| 5  | 1.50 | 2.22 | $0.46_2$ | 2.15 | 1.48 | $4.6_5$ |
| 10 | 1.50 | 2.22 | $0.47_9$ | 2.18 | 1.48 | $4.5_4$ |
| 15 | 1.50 | 2.20 | $0.49_3$ | 2.11 | 1.47 | $4.2_8$ |
| 20 | 1.50 | 2.20 | $0.50_4$ | 2.00 | 1.46 | $3.9_6$ |
| 25 | 1.50 | 2.18 | $0.51_2$ | 1.84 | 1.46 | $3.6_0$ |
| 30 | 1.50 | 2.17 | $0.51_9$ | 1.68 | 1.45 | $3.2_4$ |
| 35 | 1.50 | 2.15 | $0.52_4$ | 1.53 | 1.43 | $2.9_2$ |
| 40 | 1.50 | 2.13 | $0.52_8$ | 1.41 | 1.42 | $2.6_6$ |

It is also found that $B_s(T_o)/B_g(T_o)$ is greater than $K_s/K_g$ at

the same pressure (compare the values in table 6.11 with Appendix E).

Thus surface flow is proportionally much greater under isobaric conditions

than under isothermal ones.

Since the isobaric flux decreases at high pressures as $\theta \rightarrow 1$, then

isobaric separation will be best achieved at pressures corresponding to

the $-B(T_o)/p_o$ maximum of the most strongly sorbed component.

CHAPTER 7

CONCLUSIONS AND RECOMMENDATIONS

Isothermal permeabilities and time-lags have been determined

for the series of n-paraffins $CH_4$ to $n-C_4H_{10}$ at several temperatures

and pressures.  It has been shown that a considerable extra flow, due

to the presence of a mobile adsorbed film, occurs and that this increases

with the molecular weight of the hydrocarbon.  At 308.15K a marked

decrease in $n-C_4H_{10}$ permeability and time-lag occurred with increasing

pressure;  the $C_3H_8$ permeability also varied with pressure, tending

to reach a shallow maximum at a higher pressure.

The variation with pressure becomes more pronounced as the extent

of adsorption (and therefore of extra or surface flow) increases, ie

for more condensable gases and at lower temperatures, and is due to the

extra flow component.  The pressure dependence of the permeability was

found to be closely related to the isotherm shape.  For gases sorbed

according to Henry's law no pressure dependence is observed, since equal

pressure increments produce equal increments in adsorbate surface

concentration.  However for n-butane, not obeying the Henry law, equal

pressure increments produce progressively smaller increments in surface

concentration.  Since a gradient in surface concentration is one measure

of the driving force for isothermal surface flow, then $K_s$ and $K$ (flux

per unit increment in pressure) are found to decrease.

The relationship between $K$ and isotherm shape was further

demonstrated by evaluating a permeability defined as the flux per unit

increment in surface concentration, $c'_s$.  This was found to *increase* with

increasing sorption.

Diffusion coefficients have been evaluated for gas phase and for

extra flow;  they were found to increase with increasing temperature,

implying an increasing mobility of surface ad-atoms with temperature.

For $n-C_4H_{10}$ (and for $C_3H_8$ at 308.15K) the diffusion coefficients were

evaluated at several degrees of surface coverage, taking account of

the departure from the Henry law. Approximately constant values of

$D_{ss}$ were found at low $\theta$ (<0.3), but at high $\theta$ especially as $\theta \rightarrow 1$, a

significant increase in $D_{ss}$ occurred.

Both the increase in $D_{ss}$ and in $K$ (evaluated with respect to $c'_s$)

as $\theta \rightarrow 1$ indicates greater surface mobility at high $\theta$ and as the

monolayer is approached. It was concluded that for gases adsorbed

outside the Henry law a random walk diffusive flow mechanism occurs

at low $\theta$, but as $\theta \rightarrow 1$ a second mobile layer becomes adsorbed and there

is a possible changeover to hydrodynamic flow, accompanied by an overall

increase in adsorbate mobility and surface flux.

A linear relationship between $KL$ and $k_s$, observed by Dolphin (1971),

has been tested for this series of hydrocarbons. A good linear

relationship was obtained confirming this observation.

In the non-isothermal work thermo-osmotic steady-state pressure

ratios, $(p_o/p_\ell)_\infty$, integral heats of transport, $Q_m$, and isobaric permeabilities,

$B(T_o)/p_o$, have been obtained for He, $C_3H_8, n-C_4H_{10}$ and $neo-C_5H_{12}$. Non-

ideal values for $(p_o/p_\ell)_\infty$ and $-Q_m$ which were lower than the ideal Knudsen

gas values $((T_o/T_\ell)^{\frac{1}{2}}$ and $\frac{1}{2}RT_o$ respectively) were found with helium. The

departure from ideality, which has been observed before in these

laboratories (Ash, Barrer, Clint, Dolphin and Murray, (1973)), was

attributed to differing degrees of specular reflection for 'hot' molecules

travelling from $T_o$ to $T_\ell$ as compared with 'cold' molecules travelling

from $T_\ell$ to $T_o$. Several models for thermal transpiration, taking account

of specular reflection, have been tested for helium, neon and hydrogen

and the apparent degree of specular reflection, $\alpha$, calculated. $\alpha$ was

found to be less than 0.5 and was related to the factor $\beta$ (Ash et al, 1973).

Non-isothermal flow measurements were conducted using an apparatus which incorporated a Baratron pressure transducer. This capacitance membrane manometer was found to be both reliable and stable in use and ideally suited to these studies. A method was developed using this manometer which allowed an isobaric permeability to be determined from the initial portion of the approach curve to the thermo-osmotic steady-state.

For the hydrocarbons, where $(p_o/p_\ell)_\infty$ was found to be much larger than the Knudsen limit, a pronounced pressure dependence in $(p_o/p_\ell)_\infty$, $Q_m$ and in the isobaric permeability, $B(T_o)/p_o$, has been found. This behaviour was very similar to the pressure variation of $K$ and in the case of $-B(T_o)/p_o$ a maximum appears to occur at low pressures.

Extra flow was again found to play an important role in these non-isothermal studies and the driving force for flow was considered to be due in part to the gradient in surface concentration. The gas phase – adsorbed phase concentration relationship is important and the departure of the adsorbate from Henry law adsorption substantially affects these thermo-osmotic parameters. At high pressures it was found that the surface concentration difference per unit pressure between the membrane faces exhibited a similar variation with pressure as $-B(T_o)/p_o$.

Both $K$ and $B(T_o)/p_o$, (isothermal and isobaric permeabilities) have been divided into gas phase and surface (or extra) flow components. The ratio of surface to gas phase isobaric permeability could be very large and was generally greater than the corresponding isothermal permeability ratio. It was also found that for a given pair of gases the ratio of isobaric permeabilities was greater than the corresponding isothermal permeability ratio. Isobaric flow is therefore likely to be the more efficient means of separating binary gas mixtures, if the membrane was used as a gas separation device.

Further work could usefully be carried out in the following areas:

(i)   The range of hydrocarbons studied here should be extended and both isothermal and non-isothermal measurements made for other hydrocarbons which exist in the gas phase at ambient temperature. With the addition of heaters more condensable gases could be investigated and it would be especially interesting to study cyclohexane where the graphite ring in Graphon could act as a template for adsorption.

(ii)   Isothermal work should be carried out below ambient temperature where pressure dependence in $K$ may be observed for the less condensable gases such as propane and ethane.

(iii)   Membrane O and the capacitance manometer can be used for isothermal studies where the Baratron feature of continuous pressure recording could be used to determine isothermal permeabilities without tedious measurements using a cathetometer.

(iv)   In the non-isothermal work a more extensive study should be carried out to establish whether maxima in the thermo-osmotic parameters are observed with propane when measurements are made at much higher pressures. Measurements made at very low and very high pressures with $n-C_4H_{10}$ would also be interesting.

(v)   Non-isothermal flow measurements should be made in which $T_o$ is varied at a fixed $T_\ell$, thus enabling $Q_o$ rather than $Q_m$ to be obtained. Any variation in the pressure dependence of $Q_o$ as the temperature gradient is changed could then be observed.

(vi)   Of very great interest is the behaviour of gas mixtures, both isothermally and non-isothermally. Separation of hydrocarbon mixtures should be possible by isobaric as well as by isothermal flow. If a pressure region for flow measurements is selected corresponding to a permeability maximum for one of the components and a lower permeability for the other component, then enhanced separation may be possible. The

permeability maximum could thus be a useful tool, or variable
parameter, in selecting an area for optimum separation of a
given mixture of gases. However the effect of cross-coupling of
individual gas flows needs to be considered.

(vii) Construction of a wider, shorter plug is of interest since
a much greater flux will be generated and hence gas separation will be
more rapid. Also an improvement in the temperature gradient may be
possible by the use of a plug-holder having a narrower wall.

(viii) The pressure-dependent phenomena found in this work
require a quantitative explanation and a more rigorous relationship
with the adsorption isotherm should be developed.

## APPENDIX A

### *Notation used to describe adsorbate concentration in gas phase and*

### *surface phase flow*

From measurement of adsorption isotherms a Henry law

coefficient, $k_s$, can be obtained as

$$k_s = \frac{c'_s}{c'_g} \qquad (4.2)$$

Here $c'_s$ is the Gibbs excess surface concentration in moles per unit

area of membrane surface. $c'_g$ is the gas phase concentration (= p/RT)

in moles per unit volume of gas phase.

If $c$ is the total concentration of adsorbate within the

membrane (moles per unit volume of membrane), $\varepsilon$ is the membrane porosity

( void volume per unit volume of membrane) and A is the internal

surface area of sorbent, per unit volume of membrane, then we can write:

$$c = \varepsilon c'_g + A c'_s$$

Defining $c_s$ (= $A c'_s$) as the Gibb's excess concentration per unit

volume of membrane and $c_g$ (= $\varepsilon\ c'_g$ ) as the gas phase concentration per

unit volume of membrane, then we write

$$c = c_s + c_g$$

An alternative expression for c can be written:

$$c = c^s + c^g$$

where $c^s$ is the *absolute* concentration of adsorbate material within

the sorption volume, A$\delta$, per unit volume of membrane and $c^g$ is the gas

phase concentration, per unit volume of membrane, in the pore space

excluding the adsorbed layer (of thickness $\delta$ and volume A$\delta$). The

concept of absolute sorption is discussed further in section 4.3.

The various concentrations may be related by:

$$c^s = A(c_s' + \delta c_g')$$

$$c^g = (\varepsilon - A\delta)c_g'$$

Expressions for the flux, $J$, can be formulated in terms of either $c_s'$, $c_g'$; $c_s$, $c_g$ or $c^s$, $c^g$, and similarly for permeabilities ($K$, $K_s$, $K_g$) and diffusion coefficients ($D$, $D_{ss}$, $D_{gs}$).

It has been common practice to divide the total mass flow into two components, $J_s$ and $J_g$, which are considered to be due to flow entirely on the surface and entirely in the gas phase.

Barrer and Gabor (1960) pointed out that in a compacted carbon membrane we have very tortuous pores with bottlenecks and crevices. Consequently surface flow through a 'pore' can not be continuous because of the very nature of the membrane. Molecules in the surface phase must undergo evaporative flights, in the gas phase, while crossing crevices and discontinuities in the surface. Thus besides an equilibrium between adsorbed and gas phase molecules, there is an additional interchange of sorbed molecules between the surface and gas phase. The ratio of local gas phase to local surface phase flux will fluctuate as transport occurs through the membrane.

The surface flux or more correctly 'extra' flux, $J_s$, can therefore be divided (at any cross-section normal to the flow) into that part, $J_s'$, which is entirely in the surface, and the remainder $J - J_s'$, which is in the gas phase.

ie $$J_s = J_s' + (J_s - J_s')$$

This could be alternatively expressed as:

$$J_s' = (1 - X)J_s \text{ and } (J_s - J_s') = XJ_s$$

where X is the fraction of 'extra' flow which is in the gas phase.

Ash, Barrer, Clint, Dolphin and Murray, (1973), used this treatment

and considered that the two components of extra flow would have different diffusion coefficients, $D_1$ (surface phase) and $D_2$ (gas phase).

Hence we can write $D_{ss} = D_1 + D_2$ and therefore

$$- D_{ss} \frac{dc_s}{dx} = - D_1 \frac{dc_s}{dx} - D_2 \frac{dc_s}{dx}$$

and $\dfrac{d\ln D_{ss}}{dT} = \dfrac{E_{ss}}{RT^2} = \dfrac{d}{dT} \left\{ \ln \left[ D_{01} \exp (-E_1/RT) + D_{02} \exp (-E_2/RT) \right] \right\}$

where $D_{01}$ and $D_{02}$ are Arrhenius constants and $E_1$ and $E_2$ are activation energies pertaining to $J'_s$ and $(J_s - J'_s)$.

A third subdivision of $J$ has been proposed by Ash, Barrer and Sharma (1976). Helium is used as an internal calibrating gas to evaluate a gas phase flux of the sorbable gas, $J''_g$, in the presence of its mobile adsorbed film, which restricts the pore volume available to the gas. The remainder of the flow, $J''_s (= J - J''_g)$, is the extra flow associated with the mobile adsorbed film.

## APPENDIX B

*Calibrations and standard volumes*

(i)  Adsorption sample bulb calibrations

| $\dfrac{T_T}{K}$ | $\left(\dfrac{300\,V_1}{T_T}-1\right)/cm^3$ | | $V_1\,/\,cm^3$ | |
|---|---|---|---|---|
| | A | B | A | B |
| 77.4 | $47.9_8$ | – | $12.3_8$ | – |
| 308.15 | $12.2_1$ | $40.0_8$ | $12.5_4$ | $41.1_7$ |
| 320.65 | $11.8_0$ | $38.4_9$ | $12.6_2$ | $41.1_3$ |
| 333.15 | $11.4_2$ | $37.0_8$ | $12.6_8$ | $41.1_8$ |
| 343.15 | $11.1_2$ | $36.0_6$ | $12.7_2$ | $41.2_5$ |
| 353.15 | $10.8_2$ | $35.0_8$ | $12.7_4$ | $41.2_9$ |
| 363.15 | $10.5_4$ | $34.1_4$ | $12.7_6$ | $41.3_2$ |
| 373.15 | $10.2_7$ | $33.2_2$ | $12.7_8$ | $41.3_1$ |
| 393.15 | $9.78_8$ | $31.5_0$ | $12.8_3$ | $41.2_8$ |

$T_T$ is the isotherm temperature and $V_1$ is the volume of gas in the adsorption bulb at that temperature.

System A refers to burette 46 and 7.164g sample of Graphon

System B refers to burette 55 and $24.27_4$g sample of Graphon

(ii) McLeod gauge calibration

| Gauge | $\dfrac{V}{cm^3}$ | $\dfrac{10^5.k}{mm^{-1}}$ |
|---|---|---|
| D1 | 304.3 | $1.032_4$ |
| D2 | 301.1 | $1.043_4$ |
| D3 | 295.1 | $1.064_6$ |

$V$ = gauge volume;  $k = \pi r^2/V$ where $r$ is the capillary radius.

(iii) Buffer volumes at $25^\circ C$

| Buffer | $\dfrac{Volume}{cm^3}$ |
|---|---|
| E | $1112._0$ |
| X | $325._8$ |
| $\alpha$ | $1056._4$ |
| $\beta$ | $2271._0$ |
| $\gamma$ | $5409._6$ |
| $\epsilon$ | $1070._0$ |
| $\zeta$ | $2314._2$ |
| $\eta$ | $3214._2$ |
| $\theta$ | $3311._6$ |

# APPENDIX C

*Adsorption isotherm data*

p denotes equilibrium gas pressure (cmHg)

v denotes uptake ($cm^3$ S.T.P. $g^{-1}$)

Hydrogen isotherms

| T = 308.15K | | T = 320.65K | | T = 333.15K | | T = 343.15K | |
|---|---|---|---|---|---|---|---|
| p | v | p | v | p | v | p | v |
| 1.33 | 0.0005 | 1.80 | 0.0008 | 2.32 | 0.0003 | 2.37 | 0.0007 |
| 1.80 | 0.0009 | 3.75 | 0.0021 | 4.01 | 0.0015 | 4.13 | 0.0016 |
| 2.25 | 0.0011 | 6.95 | 0.0036 | 7.68 | 0.0032 | 7.08 | 0.0027 |
| 2.69 | 0.0015 | 11.83 | 0.0062 | 13.22 | 0.0057 | 12.36 | 0.0048 |
| 3.79 | 0.0018 | 14.47 | 0.0075 | 17.08 | 0.0074 | 17.95 | 0.0068 |
| 6.37 | 0.0034 | 18.74 | 0.0099 | 21.60 | 0.0095 | 22.81 | 0.0088 |
| 7.72 | 0.0042 | 25.51 | 0.0133 | 24.89 | 0.0108 | 26.59 | 0.0102 |
| 7.72 | 0.0042 | 28.56 | 0.0147 | 29.64 | 0.0129 | 32.35 | 0.0124 |
| 10.27 | 0.0052 | 31.71 | 0.0165 | 35.06 | 0.0154 | 37.21 | 0.0142 |
| 14.02 | 0.0073 | 36.02 | 0.0184 | 40.15 | 0.0176 | 41.70 | 0.0158 |
| 17.51 | 0.0091 | 40.59 | 0.0207 | 44.79 | 0.0195 | 47.94 | 0.0183 |
| 20.96 | 0.0110 | 46.96 | 0.0241 | 50.68 | 0.0223 | | |
| 24.89 | 0.0130 | | | | | 38.01 | 0.0144 |
| 34.00 | 0.0179 | 37.30 | 0.0196 | 40.96 | 0.0179 | 27.70 | 0.0106 |
| 37.25 | 0.0198 | 27.24 | 0.0144 | 29.91 | 0.0139 | 19.61 | 0.0074 |
| 42.38 | 0.0225 | 19.49 | 0.0101 | 21.31 | 0.0097 | 11.37 | 0.0041 |
| 48.26 | 0.0256 | 12.17 | 0.0063 | 12.86 | 0.0059 | 7.99 | 0.0027 |
| | | 6.37 | 0.0031 | 6.69 | 0.0031 | | |
| 39.11 | 0.0207 | | | | | | |
| 28.74 | 0.0155 | | | | | | |
| 17.39 | 0.0094 | | | | | | |

## Hydrogen Isotherms

| T = 353.15K | | T = 363.15K | | T = 373.15K | | T = 393.15K | |
|---|---|---|---|---|---|---|---|
| p | v | p | v | p | v | p | v |
| 2.52 | 0.0006 | 2.17 | 0.0002 | 1.82 | 0.0004 | 2.29 | 0.0003 |
| 5.43 | 0.0019 | 3.84 | 0.0011 | 3.26 | 0.0010 | 4.20 | 0.0011 |
| 8.53 | 0.0027 | 6.92 | 0.0020 | 5.86 | 0.0018 | 6.69 | 0.0016 |
| 11.80 | 0.0039 | 12.27 | 0.0040 | 10.52 | 0.0035 | 12.12 | 0.0034 |
| 15.09 | 0.0054 | 17.33 | 0.0056 | 16.25 | 0.0052 | 16.75 | 0.0048 |
| 18.66 | 0.0064 | 22.23 | 0.0077 | 22.65 | 0.0076 | 21.75 | 0.0060 |
| 23.09 | 0.0078 | 27.02 | 0.0093 | 27.37 | 0.0092 | 26.39 | 0.0076 |
| 27.99 | 0.0098 | 32.53 | 0.0113 | 32.70 | 0.0111 | 32.29 | 0.0096 |
| 33.94 | 0.0119 | 37.90 | 0.0132 | 38.25 | 0.0128 | 38.54 | 0.0109 |
| 38.22 | 0.0132 | 41.78 | 0.0146 | 43.26 | 0.0145 | 43.71 | 0.0124 |
| 42.78 | 0.0148 | 48.05 | 0.0166 | 45.79 | 0.0155 | 49.36 | 0.0137 |
| 50.51 | 0.0169 | | | | | | |
| | | 37.44 | 0.0133 | 35.84 | 0.0124 | 38.76 | 0.0112 |
| 40.14 | 0.0133 | 26.92 | 0.0099 | 25.64 | 0.0090 | 27.56 | 0.0081 |
| 29.00 | 0.0105 | 18.99 | 0.0064 | | | 19.42 | 0.0054 |
| 20.48 | 0.0064 | 11.18 | 0.0038 | | | 11.86 | 0.0033 |
| 12.53 | 0.0039 | 5.69 | 0.0013 | | | 5.93 | 0.0012 |
| 6.37 | 0.0018 | | | | | | |

Neon Isotherms

| T = 308.15K | | T = 320.65K | | T = 333.15K | | T = 343.15K | |
|---|---|---|---|---|---|---|---|
| p | v | p | v | p | v | p | v |
| 3.37 | 0.0006 | 2.83 | 0.0006 | 3.49 | 0.0005 | 2.92 | 0.0004 |
| 6.25 | 0.0010 | 5.55 | 0.0009 | 6.33 | 0.0007 | 5.97 | 0.0006 |
| 10.67 | 0.0020 | 9.58 | 0.0019 | 11.01 | 0.0017 | 10.45 | 0.0014 |
| 14.97 | 0.0023 | 14.71 | 0.0026 | 15.23 | 0.0024 | 14.48 | 0.0017 |
| 18.74 | 0.0033 | 18.46 | 0.0035 | 19.25 | 0.0028 | 18.44 | 0.0022 |
| 23.76 | 0.0041 | 24.13 | 0.0046 | 24.41 | 0.0036 | 23.97 | 0.0028 |
| 28.95 | 0.0052 | 29.94 | 0.0057 | 29.32 | 0.0045 | 29.39 | 0.0035 |
| 33.23 | 0.0060 | 35.18 | 0.0066 | 34.90 | 0.0053 | 34.39 | 0.0041 |
| 37.38 | 0.0067 | 39.85 | 0.0072 | 40.35 | 0.0056 | 39.95 | 0.0053 |
| 40.85 | 0.0072 | 45.34 | 0.0082 | 48.37 | 0.0066 | 47.74 | 0.0063 |
| 44.35 | 0.0082 | 50.56 | 0.0089 | | | | |
| 48.76 | 0.0086 | | | 38.40 | 0.0050 | 37.53 | 0.0052 |
| | | 40.72 | 0.0070 | 27.87 | 0.0038 | 27.14 | 0.0040 |
| 38.98 | 0.0070 | 29.80 | 0.0047 | 19.82 | 0.0025 | 19.19 | 0.0025 |
| 20.49 | 0.0037 | 21.21 | 0.0032 | 11.62 | 0.0015 | 12.50 | 0.0016 |
| 14.50 | 0.0027 | | | | | 6.38 | 0.0007 |
| 7.64 | 0.0012 | | | | | | |

Neon Isotherms

| T = 353.15K | | T = 363.15K | | T = 373.15K | | T = 393.15K | |
| --- | --- | --- | --- | --- | --- | --- | --- |
| p | v | p | v | p | v | p | v |
| 4.81 | 0.0005 | 4.46 | 0.0004 | 4.02 | 0.0003 | 5.18 | 0.0007 |
| 8.61 | 0.0007 | 8.19 | 0.0005 | 7.52 | 0.0004 | 8.87 | 0.0007 |
| 11.95 | 0.0012 | 11.41 | 0.0010 | 10.51 | 0.0008 | 12.49 | 0.0015 |
| 15.27 | 0.0016 | 14.63 | 0.0013 | 13.44 | 0.0011 | 16.18 | 0.0018 |
| 19.94 | 0.0021 | 19.30 | 0.0015 | 18.54 | 0.0013 | 21.28 | 0.0022 |
| 25.21 | 0.0026 | 24.81 | 0.0022 | 23.68 | 0.0018 | 27.20 | 0.0030 |
| 30.31 | 0.0029 | 30.05 | 0.0027 | 29.21 | 0.0022 | 33.19 | 0.0036 |
| 36.06 | 0.0034 | 36.22 | 0.0033 | 35.35 | 0.0028 | 39.87 | 0.0040 |
| 41.61 | 0.0041 | 41.19 | 0.0038 | 40.64 | 0.0030 | 45.61 | 0.0042 |
| 48.60 | 0.0049 | 48.90 | 0.0041 | 48.04 | 0.0033 | 51.78 | 0.0049 |
| | | | | | | | |
| 38.51 | 0.0042 | 38.15 | 0.0033 | 37.07 | 0.0023 | 41.72 | 0.0023 |
| 27.69 | 0.0030 | 27.53 | 0.0026 | 26.57 | 0.0021 | 29.65 | 0.0027 |
| 19.56 | 0.0019 | 19.39 | 0.0020 | 18.70 | 0.0010 | 20.70 | 0.0016 |
| 12.08 | 0.0011 | 11.38 | 0.0013 | | | | |
| | | 5.77 | 0.0005 | | | | |

Krypton Isotherms

| T = 308.15K | | T = 320.65K | | T = 333.15K | | T = 343.15K | |
|---|---|---|---|---|---|---|---|
| p | v | p | v | p | v | p | v |
| 1.96 | 0.0146 | 2.22 | 0.0128 | 1.28 | 0.0057 | 2.12 | 0.0093 |
| 2.96 | 0.0229 | 3.38 | 0.0192 | 1.93 | 0.0091 | 3.22 | 0.0145 |
| 4.42 | 0.0339 | 5.09 | 0.0307 | 2.76 | 0.0134 | 4.61 | 0.0210 |
| 6.17 | 0.0494 | 7.19 | 0.0442 | 4.31 | 0.0210 | 6.76 | 0.0300 |
| 8.39 | 0.0640 | 9.87 | 0.0605 | 6.54 | 0.0330 | 10.24 | 0.0459 |
| 9.67 | 0.0737 | 13.47 | 0.0824 | 9.31 | 0.0468 | 14.80 | 0.0657 |
| 13.65 | 0.1039 | 19.24 | 0.1181 | 12.80 | 0.0606 | 19.72 | 0.0859 |
| 18.70 | 0.1400 | 25.79 | 0.1561 | 19.32 | 0.0952 | 25.24 | 0.1094 |
| 23.99 | 0.1789 | 31.39 | 0.1900 | 23.46 | 0.1154 | 30.08 | 0.1306 |
| 29.44 | 0.2193 | 36.39 | 0.2190 | 29.42 | 0.1427 | 35.91 | 0.1554 |
| 33.29 | 0.2469 | 43.09 | 0.2580 | 33.65 | 0.1628 | 40.97 | 0.1760 |
| 37.68 | 0.2780 | 48.78 | 0.2921 | 38.24 | 0.1867 | 47.12 | 0.2017 |
| 44.57 | 0.3267 | | | 43.13 | 0.2116 | | |
| 50.14 | 0.3661 | 37.66 | 0.1942 | 48.69 | 0.2396 | 35.54 | 0.1503 |
| | | 24.87 | 0.1468 | | | 23.09 | 0.0960 |
| 38.75 | 0.2820 | 16.35 | 0.0911 | 36.50 | 0.1767 | 15.15 | 0.0584 |
| 25.98 | 0.1893 | 2.13 | 0.0052 | 23.98 | 0.1140 | 6.63 | 0.0225 |
| 17.08 | 0.1185 | | | 15.78 | 0.0711 | | |
| 3.60 | 0.0190 | | | 2.97 | 0.0079 | | |

Krypton Isotherms

| T = 353.15K | | T = 363.15K | | T = 373.15K | | T = 393.15K | |
|---|---|---|---|---|---|---|---|
| p | v | p | v | p | v | p | v |
| 2.27 | 0.0081 | 2.60 | 0.0075 | 2.96 | 0.0076 | 2.58 | 0.0048 |
| 3.49 | 0.0140 | 4.02 | 0.0135 | 4.57 | 0.0132 | 4.02 | 0.0094 |
| 5.39 | 0.0217 | 4.01 | 0.0156 | 7.08 | 0.0210 | 6.24 | 0.0147 |
| 7.70 | 0.0311 | 6.19 | 0.0217 | 10.34 | 0.0303 | 8.76 | 0.0209 |
| 10.74 | 0.0431 | 8.96 | 0.0310 | 15.00 | 0.0433 | 12.42 | 0.0297 |
| 14.80 | 0.0583 | 11.95 | 0.0409 | 22.02 | 0.0639 | 18.29 | 0.0437 |
| 20.54 | 0.0793 | 17.42 | 0.0593 | 27.50 | 0.0802 | 21.87 | 0.0516 |
| 26.61 | 0.1025 | 22.57 | 0.0763 | 31.70 | 0.0933 | 27.33 | 0.0652 |
| 31.32 | 0.1194 | 28.13 | 0.0952 | 36.90 | 0.1094 | 32.35 | 0.0795 |
| 36.69 | 0.1386 | 32.76 | 0.1115 | 43.70 | 0.1313 | 36.86 | 0.0884 |
| 41.89 | 0.1580 | 37.03 | 0.1247 | 48.87 | 0.1450 | 41.79 | 0.1006 |
| 47.27 | 0.1780 | 37.03 | 0.1249 | 49.29 | 0.1454 | 49.72 | 0.1197 |
| | | 43.35 | 0.1475 | | | | |
| 32.35 | 0.1201 | 50.44 | 0.1708 | 35.24 | 0.1006 | 35.86 | 0.0886 |
| 21.03 | 0.0751 | | | 22.95 | 0.0661 | 23.21 | 0.0577 |
| 13.77 | 0.0451 | 36.85 | 0.1263 | 14.80 | 0.0395 | 14.89 | 0.0350 |
| | | 24.27 | 0.0835 | | | 5.05 | 0.0127 |
| | | 15.65 | 0.0530 | | | | |

## Xenon Isotherms

| T = 308.15K | | T = 320.65K | | T = 333.15K | | T = 343.15K | |
|---|---|---|---|---|---|---|---|
| p | v | p | v | p | v | p | v |
| 1.62 | 0.054 | 2.84 | 0.071 | 1.89 | 0.035 | 1.45 | 0.023 |
| 2.31 | 0.078 | 4.14 | 0.104 | 2.76 | 0.055 | 2.15 | 0.036 |
| 3.21 | 0.106 | 5.91 | 0.146 | 4.04 | 0.078 | 3.10 | 0.052 |
| 4.13 | 0.135 | 7.64 | 0.188 | 5.34 | 0.104 | 4.26 | 0.070 |
| 6.20 | 0.197 | 11.15 | 0.269 | 6.78 | 0.130 | 5.45 | 0.089 |
| 8.92 | 0.282 | 16.44 | 0.392 | 9.66 | 0.182 | 7.62 | 0.121 |
| 12.45 | 0.389 | 23.17 | 0.548 | 14.32 | 0.270 | 11.38 | 0.180 |
| 15.98 | 0.495 | 26.99 | 0.635 | 19.95 | 0.372 | 16.52 | 0.259 |
| 18.95 | 0.583 | 31.65 | 0.741 | 26.34 | 0.486 | 20.12 | 0.313 |
| 24.50 | 0.748 | 34.50 | 0.803 | 30.61 | 0.567 | 24.55 | 0.379 |
| 28.37 | 0.862 | 39.83 | 0.922 | 34.48 | 0.630 | 30.65 | 0.469 |
| 34.37 | 1.039 | 46.22 | 1.063 | 41.31 | 0.742 | 35.70 | 0.544 |
| 40.20 | 1.208 | 51.02 | 1.171 | 47.09 | 0.844 | 39.71 | 0.603 |
| 47.42 | 1.417 | | | | | 47.33 | 0.715 |
| | | 40.15 | 0.927 | 34.64 | 0.626 | | |
| 36.49 | 1.101 | 28.55 | 0.665 | 24.02 | 0.437 | 34.39 | 0.524 |
| 26.09 | 0.795 | 19.19 | 0.449 | 16.09 | 0.292 | 23.73 | 0.364 |
| 18.14 | 0.556 | 12.91 | 0.304 | 8.19 | 0.146 | 15.76 | 0.241 |
| 10.61 | 0.329 | 5.61 | 0.131 | 2.90 | 0.045 | 7.64 | 0.116 |
| 4.16 | 0.129 | 3.83 | 0.088 | | | 2.62 | 0.035 |

Xenon Isotherms

| T = 353.15K | | T = 363.15K | | T = 373.15K | | T = 393.15K | |
|---|---|---|---|---|---|---|---|
| p | v | p | v | p | v | p | v |
| 1.81 | 0.023 | 1.17 | 0.012 | 1.62 | 0.015 | 2.03 | 0.014 |
| 2.69 | 0.038 | 1.75 | 0.020 | 2.46 | 0.025 | 3.15 | 0.023 |
| 3.91 | 0.054 | 2.61 | 0.030 | 3.64 | 0.037 | 4.69 | 0.035 |
| 5.43 | 0.074 | 3.69 | 0.042 | 5.16 | 0.052 | 6.80 | 0.050 |
| 6.56 | 0.088 | 4.85 | 0.056 | 6.72 | 0.066 | 10.53 | 0.077 |
| 9.88 | 0.134 | 6.88 | 0.077 | 10.15 | 0.100 | 15.92 | 0.116 |
| 14.38 | 0.193 | 10.17 | 0.114 | 14.27 | 0.138 | 20.92 | 0.152 |
| 20.01 | 0.265 | 14.10 | 0.159 | 19.62 | 0.188 | 25.12 | 0.180 |
| 24.16 | 0.321 | 18.91 | 0.212 | 24.80 | 0.238 | 30.93 | 0.222 |
| 29.15 | 0.383 | 23.65 | 0.266 | 30.39 | 0.293 | 35.76 | 0.251 |
| 35.81 | 0.467 | 30.56 | 0.340 | 34.87 | 0.335 | 40.66 | 0.286 |
| 38.86 | 0.506 | 35.25 | 0.390 | 39.25 | 0.377 | 45.17 | 0.316 |
| 47.15 | 0.608 | 39.98 | 0.442 | 42.43 | 0.407 | 49.74 | 0.348 |
| | | 44.29 | 0.488 | 49.29 | 0.469 | | |
| 35.16 | 0.458 | 49.63 | 0.544 | | | 36.95 | 0.258 |
| 23.56 | 0.310 | | | 36.11 | 0.345 | 24.47 | 0.169 |
| 15.83 | 0.208 | 37.75 | 0.417 | 23.89 | 0.229 | 15.84 | 0.104 |
| 7.40 | 0.098 | 25.38 | 0.285 | 15.80 | 0.150 | 6.35 | 0.036 |
| 2.43 | 0.031 | 16.69 | 0.186 | 6.97 | 0.064 | 2.91 | 0.010 |
| | | 7.51 | 0.083 | 3.25 | 0.026 | | |
| | | 2.40 | 0.024 | | | | |

Methane Isotherms

| T = 308.15K | | T = 320.65K | | T = 333.15K | | T = 343.15K | |
|---|---|---|---|---|---|---|---|
| p | v | p | v | p | v | p | v |
| 1.80 | 0.0127 | 1.80 | 0.0103 | 1.50 | 0.0062 | 2.12 | 0.0095 |
| 2.70 | 0.0194 | 2.71 | 0.0161 | 2.25 | 0.0111 | 3.23 | 0.0137 |
| 3.77 | 0.0274 | 3.85 | 0.0228 | 3.22 | 0.0157 | 4.67 | 0.0196 |
| 6.44 | 0.0462 | 7.77 | 0.0462 | 6.21 | 0.0298 | 8.35 | 0.0352 |
| 9.61 | 0.0691 | 11.73 | 0.0693 | 9.35 | 0.0452 | 12.72 | 0.0531 |
| 13.44 | 0.0962 | 16.57 | 0.0974 | 13.45 | 0.0643 | 18.17 | 0.0752 |
| 18.21 | 0.1298 | 20.73 | 0.1210 | 19.37 | 0.0923 | 23.30 | 0.0968 |
| 25.17 | 0.1790 | 25.75 | 0.1509 | 27.72 | 0.1318 | 28.58 | 0.1190 |
| 29.89 | 0.2119 | 30.85 | 0.1809 | 32.49 | 0.1537 | 34.99 | 0.1455 |
| 35.52 | 0.2518 | 36.79 | 0.2159 | 37.27 | 0.1760 | 40.60 | 0.1698 |
| 40.45 | 0.2868 | 43.39 | 0.2540 | 42.47 | 0.2014 | 46.52 | 0.1935 |
| 45.61 | 0.3230 | 49.12 | 0.2860 | 48.72 | 0.2311 | | |
| | | | | | | 32.39 | 0.1395 |
| 32.30 | 0.2318 | 35.59 | 0.2110 | 35.74 | 0.1730 | 21.22 | 0.0923 |
| 21.60 | 0.1574 | 23.74 | 0.1423 | 23.62 | 0.1161 | 13.82 | 0.0647 |
| 14.23 | 0.1043 | 15.51 | 0.0941 | 15.38 | 0.0769 | 4.87 | 0.0265 |
| 6.91 | 0.0520 | 8.71 | 0.0554 | 5.97 | 0.0324 | | |

Methane Isotherms

| T = 353.15K | | T = 363.15K | | T = 373.15K | | T = 393.15K | |
|---|---|---|---|---|---|---|---|
| p | v | p | v | p | v | p | v |
| 1.74 | 0.0067 | 2.93 | 0.0077 | 2.70 | 0.0078 | 2.15 | 0.0040 |
| 2.63 | 0.0104 | 4.47 | 0.0137 | 4.15 | 0.0122 | 3.31 | 0.0074 |
| 3.84 | 0.0141 | 6.58 | 0.0199 | 6.10 | 0.0174 | 4.87 | 0.0108 |
| 6.36 | 0.0240 | 9.89 | 0.0309 | 8.57 | 0.0244 | 8.16 | 0.0186 |
| 9.74 | 0.0358 | 15.18 | 0.0473 | 13.20 | 0.0372 | 12.64 | 0.0282 |
| 14.03 | 0.0505 | 21.88 | 0.0681 | 19.17 | 0.0539 | 18.44 | 0.0410 |
| 18.59 | 0.0673 | 26.79 | 0.0842 | 24.46 | 0.0694 | 23.41 | 0.0530 |
| 24.42 | 0.0880 | 33.16 | 0.1048 | 29.77 | 0.0843 | 28.86 | 0.0649 |
| 29.25 | 0.1054 | 38.06 | 0.1210 | 34.94 | 0.0991 | 34.00 | 0.0768 |
| 34.50 | 0.1247 | 43.00 | 0.1367 | 40.32 | 0.1143 | 39.30 | 0.0892 |
| 40.10 | 0.1458 | 48.63 | 0.1551 | 45.77 | 0.1291 | 46.44 | 0.1040 |
| 45.35 | 0.1654 | | | | | | |
| | | 34.04 | 0.1104 | 31.16 | 0.0900 | 31.14 | 0.0713 |
| 31.47 | 0.1174 | 22.13 | 0.0747 | 20.23 | 0.0601 | 20.15 | 0.0463 |
| 20.60 | 0.0791 | 14.35 | 0.0480 | 13.09 | 0.0396 | 12.99 | 0.0296 |
| 13.32 | 0.0534 | 6.14 | 0.0218 | 6.12 | 0.0197 | 5.18 | 0.0119 |
| 7.02 | 0.0303 | | | 2.56 | 0.0086 | | |

Ethane Isotherms

| T = 308.15K | | T = 320.65K | | T = 333.15K | | T = 343.15K | |
|---|---|---|---|---|---|---|---|
| p | v | p | v | p | v | p | v |
| 1.95 | 0.100 | 1.81 | 0.069 | 1.30 | 0.037 | 1.55 | 0.036 |
| 2.60 | 0.132 | 3.16 | 0.119 | 1.80 | 0.053 | 2.30 | 0.052 |
| 3.23 | 0.163 | 4.36 | 0.162 | 2.37 | 0.068 | 3.23 | 0.075 |
| 4.94 | 0.243 | 6.00 | 0.220 | 3.54 | 0.100 | 4.31 | 0.099 |
| 6.63 | 0.322 | 7.73 | 0.279 | 4.99 | 0.140 | 6.49 | 0.148 |
| 8.30 | 0.398 | 11.14 | 0.396 | 6.52 | 0.180 | 9.32 | 0.210 |
| 10.68 | 0.506 | 15.39 | 0.541 | 9.58 | 0.260 | 12.47 | 0.278 |
| 14.38 | 0.675 | 19.82 | 0.690 | 13.52 | 0.364 | 16.83 | 0.373 |
| 17.94 | 0.837 | 23.72 | 0.822 | 17.89 | 0.477 | 22.38 | 0.491 |
| 22.01 | 1.020 | 29.28 | 1.007 | 22.40 | 0.592 | 26.65 | 0.581 |
| 27.42 | 1.261 | 34.91 | 1.194 | 29.46 | 0.772 | 33.18 | 0.719 |
| 31.31 | 1.436 | 39.83 | 1.357 | 35.33 | 0.920 | 38.97 | 0.838 |
| 36.24 | 1.654 | 47.73 | 1.614 | 41.51 | 1.077 | 43.87 | 0.939 |
| 41.16 | 1.870 | | | 46.82 | 1.210 | 47.56 | 1.015 |
| 46.72 | 2.111 | 37.92 | 1.294 | | | | |
| | | 27.56 | 0.949 | 35.32 | 0.923 | 35.48 | 0.766 |
| 37.11 | 1.692 | 19.22 | 0.666 | 25.17 | 0.664 | 24.62 | 0.537 |
| 27.54 | 1.267 | 12.33 | 0.432 | 17.20 | 0.456 | 16.73 | 0.368 |
| 19.54 | 0.910 | 6.28 | 0.222 | 10.15 | 0.273 | 8.51 | 0.190 |
| 13.47 | 0.630 | | | 4.95 | 0.133 | 4.10 | 0.089 |
| 7.20 | 0.344 | | | | | | |

Ethane Isotherms

| T = 353.15K | | T = 363.15K | | T = 373.15K | | T = 393.15K | |
|---|---|---|---|---|---|---|---|
| p | v | p | v | p | v | p | v |
| 1.00 | 0.018 | 1.48 | 0.023 | 1.63 | 0.022 | 2.16 | 0.020 |
| 1.90 | 0.037 | 2.20 | 0.036 | 3.32 | 0.045 | 3.25 | 0.030 |
| 2.54 | 0.049 | 3.23 | 0.052 | 6.08 | 0.082 | 4.59 | 0.043 |
| 3.67 | 0.070 | 4.41 | 0.071 | 8.98 | 0.119 | 7.82 | 0.074 |
| 4.96 | 0.094 | 5.59 | 0.090 | 12.54 | 0.165 | 11.75 | 0.112 |
| 8.37 | 0.157 | 8.20 | 0.130 | 17.32 | 0.226 | 16.66 | 0.158 |
| 12.11 | 0.224 | 11.27 | 0.177 | 23.71 | 0.306 | 22.57 | 0.213 |
| 16.37 | 0.300 | 16.01 | 0.249 | 28.93 | 0.371 | 28.74 | 0.270 |
| 20.98 | 0.382 | 23.20 | 0.357 | 34.37 | 0.439 | 35.95 | 0.337 |
| 28.41 | 0.512 | 31.82 | 0.485 | 40.41 | 0.513 | 42.77 | 0.399 |
| 35.69 | 0.638 | 37.77 | 0.571 | 45.29 | 0.572 | 48.42 | 0.448 |
| 41.59 | 0.739 | 43.88 | 0.662 | | | | |
| 48.26 | 0.855 | 49.75 | 0.744 | 32.47 | 0.414 | 34.93 | 0.326 |
| | | | | 22.02 | 0.282 | 22.95 | 0.214 |
| 36.06 | 0.642 | 36.99 | 0.562 | 14.52 | 0.185 | 15.12 | 0.138 |
| 24.76 | 0.445 | 25.18 | 0.387 | 6.95 | 0.086 | 7.47 | 0.065 |
| 16.67 | 0.299 | 16.80 | 0.259 | | | | |
| 7.13 | 0.126 | 7.81 | 0.122 | | | | |
| 3.33 | 0.054 | | | | | | |

Propane Isotherms

| T = 308.15K | | T = 320.65K | | T = 333.15K | | T = 343.15K | |
|---|---|---|---|---|---|---|---|
| p | v | p | v | p | v | p | v |
| 0.68 | 0.189 | 0.67 | 0.132 | 1.41 | 0.184 | 1.38 | 0.143 |
| 1.29 | 0.339 | 2.32 | 0.410 | 1.97 | 0.252 | 2.95 | 0.287 |
| 2.26 | 0.571 | 5.73 | 0.968 | 5.56 | 0.665 | 6.50 | 0.601 |
| 3.65 | 0.900 | 9.68 | 1.608 | 10.93 | 1.270 | 10.06 | 0.911 |
| 5.70 | 1.394 | 14.83 | 2.419 | 15.28 | 1.751 | 14.49 | 1.290 |
| 8.05 | 1.955 | 18.94 | 3.029 | 18.76 | 2.136 | 21.61 | 1.894 |
| 11.61 | 2.780 | 25.70 | 3.948 | 21.79 | 2.456 | 25.05 | 2.175 |
| 14.55 | 3.421 | 29.68 | 4.427 | 25.26 | 2.807 | 29.79 | 2.557 |
| 19.37 | 4.351 | 36.71 | 5.149 | 31.37 | 3.400 | 33.23 | 2.816 |
| 23.12 | 4.969 | 39.89 | 5.427 | 33.54 | 3.594 | 36.86 | 3.082 |
| 27.59 | 5.591 | 45.99 | 5.900 | 36.62 | 3.859 | 43.63 | 3.550 |
| 31.66 | 6.060 | | | 40.43 | 4.167 | 48.14 | 3.838 |
| 35.06 | 6.403 | 38.68 | 5.318 | 45.43 | 4.541 | | |
| 40.33 | 6.845 | 31.13 | 4.575 | | | 40.30 | 3.315 |
| 45.63 | 7.218 | 24.30 | 3.758 | 38.07 | 3.972 | 31.24 | 2.648 |
| | | 16.33 | 2.639 | 30.11 | 3.267 | 23.35 | 2.015 |
| 38.09 | 6.663 | 8.30 | 1.363 | 23.03 | 2.565 | 13.68 | 1.196 |
| 30.58 | 5.939 | | | 15.20 | 1.721 | 6.86 | 0.601 |
| 24.05 | 5.104 | | | 8.45 | 0.962 | | |
| 14.98 | 3.505 | | | | | | |
| 9.18 | 2.212 | | | | | | |

Propane Isotherms

| T = 353.15K | | T = 363.15K | | T = 373.15K | | T = 393.15K | |
|---|---|---|---|---|---|---|---|
| p | v | p | v | p | v | p | v |
| 1.20 | 0.100 | 1.48 | 0.096 | 1.10 | 0.058 | 2.45 | 0.083 |
| 2.58 | 0.201 | 3.48 | 0.213 | 3.77 | 0.186 | 4.49 | 0.149 |
| 4.92 | 0.367 | 6.41 | 0.377 | 7.86 | 0.372 | 9.60 | 0.306 |
| 9.46 | 0.680 | 10.32 | 0.590 | 12.67 | 0.583 | 17.69 | 0.548 |
| 15.59 | 1.093 | 15.79 | 0.883 | 17.22 | 0.783 | 22.84 | 0.696 |
| 20.28 | 1.410 | 21.09 | 1.164 | 20.32 | 0.916 | 32.12 | 0.964 |
| 24.79 | 1.706 | 25.36 | 1.387 | 25.59 | 1.141 | 38.13 | 1.130 |
| 30.04 | 2.045 | 31.47 | 1.700 | 30.30 | 1.338 | 42.83 | 1.258 |
| 33.80 | 2.277 | 36.19 | 1.935 | 35.14 | 1.538 | 48.87 | 1.427 |
| 37.68 | 2.512 | 42.54 | 2.247 | 39.49 | 1.714 | | |
| 44.44 | 2.905 | 47.64 | 2.491 | 45.77 | 1.963 | 37.79 | 1.114 |
| | | | | 48.65 | 2.077 | 26.79 | 0.801 |
| 36.26 | 2.422 | 38.58 | 2.053 | | | 18.40 | 0.555 |
| 27.62 | 1.879 | 28.75 | 1.554 | 39.51 | 1.708 | 9.15 | 0.280 |
| 20.33 | 1.396 | 20.66 | 1.128 | 28.94 | 1.267 | | |
| 11.02 | 0.767 | 9.79 | 0.542 | 20.48 | 0.901 | | |
| | | | | 8.11 | 0.357 | | |

## n-Butane Isotherms

| T = 308.15K | | T = 373.15K | | T = 393.15K | |
|---|---|---|---|---|---|
| p | v | p | v | p | v |
| 0.13 | 0.198 | 1.17 | 0.226 | 1.05 | 0.128 |
| 0.36 | 0.546 | 3.03 | 0.545 | 1.65 | 0.196 |
| 0.63 | 0.951 | 6.35 | 1.087 | 2.63 | 0.301 |
| 0.90 | 1.347 | 8.43 | 1.418 | 5.14 | 0.554 |
| 1.42 | 2.036 | 11.38 | 1.866 | 9.05 | 0.937 |
| 2.58 | 3.517 | 15.38 | 2.443 | 13.28 | 1.346 |
| 2.79 | 3.731 | 19.30 | 2.930 | 16.58 | 1.646 |
| 4.95 | 5.322 | 23.70 | 3.437 | 20.98 | 2.034 |
| 9.93 | 6.754 | 27.60 | 3.838 | 24.87 | 2.362 |
| 15.55 | 7.478 | 30.73 | 4.109 | 26.81 | 2.509 |
| 19.54 | 7.836 | 35.99 | 4.499 | 29.73 | 2.721 |
| 23.36 | 8.117 | 43.24 | 4.949 | 34.14 | 3.021 |
| 29.51 | 8.487 | 49.57 | 5.286 | 39.55 | 3.359 |
| 39.17 | 9.022 | | | 45.90 | 3.714 |
| 44.84 | 9.359 | 40.97 | 4.790 | | |
| | | 31.86 | 4.123 | 37.21 | 3.185 |
| 36.13 | 8.897 | 24.15 | 3.403 | 28.74 | 2.583 |
| 27.46 | 8.389 | 11.00 | 1.794 | 21.42 | 1.994 |
| 20.39 | 7.895 | | | 9.23 | 0.870 |
| 15.39 | 7.465 | | | | |
| 9.03 | 6.574 | | | | |

Nitrogen Isotherm at 77.4K

| p | v | p | v. |
|---|---|---|---|
| 0.034 | 0.26 | 23.96 | 30.75 |
| 0.032 | 0.55 | 25.38 | 31.90 |
| 0.034 | 1.06 | 27.85 | 33.83 |
| 0.038 | 1.81 | 29.72 | 35.23 |
| 0.041 | 2.84 | 33.02 | 37.46 |
| 0.050 | 3.97 | 35.96 | 39.26 |
| 0.051 | 5.32 | 40.22 | 41.88 |
| 0.058 | 6.74 | 42.89 | 43.65 |
| 0.065 | 8.58 | 47.25 | 46.92 |
| 0.072 | 11.10 | | |
| 0.101 | 14.07 | 39.64 | 41.57 |
| 0.245 | 16.86 | 32.21 | 36.98 |
| 1.13 | 19.01 | 26.81 | 33.08 |
| 4.26 | 20.64 | 22.65 | 29.75 |
| 5.68 | 21.13 | 18.69 | 26.88 |
| 8.26 | 22.00 | 14.77 | 24.65 |
| 9.48 | 22.43 | 11.07 | 23.03 |
| 11.63 | 23.25 | 7.96 | 21.89 |
| 13.53 | 24.06 | 5.62 | 21.11 |
| 15.08 | 24.80 | 4.02 | 20.55 |
| 16.69 | 25.67 | 2.93 | 20.13 |
| 18.26 | 26.57 | 2.21 | 19.80 |
| 20.30 | 27.93 | 1.75 | 19.54 |
| 21.86 | 29.09 | 1.45 | 19.31 |

# APPENDIX D

## *Isothermal flow results*

### Helium

| $\dfrac{T}{K}$ | $\dfrac{P_o}{\text{cmHg}}$ | $\dfrac{L}{\text{min}}$ | $\dfrac{L^*}{\text{min}}$ | $\dfrac{10^5 G}{\text{J s}^{-1}}$ | $\dfrac{10^6 K}{\text{m}^2 \text{ s}^{-1}}$ |
|---|---|---|---|---|---|
| $308.1_5$ | $\cdot5.14$ | $0.4_8$ | $0.91_1$ | $0.86$ | $1.62$ |
| | $10.53$ | $0.4_2$ | | $1.75$ | $1.61$ |
| | $12.63$ | $0.8_2$ | | $2.12$ | $1.63$ |
| | $15.45$ | $0.7_2$ | | $2.57$ | $1.61$ |
| | $20.04$ | $0.2_1$ | | $3.33$ | $1.61$ |
| | $30.21$ | $0.3_2$ | | $5.02$ | $1.61$ |
| | $39.33$ | $0.4_3$ | | $6.55$ | $1.61$ |
| | $49.48$ | $0.3_6$ | | $8.22$ | $1.61$ |
| $320.6_5$ | $10.50$ | $0.4_0$ | $0.89_3$ | $1.78$ | $1.64$ |
| $333.1_5$ | $10.47$ | $0.4_0$ | $0.87_7$ | $1.82$ | $1.68$ |
| $343.1_5$ | $10.42$ | $0.2_9$ | $0.86_4$ | $1.84$ | $1.71$ |
| $353.1_5$ | $10.39$ | $0.4_8$ | $0.85_1$ | $1.87$ | $1.74$ |
| $363.1_5$ | $10.35$ | $0.5_0$ | $0.83_9$ | $1.89$ | $1.77$ |
| $373.1_5$ | $10.29$ | $0.3_9$ | $0.82_0$ | $1.91$ | $1.80$ |
| $393.1_5$ | $10.26$ | $0.3_7$ | $0.80_7$ | $1.96$ | $1.85$ |

\* Smoothed values obtained by Dolphin, R.J. (1971)

*Isothermal flow results*

Methane

| $T$ | $p_o$ | $L$ | $10^5 G$ | $10^6 \chi$ |
|---|---|---|---|---|
| $K$ | cmHg | min | $J\ s^{-1}$ | $m^2\ s^{-1}$ |
| $308.1_5$ | 10.01 | $2.6_0$ | 1.62 | 1.56 |
| | 10.08 | $2.6_1$ | 1.60 | 1.54 |
| | 18.31 | $2.6_2$ | 2.96 | 1.57 |
| | 18.38 | $2.6_3$ | 2.97 | 1.57 |
| $320.6_5$ | 10.05 | $2.3_5$ | 1.57 | 1.51 |
| $333.1_5$ | 10.02 | $2.2_5$ | 1.54 | 1.49 |
| $343.1_5$ | 9.93 | $2.1_3$ | 1.51 | 1.47 |
| $353.1_5$ | 9.92 | $2.0_1$ | 1.50 | 1.47 |
| $363.1_5$ | 9.90 | $1.9_0$ | 1.48 | 1.45 |
| $373.1_5$ | 9.86 | $1.8_9$ | 1.47 | 1.44 |
| $393.1_5$ | 9.81 | $1.6_5$ | 1.44 | 1.42 |

*Isothermal flow results*

Ethane

| $T$ | $p_o$ | $L$ | $10^5 G$ | $10^6 K$ |
|---|---|---|---|---|
| $K$ | cmHg | min | $J\ s^{-1}$ | $m^2\ s^{-1}$ |
| $308.1_5$ | 10.16 | $11.9_8$ | 1.78 | 1.70 |
| | 20.31 | $11.9_4$ | 3.58 | 1.71 |
| $320.6_5$ | 10.11 | $10.3_3$ | 1.66 | 1.59 |
| $333.1_5$ | 10.05 | $8.9_0$ | 1.56 | 1.50 |
| $343.1_5$ | 10.00 | $7.8_0$ | 1.49 | 1.44 |
| $353.1_5$ | 10.03 | $6.9_6$ | 1.45 | 1.40 |
| $363.1_5$ | 9.93 | $6.3_5$ | 1.39 | 1.36 |
| $373.1_5$ | 9.90 | $5.7_2$ | 1.36 | 1.33 |
| $393.1_5$ | 9.86 | $4.8_5$ | 1.30 | 1.27 |

*Isothermal flow results*

## Propane

| $T$ / K | $P_0$ / cmHg | $L$ / min | $10^5 G$ / J s$^{-1}$ | $10^6 K$ / m$^2$ s$^{-1}$ |
|---|---|---|---|---|
| $308.1_5$ | 5.10 | 37.8 | 1.48 | 2.80 |
| | 10.13 | 38.5 | 2.95 | 2.82 |
| | 19.80 | 37.2 | 5.75 | 2.81 |
| $320.6_5$ | 5.02 | 31.2 | 1.27 | 2.45 |
| | 10.02 | 31.5 | 2.55 | 2.47 |
| | 19.92 | 30.9 | 5.09 | 2.47 |
| $333.1_5$ | 9.91 | 25.8 | 2.26 | 2.21 |
| $343.1_5$ | 10.10 | 21.9 | 2.11 | 2.02 |
| $353.1_5$ | 10.01 | 19.7 | 1.95 | 1.89 |
| $363.1_5$ | 9.96 | 16.7 | 1.79 | 1.75 |
| $373.1_5$ | 10.07 | 14.8 | 1.71 | 1.65 |
| $393.1_5$ | 5.00 | $12.5_3$ | 0.78 | 1.51 |
| | 5.03 | $12.3_7$ | 0.78 | 1.50 |
| | 10.04 | $12.1_8$ | 1.55 | 1.49 |
| | 20.07 | $11.5_6$ | 3.09 | 1.49 |

## n-Butane

| $T$ / K | $P_0$ / cmHg | $L$ / min | $10^5 G$ / J s$^{-1}$ | $10^6 K$ / m$^2$ s$^{-1}$ |
|---|---|---|---|---|
| $308.1_5$ | 5.18 | 89.8 | 3.44 | 6.44 |
| | 9.78 | – | 5.62 | 5.57 |
| | 9.95 | 77.2 | 5.68 | 5.53 |
| | 18.21 | 64.5 | 8.53 | 4.53 |
| $320.6_5$ | 9.96 | 70.7 | 5.04 | 4.90 |
| $333.1_5$ | 5.09 | 64.2 | 2.36 | 4.49 |
| | 9.94 | 61.3 | 4.34 | 4.23 |
| | 18.17 | 54.9 | 7.26 | 3.87 |
| $343.1_5$ | 9.93 | 54.1 | 3.85 | 3.75 |
| $353.1_5$ | 5.09 | 48.3 | 1.78 | 3.39 |
| | 9.96 | 48.8 | 3.45 | 3.36 |
| | 18.29 | 44.3 | 6.06 | 3.21 |
| $363.1_5$ | 9.98 | 41.5 | 3.06 | 2.97 |
| | 18.31 | 39.9 | 5.51 | 2.91 |
| $373.1_5$ | 5.18 | 36.4 | 1.44 | 2.68 |
| | 9.96 | 35.8 | 2.75 | 2.67 |
| | 18.24 | 35.2 | 4.97 | 2.64 |
| $393.1_5$ | 5.22 | 27.3 | 1.20 | 2.22 |
| | 9.97 | 27.9 | 2.29 | 2.22 |
| | 18.15 | 27.5 | 4.15 | 2.21 |

## APPENDIX E

*Isothermal permeabilities*

| $\dfrac{T}{K}$ | $\dfrac{10^6 K_g}{m^2\ s^{-1}}$ | $\dfrac{10^6 K_s}{m^2\ s^{-1}}$ | $\dfrac{K_s}{K_g}$ |
|---|---|---|---|
| Methane | | | |
| $308.1_5$ | 0.80 | 0.76 | $0.9_5$ |
| $320.6_5$ | 0.82 | 0.69 | $0.8_4$ |
| $333.1_5$ | 0.84 | 0.65 | $0.7_7$ |
| $343.1_5$ | 0.85 | 0.62 | $0.7_3$ |
| $353.1_5$ | 0.87 | 0.60 | $0.6_9$ |
| $363.1_5$ | 0.88 | 0.57 | $0.6_5$ |
| $373.1_5$ | 0.90 | 0.54 | $0.6_0$ |
| $393.1_5$ | 0.92 | 0.50 | $0.5_4$ |
| Ethane | | | |
| $308.1_5$ | 0.59 | 1.11 | 1.9 |
| $320.6_5$ | 0.60 | 0.99 | 1.7 |
| $333.1_5$ | 0.61 | 0.89 | 1.5 |
| $343.1_5$ | 0.62 | 0.82 | 1.3 |
| $353.1_5$ | 0.63 | 0.77 | 1.2 |
| $363.1_5$ | 0.65 | 0.71 | 1.1 |
| $373.1_5$ | 0.66 | 0.67 | 1.0 |
| $393.1_5$ | 0.67 | 0.60 | $0.9_0$ |

| $\dfrac{T}{K}$ | $\dfrac{P_o}{cmHg}$ | $\dfrac{10^6 K_g}{m^2\ s^{-1}}$ | $\dfrac{10^6 K_s}{m^2\ s^{-1}}$ | $\dfrac{K_s}{K_g}$ |
|---|---|---|---|---|
| Propane | | | | |
| $308.1_5$ | 5.10 | 0.48 | 2.32 | 4.8 |
| " | 10.13 | " | 2.34 | 4.9 |
| " | 19.80 | " | 2.33 | 4.9 |
| $320.6_5$ | 5.02 | 0.50 | 1.95 | 3.9 |
| " | 10.02 | " | 1.97 | 3.9 |
| " | 19.92 | " | 1.97 | 3.9 |
| $333.1_5$ | 9.91 | 0.51 | 1.70 | 3.3 |
| $343.1_5$ | 10.10 | 0.52 | 1.50 | 2.9 |
| $353.1_5$ | 10.01 | 0.52 | 1.37 | 2.6 |
| $363.1_5$ | 9.96 | 0.53 | 1.22 | 2.3 |
| $373.1_5$ | 10.07 | 0.54 | 1.11 | 2.1 |
| $393.1_5$ | (Average) | 0.56 | 0.94 | 1.7 |

*Isothermal permeabilities*

| $\dfrac{T}{K}$ | $\dfrac{P_o}{cmHg}$ | $\dfrac{10^6 K_g}{m^2\,s^{-1}}$ | $\dfrac{10^6 K_s}{m^2\,s^{-1}}$ | $\dfrac{K_s}{K_g}$ |
|---|---|---|---|---|
| | | n – Butane | | |
| $308.1_5$ | 5.18 | 0.42 | 6.02 | $14._3$ |
| " | 9.78 | " | 5.15 | $12._3$ |
| " | 9.95 | " | 5.11 | $12._2$ |
| " | 18.21 | " | 4.11 | $9._8$ |
| $320.6_5$ | 9.96 | 0.43 | 4.47 | $10._4$ |
| $333.1_5$ | 5.09 | 0.44 | 4.05 | $9._2$ |
| " | 9.94 | " | 3.79 | 8.6 |
| " | 18.17 | " | 3.43 | 7.8 |
| $343.1_5$ | 9.93 | 0.45 | 3.30 | 7.3 |
| $353.1_5$ | 5.09 | 0.46 | 2.93 | 6.4 |
| " | 9.96 | " | 2.90 | 6.3 |
| " | 18.29 | " | 2.75 | 6.0 |
| $363.1_5$ | 9.98 | 0.46 | 2.51 | 5.5 |
| " | 18.31 | " | 2.45 | 5.3 |
| $373.1_5$ | 5.18 | 0.47 | 2.21 | 4.7 |
| " | 9.96 | " | 2.20 | 4.7 |
| " | 18.24 | " | 2.17 | 4.6 |
| $393.1_5$ | 5.22 | 0.49 | 1.73 | 3.5 |
| " | 9.97 | " | 1.73 | 3.5 |
| " | 18.15 | " | 1.72 | 3.5 |

# REFERENCES

ADZUMI, H., 1937a, Bull. Chem. Soc. Japan, 12, 285.

ADZUMI, H., 1937b, Bull. Chem. Soc. Japan, 12, 292.

ADZUMI, H., 1937c, Bull. Chem. Soc. Japan, 12, 304.

ADZUMI, H., 1939, Bull. Chem. Soc. Japan, 14, 343.

ASH, R., BAKER, R.W. and BARRER, R.M., 1967, Proc. Roy. Soc. A., 299, 434.

ASH, R., BAKER, R.W. and BARRER, R.M., 1968, Proc. Roy. Soc. A., 304, 407.

ASH, R. and BARRER, R.M., 1963, Trans. Farad. Soc., 59, 2260.

ASH, R., BARRER, R.M., CLINT, J.H., DOLPHIN, R.J. and MURRAY, C.L., 1973, Phil. Trans. Roy. Soc. Lond. A., 275, 255.

ASH, R., BARRER, R.M. and LOWSON, R.T., 1970, Surf. Sci., 21, 265.

ASH, R., BARRER, R.M. and LOWSON, R.T., 1973, J.C.S. Farad. I., 69, 2166.

ASH, R., BARRER, R.M. and POPE, C.G., 1963a, Proc. Roy. Soc. A., 271, 1.

ASH, R., BARRER, R.M. and POPE, C.G., 1963b, Proc. Roy. Soc. A., 271, 19.

ASH, R., BARRER, R.M. and SHARMA, P., 1976, J. Membrane Sci., 1, 17.

ASH, R, and GROVE, D.M., 1960, Trans. Farad. Soc., 56, 1357.

ATKINS, J.A., 1964, Anal. Chem., 36, 579.

AYLMORE, L.A.G. and BARRER, R.M., 1966, Proc. Roy. Soc. A., 290, 477.

BABBITT, J.D., 1950, Canad. J. Res., 28A, 449.

BABBITT, J.D., 1951, Canad. J. Phys., 29, 427, 437.

BALDWIN, G.C. and GAERTTNER, M.R., 1973, J. Vac. Sci. Tech., 10, 215.

BARBER, C.G., 1971, The Calibration of Thermometers, London: H.M.S.O.

BARRER, R.M., 1939, Trans. Farad. Soc., 35, 628.

BARRER, R.M., 1963a, Appl. Mat. Res., 2, 129.

BARRER, R.M., 1963b, Canad. J. Chem., 41, 1768.

BARRER, R.M. and BARRIE, J.A., 1952, Proc. Roy. Soc. A., 213, 250.

BARRER, R.M. and GABOR, T., 1959, Proc. Roy. Soc. A., 251, 353.

BARRER, R.M. and GABOR, T., 1960, Proc. Roy. Soc. A., 256, 267.

BARRER, R.M. and GROVE, D.M., 1951a, Trans. Farad. Soc., 47, 826.

BARRER, R.M. and GROVE, D.M., 1951b, Trans. Farad. Soc., 47, 837.

BARRER, R.M. and JOST, W., 1949, Trans. Farad. Soc., 45, 928.

BARRER, R.M. and PAPADOPOULOS, R., 1972, Proc. Roy. Soc. A., 326, 315.

BARRER, R.M. and REES, L.V.C., 1959, Trans. Farad. Soc., 55, 992.

BARRER, R.M. and REES, L.V.C., 1961, Trans. Farad. Soc., 57, 999.

BARRER, R.M. and RUZICKA, D.J., 1962, Trans. Farad. Soc., 58, 2253.

BARRER, R.M. and STRACHAN, E., 1955, Proc. Roy. Soc. A., 231, 52.

BEARMAN, R.J., 1957, J. Phys. Chem., 61, 708.

BEARMAN, M.Y. and BEARMAN, R.J., 1966, J. Phys. Chem., 70, 3010.

BEEBE, R.A., BISCOE, J., SMITH, W.R. and WENDELL, C.B., 1947, J. Am. Chem. Soc., 69, 95.

BEEBE, R.A., MILLARD, B. and CYNARSKI, J., 1953, J. Am. Chem . Soc., 75, 839.

BEEBE, R.A., POLLEY, M.H., SMITH, W.R. and WENDELL, C.B., 1947, J. Am. Chem. Soc., 69, 2294.

BENNETT, M.J. and TOMPKINS, F.C., 1957, Trans. Farad. Soc., 53, 185.

BERMAN, A.S. and LUND, L.M., 1958, Proc. 2nd U.N. Int. Conf. on Peaceful Uses of Atomic Energy, 4, 359.

BISCOE, J. and WARREN, B.E., 1942, J. Appl. Phys., 13, 364.

BLAKE, F.C., 1922, Trans. Am. Inst. Chem. Engnrs., 14, 415.

BODDENBERG, B., HAUL, R. and OPPERMANN, G., 1970, Surf. Sci., 22, 29.

BRITISH STANDARDS INSTITUTE, 1952, B.S. 1827, London.

BRITISH STANDARDS INSTITUTE, 1961, B.S. 1828, London.

BROMBERG, J.P., 1969, J. Vac. Sci. Tech., 6, 801.

BROWN, G.P., Di NARDO, A., CHENG, G.K. and SHERWOOD, T.K., 1946, J. Appl. Phys., 17, 802.

BRUNAUER, S., EMMETT, P.H. and TELLER, E., 1938, J. Am. Chem. Soc., 60, 309.

CABOT, Technical Data Sheet.

CARMAN, P.C., 1950, Proc. Roy. Soc. A., 203, 55.

CARMAN, P.C. and MALHERBE, P. le R., 1950, Proc. Roy. Soc. A., 203, 165.

CARMAN, P.C. and RAAL, F.A., 1951a, Proc. Roy. Soc. A., 209, 38.

CARMAN, P.C. and RAAL, F.A., 1951b, Proc. Roy. Soc. A., 209, 59.

CARMAN, P.C. and RAAL, F.A., 1954, Trans. Farad. Soc., 50, 842.

CARR, P.H., 1964, Vacuum, 14, 37.

CHA, C.Y., and McCOY, B.J., 1972, J. Chem. Phys., 56, 3273.

CHIRNSIDE, G.C. and POPE, C.G., 1964, J. Phys. Chem., 68, 2377.

CLAUSING, P., 1930, Ann. d. Physik (5), 7, 489.

CLAUSING, P., 1932, Ann. d. Physik (5), 12, 961.

CLINT, J.H., 1966, Ph.D. Thesis, University of London.

CORRIN, M.L., 1951, J. Am. Chem. Soc., 73, 4061.

CROWE, C.M., 1957, Trans. Farad. Soc., 53, 1413.

CROWE, C.M., 1963, Trans. Farad. Soc ., 59, 2515.

DAVIS , R.T. Jr., DeWITT, T.W. and EMMETT, P.H., 1947, J. Phys. Chem.,
51, 1232.

DeBOER, J.H. and CUSTERS, J.F.H., 1934, Z. Phys. Chem. B., 25, 225.

DENBIGH, K.G., 1951, The Thermodynamics of the Steady State, London : Methuen.

DENBIGH, K.G. and RAUMANN, G., 1952a, Proc. Roy. Soc. A., 210, 377.

DENBIGH, K.G. and RAUMANN, G., 1952b, Proc. Roy. Soc. A., 210, 518.

DERIAGIN, B.V. and BAKANOV, S.P., 1957a, Sov. Phys. Doklady., 2, 326.

DERIAGIN, B.V. and BAKANOV, S.P., 1957b, Sov. Phys. - Tech. Phys., 2, 1904.

DiCORCIA, A. and SAMPERI, R., 1973, J. Phys. Chem., 77, 1301.

DOLPHIN, R.J., 1971, Ph.D. Thesis, University of London.

DUSHMAN, S. and LAFFERTY, J.M., 1965, Scientific Foundations of Vacuum
Technique, 2nd Edn., New York : John Wiley.

EDMONDS, T. and HOBSON, J.P., 1965, J. Vac. Sci. Tech., 2, 182.

ELKINGTON, P.A. and CURTHOYS, G., 1969, J. Phys. Chem., 73, 2321.

EMMETT, P.H. and BRUNAUER, S., 1937, J. Am. Chem. Soc., 59, 1553.

EVERETT, D.H., 1950, Trans. Farad. Soc., 46, 453, 942, 957.

FEDDERSON, W., 1873, Pogg. Ann., 148, 308.

FENG, C. and STEWART, W.E., 1973, Ind. Eng. Chem. Fundam., 12, 143.

FLOOD, E.A., TOMLINSON, R.H. and LEGER, A.E., 1952a, Canad. J. Chem.,
30, 348.

FLOOD, E.A., TOMLINSON, R.H. and LEGER, A.E., 1952b, Canad. J. Chem.,
30, 372.

FLOOD, E.A., TOMLINSON, R.H. and LEGER, A.E., 1952c, Canad. J. Chem., 30, 389.

FRANK, H.S., 1945, J.Chem. Phys., 13, 493.

FRISCH, H.L., 1957, J Phys. Chem.., 61, 93.

FRISCH, H.L., 1958, J. Phys. Chem., 62, 401.

FRISCH, H.L., 1959, J. Phys. Chem., 63, 1249.

GAEDE, W., 1913, Ann. d. Physik (4), 41, 289.

GASCOIGNE, J., 1971, Vacuum, 21, 21.

GILLILAND, E.R. BADDOUR, R.F. and ENGEL, H.H., 1962, A.I.Ch.E.J., 8, 530.

GILLILAND, E.R., BADDOUR, R.F., PERKINSON, G.P. and SLADEK, K.J., 1974, Ind. Eng. Chem. Fundam., 13, 95.

GILLILAND, E.R., BADDOUR, R.F. and RUSSELL, J.L., 1958, A.I.Ch.E.J., 4, 90.

GOODKNIGHT, R.C. and FATT, I., 1961, J. Phys. Chem., 65, 1709.

GOULD, F.A. and VICKERS, T., 1952, J. Sci. Instruments, 29, 85.

GRAHAM, D., 1957, J. Phys. Chem., 61, 1310.

GRAHAM, T., 1846, Phil. Trans. Roy. Soc. Lond., 136, 573.

HALL, C.E., 1948, J. Appl. Phys., 19, 271.

HANLEY, H.J.M., 1965, J. Chem. Phys., 43, 1510.

HANLEY, H.J.M., 1966, Trans. Farad. Soc., 62, 2395.

HANLEY, H.J.M. and STEELE, W.A., 1964, J. Phys. Chem., 68, 3087.

HANLEY, H.J.M. and STEELE, W.A., 1965, Trans. Farad. Soc., 61, 2661.

HAÜL, R.A.W., 1950, Angewandte Chemie, 62, 10.

HAUL, R.A.W. and PEERBOOMS, R., 1958, Naturwiss., 45, 109.

HIBY, J.W. and PAHL, M., 1956, Z. Naturforschung, 11a, 80.

HIGASHI, K., ITO, H. and OISHI, J., 1964, J. Nucl. Sci. Tech., 1, 298.

HILL, T.L., 1952, Adv. in Catalysis, 4, 211.

HILL, T.L., 1956, J. Chem. Phys., 25, 730.

HIRSCH, E.H., 1961, J. Appl. Phys., 32, 977.

HIRSCHFELDER, J.O., CURTISS, C.F. and BIRD, R.B., 1964, Molecular Theory of Gases and Liquids, New York : John Wiley.

HOBSON, J.P., 1969, J. Vac. Sci. Tech., 6, 257.

HOBSON, J.P., EDMONDS, T. and VERREAULT, R., 1963, Canad. J. Phys., 41, 983.

HOPFINGER, E.J. and ALTMAN, M., 1969, J. Chem. Phys., 50, 2417.

HORIGUCHI, Y., HUDGINS, R.R. and SILVESTON, P.L., 1971, Canad. J. Chem. Eng., 49, 76.

HOUSKA, C.R. and WARREN, B.E., 1954, J. Appl. Phys., 25, 1503.

HUGGILL, J.A.W., 1952, Proc. Roy. Soc. A., 212, 123.

HWANG, S.T. and KAMMERMEYER, K., 1966a, Canad. J. Chem. Eng., 44, 82.

HWANG, S.T. and KAMMERMEYER, K., 1966b, Separation Sci., 1, 629.

HWANG, S.T. and KAMMERMEYER, K., 1967, Separation Sci., 2, 555.

ISIRIKYAN, A.A. and KISELEV, A.V., 1962, J. Phys. Chem., 66, 205.

JOHNSON, M.F.L. and STEWART, W.E., 1965, J. Catalysis, 4, 248.

JOYNER, L.G. and EMMETT, P.H., 1948, J. Am. Chem. Soc., 70, 2353.

KAMMERMEYER, K., 1958, Ind. Eng. Chem., 50, 697.

KENNARD, E.H., 1938, Kinetic Theory of Gases, New York : McGraw-Hill.

KIRKWOOD, J.G., 1932, Phys. Z., 33, 57.

KLOSE, W., 1931, Ann. d. Physik (5), 11, 73.

KNUDSEN, M., 1909, Ann. d. Physik (4), 28, 75.

KNUDSEN, M., 1910a, Ann. d. Physik (4), 31, 205.

KNUDSEN, M., 1910b, Ann. d. Physik (4), 31, 633.

KOZENY, J., 1927, S.B. Akad. Wiss., Wien , Abt. IIa., 136, 271.

KRUYER, S., 1953, Proc. Acad. Sci. Amst. B., 56, 274.

LAL, M. and SPENCER, D., 1974, J.C.S. Farad. II., 70, 910.

LASSETTRE, E.N., 1956, American Atomic Energy Commission Research Report, K - 1258.

LASSETTRE, E.N., 1958, American Atomic Energy Commission Research Report, K - 1403.

LASSETTRE, E.N. and BROOKS, A.A., 1961, American Atomic Energy Commission Research Report, K- 1464.

LEE, C.S. and O'CONNELL, J.P., 1972, J. Coll. Intf. Sci., 41, 415.

LIANG, S.C., 1951, J. Appl. Phys., 22, 148.

LIANG, S.C., 1952, J. Phys. Chem., 56, 660.

LIANG,S.C., 1953, J.Phys. Chem., 57, 910.

LIANG, S.C., 1955, Canad. J. Chem., 33, 279.

LONDON,F., 1930, Z. Phys., 63, 245.

LOS,J.M. and FERGUSSON,R.P., 1952, Trans. Farad. Soc., 48, 730.

MASON,E.A., EVANS,R.B. III. and WATSON,G.M., 1961, J. Chem. Phys.,35, 2076.

MASON, E.A., EVANS, R.B. III. and WATSON, G.M., 1963, J. Chem. Phys., 38, 1808.

MASON, E.A. and MALINAUSKAS, A.P., 1964, J. Chem. Phys., 41, 3815.

MAXWELL, J.C., 1860, Phil. Mag. (4)., 20, 21.

MAXWELL, J.C., 1879, Phil. Trans. Roy. Soc. Lond., 170, 231.

McCORMICK, N.J. and KUŠČER, I., 1972, Phys. Fluids, 15, 1567.

MILLER, G.A., 1963, J. Phys. Chem., 67, 1359.

MILLER, G.A. and BUICE, R.L. Jr., 1966, J. Phys. Chem., 70, 3874.

MÜLLER, A., 1936, Proc. Roy. Soc. A., 154, 624.

NEUMANN, C., 1872, Ber. d. Könige Sächs. Akad. d. Wiss., 24, 49.

NICHOLSON, D. and PETROPOULOS, J.H, 1971, J. Phys. D., 4, 181.

NICHOLSON, D. and PETROPOULOS, J.H., 1973, J. Coll. Intf. Sci., 45, 459.

ONSAGER, L., 1931, Phys. Rev., 37, 405; 38, 2265.

PARKINSON, C. and GRAY, P., 1972, J.C.S. Farad. I., 68, 1065.

PARSONAGE, N.G. and STAVELEY, L.A.K., 1959, Quart. Rev., 13, no.4.

PATEL, P.V. and BUTT, J.B., 1972, Chem. Eng. Sci., 27, 2175.

PERRY, R.H. and CHILTON, C.H., Eds., 1973, Chemical Engineers Handbook, 5th Edn., New York : McGraw - Hill.

PIERCE, C. and EWING, B., 1964, J. Phys. Chem., 68, 2562.

PODGURSKI, H.H. and DAVIS, F.N., 1961, J. Phys. Chem., 65, 1343.

POLLARD, W.G. and PRESENT, R.D., 1948, Phys. Rev., 73, 762.

POPE, C.G., 1961, Ph.D. Thesis, University of London.

POPE, C.G., 1967, Trans. Farad. Soc., 63, 734.

POPIELAWSKI, J., 1967, J. Catalysis, 7, 263.

RASTOGI, R.P. and RAI, A.P., 1974, J. Phys. Chem., 78, 2693.

RASTOGI, R.P., RAI, A.P. and YADAVA, M.L., 1974, Indian. J. Chem., 12, 1273.

RASTOGI, R.P., SINGH, K. and SINGH, H.P., 1969, J. Phys. Chem., 73, 2798.

REYNOLDS, O., 1879, Phil. Trans. Roy. Soc., 170, 727.

ROSENBERG, A.J., 1956, J. Am. Chem. Soc., 78, 2929.

ROSS, J.W. and GOOD, R.J., 1956, J. Phys. Chem., 60, 1167.

ROSSINI, F.D., PITZER, K.S., TAYLOR, W.J., EBERT, J.P., KILPATRICK, J.E.,
        BECKETT, C.W., WILLIAMS, M.G. and WERNER, H.G., 1947,
        Selected Values of Properties of Hydrocarbons, Washington:
        U.S. Dept. of Commerce, N.B.S. Circular 471.

ROYBAL, L.A. and SANDLER, S.I., 1972, A.I.Ch.E.J., 18, 39.

SANDLER, S.I., 1972a, Ind. Eng. Chem. Fundam., 11, 424.

SANDLER, S.I., 1972b, A.I.Ch.E.J., 18, 856.

SCHAEFFER, W.D., SMITH, W.R. and POLLEY, M.H., 1953, Ind. Eng. Chem., 45, 1721.

SEARS, G.W., 1954, J. Chem. Phys., 22, 1252.

SINGH, H.P., 1971, Indian J. Chem., 9, 52.

SIU, M.C.I., 1973, J. Vac. Sci. Tech., 10, 368.

SLADEK, K.J., GILLILAND, E.R. and BADDOUR, R.F., 1974, Ind. Eng. Chem.
                                                 Fundam., 13, 100.

SLATER, J.C. and KIRKWOOD, J.G., 1931, Phys. Rev., 37, 682.

SMITH, R.K. and METZNER, A.B., 1964, J. Phys. Chem., 68, 2741.

SMOLUCHOWSKI, M., 1910, Ann. d. Physik (4), 33, 1559.

STEELE, W.A. and HANLEY, H.J.M., 1971, Trans. Farad. Soc., 67, 3484.

TAKAISHI, T. and SENSUI, Y., 1963, Trans. Farad. Soc., 59, 2503.

UTTERBACK, N.G., and GRIFFITH, T. Jr., 1966, Rev. Sci. Inst., 37, 866.

VAN ITTERBEEK, A. and De GRANDE, E., 1947, Physika, 13, 289.

VOLMER, M. and ESTERMAN, J., 1921, Z. Physik, 7, 13.

WEAST, R.C., Ed., 1970, Handbook of Chemistry and Physics, 51st Edn.,
                        Cleveland : The Chemical Rubber Co.

WEAVER, J.A. and METZNER, A.B., 1966, A.I.Ch.E.J., 12, 655.

WEBER, S., 1954, Mat. fys. Medd. Kong. Dansk. vid. sels., 28, no 2.

WEBER, S., KEESOM, W.H. and SCHMIDT, G., 1936, Comm. Kam. Onnes. Lab.,
                                               Leiden, 22, no 246 a-d.

WEISSBERG, H.L., 1963, J. Appl. Phys., 34, 2636.

WICKE, E. and KALLENBACH, R., 1941, Kolloid. Zschr., 97, 135.

WILLIAMS, J.C. III., 1971, J. Vac. Sci. Tech., $\underline{8}$, 446.

WILLIAMS, M.M.R., 1973, J. Phys. D., $\underline{6}$, 759.

WRIGHT, P.G., 1971, Trans. Farad. Soc., $\underline{67}$, 2551.

WU, Y., 1968, J. Chem. Phys., $\underline{48}$, 889.

WYNNE-JONES, W.F.K., 1958, Proc. Colston. Symposium : The Structure
        and Properties of Porous Materials, p35, London : Butterworths.

YANG, R.T., FENN, J.B. and HALLER, G.L., 1973, A.I.Ch.E.J., $\underline{19}$, 1052.

YOUNG, D.M. and CROWELL, A.D., 1962, Physical Adsorption of Gases,
                                London : Butterworths.